Electronic ISSN: 1309-0267

# International Journal of Engineering & Applied Sciences

IJEAS

I J E A S

Volume 10, Issue 3
2018

Published by Akdeniz University

## Editorial Board

*(The name listed below is not Alphabetical or any title scale)*

## Abstracting & Indexing

**IJEAS** provides unique **DOI** link to every paper published.

## Editorial Scope

The journal presents its readers with broad coverage across some branches of engineering and science of the latest development and application of new solution algorithms, artificial intelligent techniques innovative numerical methods and/or solution techniques directed at the utilization of computational methods in solid and nano-scaled mechanics.

International Journal of Engineering & Applied Sciences (IJEAS) is an Open Access Journal

International Journal of Engineering & Applied Sciences (IJEAS) publish original contributions on the following topics:

Numerical Methods in Solid Mechanics

Nanomechanic and applications

Microelectromechanical systems (MEMS)

Vibration Problems in Engineering

Higher order elasticity (Strain gradient, couple stress, surface elasticity, nonlocal elasticity)

Applied Mathematics

# CONTENTS

*International Journal of Engineering & Applied Sciences (IJEAS)*
*Vol.10, Issue 3 (2018) 140-158*
*http://dx.doi.org/10.24107/ijeas.422906*
Int J Eng Appl Sci 10(3) (2018) 140-158

# Nonlinear Wave Modulation in Nanorods Based on Nonlocal Elasticity Theory by Using Multiple-Scale Formalism

*Guler Gaygusuzoglu*

*Namık Kemal University, Corlu Faculty of Engineering, Department of Civil Engineering, Corlu-Tekirdag.*
*E-mail address*: ggaygusuzoglu@nku.edu.tr

*Received date: 11.05.2018*
*Accepted date: 26.09.2018*

**Abstract**

*Many systems in physics, engineering, and natural sciences are nonlinear and modeled with nonlinear equations. Wave propagation, as a branch of nonlinear science, is one of the most widely studied subjects in recent years. Nonlocal elasticity theory represents a common growing technique used for conducting the mechanical analysis of microelectromechanical and nanoelectromechanical systems. In this study, nonlinear wave modulation in nanorods was examined by means of nonlocal elasticity theory. The nonlocal constitutive equations of Eringen were utilized in the formulation, and the nonlinear equation of motion of nanorods was obtained. By applying the multiple scale formalism, the propagation of weakly nonlinear and strongly dispersive waves was investigated, and the Nonlinear Schrödinger (NLS) equation was obtained as the evolution equation. A part of spacial solutions of the NLS equation, i.e. nonlinear plane wave, solitary wave and phase jump solutions, were presented. In order to investigate the nonlocal impacts on the NLS equation numerically, whether envelope solitary wave solutions exist was investigated by utilizing the physical and geometric features of carbon nanotubes (CNTs).*

**Keywords:** Nanorods, nonlinear wave modulation, nonlocal elasticity theory, multiple-scale method.

## 1. Introduction

The accurate characterization of the actual mechanical behavior of nanoscale devices is significant in the design of the devices in question, including CNTs. However, the application of a classical continuum theory is questionable while carrying out the mechanical analysis of carbon nanotubes. The classical continuum theory (classical elasticity theory) is length scale-free. Hence, it cannot accurately account for very small-sized effects. To eliminate the deficiencies of the classical continuum theory, different higher-order continuum theories, such as micro-polar elasticity theory [1-4], nonlocal elasticity theory [5-7], couple stress theory [8] and the modified couple stress approach [9, 10], have received significant attention in the analysis of micro- and nanostructures. Due to the high cost of experiments that operate on the nanoscale, it is of vital importance to introduce suitable physical models for nanobeams (carbon nanotubes) for the establishment of an appropriate theoretical and mathematical framework for nanosized structures [11-13]. Eringen [14] and Eringen and Edelen [15] proposed nonlocal elasticity theory in the 1970s for the purpose of overcoming the deficiencies of classical

elasticity models. Unlike the conventional theory of elasticity, in the nonlocal theory of elasticity, it is assumed that the strain at a particular point in a continuous domain and the strain at all points in the domain determine the stress at the point in question. Several studies have been performed using this nonlocal model to conduct the analysis of the mechanical behavior of nanosized structures [16-18].

Wave propagation is a very effective, nondestructive method used for the characterization of nanostructures. Nanosensor transducers also work on the wave propagation principle. The wave propagation issue has attracted attention around the world [19-25] in various domains of science and engineering due to its importance. In the study carried out by Lim and Yang [19], the researchers investigated wave propagation in CNTs based on nonlocal elastic stress field theory and Timoshenko beam theory and acquired a novel dispersion and spectrum correlation. In the study of Hu et al. [20], transverse and torsional waves in single-walled carbon nanotubes (SWCNTs) and double-walled carbon nanotubes (DWCNTs) were investigated on the basis of nonlocal elastic cylindrical shell theory. The researchers compared the wave dispersion that was estimated by utilizing their model with molecular dynamics simulations in the terahertz area and concluded that it was possible to acquire a better prediction of dispersion relations by the nonlocal model. Wu and Dzenis [26] investigated wave propagation in nanofibers. The researchers studied longitudinal and flexural wave propagation in nanofibers by employing local theories in terms of surface impacts. Challamel [27] suggested a dispersive wave equation by utilizing nonlocal elasticity. The researcher introduced a mixture theory of a local and nonlocal strain. Narendar and Gopalakrishnan [28] investigated the nonlocal scale impacts on the ultrasonic wave feature of nanorods by employing the nonlocal Love rod theory. In the study of Narendar [29], the nonlocal Love-Rayleigh rod theory was used to examine wave propagation in uniform nanorods.

It is well-known that in the case of a sufficiently small amplitude of a wave, a lot of nonlinear systems allow for harmonic wave solutions with sufficiently small nonlinear terms for ignoring them, and the amplitude stays unchanged over time. In case of a small-but-finite amplitude of the wave, it is not possible to ignore the nonlinear terms, which causes an alteration in amplitude in space as well as time. In case of the slow variation of the amplitude during the period of oscillation, a stretching transformation allows the separation of the system into a quickly changing component related to the oscillation and a slowly changing component, for example, the amplitude. It is possible to present a formal solution as an asymptotic expansion, and it is possible to derive an equation that identifies the modulation of the first order amplitude. For example, the nonlinear Schrödinger (NLS) equation represents the most elementary representative equation that defines the self-modulation of one-dimensional monochromatic plane waves in dispersive media. The equilibrium between dispersion and nonlinearity is presented by it. The problem of nonlinear wave modulation was studied by Erbay, Erbay, and Dost [30] in micropolar elastic media longitudinal waves. They showed that the nonlinear Schrödinger (NLS) equation, originating from the equilibrium between nonlinearity and dispersion, governs the nonlinear self-modulation of a longitudinal microrotation wave in micropolar elastic media. Erbay and Erbay [31] studied nonlinear self-modulation in distensible tubes filled with fluid by utilizing the nonlinear equations of a thin viscoelastic tube and the approximate fluid equations. As a result of the study, the researchers indicated that the dissipative NLS equation governs the nonlinear modulation of pressure waves. The amplitude modulation of the fluid-filled viscoelastic tube was investigated in the study of Akgun and Demiray [32], and the dissipative NLS equation was acquired. Furthermore, Akgun and Demiray [33] studied the modulation of non-linear axial and transverse waves in a thin elastic

tube filled with fluid and obtained nonlinear Schrödinger equation which corresponds to two nonlinear equations related to the axial and transverse motions of the tube material. Erbay, Erbay, and Erkip [34] studied a unidirectional wave motion in a nonlocally and nonlinearly elastic medium. Duruk, Erbay, and Erkip [35] investigated the blow-up and global existence for a general class of nonlocal nonlinear coupled wave equations. In the previous studies, nonlinear wave modulation in nanotubes has not been considered.

In this study, the amplitude modulation of nonlinear wave propagation in nanorods based on the nonlocal theory was studied by employing the reductive perturbation technique. Firstly, a one-dimensional nonlinear field equation was obtained. The linear dispersion relation of axial waves was also presented for observing the dispersive characteristic of the medium. It is shown that the nonlinear Schrödinger (NLS) equation governs the nonlinear self-modulation of axial waves in nonlocal elastic media and it is given as an analytical plane wave, envelope solitary wave and a phase jump solution for the NLS equation. For the purpose of numerical investigation of the nonlocal impacts on the NLS equation, whether envelope solitary wave solutions exist was investigated by utilizing the physical and geometric features of carbon nanotubes.

The organization of the current study is presented below. Section 2 contains information on nonlocal elasticity theory and the governing equation of the system. The basics of the method of multiple scale formalism and self-modulation of nonlinear waves are discussed in Section 3. Section 4 contains the numerical and graphical presentation of the findings. In Section 5, some discussions and conclusions are given.

## 2. Basic equations and theoretical preliminaries

In the present section, the basic equation that governs the motion of nanorods in nonlocal elastic media should be derived. The constitutive equation of the nonlocal linear vibration of a nanorod which is provided by Eringen [15], Aydogdu [17] is as follows;

$$\left[1-(\mathrm{e}_0 a)^2\frac{\partial}{\partial \mathrm{x}^2}\right]\tau_{kl} = \lambda_L\,\varepsilon_{\mathrm{rr}}\delta_{kl} + 2\,\mu_L\,\varepsilon_{kl} \tag{1}$$

where $\tau_{kl}$ represents the nonlocal stress tensor, $\varepsilon_{kl}$ represents the strain tensor, $\lambda_L$ and $\mu_L$ represent Lame constants, $a$ represents the internal characteristic length, and $\mathrm{e}_0$ represents a constant. From now on, the nonlocal parameter μ will be used as $(\mathrm{e}_0 a)^2 = \mu$.

Selection of the $\mathrm{e}_0$ parameter (in a unit of length) is very important in ensuring the accuracy of nonlocal models. It is possible to write Eq.(1) for one-dimensional rod case as follows;

$$\left[1-\mu\frac{\partial}{\partial \mathrm{x}^2}\right]\tau_{\mathrm{kl}} = \mathrm{E}_{\mathrm{E}}\,\varepsilon_{kl} \tag{2}$$

where $E_E$ represents the modulus of elasticity. It is possible to write the equation of motion for a rod with axial vibration motion as follows;

$$\frac{\partial N^L}{\partial x} = m\frac{\partial^2 u(x,t)}{\partial t^2} \tag{3}$$

where u(x,t) denotes the axial displacement, and m gives the mass per unit length, while $N^L$ provides the axial force per unit length for local elasticity and is presented as follows;

$$N^L = \int_A \sigma_{xx} dA \tag{4}$$

where A represents the cross-sectional area, $\sigma_{xx}$ represents the local stress component in the x-direction. By taking the area integral of equation (2), the following equation can be obtained;

$$N - \mu\frac{\partial^2}{\partial x^2}N = N^L \tag{5}$$

Here $N = \int_A \sigma_{xx} dA$ indicates axial force per unit length in nonlocal elasticity. The axial vibration equation of the rod in nonlocal elasticity may be reached using equations (3) and (5) in terms of the displacement component as follows;

$$E_E A\frac{\partial^2 u}{\partial x^2} = \left[1 - \mu\frac{\partial}{\partial x^2}\right] m\frac{\partial^2 u(x,t)}{\partial t^2} \tag{6}$$

The equation above represents the basic equation of the nonlocal rod model for axial vibration in a thin rod. In case of $\mu = e_0 a = 0$, the reduction of the equation to the equation of the classical rod model is performed. To obtain the nonlinear vibration equation of the nanotube in an elastic medium, first we introduce the deformation gradient tensor that was described by Malvern [36] as follows;

$$F = \vec{\nabla} u + I \tag{7}$$

Here, u represents the displacement component of the motion, while I is the unit matrix. If body forces on the element are absent in a medium exposed to a finite extension, in terms of material coordinates, it is possible to write the equations of motion as follows;

$$\nabla . [SF^T] = \rho_0 \frac{\partial^2 u}{\partial t^2} \tag{8}$$

Here $\rho_0$ is the non-deformed density of the medium, while S is the second Piola-Kirchoff stress tensor. The second Piola-Kirchoff stress tensor represents a conjugate of the Green strain tensor

in terms of energy. Therefore, Hook's law can be used as the governing equation. The equation is written as follows;

$$S = cE \tag{9}$$

Here, c denotes the fourth-order tensor that represents the elastic behavior of the material, while E denotes the Green strain tensor written as follows;

$$E = \frac{1}{2}[F^T F - 1] \tag{10}$$

If limiting the boundary conditions of the rod and assuming only the radial deformation U(x,t) take place in the medium, the gradient deformation tensor in the cartesian coordinates becomes a diagonal matrix.

$$F_{xx} = 1 + \frac{\partial U}{\partial x} \tag{11}$$

$$F_{zz} = 1 \tag{12}$$

$$F_{yy} = 1 \tag{13}$$

By referring only to the non-zero element in the Green strain tensor, the following equation can be obtained:

$$E_{xx} = \left(1 + \frac{1}{2}\frac{\partial U}{\partial x}\right)\frac{\partial U}{\partial x}. \tag{14}$$

The stress-strain relations of isotropic materials with the modulus of elasticity $E_E$ and Poisson's ratio $\nu$ become as follows;

$$S_{ij} = \frac{E_E}{(1+\nu)}\left[E_{ij} + \frac{\nu}{1-2\nu}E_{kk}\delta_{ij}\right] \tag{15}$$

$\delta_{ij}$ denotes the Kronecker delta. If we replace equation (14) into equation (15), it is observed that shear stresses are eliminated, while normal stress elements are shown as below:

$$S_{xx} = \frac{E_E(1-\nu)}{(1+\nu)(1-2\nu)}\left(1 + \frac{1}{2}\frac{\partial U}{\partial x}\right)\frac{\partial U}{\partial x} \tag{16}$$

$$S_{yy} = S_{zz} = \frac{E_E\,\nu}{(1+\nu)(1-2\nu)}\left(1 + \frac{1}{2}\frac{\partial U}{\partial x}\right)\frac{\partial U}{\partial x} \tag{17}$$

Equation (8) can be obtained as follows by rearranging equations (16), (17) and using equations (11), (12), (13):

$$\left[\left(\frac{\partial U}{\partial x}\right)^2 + 2\frac{\partial U}{\partial x} + \frac{2}{3}\right]\frac{\partial^2 U}{\partial x^2} = \frac{2\rho_0(1+\nu)(1-2\nu)}{3\,E_E\,(1-\nu)}\frac{\partial^2 U}{\partial t^2} \tag{18}$$

In a special case, the infinite deformation of the medium, the nonlinear terms in equation (18) become insignificant, and equation (18) is reduced to the following equation.

$$\frac{\partial^2 U}{\partial x^2} = \frac{\rho_0(1+\nu)(1-2\nu)}{E_E\,(1-\nu)}\frac{\partial^2 U}{\partial t^2} \tag{19}$$

By making the equation non-dimensional, let us introduce the following non-dimensional variables:

$$\Psi = \frac{U}{r_0} \tag{21}$$

$$\zeta = \frac{x}{r_0} \tag{22}$$

here $r_0$ defines the radius of the rod. If equations (18) and (19) are reorganized by using equations (21) and (22), the following non-dimensional equations can be obtained as has been described by Mousavi and Fariborz [37] ;

$$\left[\left(\frac{\partial \psi}{\partial \zeta}\right)^2 + 2\left(\frac{\partial \psi}{\partial \zeta}\right) + \frac{2}{3}\right]\frac{\partial^2 \psi}{\partial \zeta^2} = \frac{2}{3}\delta\frac{\partial^2 \psi}{\partial t^2} \tag{23}$$

and

$$\frac{\partial^2 \psi}{\partial \zeta^2} = \delta\frac{\partial^2 \psi}{\partial t^2} \tag{24}$$

where the coefficient $\delta$ is defined as follows:

$$\delta = \frac{\rho_0\, {r_0}^2(1+\nu)(1-2\nu)}{E_E\,(1-\nu)}. \tag{25}$$

By using Eqs. (2), (8), (16) and (17), the following nonlinear equation of motion in terms of nonlocal elasticity is obtained:

$$\left[\left(\frac{\partial\psi}{\partial\zeta}\right)^2 + 2\left(\frac{\partial\psi}{\partial\zeta}\right) + \frac{2}{3}\right]\frac{\partial^2\psi}{\partial\zeta^2} = \frac{2}{3}\delta\frac{\partial^2\psi}{\partial t^2} - \frac{2}{3}\delta\,\mu\,\frac{\delta^4\psi}{\delta\zeta^2\delta t^2}. \tag{26}$$

A similar equation was obtained by Fernandes et al. [38]. The main difference is that they neglected y and z component contributions.

Setting $\mu = 0$ leads to the nonlinear equation of motion of classical elasticity.

## 3. Nonlinear wave modulation in nanorods by using the multiple-scale method

Finding precise solutions for nonlinear problems is usually hard. This especially applies to nonlinear dynamics under the nonlocal elasticity theory due to the apparent complexity of the governing equations. Nevertheless, handling nonlinear problems in case of sufficiently weak nonlinearity is relatively straightforward. In this situation, evolution equations originating from the equilibrium between dispersion and nonlinearity can be obtained using the dispersive nature of the medium. As a result of the above-mentioned characteristic, it is possible to apply the far-field theory of weakly nonlinear waves, the complete development of which has been performed in different areas of engineering and physics, to nonlocal elasticity theory in case of equilibrium between nonlinearity and dispersion.

In the present section, the modulation of the axial waves in nonlocal elastic media due to nonlinear effects is examined. Therefore, the multiple scale technique [39] is used, and the coordinate stretching below is presented:

$$\zeta_n = \varepsilon^n\zeta \quad , \quad t_n = \varepsilon^n t \quad , \quad (n = 0,1,2,\dots) \tag{27}$$

where $\varepsilon$ represents a small parameter measuring the weakness of non-linearity.

It should be assumed that the field quantities represent the functions of fast variables $(\zeta, t)$, as well as slow variables $(\zeta_0, \zeta_1, \zeta_2, \dots; t_0, t_1, t_2, \dots.)$. Therefore, the substitution presented below can be performed:

$$\frac{\partial}{\partial\zeta} = \sum_{n=0}^{N}\varepsilon^n\frac{\partial}{\partial\zeta_n} \qquad , \qquad \frac{\partial}{\partial t} = \sum_{n=0}^{N}\varepsilon^n\frac{\partial}{\partial t_n} \tag{28}$$

By performing the expansion of the field quantities into an asymptotic series of $\varepsilon$ as:

$$\psi = \sum_{n=1}^{\infty}\varepsilon^n\psi_n\,(\zeta_0,\zeta_1,\zeta_2,\dots;t_0,t_1,t_2,\dots.) = \varepsilon\psi_1 + \varepsilon^2\psi_2 + \varepsilon^3\psi_3{+}\dots \tag{29}$$

and introducing the above-mentioned expansion into Eq. (26), the differential equation presented below is acquired.

$$\left[\left(\varepsilon\frac{\partial\psi_1}{\partial\zeta_0}\right)^2+2\varepsilon^3\frac{\partial\psi_1}{\partial\zeta_0}\frac{\partial\psi_1}{\partial\zeta_1}+2\varepsilon\frac{\partial\psi_1}{\partial\zeta_0}+2\varepsilon^2\frac{\partial\psi_2}{\partial\zeta_0}+2\varepsilon^2\frac{\partial\psi_1}{\partial\zeta_1}+\cdots\frac{2}{3}\right]\times\left[\varepsilon\frac{\partial^2\psi_1}{\partial{\zeta_0}^2}+\varepsilon^2\frac{\partial^2\psi_2}{\partial{\zeta_0}^2}+\varepsilon^3\frac{\partial^2\psi_3}{\partial{\zeta_0}^2}+2\varepsilon^2\frac{\partial^2\psi_1}{\partial\zeta_0\,\partial\zeta_1}+2\varepsilon^3\frac{\partial^2\psi_2}{\partial\zeta_0\,\partial\zeta_1}+2\varepsilon^3\frac{\partial^2\psi_1}{\partial\zeta_0\,\partial\zeta_2}+\varepsilon^3\frac{\partial^2\psi_1}{\partial{\zeta_1}^2}\right]=\frac{2\delta}{3}\left[\varepsilon\frac{\partial^2\psi_1}{\partial{t_0}^2}+\varepsilon^2\frac{\partial^2\psi_2}{\partial{t_0}^2}+\varepsilon^3\frac{\partial^2\psi_3}{\partial{t_0}^2}+2\varepsilon^2\frac{\partial^2\psi_1}{\partial t_0\,\partial t_1}+2\varepsilon^3\frac{\partial^2\psi_2}{\partial t_0\,\partial t_1}+2\varepsilon^3\frac{\partial^2\psi_1}{\partial t_0\,\partial t_2}+\varepsilon^3\frac{\partial^2\psi_1}{\partial{t_1}^2}\right]-\frac{2\delta\mu}{3}\left[\varepsilon\frac{\partial^4\psi_1}{\partial{t_0}^2\partial{\zeta_0}^2}+\varepsilon^2\frac{\partial^4\psi_2}{\partial{t_0}^2\partial{\zeta_0}^2}+\varepsilon^3\frac{\partial^4\psi_3}{\partial{t_0}^2\partial{\zeta_0}^2}+2\varepsilon^2\frac{\partial^4\psi_1}{\partial{t_0}^2\partial\zeta_0\,\partial\zeta_1}+2\varepsilon^3\frac{\partial^4\psi_2}{\partial{t_0}^2\partial\zeta_0\,\partial\zeta_1}+2\varepsilon^3\frac{\partial^4\psi_1}{\partial{t_0}^2\partial\zeta_0\,\partial\zeta_1}+\varepsilon^3\frac{\partial^4\psi_1}{\partial{t_0}^2\partial{\zeta_1}^2}+2\varepsilon^2\frac{\partial^4\psi_1}{\partial{\zeta_0}^2\partial t_0\,\partial t_1}+2\varepsilon^3\frac{\partial^4\psi_2}{\partial{\zeta_0}^2\partial t_0\,\partial t_1}+4\varepsilon^3\frac{\partial^4\psi_1}{\partial t_0\,\partial t_1\partial\zeta_0\,\partial\zeta_1}+2\varepsilon^3\frac{\partial^4\psi_1}{\partial{\zeta_0}^2\partial t_0\,\partial t_2}+\varepsilon^3\frac{\partial^4\psi_1}{\partial{t_1}^2\partial{\zeta_0}^2}\right] \tag{30}$$

The set of differential equations presented below is acquired as a result of setting the coefficients of like powers of $\varepsilon$ equal to zero;

*First-order, O(ε), equation:*

$$\frac{\partial^2\psi_1}{\partial{\zeta_0}^2}=\delta\frac{\partial^2\psi_1}{\partial{t_0}^2}-\delta\mu\frac{\partial^4\psi_1}{\partial{t_0}^2\partial{\zeta_0}^2} \tag{31}$$

*Second-order, O($\varepsilon^2$),equation:*

$$2\frac{\partial\psi_1}{\partial\zeta_0}\frac{\partial^2\psi_1}{\partial{\zeta_0}^2}+\frac{2}{3}\frac{\partial^2\psi_2}{\partial{\zeta_0}^2}+\frac{4}{3}\frac{\partial^2\psi_1}{\partial\zeta_0\,\partial\zeta_1}=\frac{2\delta}{3}\frac{\partial^2\psi_2}{\partial{t_0}^2}+\frac{4\delta}{3}\frac{\partial^2\psi_1}{\partial t_0\,\partial t_1}-\frac{2\delta\mu}{3}\frac{\partial^4\psi_2}{\partial{t_0}^2\partial{\zeta_0}^2}-\frac{4\delta\mu}{3}\frac{\partial^4\psi_1}{\partial{t_0}^2\partial\zeta_0\,\partial\zeta_1}-\frac{4\delta\mu}{3}\frac{\partial^4\psi_1}{\partial{\zeta_0}^2\partial t_0\,\partial t_1} \tag{32}$$

*Third-order, O($\varepsilon^3$),equation:*

$$\left(\frac{\partial\psi_1}{\partial\zeta_0}\right)^2\frac{\partial^2\psi_1}{\partial{\zeta_0}^2}+2\frac{\partial\psi_1}{\partial\zeta_0}\frac{\partial^2\psi_2}{\partial{\zeta_0}^2}+2\frac{\partial\psi_2}{\partial\zeta_0}\frac{\partial^2\psi_1}{\partial{\zeta_0}^2}+2\frac{\partial\psi_1}{\partial\zeta_1}\frac{\partial^2\psi_1}{\partial{\zeta_0}^2}+\frac{4}{3}\frac{\partial^2\psi_1}{\partial\zeta_0\,\partial\zeta_1}+\frac{2}{3}\frac{\partial^2\psi_3}{\partial{\zeta_0}^2}+\frac{4}{3}\frac{\partial^2\psi_2}{\partial\zeta_0\,\partial\zeta_1}+\frac{2}{3}\frac{\partial^2\psi_1}{\partial{\zeta_1}^2}+4\frac{\partial\psi_1}{\partial\zeta_0}\frac{\partial^2\psi_1}{\partial\zeta_0\,\partial\zeta_1}=\frac{2\delta}{3}\frac{\partial^2\psi_3}{\partial{t_0}^2}+\frac{4\delta}{3}\frac{\partial^2\psi_2}{\partial t_0\,\partial t_1}+\frac{4\delta}{3}\frac{\partial^2\psi_1}{\partial t_0\,\partial t_2}+\frac{2\delta}{3}\frac{\partial^2\psi_1}{\partial{t_1}^2}-\frac{2\delta\mu}{3}\frac{\partial^4\psi_3}{\partial{t_0}^2\partial{\zeta_0}^2}-\frac{4\delta\mu}{3}\frac{\partial^4\psi_2}{\partial{t_0}^2\partial\zeta_0\,\partial\zeta_1}-\frac{4\delta\mu}{3}\frac{\partial^4\psi_1}{\partial{t_0}^2\partial\zeta_0\,\partial\zeta_2}-\frac{4\delta\mu}{3}\frac{\partial^4\psi_2}{\partial{\zeta_0}^2\partial t_0\,\partial t_1}-\frac{8\delta\mu}{3}\frac{\partial^4\psi_1}{\partial t_0\,\partial t_1\partial\zeta_0\,\partial\zeta_1}-\frac{4\delta\mu}{3}\frac{\partial^4\psi_1}{\partial{\zeta_0}^2\partial t_0\,\partial t_2}-\frac{2\delta\mu}{3}\frac{\partial^4\psi_1}{\partial{t_0}^2\partial{\zeta_1}^2}-\frac{2\delta\mu}{3}\frac{\partial^4\psi_1}{\partial{t_1}^2\partial{\zeta_0}^2} \tag{33}$$

where $\psi_1$ is the function of fast as well as slow variables.

### 3.1 The solution of field equations:

In the present section, an attempt should be made to acquire the solution of the field equations that govern different order terms in the perturbation expansion.

#### 3.1.1 The solution of O($\varepsilon$) order equation:

The form of the differential equation presented in Eq. (31) indicates that we should look for the type of solution presented below:

$$\psi_1 = \varphi(\zeta_1, \zeta_2, \dots; t_1, t_2, \dots) exp[\,\mathrm{i}(\omega t_0 - k\,\zeta_0)] + \mathrm{c.c.} \tag{34}$$

where ω denotes the angular frequency, $k$ denotes the wave number, $\varphi(\zeta_1, \zeta_2, \dots; t_1, t_2, \dots)$ denotes the amplitude function depending on the slow variables, and c. c. denotes the complex conjugate of the equivalent quantity. As a result of introducing Eq. (34) into Eq. (31) and requiring the non-vanishing solution for $\varphi(\zeta_1, \zeta_2, \dots; t_1, t_2, \dots)$, the following dispersion relation is obtained:

$$\mathrm{D}(\omega, \mathrm{k}) = \mathrm{k}^2 - \delta\omega^2 - \delta\mu\mathrm{k}^2\omega^2 = 0\,. \tag{35}$$

Here $\varphi(\zeta_1, \zeta_2, \dots; t_1, t_2, \dots)$ stands for an unknown function, the governing equation of which will be acquired afterwards.

#### 3.1.2 The solution of O($\varepsilon^2$), order equation:

The form of Eq. (32) indicates that it is necessary to look for the type of solution for $\psi_2$ presented below:

$$\psi_2 = \sum_{\alpha=1}^{2} \Psi_2^{(\alpha)} e^{i\alpha\theta} + c.c. \tag{36}$$

Here, the phasor $\theta$ is defined by $\theta = \omega t_0 - k\,\zeta_0$ and $\Psi_2^{(1)}, .., \Psi_2^{(-2)}$ are functions of slow variables of $\zeta_0$ and $t_0$. The equation for α=1 mode presented below is acquired by introducing Eq. (34) and Eq. (36) into Eq. (32);

$$[\mathrm{k}^2 - \delta\omega^2(1 + \mu\mathrm{k}^2)]\Psi_2^{(1)} + 2ik(1 - \delta\mu\omega^2)\frac{\partial\varphi}{\partial\zeta_1} + 2i\delta\omega(1 + \mu\mathrm{k}^2]\frac{\partial\varphi}{\partial t_1} = 0 \tag{37}$$

Here, the coefficient of $\Psi_2^{(1)}$ is the dispersion relation and must be zero. The following is obtained by employing the dispersion relation:

$$2ik(1-\ \delta\mu\omega^2)\frac{\partial\varphi}{\partial\zeta_1}\ +2i\delta\omega(1+\mu k^2]\frac{\partial\varphi}{\partial t_1}=0 \tag{38}$$

For obtaining non-zero solution for φ that satisfies Eq. (38), it should have the form below:

$$\varphi=\varphi(\ \xi\ ,\zeta_2\ ,\ldots;\ t_2,\ldots.)\quad ,\quad \xi=\zeta_1-\lambda\ t_1 \tag{39}$$

Here, $\lambda$ stands for the group velocity of the wave, and it is described by:

$$v_g=\lambda\ =\frac{k}{\omega\ \delta\ (1+\mu k^2)^2}. \tag{40}$$

Here, the function $\Psi_2^{(1)}$ represents another function, the governing equation of which is acquired from the higher-order expansion of the field quantities. The solution of Eq. (32) for α=2 mode is obtained as follows:

$$\Psi_2^{(2)}=\frac{3ik^3}{\left[4k^2-4\delta\omega^2-16\delta\mu k^2\omega^2\right]}\varphi^2=\frac{3ik^3}{D(2k,2\omega)}\varphi^2. \tag{41}$$

Here $D(lk,l\omega)\neq\ 0$ for $l=2,3,..\ .$

### 3.1.3 The solution of O($\varepsilon^3$), order equation:

It is generally possible to express the solution for the order in question in terms of the phasor as follows:

$$\psi_3=\sum_{\alpha=1}^{3}\Psi_3^{(\alpha)}e^{i\alpha\theta}+c.c.\qquad ,\qquad \theta=\ \omega\ t_0-k\ \zeta_0 \tag{42}$$

Only the first order equation in terms of the phasor is required for completing the solution for the unknown function $\varphi(\ \xi\ ,\zeta_2\ ,\ldots;\ t_2,\ldots.)$. By introducing Eqs. (34), (36) and (42) into Eq. (33), we obtain:

$$\begin{aligned}&\frac{2}{3}[k^2-\delta\omega^2(1+\mu k^2)]\Psi_3^{(1)}\ +\frac{4i\delta\omega}{3}[1+\mu k^2\ ]\frac{\partial\Psi_2^{(1)}}{\partial t_1}+\frac{4ik}{3}[1-\delta\mu\omega^2\ ]\frac{\partial\Psi_2^{(1)}}{\partial\zeta_1}+\\&\frac{4i\delta\omega}{3}[1+\mu k^2\ ]\frac{\partial\varphi}{\partial t_2}+\frac{4ik}{3}[1-\delta\mu\omega^2\ ]\frac{\partial\varphi}{\partial\zeta_2}\ +\frac{2}{3}\delta(1+\mu k^2)\frac{\partial^2\varphi}{\partial{t_1}^2}-\frac{8}{3}\delta\mu k\omega\frac{\partial^2\varphi}{\partial t_1\,\partial\zeta_1}-\\&-\frac{2}{3}[1-\delta\mu\omega^2\ ]\frac{\partial^2\varphi}{\partial{\zeta_1}^2}-k^4|\varphi|^2\varphi+\ 4ik^3\Psi_2^{(2)}\varphi^*=\ 0.\end{aligned} \tag{43}$$

Here, the coefficient of $\Psi_3^{(1)}$ is the dispersion relation and must be zero. By rearranging Eq. (43), we have:

$$\frac{4\delta\omega}{3}[1+\mu k^2\,]\times\left\{i\left(\frac{\partial\Psi_2^{(1)}}{\partial t_1}+\lambda\frac{\partial\Psi_2^{(1)}}{\partial\zeta_1}\right)+i\left(\frac{\partial\varphi}{\partial t_2}+\lambda\frac{\partial\varphi}{\partial\zeta_2}\right)\right\}-\frac{2}{3}[1-\delta\mu\omega^2-4\delta\mu\lambda k\omega-\delta\lambda^2(1+\mu k^2)\,]\frac{\partial^2\varphi}{\partial\xi^2}-k^4|\varphi|^2\varphi+4ik^3\Psi_2^{(2)}\varphi^*=0. \quad (44)$$

Here, the dependence of φ on ξ has been already utilized. Furthermore, in case of assuming that $\Psi_2^{(1)}$ depends on $t_1$ and $\zeta_1$ through ξ, then the drop occurs in the first terms in (44). As a result of presenting a new variable τ as $t_2=\tau$ , $\zeta_2=\varepsilon\xi+\lambda\tau$ , it is possible to read the second term in Eq. (44) as follows:

$$\frac{\partial\varphi}{\partial t_2}+\lambda\frac{\partial\varphi}{\partial\zeta_2}=\frac{1}{\varepsilon}\frac{\partial\varphi}{\partial\xi}-\frac{1}{\varepsilon}\frac{\partial\varphi}{\partial\xi}+\frac{\partial\varphi}{\partial\tau}=\frac{\partial\varphi}{\partial\tau} \quad (45)$$

By introducing the expression of $\Psi_2^{(2)}$ into (44), the nonlinear Schrödinger equation presented below is acquired:

$$i\frac{\partial\varphi}{\partial\tau}+\nu_1\frac{\partial^2\varphi}{\partial\xi^2}+\nu_2|\varphi|^2\varphi=0 \quad (46)$$

where the coefficients $\nu_1$ and $\nu_2$ are defined by:

$$\nu_1=\frac{1}{2}\frac{\partial v_g}{\partial k}=-\frac{1}{2}\frac{[1-\delta\mu\omega^2-4\delta\mu\lambda k\omega-\delta\lambda^2(1+\mu k^2)\,]}{\delta\omega(1+\mu k^2)}$$

$$\nu_2=\frac{3}{4}\lambda k^3(1+\mu k^2)\left\{1-\frac{3k^2}{[k^2-\delta\omega^2-4\delta\mu k^2\omega^2]}\right\} \quad (47)$$

The NLS equation appears in different fields as an equation that defines the self-modulation of one-dimensional monochromatic plane waves in dispersive media. The steady-state solution of the NLS equation, usually representing the wave trains that can be expressed in terms of Jacobian elliptic functions, contains bright and dark envelope solitons, a phase jump, and a plane wave with a constant amplitude as special cases. In order to determine how the presented initial data will develop in the long term for the asymptotic NLS equation in the form [40], the criterion of whether $\nu_1\nu_2>0$ or $\nu_1\nu_2<0$ is significant:

$$A(\xi,\tau)=V(\eta)\exp[\,i\,(K\,\xi-\Omega\,\tau)],\quad \eta=\xi-v_0\,\tau\,,\quad v_0=const, \quad (48)$$

where $V(\eta)$ stands for a real function of η. In the mentioned situation, in case of $|\varphi|$ approaching a constant $V_0$ at infinity, the solution is presented by a non-linear plane wave:

$$\varphi(\eta)=V_0\exp[\,i\,(K\,\xi-\Omega\,\tau)], \quad (49)$$

where $\Omega = \sigma_1 K^2 - \sigma_2 {V_0}^2$. It is generally possible to acquire the solution in terms of the Jacobian elliptic functions by assuming that $v_0 = 2\sigma_1 K$. The specific functional form of the solution in question will be presented only for the limiting cases below. If there is an assumption that $V \to 0$ and $\frac{\partial \mathrm{V}}{\partial \eta} \to 0$

as $|\eta| \to \infty$, for $\sigma_1 \sigma_2 > 0$, the solution is presented by:

$$\mathrm{V}(\eta) = A_0 \operatorname{sech}\left[\left(\frac{\nu_2}{2\nu_1}\right)^{1/2} A_0 \eta\right] \tag{46}$$

where $\Omega = \sigma_1 K^2 - \sigma_2 {A_0}^2/2$. For $\nu_1 \nu_2 < 0$, if $\varphi \to V_0$ and $\frac{\partial \varphi}{\partial \eta} \to 0$ as $|\eta| \to \infty$, the solution is given as follows:

$$\mathrm{V} = V_0 \tanh\left[\left(-\frac{\nu_2}{2\nu_1}\right)^{1/2} V_0 \eta\right] \tag{47}$$

where $\Omega = \sigma_1 K^2 - \sigma_2 {V_0}^2$. The mentioned solutions correlate to an envelope solitary wave and a phase jump, respectively. On the contrary, it is a well-known fact that the plane wave solution of the NLS equation is modulationally unstable in case of $\nu_1 \nu_2 > 0$ or stable in case of $\nu_1 \nu_2 < 0$.

## 4. Numerical Results and Discussion

This study examines nonlinear wave modulation in nanorods on the basis of nonlocal elasticity theory. In this study, numerical results are given for SWCNT with material and geometrical properties. In the light of the open literature, no consensus has been achieved on Poisson's ratio of nanotubes. The suggested values vary in a wide band 0.19 ~ 0.34 [41]. Therefore, in the present study, ν is selected as 0.3, and the nonlocal parameter μ is taken as $0 \sim 4\text{x}10^{-18} nm^2$. Some material properties are taken as $\rho_0 = 2300\ kg/m^3$ , $r_0 = 10^{-9} m$ , $\mathrm{E} = 1\ TPa$.

As mentioned previously, the features of both solutions of the NLS equation and the stability of the plane wave solution significantly depend on the sign of $\nu_1 \nu_2$. Thus, giving more details on the change of $\nu_1 \nu_2$ with the wave number will be interesting. The variation in $\nu_1$ for axial waves by wave number for three nonlocal parameter values are depicted in Fig 1. As is seen from this figure for each selected values of μ, $\nu_1$ values remain positive ($\nu_1 > 0$). To clearly see the effect of μ on $\nu_2$ , the graphs of $\nu_2$ by wave number are plotted in Fig 2. This figure also shows that for each selected values of μ, $\nu_2$ values remain positive ($\nu_2 > 0$). The alterations of $\nu_1 \nu_2$ for axial (longitudinal) waves and the wave number are presented in Fig 3. As is seen from the mentioned figure, the plane wave solution for the wave in question is unstable for all values of the wave number for all nonlocal parameter values.

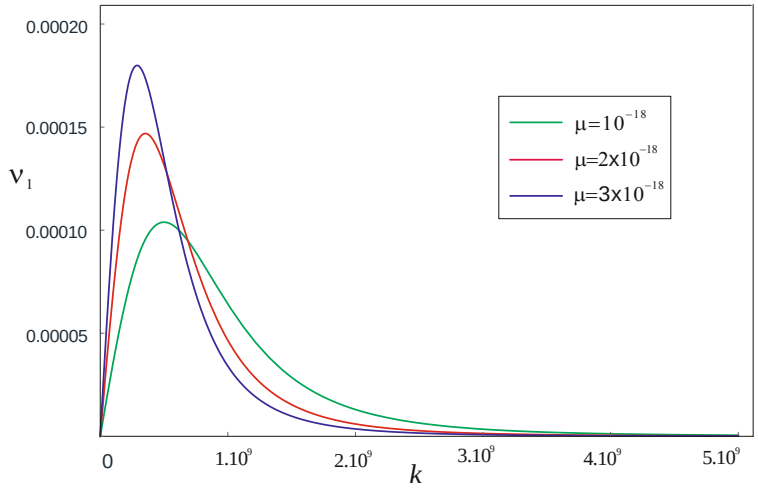


Fig. 1. Variation in the $\nu_1$ for axial waves by wave number for three nonlocal parameter values.

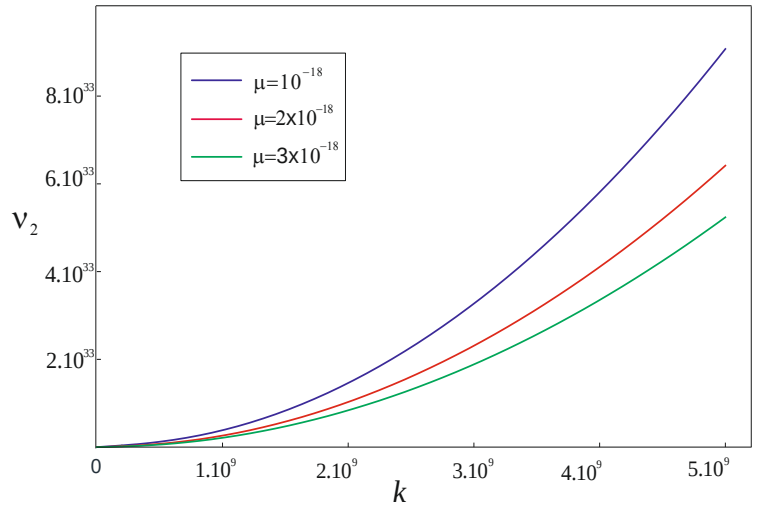


Fig. 2. Variation in the $\nu_2$ for axial waves by wave number for three nonlocal parameter values.

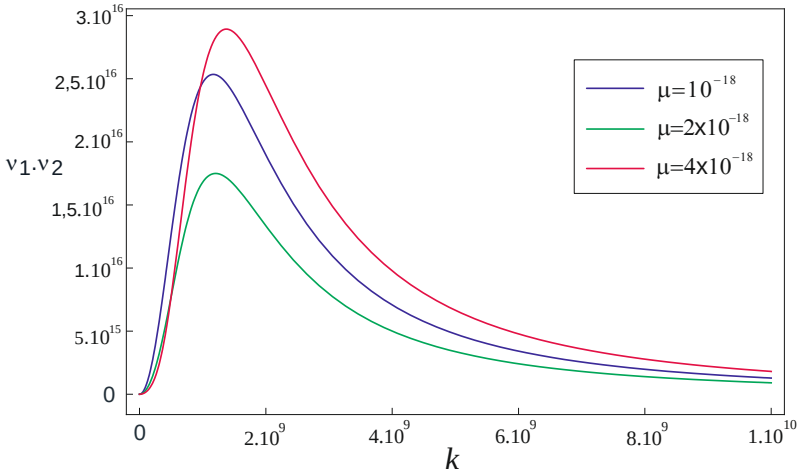


Fig. 3. Variation in the $\nu_1\nu_2$ for axial waves by wave number for three nonlocal parameter values.

Regarding the alteration of the solution profile of the nonlinear Schrödinger equation, the split-step Fourier method [42] was utilized, and the evolution equation was solved numerically. The change of the solution profile with variable η at spatial time is presented in Fig. 4. Here, the nonlocal parameter was taken as $\mu = 10^{-18}$. For $\mu = 0$, there is no solitary wave profile because of non-dispersion.

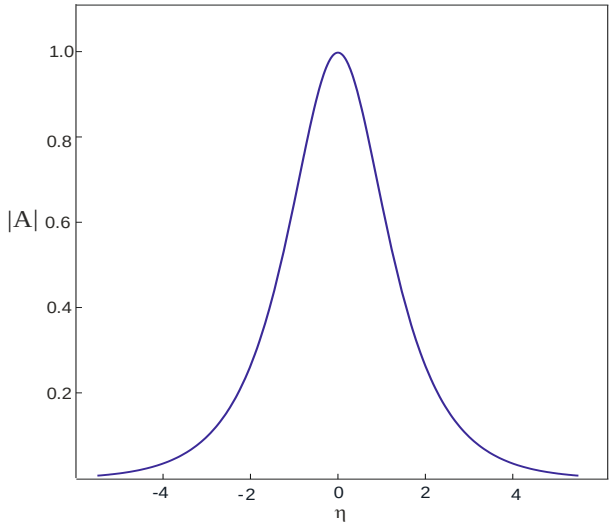


Fig. 4. Variation in the solution profile of the NLS equation by variable η (at $\mu = 10^{-18}$)

The variation of wave frequency with the nonlocal parameter μ for various values of the wave number is given in Fig. 5. From the mentioned figure, it can be observed that a decrease in frequencies occurs with an increase in the nonlocal parameter. The frequency curves get closer to each other with an increase in nonlocal parameters.

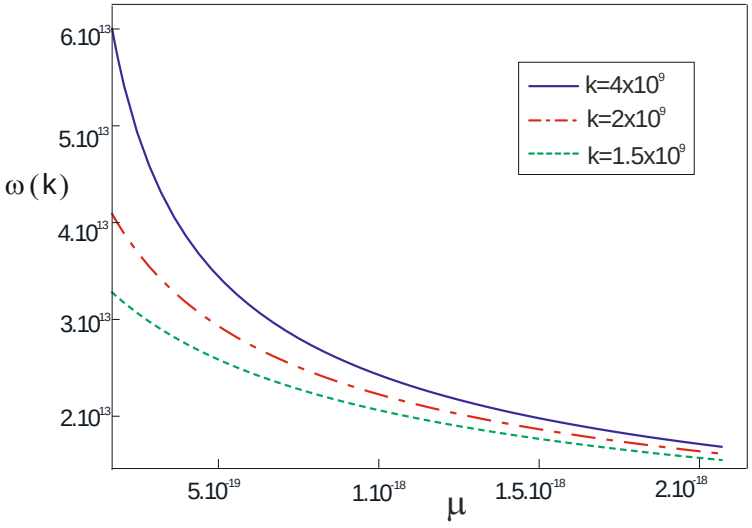


Fig. 5. Variation of wave frequency with the nonlocal parameter values for various values of the wave numbers

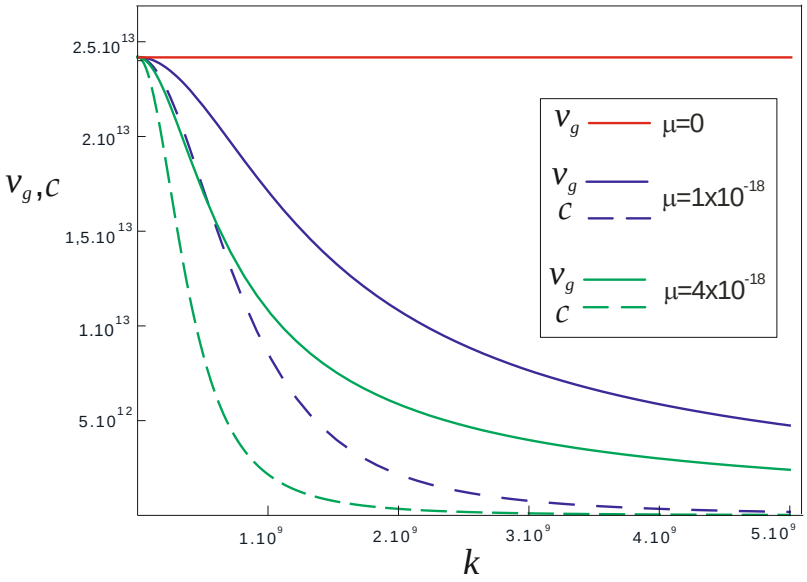


Fig. 6. Variation of phase and group velocities by the wave numbers for different nonlocal parameter values.

The impact of the nonlocal parameter on the velocities of nanotubes is plotted in Fig.6. From this figure, it can be observed that group and phase velocities decrease with increasing nonlocal parameters and wave numbers. For μ=0, the group velocity is equal to phase velocity, which shows the non-dispersive situation.

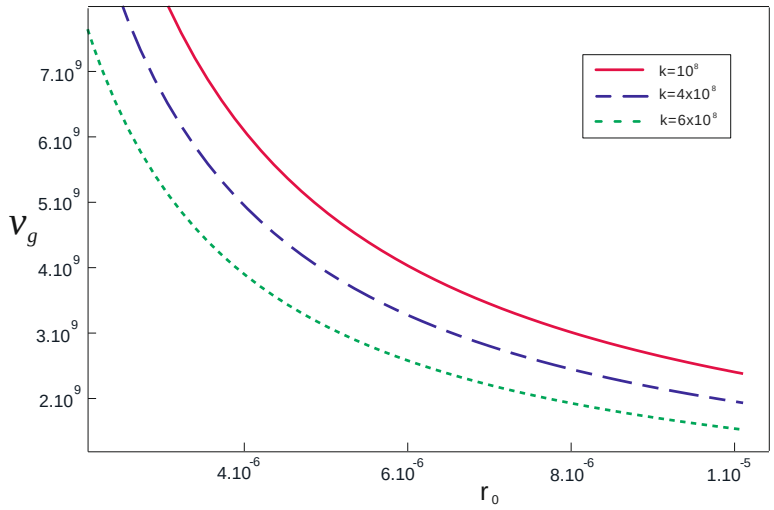


Fig. 7. Variation of group velocity with the radius for some different values of wave numbers.

The variation of group velocity with the radius for some different values of the wave number is presented in Fig.7. As is seen from the figure in question, with the increasing values of the radius, it is observed that group velocities decrease rapidly for different wave numbers.

## 5. Conclusions

In the present study, the self-modulation of weakly nonlinear and strongly dispersive waves in nanorods was examined, and the nonlinear Schrödinger (NLS) equation was obtained as an evolution equation of a slowly changing amplitude of the carrier wave. Solutions for the NLS equation for nonlinear plane waves, envelope solitary waves, and phase jump solutions are also provided. In addition to these, in the present study, due to nonlocality, the elastic medium has a dispersive character. The nonlocal parameter μ represents the dispersive character of the medium. If $\mu = 0$, this leads to the nonlinear motion of classical elasticity. In the wave propagation analysis, together a linear and local situation represents a non-dispersive character. A linear and non-local situation represents a dispersive character. Besides, the nonlinear and local situation represents a non-dispersive character. However, in case of a non-linear and nonlocal situation, nonlinearity and dispersion balance with each other and a solitary wave profile arise.

In numerical calculations, it is shown that the plane wave solution of the NLS equation is modulationally unstable in case of $\nu_1\nu_2 > 0$ for all values of the wave number for all nonlocal parameter values. This situation corresponds to the envelope solitary wave solution. For $\mu = 0$, there is no solitary wave profile because of a non-dispersion. Wave frequency curves and group velocity curves are plotted with the wave number, and it is shown that nonlocal frequency and velocity curves are approximately the same with the literature [24,43]. To see the small-scale effect of nanorods, the variation of wave frequencies was examined, and group velocities changed with the radius of a nanorod. It is shown that frequencies and group velocities are decreasing with the increasing nanorod radius. It is observed that the nonlocal parameter has an obvious effect on wave frequencies and velocities. It is expected that the nonlinear modulation introduced herein will be useful for studies on the nanostructure.

## References

[1] Eringen, A. C., Suhubi, E. S., Nonlinear theory of simple micro-elastic solids-I, *International Journal of Engineering Science,* 2, 189-203, 1964.

[2] Eringen, A. C., Simple microfluids, *International Journal of Engineering Science,* 2, 205-217, 1964.

[3] Eringen, A. C., Theory of micropolar elastisity in Fracture (Edited by H. Liebowitz), Vol. II Academic Press, New York, 1968.

[4] Kafadar, C. B., Eringen A. C., Micropolar Media-I. The classical theory, *International Journal of Engineering Science,* 9, 271-305, 1971.

[5] Eringen, A. C., Nonlocal polar elastic continua, *International Journal of Engineering Science,* 10, 1-16, 1972.

[6] Demiray, H., A nonlocal continuum theory for diatomic elastic solids, *Int. J. Eng. Sci.,* 15, 623-644, 1977

[7] Eringen, A. C., On differential equations of nonlocal elasticity and solutions of screw dislocation and surface waves, *Journal of Applied Physics,* 54, 4703-4710,1983.

[8] Toupin, R. A., Elastic materials with coupled stresses, *Archive for Rational Mechanics and Analysis*, 11, 385, 1962.

[9] Park, S. K., Gao, X. L., Bernoulli-Euler beam model based on a modified coupled stress theory, *Journal of Micromechanics and Microengineering*, 16 (11),23055-2359, 2006.

[10] Ma, H. M., Gao, X. L., Reddy J. N., A microstructure-dependent Timoshenko beam model based on a modified couple stress theory, *Journal of the Mechanics and Physics of Solids*, 56(12), *3379-3391*, 2008.

[11] Murmu, T., Pradhan, S. C., Small-scale effect on the vibration on the nonuniform nanocantiliver based on nonlocal elasticity theory, *Physica E*, 41, 1451-1456, 2009.

[12] Senthilkumar, V., Pradhan, S. C., Pratap, G., Small-scale effect on buckling analysis of carbon nanotube with Timoshenko theory by using differential transform method, *Adv. Sci. Lett.*, 3, 1-7, 2010.

[13] Rahmani, O., Pedram, O., Analysis and modelling the size effect on vibration of functionally graded nanobeams based on nonlocal Timoshenko beam theory, *International Journal of Engineering Science*, 77, 55-70, 2014.

[14] Eringen, A. C., Linear theory of nonlocal elasticity and dispersion of plane waves, *International Journal of Engineering Science*,10, 1-16, 1972.

[15] Eringen, A. C., Edelen, D. G. B., On nonlocal elasticity, *International Journal of Engineering Science*, 10, 233-248, 1972.

[16] Thai, H. T., A nonlocal beam theory for bending, buckling and vibration of nanobeams, *International Journal of Engineering Science*, 52, 56-64, 2012.

[17] Aydogdu, M., Axial vibration of the nanorods with the nonlocal continuum rod model, *Physica E: Low-dimensional Systems and Nanostructures*, 41(5), 861-864, 2009.

[18] Aydogdu, M., Axial vibration analysis of nanorods (carbon nanotubes) embedded in an elastic medium using nonlocal theory, *Mechanics Research Communications*, 43, 34-40, 2012.

[19] Lim, C. W. and Yang, Y., Wave propagation in carbon nanotubes: nonlocal elasticity-induced stiffness and velocity enhancement effects, *J. Mech. Mater. Struct.*, 5, 459-476, 2010.

[20] Hu, Y. G., Liew, K. M., Wang, Q., He, X. Q., Yakobson, B. I., Nonlocal shell model for elastic wave propagation single- and double-walled carbon nanotubes, *J. Mech. Phys. Solids*, 56: 3475-3485, 2008.

[21] Wang, Q., Varadan, V. K., Wave characteristics of carbon nanotubes, *Int. J. Solids Struct*., 43, 254-265, 2006.

[22] Narendar, S., Gopalakrishnan, S., Temperature effects on wave propagation in nanoplates, *Compos. Part B*, 43, 1275-1281, 2012.

[23] Narendar, S., Gopalakrishnan, S., Nonlocal scale effects on wave propagation in multi-walled carbon nanotubes, *Comput. Mater. Sci.,* 47, 526-538, 2009.

[24] Aydogdu, M., Longitudinal wave propagation in nanorods using a general nonlocal unimodal rod theory and calibration of nonlocal parameter with lattice dynamics, *Int. J. Eng. Sci.,* 56, 17-28 ,2012.

[25] Aydogdu, M., Longitudinal wave propagation in multiwalled carbon nanotubes, *Composite Structures,* 107: 578-584, 2014.

[26] Wu, X. F., Dzenis, Y. A. ,Wave propagation in nanofibers, *J. App. Phys.,* 100, 124318, 2006.

[27] Challamel, N., Rakotomanana, L., Marrec, L. L., A dispersive wave equation using nonlocal elasticity, *Comptes Rendus Mecanique,* 337, 591-595, 2009.

[28] Narendar, S., Gopalakrishnan, S., Nonlocal scale effects on wave propagation in multi-walled carbon nanotubes, *Comput. Mater. Sci.,* 47, 526-538, 2009.

[29] Narendar, S., Terahertz wave propagation in uniform nanorods: a nonlocal continuum mechanics formulation including the effect of lateral inertia, *Physica E: Low-dimensional Syst. Nanostruct.,* 43, 1015-1020, 2011.

[30] Erbay, S., Erbay, H. A., Dost, S., Nonlinear wave modulation in micropolar elastic media-I. Longitudional waves, *International Journal of Engineering Science,* 29 (7), 845-858, 1991.

[31] Erbay, H. A., Erbay, S., Nonlinear wave modulation in fluid filled distensible tubes, *Acta Mechanica,* 104, 201-214, 1994.

[32] Akgun, G., Demiray, H., Nonlinear wave modulation in a pre-stressed viscoelastic thin tube filled with an inviscid fluid, *Int. J. Non-linear Mech.,* 34, 571-588, 1999.

[33] Akgun, G., Demiray, H., Modulation of non-linear axial and transverse waves in a fluid-filled thin elastic tube, *Int. J. Non-linear Mech.,* 35, 597-611, 2000.

[34] Erbay, H. A., Erbay, S., Erkip, A., Unidirectional wave motion in nonlocally and nonlinearly elastic medium: the KdV, BBM and CH equations, *Nonlinear Waves,* 64, 256-264, 2015.

[35] Duruk, N., Erbay, H. A., Erkip, A., Blow-up and global existence for a general class of nonlocal nonlinear coupled wave equations, *J. Differ. Equations,* 250, 1448-1459, 2011.

[36] Malvern, L. E., Introduction to the Mechanics of a Continuum Medium, *Prentice Hall,* Englwood Cliffs, New Jersey, 1969.

[37] Mousavi, S. M., Fariborz, S. J., Free vibration of a rod undergoing finite strain, *J. of Physics Conferans Series,* 382(1), 2012.

[38] Fernandes, R., El-Borgi, S., Mousavi, S. M., Reddy, J.N., Mechmoum, A., Nonlinear size-dependent longitudinal vibration of carbon nanotubes embedded in an elastic medium, *Phisica E,* 88, 18-25, 2017.

[39] Jeffrey, A., Kawahara, T., *Asymptotic Methods in Nonlinear Wave Theory*, Pitman, Boston, 1982.

[40] Lamb Jr., G. L., Mc Laughlin, D. W., in: Bullough, R. K., Coudrey, P. J. (Eds), *Aspect of Soliton Physics:in Solitons*, Springer, Berlin, 1980.

[41] Tu, Z-C., Single walled and multiwalled carbon nanotubes viewed as elastic tubes with the effective Young's moduli dependent on layer number, *Physics Rev. B*, 65, 233-237, 2002

[42] Taha, T. R., Ablowitz, M. J., Analytical and numerical aspects of certain nonlinear evolution equations. II Numerical nonlinear Schrödinger equation, *J. Comput. Phys*., 55, 203-230, 1984

[43] Wang, H., Dong, K., Men, F., Yan, Y. J., Wang, X., Influences of longitudinal magnetic field on wave propagation in carbon nanotubes embedded in elastic matrix, *Appl. Math. Model.*, 34, 878-889, 2010.

*International Journal of Engineering & Applied Sciences (IJEAS)*
*Vol.10, Issue 3 (2018) 159-175*
*http://dx.doi.org/10.24107/ijeas.457535*
Int J Eng Appl Sci 10(3) (2018) 159-175

# Some closed-form solutions for buckling of straight beams with varying cross-section by Variational Iteration Method with Generalized Lagrange Multipliers

*Ugurcan Eroglu* [a], *Ekrem Tufekci* [b*]

[a,b] *Istanbul Technical University, Faculty of Mechanical Engineering*

[*]*E-mail address*: ueroglu@itu.edu.tr [a], tufekcie@itu.edu.tr [b*]

*Received date: 05.09.2018*
*Accepted date: 02.10.2018*

*ORCID numbers of authors*
0000-0002-2446-0947[a], 0000-0003-3991-4005[b]

**Abstract**

*This study aims to derive approximate closed-form solutions for critical loads of straight beams with variable cross-section. The governing equations are derived for purely flexible beam for small displacements and rotation and turned into non-dimensional form. Approximate solutions to the set of equations for stability problems are searched by Variational Iteration Method with Generalized Lagrange Multipliers. It turns out that highly accurate approximate buckling loads for cantilever beams with constant or variable section can be obtained in closed-form. Many novel closed-form solutions for critical load of such structures, which may serve as benchmark solutions, are presented.*

**Keywords:** beam theory, closed-form solutions, variational iteration method, buckling.

## 1. Introduction

Closed-form solutions are of practical importance to engineers and designers as they help to better understand the contributions of different physical parameters involved in a problem to the output, which may be static deflection, state of stress at a point, natural frequency, etc. This is important as it paves the way to essential elements of modern engineering, such as of optimum design and monitoring of structures. In addition, closed-form solutions may serve as benchmark solutions to numerical methods which are frequently used in modern time. Unfortunately, it is possible to obtain exact solutions in closed-form only for very special cases.

Not surprisingly, majority of closed-form solutions are presented in the literature for one dimensional structures [1], which is a reduced representation of 3-dimensional continua under reasonable assumptions and simplifications [2, 3]. There are, of course, almost countless contributions on the field of mechanics of beam-like structures since the middle of 18$^{th}$ century, but reviewing the entire bibliography would be out of the scope of this study. Rather, dedicated readers are kindly referred to the monographs by Love [3] and Timoshenko [4], to have a better insight about especially early works on this subject, which eventually formed the basis of structural engineering.

Earliest investigation on the buckling of columns is due to Euler [5,6]. Without being exhaustive, one may quote Engesser [7], Dinnik [8], and Duncan [9] as other early contributors in the field. Moving on to the more recent investigations, one may quote contributions by Elishakoff and his co-workers [1, 10-14] concerning semi-inverse solutions for buckling of straight beams with continuously varying bending rigidity. These solutions make sense considering the introduction of functionally graded materials [15], and advances in their manufacturing [16]. Indeed, variation of bending rigidity along the beam axis may be due to smooth variation of cross-section, functional grading of the material, or both. Nevertheless, solution of a direct problem in closed-form, *i.e.* determination of critical load for a known material property and geometry, is still a challenging one. Yet, there are valuable contributions in the modern literature, such as the ones by Ruta *et al.* [17, 18], based on a one-dimensional model for thin-walled beams [19], which provides exact solution to critical loads in closed-form, by Gupta *et al.* [20] for post-buckling behavior of laminated beams, Mercan and Civalek [21] for critical load of nanobeams, and Abbondanza *et al.* [22] for vibration frequencies and buckling loads of nanobeams. In addition, there are numerous studies which focus on numerical solutions of such problems, which ensures required accuracy for engineering applications when tackled the numerical problems, such as locking, but lack generality as they require the numerical values of the parameters of the problem. Instead, an approximate solution is aimed here. For this purpose, Variational Iteration Method (VIM), which has been shown to be a very simple and effective semi-analytical technique, is utilized. This method is developed by He [23-25], basically for solutions of non-linear problems. Reviews and more detailed explanations about the method can be seen in [26,27]. Since the initiation of the method, there have been many modifications and improvements introduced to it [28-32], for the reviews of which we refer to the note by He [33]. VIM is recently used for solutions of many different structural problems, see for example [34-38].

In this contribution, the aim is to present some approximate, yet accurate, solutions for buckling loads of straight beams of variable section. For this purpose, the system of equations is briefly derived and turned into non-dimensional form. As the solution technique, Variational Iteration Method with Generalized Lagrange Multiplier, which has been shown recently to be a very neat procedure for linear differential equation systems, is used. Amongst the classical boundary conditions, we focus on cantilevered beams as it is the only case that one can obtain real roots of the characteristic equation in closed-form. This may seem limiting, however, cantilevered beams of variable section may be an accurate model for many practical engineering problems. Moreover, being in closed-form, presented results may be used for benchmark purposes for different approximate and numerical techniques. To this aim, considering different variations of the cross-section, some new closed-form solutions for cantilevered beams are presented.

## 2. Governing Equations

Consider copies of a plane region, $\Re \subset \mathbb{R}^2$, attached orthogonally to a line of length $L$, $C_0$, through their centroids. The region occupied by this construction represents the reference configuration of the beam, $B^0$, for parameterization of which a Cartesian coordinate system, $\{x, y, z\}$, with base vectors $\{\mathbf{i}, \mathbf{j}, \mathbf{k}\}$ is introduced. With proper selection of an origin, it is assumed that $C_0$ is along $\mathbf{k}$, and, therefore, $\Re$ lies on coordinate plane $\{\mathbf{i}, \mathbf{j}\}$, which yields

$B^0 = \Re \times [0, L]$. Furthermore, principal axes of $\Re$ is assumed to be coincident with axes *x* and *y*, for simplicity in constitutive modelling.

Current configuration of the beam, *B*, is described by regular vector field $\mathbf{r}(z)(=\mathbf{k}+\mathbf{u}(z))$ which represents the positions of each point, *C*, initially on $C_0$ and with coordinate *z*, and an orthogonal tensor $\mathbf{R}(z)$, providing the rotation of cross-sections, assumed to remain planar.

The expressions of finite deformation measures in current configuration [17,18],

$$\boldsymbol{\varepsilon}(z) = \frac{d}{dz}\left(z\mathbf{k} + \mathbf{u}(z)\right) - \mathbf{R}(z)\mathbf{k}, \quad \boldsymbol{\chi}(z) = \frac{d\mathbf{R}(z)}{dz}\mathbf{R}^T(z), \tag{1}$$

where $\boldsymbol{\varepsilon}(z)$ is the difference between the tangents of *C* and $C_0$, pushed-forward from $B^0$ to *B*, and $\boldsymbol{\chi}(z)$ presents the curvature of *C*.

The balance equations in actual configuration reads [2, 18],

$$\frac{d\mathbf{F}(z)}{dz} + \mathbf{p}(z) = 0, \quad \frac{d\mathbf{M}(z)}{dz} + \frac{d}{dz}\left(z\mathbf{k} + \mathbf{u}(z)\right) \times \mathbf{F}(z) + \mathbf{m}(z) = 0 \tag{2}$$

where $\mathbf{F}(z), \mathbf{M}(z), \mathbf{p}(z)$ and $\mathbf{m}(z)$ stand for internal force, internal couple, distributed external force and distributed external couple, respectively.

The analysis herein is limited such that the curve *C* remains at $\{\mathbf{j}, \mathbf{k}\}$ plane. Then,

$$\begin{gathered}
\mathbf{u} = u_y \mathbf{j} + u_z \mathbf{k}, \\
\mathbf{R} = \begin{pmatrix} 1 & 0 & 0 \\ 0 & \cos\Omega_x & -\sin\Omega_x \\ 0 & \sin\Omega_x & \cos\Omega_x \end{pmatrix}, \\
\boldsymbol{\varepsilon} = \gamma_y \mathbf{j} + \varepsilon_z \mathbf{k}, \\
\boldsymbol{\chi} = \chi_x \mathbf{j} \wedge \mathbf{k}, \\
\mathbf{F} = F_y \mathbf{j} + F_z \mathbf{k} \\
\mathbf{M} = M_x \mathbf{i},
\end{gathered} \tag{3}$$

where the dependence of each field on *z* is omitted for simplicity of the notation.

Let us assume vanishing of the axial strain and shear strain, and a linear relation between the curvature of the deformed beam axis and the bending couple in the form,

$$\varepsilon_z(z)=0,\quad \gamma_y(z)=0,\quad \chi_x(z)=\frac{M_x(z)}{EI_x(z)} \tag{4}$$

where $E$ is the modulus of elasticity of the material and $I_x$ is the moment of inertia of the cross-sections about the axis $x$. The bending rigidity $EI_x(z)\left(=EI_{x0}f(z)\right)$ is assumed to depend on the position along the axis, $z$, which may be due to variation of material properties, or smooth variation of cross-sectional dimensions, or both.

Let us further assume that $B^0$ is pre-loaded by what results an axial compressive force $N(z)$, which is assumed to be known and may be due to self-weight or an external action.

The system of differential equation for determination of configuration $B$ which is assumed to be in the neighborhood of $B^0$, thus linearized, by static perturbation technique [17, 18, 39], reads,

$$\begin{aligned}&\frac{d\bar{u}_z}{dz}+\bar{\Omega}_x=0,\ \frac{d\bar{\Omega}_x}{dz}=\frac{\bar{M}_x}{EI_x}\\&\frac{d\bar{F}_y}{dz}=0,\quad \frac{d\bar{M}_x}{dz}=\bar{F}_y-\bar{\Omega}_x N\ ,\end{aligned} \tag{5}$$

where, superimposed bar denotes the first order derivative of indicated field with respect to an evolution parameter, hence the first order increments to the fields given in (3) [17, 18, 39].

Equation system (5) is identical to that given in [40]. With the following non-dimensional quantities,

$$\begin{aligned}&Z=\frac{z}{L},\quad T=\frac{\bar{F}_y L^2}{EI_{x0}},\quad P=\frac{NL^2}{EI_{x0}}\\&M=\frac{\bar{M}_x L}{EI_{x0}},\quad U=\frac{\bar{u}_z}{L},\quad \theta=\bar{\Omega}_x,\end{aligned} \tag{6}$$

System of equations given in (6) may be represented in matrix form as below.

$$\frac{d\mathbf{y}}{dZ}=\mathbf{A}(Z)\mathbf{y},\qquad \mathbf{y}=\{U\quad \theta\quad T\quad M\}^{\mathrm{T}}$$
$$\mathbf{A}(Z)=\begin{pmatrix}0 & -1 & 0 & 0\\ 0 & 0 & 0 & \dfrac{1}{f(Z)}\\ 0 & 0 & 0 & 0\\ 0 & -P & 1 & 0\end{pmatrix}. \tag{7}$$

with solution,

$$\mathbf{y}=\mathbf{Y}(Z,Z_0)\mathbf{y}(Z_0) \tag{8}$$

where $\mathbf{Y}(Z,Z_0)$ is the matricant of system $(7)_1$ about an initial point $Z_0$, and $\mathbf{y}(Z_0)$ lists the initial values of field functions [41]. Note that when the coefficients matrix **A** consists of constant components, matricant of Eq. $(7)_1$ is given by matrix exponential of $z\mathbf{A}$, which may be obtained exactly by Cayley-Hamilton theorem [42], or approximately by power series expansion**.** If the matrix **A** can be reduced into a triangular form, then again an exact solution may be found to Eq.(7) by successive integrations of the equations [43], similar to solution of an algebraic equation system by Gauss elimination method. Neither of these conditions hold in our case. Even in such situations, it might be possible to find an exact solution to the system of equations which requires a commutativity between **A** and matrix exponential of its integral. This is a very restrictive condition in practical point of view hence, search for approximate solution to Eq. (7) becomes inevitable.

## 3. Variational Iteration Method

A kind of VIM with a suitably modified Lagrange Multipliers for system of differential equations proposed by Altintan and Ugur [32] will be followed here. Even if the essence of the method is to tackle the nonlinear problems, here we will apply restricted variation to the part of matrix **A** which makes an exact solution to Eq.(7) impossible.

$$\mathbf{y}_{k+1}(Z)=\mathbf{y}_k(Z)+\int_{Z_0}^{Z}\mathbf{\Lambda}(\zeta;Z)\left(\frac{d\mathbf{y}_k(\zeta)}{d\zeta}-L_1\mathbf{y}_k(\zeta)-L_2\tilde{\mathbf{y}}_k(\zeta)\right)d\zeta \tag{9}$$

where subscript $k$ denotes the order of approximation, and superimposed tilde denotes the variation of the indicated field is restricted. $L_1$ and $L_2$ are linear operators defined as below.

$$L_1\mathbf{y}=\mathbf{A}_1\mathbf{y},\quad L_2\mathbf{y}=\mathbf{A}_2\mathbf{y}, \tag{10}$$

where,

$$\mathbf{A}_1 = \begin{pmatrix} 0 & -1 & 0 & 0 \\ 0 & 0 & 0 & \dfrac{1}{f(Z)} \\ 0 & 0 & 0 & 0 \\ 0 & 0 & 1 & 0 \end{pmatrix}, \ \mathbf{A}_2 = \begin{pmatrix} 0 & 0 & 0 & 0 \\ 0 & 0 & 0 & 0 \\ 0 & 0 & 0 & 0 \\ 0 & -P & 0 & 0 \end{pmatrix}. \tag{11}$$

With those definitions at hand, the so-called Generalized Lagrange Multiplier in Eq. (9), $\mathbf{\Lambda}(\zeta;Z)$ becomes [32],

$$\mathbf{\Lambda}(\zeta;Z) = -\mathbf{\Psi}(\zeta,Z) \tag{12}$$

Where $\mathbf{\Psi}(\zeta,Z)$ is the matricant of system $d\mathbf{y}/d\zeta = \mathbf{A}_1\mathbf{y}$, about *Z*. Properties of matricant yields [32, 42],

$$\mathbf{\Lambda}(\zeta;Z) = \mathbf{\Psi}(Z,Z_0)\mathbf{\Psi}^{-1}(\zeta,Z_0). \tag{13}$$

A recent contribution by Yildirim [44] provides the components of matricant, also known as *fundamental matrix* or *transfer matrix*, for constant cross-section.

If $(k+1)^{\text{th}}$ approximation of **y** is written similar to Eq. (8),

$$\mathbf{y}_{k+1}(Z) = \mathbf{Y}_{k+1}(Z,Z_0)\mathbf{y}(Z_0), \tag{14}$$

where, with the help of Eqs. (7, 12, 13),

$$\mathbf{Y}_{k+1}(Z,Z_0) = \mathbf{Y}_k(Z,Z_0) + \mathbf{\Psi}(Z,Z_0)\int_{Z_0}^{Z}\mathbf{\Psi}^{-1}(\zeta,\zeta_0)\left[\frac{d\mathbf{Y}_k(\zeta,Z_0)}{d\zeta} - \mathbf{A}(\zeta)\right]d\zeta. \tag{15}$$

Once an initial approximation to the matricant, $\mathbf{Y}_0(Z,Z_0)$, is made, successive iterations provided in Eq. (15) will yield the approximate matricant of the system $(7)_1$. Then, it is a matter of solving the initial values $\mathbf{y}(Z_0)$, or looking for mathematical requirements for a non-trivial solution of them. In our case the latter holds true. These conditions for classical boundary conditions are listed below.

$$\begin{aligned}
&\textit{Clamped}-\textit{free} && U(0)=0,\ \theta(0)=0, && \begin{vmatrix} Y_{33,k} & Y_{34,k} \\ Y_{43,k} & Y_{44,k} \end{vmatrix}=0 \\
& && T(1)=0,\ M(1)=0. && \\
&\textit{Pinned}-\textit{pinned} && U(0)=0,\ M(0)=0, && \begin{vmatrix} Y_{12,k} & Y_{13,k} \\ Y_{42,k} & Y_{43,k} \end{vmatrix}=0 \\
& && U(1)=0,\ M(1)=0. && \\
&\textit{Clamped}-\textit{clamped} && U(0)=0,\ \theta(0)=0, && \begin{vmatrix} Y_{13,k} & Y_{14,k} \\ Y_{23,k} & Y_{24,k} \end{vmatrix}=0 \\
& && U(1)=0,\ \theta(1)=0. && 
\end{aligned} \tag{16}$$

where $Y_{ij,k}$ denote the components of $k^{\text{th}}$ order of approximation to matricant at $i^{\text{th}}$ row and $j^{\text{th}}$ column. It turns out it is possible to find closed form solutions only for clamped-free column as that is the only case yielding a characteristic equation of third order with real roots.

In the next section, we will search for closed form expressions exploiting Eq. (15) for different variations of cross-section.

## 4. Closed-Form Solutions

As the initial approximation of the matricant, we will use the solution of $(7)_1$ for $\mathbf{A}_2 = 0$, that is, the elastic curve in the absence of pre-loads:

$$\mathbf{Y}_0(Z, Z_0) = \mathbf{\Psi}(Z, Z_0). \tag{17}$$

A suitable selection of the initial point is $Z_0 = 0$, for the simplicity of solutions. The explicit expressions of matricant components at each iteration are provided for specific variations of cross-section and pre-load in the following sub-sections.

### 4.1 Polynomial Bending Rigidity

Here we present some solutions bending rigidity given by a polynomial function specified as below.

$$f(Z) \equiv (1-\alpha_1 Z)(1-\alpha_2 Z)^3 \tag{18}$$

This variation of the bending rigidity may be interpreted as that of a rectangular cross-section with linearly varying height and width, and has been considered recently in [45].

For such a variation of bending rigidity, components of the *zeroth* order of approximation to matricant are listed below.

$$Y_{11,0}=1,\ Y_{12,0}=-Z,$$

$$Y_{13,0}=-\frac{Z(\alpha_1\text{-}\alpha_2)(Z(\alpha_1+\alpha_2)\text{-}2)\text{-}2(\alpha_1 Z\text{-}1)(\alpha_2 Z\text{-}1)\ln(1\text{-}\alpha_1 Z)+2(\alpha_1 Z\text{-}1)(\alpha_2 Z\text{-}1)\ln(1\text{-}\alpha_2 Z)}{2(\alpha_1\text{-}\alpha_2)^3(\alpha_2 Z\text{-}1)},$$

$$Y_{14,0}=-\frac{Z(\alpha_1\text{-}\alpha_2)\left(\alpha_1(3\alpha_2 Z\text{-}2)\text{-}\alpha_2^2 Z\right)-2\alpha_1(\alpha_1 Z\text{-}1)(\alpha_2 Z\text{-}1)\ln(1\text{-}\alpha_1 Z)+2\alpha_1(\alpha_1 Z\text{-}1)(\alpha_2 Z\text{-}1)\ln(1\text{-}\alpha_2 Z)}{2(\alpha_1\text{-}\alpha_2)^3(\alpha_2 Z\text{-}1)},$$

$$Y_{21,0}=0,\ Y_{22,0}=0,$$

(19)

$$Y_{23,0}=\frac{Z(\alpha_1\text{-}\alpha_2)\left(-2\alpha_1+\alpha_1\alpha_2 Z+\alpha_2^2 Z\right)-2\alpha_1(\alpha_2 Z\text{-}1)^2\ln(1\text{-}\alpha_1 Z)+2\alpha_1(\alpha_2 Z\text{-}1)^2\ln(1\text{-}\alpha_2 Z)}{2(\alpha_1\text{-}\alpha_2)^3(\alpha_2 Z\text{-}1)^2},$$

$$Y_{24,0}=\frac{-2\alpha_1^2(\alpha_2 Z\text{-}1)^2\ln(1\text{-}\alpha_1 Z)+2\alpha_1^2(\alpha_2 Z\text{-}1)^2\ln(1\text{-}\alpha_2 Z)+\alpha_2 Z(\alpha_1\text{-}\alpha_2)(\alpha_1(3\alpha_2 Z\text{-}4)+\alpha_2(2\text{-}\alpha_2 Z))}{2(\alpha_1\text{-}\alpha_2)^3(\alpha_2 Z\text{-}1)^2},$$

$$Y_{31,0}=0,\ Y_{32,0}=0,\ Y_{33,0}=1,\ Y_{34,0}=0$$

$$Y_{41,0}=0,\ Y_{42,0}=0,\ Y_{43,0}=Z,\ Y_{44,0}=1$$

We list below the characteristic equations of different orders of approximations for clamped-free column with polynomial bending rigidity.

$$k=1:\quad 2(\alpha_2\text{-}1)(\alpha_1\text{-}\alpha_2)^3+P\left((\alpha_1\text{-}\alpha_2)\left(\alpha_1(2\text{-}3\alpha_2)+\alpha_2^2\right)+2(\alpha_1\text{-}1)\alpha_1(\alpha_2\text{-}1)(\ln(1\text{-}\alpha_1)\text{-}\ln(1\text{-}\alpha_2))\right)=0$$

(20)

$$\begin{aligned}k=2:\quad & 12(\alpha_2\text{-}1)^2(\alpha_1\text{-}\alpha_2)^5+P\Big[12(\alpha_1\text{-}1)\alpha_1(\alpha_2\text{-}1)^2(\alpha_1\text{-}\alpha_2)^2(\ln(1\text{-}\alpha_1)\text{-}\ln(1\text{-}\alpha_2))\\ & \text{-}6(\alpha_2\text{-}1)(\alpha_1\text{-}\alpha_2)^3\left(\alpha_1(3\alpha_2\text{-}2)\text{-}\alpha_2^2\right)\Big]+P^2\Big[(\alpha_1\text{-}\alpha_2)\left(\alpha_1^2(16\alpha_2\text{-}15)\text{-}2\alpha_1(\alpha_2(\alpha_2+9)\text{-}9)\right.\\ & \left.+\alpha_2((9\text{-}2\alpha_2)\alpha_2\text{-}6)\right)-6(\alpha_1\text{-}1)(\alpha_2\text{-}1)\left(2\alpha_1\alpha_2+(\alpha_1\text{-}3)\alpha_1-\alpha_2^2+\alpha_2\right)(\ln(1-\alpha_1)\text{-}\ln(1\text{-}\alpha_2))\Big]=0\end{aligned}$$

(21)

$$k=3:\quad \begin{aligned}&144(\alpha_2\text{-}1)^3(\alpha_1\text{-}\alpha_2)^7+P\Big[144(\alpha_1\text{-}1)\alpha_1(\alpha_2\text{-}1)^3(\alpha_1\text{-}\alpha_2)^4(\ln(1\text{-}\alpha_1)\text{-}\log(1\text{-}\alpha_2))\\&\text{-}72(\alpha_2\text{-}1)^2(\alpha_1\text{-}\alpha_2)^5\left(\alpha_1(3\alpha_2\text{-}2)\text{-}\alpha_2^2\right)\Big]+P^2\Big[12(\alpha_2\text{-}1)(\alpha_1\text{-}\alpha_2)^3\left(\alpha_1^2(16\alpha_2\text{-}15)\right.\\&\text{-}2\alpha_1(\alpha_2(\alpha_2+9)\text{-}9)+\alpha_2((9\text{-}2\alpha_2)\alpha_2\text{-}6)\big)-72(\alpha_1\text{-}1)(\alpha_2\text{-}1)^2(\alpha_1\text{-}\alpha_2)^2\left(2\alpha_1\alpha_2+(\alpha_1\text{-}3)\alpha_1\right.\\&\left.\text{-}\alpha_2^2+\alpha_2\right)\left(\ln(1-\alpha_1)\text{-}\ln(1\text{-}\alpha_2)\right)\Big]+P^3\Big[(\alpha_2\text{-}\alpha_1)\left(\alpha_1^3(41\alpha_2\text{-}40)+\alpha_1^2(\alpha_2(65\alpha_2\text{-}224)+156)\right.\\&+\alpha_1(\alpha_2((28\text{-}43\alpha_2)\alpha_2+138)\text{-}120)+\alpha_2(\alpha_2((56\text{-}3\alpha_2)\alpha_2\text{-}114)+60))+12(\alpha_1\text{-}1)(\alpha_2\text{-}1)\left(\alpha_1^3\right.\\&\left.+\alpha_1^2(6\alpha_2\text{-}8)+\alpha_1(10\text{-}9\alpha_2)+\alpha_2((7\text{-}2\alpha_2)\alpha_2\text{-}5)\right)\left(\ln(1-\alpha_1)\text{-}\ln(1\text{-}\alpha_2)\right)\Big]=0\end{aligned} \tag{22}$$

Solutions of Eqs.(20-22) provide the critical buckling loads at $k^{\text{th}}$ order, $P_{cr,k}$ .

$$P_{cr,1}=-\frac{2(\alpha_2\text{-}1)(\alpha_1\text{-}\alpha_2)^3}{(\alpha_1\text{-}\alpha_2)\left(\alpha_1(2\text{-}3\alpha_2)+\alpha_2^2\right)+2(\alpha_1\text{-}1)\alpha_1(\alpha_2\text{-}1)\ln\left(\frac{\alpha_1\text{-}1}{\alpha_2\text{-}1}\right)} \tag{23}$$

$$\alpha_1=0\Rightarrow P_{cr,2}=\frac{(\alpha_2\text{-}1)\alpha_2^2\left(3\alpha_2^2\text{-}\sqrt{3\alpha_2(\alpha_2(\alpha_2(3\alpha_2+8)\text{-}36)+24)+72(\alpha_2\text{-}1)^2\ln(1\text{-}\alpha_2)}\right)}{\alpha_2(\alpha_2(2\alpha_2\text{-}9)+6)+6(\alpha_2\text{-}1)^2\ln(1\text{-}\alpha_2)} \tag{24}$$

$$\alpha_2=0\Rightarrow P_{cr,2}=\frac{2\alpha_1^2}{\sqrt{(\alpha_1\text{-}1)(6\alpha_1+\ln(1\text{-}\alpha_1)(\text{-}4\alpha_1+(\alpha_1\text{-}1)\ln(1\text{-}\alpha_1)+6))}+\alpha_1\text{-}(\alpha_1\text{-}1)\ln(1\text{-}\alpha_1)} \tag{25}$$

$$\begin{aligned}\alpha_1=0\Rightarrow P_{cr,3}=\frac{2}{c_1}\Bigg[&-\frac{2(\alpha_2\text{-}1)^2\alpha_2^4}{\sqrt[3]{c_2}}\left(12\alpha_2\left(2\alpha_2^2+3\alpha_2\text{-}12\right)(\alpha_2\text{-}1)^2\ln(1\text{-}\alpha_2)\text{-}72(\alpha_2\text{-}1)^4\ln^2(1\text{-}\alpha_2)\right.\\&\left.+\alpha_2^2\left(\alpha_2^4\text{-}96\alpha_2^3+132\alpha_2^2+36\alpha_2\text{-}72\right)\right)+\sqrt[3]{c_2}+2(\alpha_2\text{-}1)\alpha_2^2\left(\alpha_2\left(2\alpha_2^2\text{-}9\alpha_2+6\right)\right.\\&\left.+6(\alpha_2\text{-}1)^2\ln(1\text{-}\alpha_2)\right)\Bigg]\end{aligned} \tag{26}$$

$$\begin{aligned}\alpha_2=0\Rightarrow P_{cr,3}=\frac{1}{c_3}\Bigg[&-\frac{3\alpha_1^4}{\sqrt[3]{c_4}}\left(\left(\text{-}35\alpha_1^2+24\alpha_1+12\right)\alpha_1^2+8\left(\alpha_1^3\text{-}\alpha_1^2\text{-}3\alpha_1+3\right)\alpha_1\ln(1\text{-}\alpha_1)\right.\\&\left.\text{-}12(\alpha_1\text{-}1)^2(2\alpha_1\text{-}1)\ln^2(1\text{-}\alpha_1)\right)+\sqrt[3]{c_4}-3\alpha_1^2\left((6\text{-}5\alpha_1)\alpha_1\right.\\&\left.+2\left(\alpha_1^2\text{-}4\alpha_1+3\right)\ln(1\text{-}\alpha_1)\right)\Bigg]\end{aligned} \tag{27}$$

$$c_1=\alpha_2\left(3\alpha_2^3\text{-}56\alpha_2^2+114\alpha_2\text{-}60\right)+12(2\alpha_2\text{-}5)(\alpha_2\text{-}1)^2\ln(1\text{-}\alpha_2) \tag{28}$$

$$
\begin{aligned}
c_2 = {} & -36\alpha_2^7\left(17\alpha_2^5-156\alpha_2^4-498\alpha_2^3+3120\alpha_2^2-4284\alpha_2+1800\right)(\alpha_2-1)^5\ln(1-\alpha_2)+650484\alpha_2^{10} \\
& -432\alpha_2^6\left(2\alpha_2^3+15\alpha_2^2-72\alpha_2+75\right)(\alpha_2-1)^7\ln^2(1-\alpha_2)+32400\alpha_2^8-222048\alpha_2^9+1728\alpha_2^6(\alpha_2-1)^9\ln^3(1-\alpha_2) \\
& -1052676\alpha_2^{11}+1008324\alpha_2^{12}-557424\alpha_2^{13}+146079\alpha_2^{14}+4031\alpha_2^{15}-10815\alpha_2^{16}+1689\alpha_2^{17}-44\alpha_2^{18} \\
& +3\Big[\Big(-432\left(\alpha_2^4-4\alpha_2^3-18\alpha_2^2+84\alpha_2-75\right)(\alpha_2-1)^4\ln^2(1-\alpha_2)-3456(\alpha_2-1)^6\ln^3(1-\alpha_2) \\
& +72\alpha_2\left(4\alpha_2^6+15\alpha_2^5-186\alpha_2^4-117\alpha_2^3+1596\alpha_2^2-2214\alpha_2+900\right)(\alpha_2-1)^2\ln(1-\alpha_2) \\
& +\alpha_2^2\left(24\alpha_2^8-824\alpha_2^7-1719\alpha_2^6+14904\alpha_2^5+2628\alpha_2^4-100872\alpha_2^3+180036\alpha_2^2\right. \\
& \left.-126576\alpha_2+32400\right)\Big)(\alpha_2-1)^6\alpha_2^{12}\left(\alpha_2\left(3\alpha_2^3-56\alpha_2^2+114\alpha_2-60\right)+12(2\alpha_2-5)(\alpha_2-1)^2\ln(1-\alpha_2)\right)^2\Big]^{1/2}
\end{aligned}
\tag{29}
$$

$$
c_3 = \alpha_1\left(-10\alpha_1^2+39\alpha_1-30\right)+3\left(\alpha_1^3-9\alpha_1^2+18\alpha_1-10\right)\ln(1-\alpha_1) \tag{30}
$$

$$
\begin{aligned}
c_4 = {} & 3\Big[-375\alpha_1^{12}+5220\alpha_1^{11}-14778\alpha_1^{10}+15336\alpha_1^9-5400\alpha_1^8+36(\alpha_1-1)^3\left(\alpha_1^3-15\alpha_1^2\right. \\
& \left.+48\alpha_1-36\right)\alpha_1^6\ln^3(1-\alpha_1)-36(\alpha_1-1)^2\left(7\alpha_1^4-87\alpha_1^3+279\alpha_1^2-348\alpha_1+150\right)\alpha_1^6\ln^2(1-\alpha_1) \\
& +36\left(15\alpha_1^5-197\alpha_1^4+786\alpha_1^3-1342\alpha_1^2+1038\alpha_1-300\right)\alpha_1^7\ln(1-\alpha_1)+2\sqrt{3}\Big(\alpha_1^{12}\Big(\alpha_1\left(-10\alpha_1^2\right. \\
& \left.+39\alpha_1-30\right)+3\left(\alpha_1^3-9\alpha_1^2+18\alpha_1-10\right)\ln(1-\alpha_1)\Big)^2\Big(-8\left(11\alpha_1^3-141\alpha_1^2+294\alpha_1-162\right)(\alpha_1-1)^3\ln^3(1-\alpha_1) \\
& +\alpha_1^2\left(10\alpha_1^4-2964\alpha_1^3+8571\alpha_1^2-8316\alpha_1+2700\right)+12(\alpha_1-13)(\alpha_1-1)^5\ln^4(1-\alpha_1)+12\left(19\alpha_1^4-288\alpha_1^3\right. \\
& \left.+726\alpha_1^2-684\alpha_1+225\right)(\alpha_1-1)^2\ln^2(1-\alpha_1)-6\alpha_1\ln(1-\alpha_1)\left(43\alpha_1^5-848\alpha_1^4+3207\alpha_1^3-4940\alpha_1^2\right. \\
& \left.+3438\alpha_1-900\right)\Big)\Big)^{1/2}\Big]
\end{aligned}
\tag{31}
$$

Note that Eqs.(23-27) are the lowest roots of the characteristic equations for $1>\alpha_1,\alpha_2\geq 0$.

Table 1. Critical loads for variable height ($\alpha_1 = 0$)

| $\alpha_2$ | Present | | | [45] |
|---|---|---|---|---|
| | $P_{cr,1}$ | $P_{cr,2}$ | $P_{cr,3}$ | |
| 0 | 2 | 2.536 | 2.465 | 2.467 |
| 0.2 | 1.6 | 2.101 | 2.023 | 2.023 |
| 0.4 | 1.2 | 1.660 | 1.565 | 1.569 |
| 0.6 | 0.8 | 1.218 | 1.093 | 1.098 |
| 0.8 | 0.4 | - | 0.588 | 0.597 |

Numerical results are given for constant width, variable height and constant height, variable width, in Table 1 and Table 2, respectively, from which one may see their convergence and accuracy. Very simple first order approximations of the critical loads seem to be impractical, while third order solutions are very accurate. The simplicity versus the relatively low accuracy of second order approximations may be debated; but the effects of geometrical parameters on the critical load are well represented. On the other hand, solution of second

order approximation yields an imaginary root for $\alpha_1 = 0$, $\alpha_2 = 0.8$, which is possibly due to inability of the approximate displacement function to represent the actual mode shape.

Table 2. Critical loads for variable width ($\alpha_2 = 0$)

| $\alpha_1$ | Present | | | [45] |
|---|---|---|---|---|
| | $P_{cr,1}$ | $P_{cr,2}$ | $P_{cr,3}$ | |
| 0 | 2 | 2.536 | 2.465 | 2.467 |
| 0.2 | 1.862 | 2.387 | 2.314 | 2.316 |
| 0.4 | 1.711 | 2.227 | 2.148 | 2.151 |
| 0.6 | 1.542 | 2.052 | 1.964 | 1.968 |
| 0.8 | 1.339 | 1.855 | 1.747 | 1.752 |

In case of a square cross-section, i.e. $\alpha_1 = \alpha_2 = \alpha$,

$$P_{cr,1} = -\frac{6(-1+\alpha)^2}{-3+2\alpha} \tag{32}$$

$$P_{cr,2} = \frac{10\alpha(\alpha(2\alpha-7)+8)+2\sqrt{5}\sqrt{(\alpha-1)^4(4\alpha(5\alpha-9)+15)}-30}{4\alpha-5} \tag{33}$$

$$P_{cr,3} = \frac{2(-1+\alpha)^2(-128.076-35c_5^{1/3}+1.913c_5^{2/3}+146.372\alpha+28c_5^{1/3}\alpha-29.274\alpha^2)}{c_5^{1/3}(-7+6\alpha)} \tag{34}$$

$$\begin{aligned} c_5 = {} & (6360\alpha^2-1904\alpha^3+7(385+\sqrt{10}\sqrt{15435-54180\alpha+72600\alpha^2-43904\alpha^3+10080\alpha^4}) \\ & -6\alpha(1190+\sqrt{10}\sqrt{15435-54180\alpha+72600\alpha^2-43904\alpha^3+10080\alpha^4})) \end{aligned} \tag{35}$$

Table 3. Critical loads of column with square cross-section ($\alpha_1 = \alpha_2 = \alpha$)

| $\alpha$ | Present | | | [45] |
|---|---|---|---|---|
| | $P_{cr,1}$ | $P_{cr,2}$ | $P_{cr,3}$ | |
| 0 | 2 | 2.536 | 2.465 | 2.467 |
| 0.2 | 1.477 | 1.963 | 1.880 | 1.884 |
| 0.4 | 0.982 | 1.406 | 1.304 | 1.309 |
| 0.6 | 0.533 | 0.894 | 0.750 | 0.757 |
| 0.8 | 0.171 | - | 0.259 | 0.265 |

Critical loads of different orders of approximations for variable square section is presented in Table 3. The outlook is very similar to first two tables: first order solutions are not accurate while the third order solutions are in a very good agreement with the literature. Second order solution in case of a very sharp change in cross-section results an imaginary root, again possibly due to inadequate prediction of the mode shape. This situation may be seen as a

drawback but the use of classical beam theories for structures with rapid change of section can also be debated.

### 4.2 Exponential Bending Rigidity

Here the bending rigidity is assumed to vary exponentially, as it is common in the literature [34, 46].

$$f\left(Z\right)\equiv e^{-\alpha Z} \tag{36}$$

For such a variation of bending rigidity, components of the *zeroth* order of approximation to matricant are listed below.

$$\begin{gathered} Y_{11,0}=1,\;\; Y_{12,0}=-Z,\;\; Y_{13,0}=\frac{\alpha(-Z)+e^{\alpha Z}(2-\alpha Z)-2}{\alpha^3},\;\; Y_{14,0}=\frac{\alpha Z-e^{\alpha Z}+1}{\alpha^2} \\ Y_{22,0}=1,\;\; Y_{23,0}=\frac{e^{\alpha Z}(\alpha Z-1)+1}{\alpha^2},\;\; Y_{24,0}=\frac{e^{\alpha Z}-1}{\alpha} \\ Y_{33,0}=1,\;\; Y_{43,0}=Z,\;\; Y_{44,0}=1 \end{gathered} \tag{37}$$

We list below the characteristic equations of different orders of approximations for clamped-free column with exponential bending rigidity.

$$k=1:\quad \alpha^2+\left(\alpha-e^{\alpha}+1\right)P=0 \tag{38}$$

$$k=2:\quad \left(-4e^{\alpha}(\alpha-1)+e^{2\alpha}-2\alpha-5\right)P^2+4\left(\alpha-e^{\alpha}+1\right)\alpha^2P+4\alpha^4=0 \tag{39}$$

$$k=3:\quad \begin{gathered} \left(9e^{2\alpha}(\alpha-2)-e^{3\alpha}+3\alpha+9e^{\alpha}(2\alpha+1)+10\right)P^3 \\ -9\left(4e^{\alpha}(\alpha-1)-e^{2\alpha}+2\alpha+5\right)\alpha^2P^2+36\left(\alpha-e^{\alpha}+1\right)\alpha^4P+36\alpha^6=0 \end{gathered} \tag{40}$$

Solutions of Eqs.(38-40) provide the critical buckling loads at $k^{\text{th}}$ order, $P_{cr,k}$ .

$$P_{cr,1}=\frac{\alpha^2}{-1+e^{\alpha}-\alpha} \tag{41}$$

$$P_{cr,2}=-\frac{2\alpha^2}{(1-e^{\alpha}+\alpha)-\sqrt{(6+2e^{\alpha}(-3+\alpha)+\alpha(4+\alpha))}} \tag{42}$$

$$P_{cr,3}=\frac{\alpha^2}{c_6\sqrt[3]{c_7}}\Big[\sqrt[3]{3}c_7^{\,2/3}-3^{2/3}\left(-6e^{2\alpha}\left(2\alpha^2+21\right)+4e^{\alpha}\left(6\alpha^2+6\alpha+29\right)+e^{3\alpha}(44-16\alpha)\right.$$
$$\left.+e^{4\alpha}-8\alpha-35\right)-3\sqrt[3]{c_7}\left(-4e^{\alpha}(\alpha-1)+e^{2\alpha}-2\alpha-5\right)\Big] \tag{43}$$

where,

$$c_6=\left(9e^{2\alpha}(\alpha-2)-e^{3\alpha}+3\alpha+9e^{\alpha}(2\alpha+1)+10\right) \tag{44}$$

$$c_7=-3\left(12\alpha^3+84\alpha^2+3e^{4\alpha}\left(4\alpha^2-68\alpha+165\right)+4e^{3\alpha}\left(6\alpha^3+69\alpha^2-396\alpha+77\right)\right.$$
$$+6e^{\alpha}\left(24\alpha^3+118\alpha^2+214\alpha+165\right)+3e^{2\alpha}\left(84\alpha^3+240\alpha^2+104\alpha-633\right)+180\alpha$$
$$\left.-e^{6\alpha}+6e^{5\alpha}(2\alpha-3)+125\right)-2\sqrt{3}\left(9e^{2\alpha}(\alpha-2)-e^{3\alpha}+3\alpha+9e^{\alpha}(2\alpha+1)+10\right)\left(-12e^{5\alpha}(\alpha-2)\right.$$
$$-6e^{4\alpha}\left(4\alpha^2-25\alpha+52\right)-8e^{3\alpha}\left(2\alpha^3-30\alpha^2+201\alpha-434\right)+3e^{2\alpha}\left(120\alpha^3-96\alpha^2-776\alpha-2033\right)$$
$$\left.+2\left(6\alpha^4+44\alpha^3+114\alpha^2+129\alpha+5\right)+12e^{\alpha}\left(12\alpha^4+72\alpha^3+212\alpha^2+295\alpha+242\right)+e^{6\alpha}\right)^{1/2} \tag{45}$$

The numerical results for different geometries with comparison are given in Table 4. Very similar to the previous problem, convergence of the numerical results with the order of approximations are apparent. Also, agreement of the results with the literature are encouraging.

Table 4. Critical loads of clamped-free column with exponentially varying bending rigidity

| $\alpha$ | Present | | | [46] |
|---|---|---|---|---|
| | $P_{cr,1}$ | $P_{cr,2}$ | $P_{cr,3}$ | |
| 0 | 2 | 2.536 | 2.465 | 2.467 |
| 0.1 | 1.934 | 2.464 | 2.392 | 2.394 |
| 0.5 | 1.681 | 2.187 | 2.109 | 2.110 |
| 1.0 | 1.392 | 1.861 | 1.778 | 1.782 |
| 1.5 | 1.135 | 1.531 | 1.476 | 1.480 |
| 2.0 | 0.911 | 1.294 | 1.205 | 1.209 |

The essence and practical importance of the results provided herein is evident from the very good agreement of the numerical results with the existing literature. It must be noted that this approach to the solution of critical buckling load of columns provides very accurate closed-form solutions by very simple integrations and determination of roots of polynomial equations. *Classical* VIM approaches to this problem may require dealing with heavy integrations, and consideration of higher order of approximations for convergence, which inevitably require numerical solution techniques to solve the characteristic equation. Indeed, it is reported in [34], for a very similar problem, that nine iterations are conducted, and series expansions of the variations of bending rigidity up to nine terms are used to obtain the

numerical results. Even though their results are almost overlap with the exact solutions, the heavy integrations and computational cost must be taken into consideration.

## 5. Conclusions

This paper aims to derive some closed-form solutions for critical loads of columns with variable section. To this aim, Variational Iteration Method, modified for the system of linear differential equations, is utilized. It is found that the solutions to the approximate characteristic equations of up to third order are highly accurate for cantilevered beams, while other boundary conditions require the consideration of higher order approximations. Hence, some approximate closed-form solutions are presented, for the first time, for cantilevered columns of variable cross-section. The accuracy and versatility of the solution procedure are demonstrated by comparing the results presented in the literature, and a very good agreement is observed. The closed-form solutions presented herein, therefore, may well be used as benchmark solutions for other approximate solution procedures. Further approximations by selecting different trial functions, which may enlarge the present investigation also to the other boundary conditions, are possible. In addition, even one confines oneself to the trial functions used herein, many other closed-form solutions to direct problem of clamped-free column buckling seem to be at ease. This contribution may also be interpreted as the first step towards the closed-form solutions of eigenvalue problems of structural elements in closed-form, which may be used in their monitoring and identification.

## References

[1] Elishakoff, I., *Eigenvalues of Inhomogeneous Structures: Unusual Closed-Form Solutions*, CRC Press, Boca Raton, 2005.

[2] Antman, S.S., *The theory of rods*, pp.641-703 of *Linear Theories of Elasticity and Thermoelasticity*, Truesdell C. (ed.), Berlin, Springer, 1973.

[3] Love, A.E.H., *A Treatise on the Mathematical Theory of Elasticity*, Cambridge, at the University press, 4th edition, 1927.

[4] Timoshenko, S., *History of Strength of Materials*, McGraw-Hill, New York, 1953.

[5] Oldfather, W.A., Ellis C.A., Brown D.M., Leonhard Euler's Elastic Curves. *Isis*, 20(1), 72-160, 1933.

[6] Euler, L., Sur la force des callones. *Memories de L'Academie des Sciences et Belles-Letteres* (Berlin) 13, 252–282, 1759. (in French)

[7] Engesser, F., Ueber Krickfestigkeit gerader Staebe. *Zeitschrift Architekten und Ingineure in Hannover* 35, 455 (1899). (in German).

[8] Dinnik, A.N., *Design of columns of varying cross-section*, Transactions of the ASME, Applied Mechanics, 1929.

[9] Duncan, N.J., *Galerkin's method in mechanics and differential equations*. Aeronautical Research Committee Reports and Memoranda, No. 1798, 1937.

[10] Elishakoff, I., Pellegrini, F., Exact and effective approximate solutions of some divergent type non-conservative problems. *Journal of Sound and Vibration,* 114, 144-148, 1987.

[11] Elishakoff, I., Pellegrini, F., Application of Bessel and Lommel functions and undetermined multiplier Galerkin method version for instability of non-uniform column. *Journal of Sound and Vibration,* 115, 182-186, 1987

[12] Elishakoff, I., Pellegrini, F., Exact solution for buckling of some divergence type non-conservative systems in terms of Bessel and Lommel functions. *Computer Methods in Applied Mechanics and Engineering,* 66, 107-119, 1988

[13] Elishakoff, I., Inverse buckling problem for inhomogeneous columns. *International Journal of Solids and Structures,* 38(3), 457–464, 2001.

[14] Elishakoff, I., Eisenberger, M., Delmas, A., Buckling and vibration of functionally graded columns sharing Duncan's mode shape, and new cases. *Structures,* 5, 170–174, 2016.

[15] Suresh S, Mortensen A. Fundamentals of functionally graded materials. London, UK: IOM Communications Limited, 1998.

[16] Mahamood, R.S., Akinlabi, E.T., *Functionally Graded Materials,* Springer, 2017.

[17] Ruta, G.C., Varano, V., Pignataro, M., Rizzi N.L., A beam model for the flexural-torsional buckling of thin-walled memberse with some applications. *Thin-Walled Structures,* 46, 816,822, 2008.

[18] Ruta, G., Pignataro, M., Rizzi, N., A direct one-dimensional beam model for the flexural-torsional buckling of thin-walled beams. *Journal of Mechanics of Materials and Structures,* 1(8), 1479-1496, 2006.

[19] Tatone, A., Rizzi, N., A one-dimensional model for thin-walled beams, pp. 312–320 in *Trends in applications of mathematics to mechanics,* edited by W. ed. Schneider et al., Longman, Avon, 1991.

[20] Gupta, R.K., Gunda, J.B., Janardhan, G.R., Rao, G.V., Post-buckling analysis of composite beams: Simple and accurate closed-form expressions. *Composite Structures,* 92, 1947-1956, 2010.

[21] Mercan, K., Civalek, O., Comparison of Small Scale Effect Theories for Buckling Analysis of Nanobeam. *International Journal of Engineering and Applied Sciences,* 9(3), 87-97, 2016.

[22] Abbondanza, D., Battista, D., Morabito, F., Pallante, C., Barretta, R., Luciano, R., de Sciarra, F.M., Ruta, G., Modulated linear dynamics of nanobeams accounting for higher gradient effects. *International Journal of Engineering and Applied Sciences,* 8(2), 1-20, 2016.

[23] He, J.H., A new approach to non-linear partial differential equations. *Communications in Nonlinear Science and Numerical Simulation,* 2, 230–235, 1997.

[24] He, J.H., Variational iteration method for delay differential equations, *Communications in Nonlinear Science and Numerical Simulation,* 2, 235–236, 1997.

[25] He, J.H., Variational iteration method a kind of non-linear analytical technique: some examples. *International Journal of Nonlinear Mechanics,* 34, 699–708, 1999.

[26] He, J.H., Variational iteration method some recent results and new interpretations. *Journal of Computational and Applied Mathematics,* 207, 3–17, 2007.

[27] He, J.H., Wu, X.H., Variational iteration method: new development and applications. *Computers and Mathematics with Applications,* 54,881–894, 2007.

[28] Turkyilmazoglu, M., An optimal variational iteration method. *Applied Mathematics Letters,* 24(5), 762–765, 2011.

[29] Yilmaz, E., Inc, M., Numerical simulation of the squeezing flow between two infinite plates by means of the modified variational iteration method with an auxiliary parameter. *Nonlinear Science Letters A,* 1, 297–306, 2010.

[30] Hosseini, M.M., Mohyud-Din, S.T., Ghaneai H., Usman, M., Auxiliary parameter in the variational iteration method and its optimal determination. *International Journal of Nonlinear Sciences and Numerical Simulation,* 11(7), 495–502, 2010.

[31] Herişanu, N., Marinca, V., A modified variational iteration method for strongly nonlinear problems. *Nonlinear Science Letters A,* 1, 183–192, 2010.

[32] Altintan, D., Ugur, O., Generalisation of the Lagrange multipliers for variational iterations applied to systems of differential equations. *Mathematical and Computer Modelling.* 54, 2040-2050, 2011.

[33] He, J.H., Notes on the optimal variational iteration method. Applied Mathematics Letters. 25(10), 1579-1581, 2012.

[34] Coskun, S.B., Atay, M.T., Determination of critical buckling load for elastic columns of constant and variable cross-sections using variational iteration method. *Computers and Mathematics with Applications,* 58, 2260,2266, 2009.

[35] Chen, Y., Zhang, J., Zhang, Z., Flapwise bending vibration of rotating tapered beams using variational iteration method. *Journal of Vibration and Control,* 22(15), 3384-3395, 2016.

[36] Eroglu, U., Large deflection analysis of planar curved beams made of functionally graded materials using variational iterational method. *Composite Structures,* 136, 204–216, 2016.

[37] Yun-dong, L., Yi-ren, Y., Vibration analysis of conveying fluid pipe via He's variational iteration method. *Applied Mathematical Modelling,* 43, 409,420.

[38] Eroglu, U., Tufekci, E., Small-Amplitude free vibrations of straight beams subjected to large displacements and rotation. *Applied Mathematical Modelling,* 53, 223-241, 2018.

[39] Budiansky, B., Theory of buckling and postbuckling behavior of elastic structures, pp. 1–65 in *Advances in applied mechanics,*14, Academic Press, New York, 1974.

[40] Timoshenko, S.P., Gere, J.M., *Theory of Elastic Stability*. McGraw-Hill, New York, 1961.

[41] Pease, M.C., *Methods of Matrix Algebra*. Academic Press, New York, 1965.

[42] Tufekci, E., Arpaci, A., Exact solution of in-plane vibrations of circular arches with account taken of axial extension, transverse shear and rotatory inertia effects. *Journal of Sound and Vibration* 209 (5):845–56, 1998.

[43] Tufekci, E., Arpacı, A., Analytical solutions of in-plane static problems for non-uniform curved beams including axial and shear deformations. *Structural Engineering and Mechanics*, 22 (2):131–50, 2006.

[44] Yildirim, V., Several Stress Resultant and Deflection Formulas for Euler-Bernoulli Beams under Concentrated and Generalized Power/Sinusoidal Distributed Loads, *International Journal of Engineering and Applied Sciences*, 10(2), 35-63, 2018.

[45] Wei, D.J., Xani S.X., Zhang, Z.P., Li, X.F., Critical load for buckling of non-prismatic columns under self-weight and tip force. *Mechanics Research Communications,* 37, 554-558- 2010.

[46] Wang, C.M., Wang, C.Y., Reddy, J.N., *Exact Solutions for Buckling of Structural Members*. CRC Press, Boca Raton, 2005.

*International Journal of Engineering & Applied Sciences (IJEAS)*
*Vol.10, Issue 3 (2018) 176-189*
*http://dx.doi.org/10.24107/ijeas.456755*
Int J Eng Appl Sci 10(3) (2018) 176-189

# Free Vibration Analysis of a Cross-Ply Laminated Plate in Thermal Environment

*Yusuf Ziya YÜKSEL* [a*] *and Şeref Doğuşcan AKBAŞ* [b]

[a,b] *Bursa Technical University, Department of Civil Engineering, Bursa, Turkey.*
*E-mail address*: yusuf.yuksel@btu.edu.tr [a*], seref.akbas@btu.edu.tr [b]

*Received date: 03.09.2018*
*Accepted date: 30.10.2018*

*ORCID numbers of authors*
0000-0002-2615-1590[a], 0000-0001-5327-3406[b]

**Abstract**

*This paper presents free vibration analysis of a cross-ply laminated plate under temperature rising with considering temperature-dependent physically properties. Material properties of laminas are orthotropic and temperature-dependent. In the kinematic model of the plate, first-order shear deformation plate theory is used. In solution method, the Navier procedure is used for a simply supported plate. The vibration frequencies of the laminated plate are obtained and discussed for different values of temperature, sequence of laminas and orientation angle of layers. Also, the difference between temperature dependent and independent physical properties is investigated.*

**Keywords:** Composite Materials; Laminated Plates; Free Vibration; Temperature Rising.

## 1. Introduction

Laminated composite structures have been used a lot of engineering applications, for example; aircrafts, space vehicles, automotive engineering, defence industries and civil engineering applications because these structures have higher strength-weight ratios, more lightweight and ductile properties than classical materials. In generally, laminated composite structures are used in higher thermal systems. Hence, the temperature effect is very important issue of laminated composite structures and their design. In the literature, studies about temperature problems in composite plates are; Pal [1] analyzed nonlinear vibrations of plates under thermal loading. Chen and Chen [2] examined thermal buckling of laminated plates by finite element method. Chen and Chen [3] studied thermal post-buckling of laminated plates under thermal loading. Liu and Huang [4] analyzed vibration of laminated plates under thermal loading with first shear deformation plate theory (FSDPT). F. Lee et al. [5] studied free vibration of symmetrically laminated plates with FSDPT. Reddy and Chin [6] investigated dynamic thermo-elastic analysis of functionally graded cylinders and plates. Lee and Saravanos [7] studied thermo-piezoelectric composite materials with thermal effects with temperature dependent material properties. Reddy [8] performed static analysis of functionally graded plates by using FSDPT. Jane and Hong [9] investigated thermal problems of thin laminated rectangular orthotropic plates by

using generalized differential quadrature method. Shen [10] examined thermal post-buckling of laminated plate resting on elastic foundation. Singha et al. [11] studied thermal postbuckling of graphite/epoxy laminated plates of various by finite element method. Sayman [12] analyzed elastic-plastic behavior of aluminum metal-matrix laminated plate under temperature effect. Patel et al. [13] examined flexural analysis of laminated plates of bimodulus materials under temperature effect. Shukla et al. [14] investigated postbuckling of laminated plates under temperature effect. Liew et al. [15] examined thermal buckling/post-buckling of thick laminated plates uniform temperature rising. Emery et al. [16] investigated thermoelastic stress analysis of laminated orthotropic plates. Shen [17] examined nonlinear analysis of functionally graded nanocomposite plates reinforced by single-walled carbon nanotubes under temperature effect. Zenkour and Alghamdi [18] examined bending of functional graded layered plates under thermal and mechanical loads. Vosoughi et al. [19] examined thermal postbuckling thermal postbuckling behavior of laminated composite skew with temperature dependent material properties. Kishore et al. [20] investigated nonlinear analysis of magnetostrictive layered plate by using third order shear deformation theory. Sahoo and Singh [21] presented static analysis of layered plates by using the hyperbolic zigzag theory. Carrera et al. [22] analyzed static stress problems in multi-layer plates. Sahoo and Singh [23] examined static analysis of layered plates by using a new inverse trigonometric ZigZag theory. Chen et al. [24] investigated thermal buckling and vibration of composite plates with temperature-dependent material properties and initially stressed. Torabizadeh and Fereidoon [25] solved general laminated composite plates under mechanical and thermal loading. Houmat [26] investigated the geometrically nonlinear free vibration of laminated composite rectangular plates with curvilinear fibers. Khorshid and Farhadi [27] investigated hydrostatic vibration analysis of a laminated composite rectangular plate partially contacting with a bounded fluid. Akbaş [28,29,30,31,32,33,34,35,36,37,38] investigated dynamics and stability of functionally graded composite beams by using finite element method. Sayyad et al. [39,40] solved thermoelastic analysis of laminated plates under thermal loading. Li and Qiao [41,42] examined thermal postbuckling analysis of laminated composite beams under thermal loading. Akbaş [43] examined a nano-plate by using generalized differential quadrature method. Ramos et al. [44] investigated thermoelastic static analysis of composite plates by using a new combined trigonometric equation. Akbaş [45,46] investigated functionally graded porous plates. Choudhury et al. [47] solved stress analysis of composite plate under thermo mechanical loads. Akbaş [48,49,50] investigated thee laminated beams with nonlinear behavior. Akbaş [51] examined bi-material composite beams by using finite element method. Yüksel et al. [52] examined temperature dependent vibration of a simply supported plate by using the Navier method. Yüksel and Akbaş [53] investigated the stress analysis of a laminated composite plate under temperature rising. Also, many researchers investigated vibration, buckling, post-buckling analysis of nano composites, functionally graded composite structures in thermal and mechanical loads [54-73].

In this paper, free vibration of cross-play laminated plate examined under thermal effects. In constitute model of laminas, orthotropic and temperature-dependent properties are used. FSDPT is used in plate model. The Navier procedure is used for a simply supported plate. Effects of temperature, sequence of laminas and orientation angle of layers on the vibration characterises of laminated plate are investigated in temperature-dependent physically property.

## 2. Theory and Formulations

In figure 1, a simply supported rectangular cross-ply laminated composite plate with thickness $h$, the length of $L_{X_1}$ and $L_{X_2}$ is displayed. Laminated composite plate is subjected to a non-uniform temperature rising with temperature rising values at the bottom surface $\Delta T_B$ and top surface $\Delta T_T$. Height of face sheet layers is equal to each other. In this study, numbers of the laminas are selected as two and three.

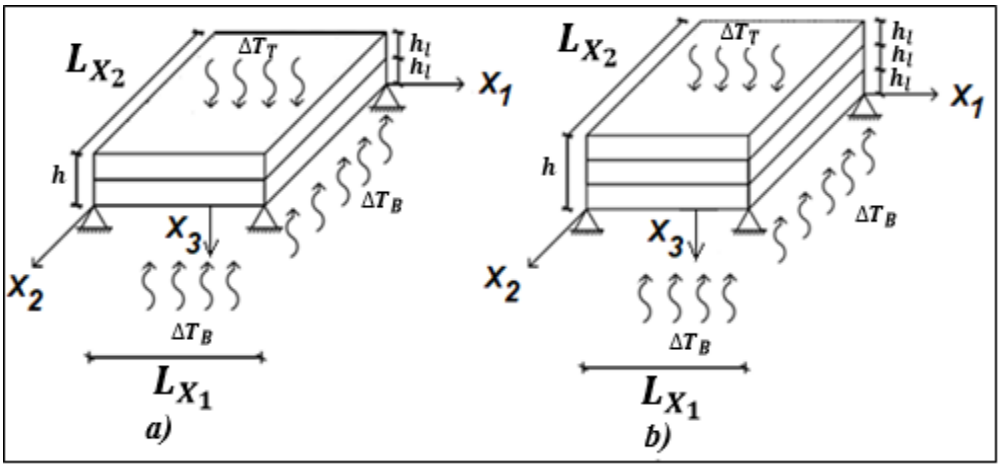


Fig. 1. A simply supported laminated rectangular composite plate under non-uniform temperature rising for a) two layer and b) three layer.

Based on FSDPT, the strain-displacement relations are expressed as;

$$\varepsilon_{X_1X_1} = \frac{\partial u_{01}}{\partial X_1} + X_3 \frac{\partial \emptyset_{X_1}}{\partial X_1} \qquad \varepsilon_{X_2X_2} = \frac{\partial u_{02}}{\partial X_2} + X_3 \frac{\partial \emptyset_{X_2}}{\partial X_2} \tag{1}$$

$$\gamma_{X_1X_2} = \frac{\partial u_{02}}{\partial X_2} + \frac{\partial u_{02}}{\partial X_1} + X_3 \left( \frac{\partial \emptyset_{X_1}}{\partial X_2} + \frac{\partial \emptyset_{X_2}}{\partial X_1} \right) \tag{2}$$

$$\gamma_{X_1X_3} = \frac{\partial u_{03}}{\partial X_1} + \emptyset_{X_1}\,,\ \gamma_{X_2X_3} = \frac{\partial u_{03}}{\partial X_2} + \emptyset_{X_2}\,,\ \varepsilon_{X_3X_3} = 0 \tag{3}$$

where $u_{01}$, $u_{02}$, $u_{03}$ indicate displacements in $X_1$, $X_2$ and $X_3$ directions, respectively. Constitutive expressions of orthotropic laminated plate for *n*th layer with temperature effect are given as follows:

$$\begin{Bmatrix} \sigma_{X_1X_1} \\ \sigma_{X_2X_2} \\ \sigma_{X_1X_2} \end{Bmatrix}^{(n)} = \begin{bmatrix} \overline{Q}_{11}(T) & \overline{Q}_{12}(T) & \overline{Q}_{16}(T) \\ \overline{Q}_{12}(T) & \overline{Q}_{22}(T) & \overline{Q}_{26}(T) \\ \overline{Q}_{16}(T) & \overline{Q}_{26}(T) & \overline{Q}_{66}(T) \end{bmatrix}^{(n)} \begin{Bmatrix} \frac{\partial u_{01}}{\partial X_1} - X_3 \frac{\partial^2 u_{03}}{\partial {X_1}^2} - \bar{\alpha}_{11}(T)\Delta T \\ \frac{\partial u_{02}}{\partial X_2} - X_3 \frac{\partial^2 u_{03}}{\partial {X_2}^2} - \bar{\alpha}_{22}(T)\Delta T \\ \frac{\partial u_{01}}{\partial X_2} + \frac{\partial u_{02}}{\partial X_1} - X_3 \frac{\partial^2 u_{03}}{\partial {X_2}^2} - X_3 \frac{\partial^2 u_{03}}{\partial {X_1}^2} - 2\bar{\alpha}_{12}(T)\Delta T \end{Bmatrix}^{(n)} \tag{4a}$$

$$\begin{Bmatrix} \sigma_{X_2X_3} \\ \sigma_{X_1X_3} \end{Bmatrix}^{(n)} = \begin{bmatrix} \overline{Q}_{44}(T) & \overline{Q}_{45}(T) \\ \overline{Q}_{45}(T) & \overline{Q}_{55}(T) \end{bmatrix}^{(n)} \begin{Bmatrix} \frac{\partial u_{02}}{\partial X_2} - \frac{\partial u_{03}}{\partial X_2} \\ \frac{\partial u_{03}}{\partial X_1} - \frac{\partial u_{03}}{\partial X_1} \end{Bmatrix}^{(n)} \tag{4b}$$

where $\bar{Q}_{ij}(T)$ is the transformed reduced material properties which depends the temperature ($T$) are given as follows:

$$\overline{Q}_{11}(T) = Q_{11}(T)cos^4\theta + 2(Q_{12}(T) + 2Q_{66}(T))sin^2\theta cos^2\theta + Q_{22}(T)sin^4\theta$$
$$\overline{Q}_{12}(T) = \big(Q_{11}(T) + Q_{22}(T) - 4Q_{66}(T)\big)sin^2\theta cos^2\theta + Q_{12}(T)(sin^4\theta + cos^4\theta)$$
$$\overline{Q}_{22}(T) = Q_{11}(T)sin^4\theta + 2\big(Q_{12}(T) + 2Q_{66}(T)\big)sin^2\theta cos^2\theta + Q_{22}(T)cos^4\theta$$
$$\overline{Q}_{16}(T) = \big(Q_{11}(T) - Q_{12}(T) - 2Q_{66}(T)\big)sin\theta cos^3\theta + (Q_{12}(T) - Q_{22}(T) + 2Q_{66}(T))sin^3\theta cos\theta$$
$$\overline{Q}_{26}(T) = \big(Q_{11}(T) - Q_{12}(T) - 2Q_{66}(T)\big)sin^3\theta cos\theta + (Q_{12}(T) - Q_{22}(T) + 2Q_{66}(T))sin\theta cos^3\theta$$

$$\overline{Q}_{66}(T) = \left(Q_{11}(T) + Q_{22}(T) - 2Q_{12}(T) - 2Q_{66}(T)\right)sin^2\theta cos^2 + Q_{66}(T)(sin^4\theta + cos^4\theta)$$
$$\bar{Q}_{44}(T) = Q_{44}(T)\cos^2\theta + Q_{55}(T)\sin^2\theta$$
$$\bar{Q}_{45}(T) = (Q_{55}(T) - Q_{44}(T))\cos\theta\sin\theta$$
$$\bar{Q}_{55}(T) = Q_{44}(T)\sin^2\theta + Q_{55}(T)\cos^2\theta \quad (5)$$

where, $\theta$ is the fiber orientation angle. Components of the $Q_{ij}$ are given as follows;

$$Q_{11}(T) = \frac{E_1(T)}{1-\nu_{12}\nu_{21}}\ , \qquad Q_{22}(T) = \frac{E_2(T)}{1-\nu_{12}\nu_{21}}$$
$$Q_{12}(T) = \frac{\nu_{12}E_2(T)}{1-\nu_{12}\nu_{21}} = \frac{\nu_{21}E_1(T)}{1-\nu_{12}\nu_{21}} \qquad Q_{44}^{(n)}(T) = G_{23}^{(n)}(T) \qquad Q_{55}^{(n)}(T) = G_{13}^{(n)}(T)$$
$$Q_{21}(T) = \frac{\nu_{12}E_2(T)}{1-\nu_{12}\nu_{21}} = \frac{\nu_{21}E_1(T)}{1-\nu_{12}\nu_{21}} \qquad Q_{66}(T) = G_{12}(T) \quad (6)$$

The material properties of orthotropic laminated plate is a function of temperature ($T$) as follows (Shen[67]; Li and Qiao[68]).

$$E_1(T) = E_1(1 - 0{,}5 * 10^{-3}\Delta T)GPa$$
$$E_2(T) = E_2(1 - 0{,}2 * 10^{-3}\Delta T)GPa$$
$$G_{12}(T) = G_{13}(T) = G_{12}(1 - 0{,}2 * 10^{-3}\Delta T)GPa$$
$$G_{23}(T) = G_{23}(1 - 0{,}2 * 10^{-3}\Delta T)GPa$$
$$\alpha_1(T) = \alpha_1(1 + 0{,}5 * 10^{-3}\Delta T)/℃$$
$$\alpha_2(T) = \alpha_2(1 + 0{,}5 * 10^{-3}\Delta T)/℃ \quad (7)$$

The transformed the thermal expansion coefficients $\alpha_{X_1X_1}$, $\alpha_{X_2X_2}$, $\alpha_{X_1X_2}$ are given as follows;

$$\alpha_{X_1X_1} = \alpha_1 cos^2\theta + \alpha_2 sin^2\theta$$
$$\alpha_{X_2X_2} = \alpha_2 cos^2\theta + \alpha_1 sin^2\theta$$
$$2\alpha_{X_1X_2} = 2(\alpha_1 - \alpha_2)sin\theta cos\theta \quad (8)$$

where $\alpha_1$ and $\alpha_2$ are thermal expansion coefficients in $X_1$ and $X_2$ directions, respectively. Stress resultants are given as follows;

$$\begin{Bmatrix}\{N\}\\ \{M\}\end{Bmatrix} = \begin{bmatrix}[A(T)] & [B(T)]\\ [B(T)] & [D(T)]\end{bmatrix}\begin{Bmatrix}\{\varepsilon^0\}\\ \{\varepsilon^1\}\end{Bmatrix} - \begin{Bmatrix}\{N^T\}\\ \{M^T\}\end{Bmatrix} \quad (9)$$

where $N$ is normal force and $M$ is moment. $\{N^T\}$ and $\{M^T\}$ are thermal force resultants:

$$\{N^T\} = \sum_{n=1}^{N}\int_{z_n}^{z_{n+1}}\overline{Q}_{ij}(T)^n\{\bar{\alpha}(T)\}^n\,\Delta T dX_3 \quad (10a)$$
$$\{M^T\} = \sum_{n=1}^{N}\int_{z_n}^{z_{n+1}}\overline{Q}_{ij}(T)^n\{\bar{\alpha}(T)\}^n\,\Delta T X_3 dX_3 \quad (10b)$$

$\{\varepsilon^0\}$ and $\{\varepsilon^1\}$ are given as follows;

$$\{\varepsilon^0\} = \begin{Bmatrix}\frac{\partial u_{01}}{\partial X_1}\\ \frac{\partial u_{02}}{\partial X_2}\\ \frac{\partial u_{01}}{\partial X_2} + \frac{\partial u_{02}}{\partial X_1}\end{Bmatrix}, \quad \{\varepsilon^1\} = \begin{Bmatrix}\frac{\partial \emptyset_{X_1}}{\partial X_1}\\ \frac{\partial \emptyset_{X_2}}{\partial X_2}\\ \frac{\partial \emptyset_{X_1}}{\partial X_2} + \frac{\partial \emptyset_{X_2}}{\partial X_1}\end{Bmatrix} \quad (11)$$

where $A_{ij}$ is extensional stiffness, $D_{ij}$ is bending stiffness, and $B_{ij}$ is bending – extensional coupling stiffness. $A_{ij}$, $B_{ij}$ and $D_{ij}$ are expressed as follows:

$$A_{ij} = \sum_{k=1}^{n} \overline{Q}_{ij}^{(n)} (z_{n+1} - z_n) \quad (12a)$$

$$B_{ij} = \frac{1}{2} \sum_{k=1}^{n} \overline{Q}_{ij}^{(n)} (z_{n+1}^2 - z_n^2) \quad (12b)$$

$$D_{ij} = \frac{1}{3} \sum_{k=1}^{n} \overline{Q}_{ij}^{(n)} (z_{n+1}^3 - z_n^3) \quad (12c)$$

The elastic strain energy ($U_i$) and the kinetic energy ($T$) of laminated plate are expressed as follows:

$$U_i = \frac{1}{2} \int_V \sigma_{ij} \, \varepsilon_{ij} \, dV \quad (13a)$$

$$T = \frac{1}{2} \int_V \rho \left[ \left( \frac{\partial u_{01}}{\partial t} \right)^2 + \left( \frac{\partial u_{02}}{\partial t} \right)^2 + \left( \frac{\partial u_{03}}{\partial t} \right)^2 \right] dV \quad (13b)$$

The Hamilton's principle of the problem is as follows;

$$\delta \int_0^t [T - U_i] dt \quad (14)$$

After using Hamilton's principle, governing equations of the laminated plate can be obtained;

$$\frac{\partial N_{X_1X_1}}{\partial X_1} + \frac{\partial N_{X_1X_2}}{\partial X_2} = I_0 \frac{\partial^2 u_{01}}{\partial t^2} + I_1 \frac{\partial^2 \emptyset_{X_1}}{\partial t^2} \quad (15a)$$

$$\frac{\partial N_{X_1X_2}}{\partial X_1} + \frac{\partial N_{X_2X_2}}{\partial X_2} = I_0 \frac{\partial^2 u_{02}}{\partial t^2} + I_1 \frac{\partial^2 \emptyset_{X_2}}{\partial t^2} \quad (15b)$$

$$\frac{\partial Q_{X_1}}{\partial X_1} + \frac{\partial Q_{X_2}}{\partial X_2} = I_0 \frac{\partial^2 u_{03}}{\partial t^2} \quad (15c)$$

$$\frac{\partial M_{X_1X_1}}{\partial X_1} + \frac{\partial M_{X_1X_2}}{\partial X_2} - Q_{X_1} = I_2 \frac{\partial^2 \emptyset_{X_1}}{\partial t^2} + I_1 \frac{\partial^2 u_{01}}{\partial t^2} \quad (15d)$$

$$\frac{\partial M_{X_1X_2}}{\partial X_1} + \frac{\partial M_{X_2X_2}}{\partial X_2} - Q_{X_2} = I_2 \frac{\partial^2 \emptyset_{X_2}}{\partial t^2} + I_1 \frac{\partial^2 u_{02}}{\partial t^2} \quad (15e)$$

where

$$\begin{Bmatrix} N_{X_1X_1} \\ N_{X_2X_2} \\ N_{X_1X_2} \end{Bmatrix} = \int_{-\frac{h}{2}}^{\frac{h}{2}} \begin{Bmatrix} \sigma_{X_1X_1} \\ \sigma_{X_2X_2} \\ \sigma_{X_1X_2} \end{Bmatrix} dX_3 \quad (16a)$$

$$\begin{Bmatrix} M_{X_1X_1} \\ M_{X_2X_2} \\ M_{X_1X_2} \end{Bmatrix} = \int_{-\frac{h}{2}}^{\frac{h}{2}} \begin{Bmatrix} \sigma_{X_1X_1} \\ \sigma_{X_2X_2} \\ \sigma_{X_1X_2} \end{Bmatrix} X_3 dX_3 \quad (16b)$$

$$\begin{Bmatrix} Q_{X_2} \\ Q_{X_1} \end{Bmatrix} = K \begin{bmatrix} A_{44}(T) & A_{45}(T) \\ A_{45}(T) & A_{55}(T) \end{bmatrix} \begin{bmatrix} \frac{\partial u_{03}}{\partial X_2} + \emptyset_{X_2} \\ \frac{\partial u_{03}}{\partial X_1} + \emptyset_{X_1} \end{bmatrix} \quad (16c)$$

$$\begin{Bmatrix} I_0 \\ I_1 \\ I_2 \end{Bmatrix} = \int_{-\frac{h}{2}}^{\frac{h}{2}} \begin{Bmatrix} 1 \\ X_3 \\ {X_3}^2 \end{Bmatrix} \rho_0 dX_3 \quad (16d)$$

In solution of problem, Navier method is implemented in the solution of the problem. In Navier solution, boundary conditions and displacement fields the plate are given the following equations:

$$u_{01}(X_1, 0, t) = 0, \quad u_{01}(X_1, b, t) = 0, \quad u_{02}(0, X_2, t) = 0, \quad u_{02}(a, X_2, t) = 0, \quad (17a)$$

$$u_{03}(X_1,0,t)=0,\quad u_{03}(X_1,b,t)=0,\quad u_{03}(0,X_2,t)=0,\quad u_{03}(a,X_2,t)=0, \tag{17b}$$

$$\emptyset_{X_1}(X_1,0,t)=0,\quad \emptyset_{X_1}(X_1,b,t)=0,\quad \emptyset_{X_2}(0,X_2,t)=0,\quad \emptyset_{X_2}(a,X_2,t)=0, \tag{17c}$$

$$N^T_{X_1X_1}(0,X_2,t)=0,\quad N^T_{X_1X_1}(a,X_2,t)=0,\quad N^T_{X_2X_2}(X_1,0,t)=0,\quad N^T_{X_2X_2}(X_1,b,t)=0 \tag{17d}$$

$$M^T_{X_1X_1}(0,X_2,t)=0,\quad M^T_{X_1X_1}(a,X_2,t)=0,\quad M^T_{X_2X_2}(X_1,0,t)=0,\quad M^T_{X_2X_2}(X_1,b,t)=0 \tag{17e}$$

$$u_{01}(X_1,X_2,t)=\sum_{n=1}^{\infty}\sum_{m=1}^{\infty}U_{1_{mn}}(t)coskX_1\ sinlX_2\ e^{-i\beta t} \tag{18a}$$

$$u_{02}(X_1,X_2,t)=\sum_{n=1}^{\infty}\sum_{m=1}^{\infty}U_{2_{mn}}(t)sinkX_1\ coslX_2\ e^{-i\beta t} \tag{18b}$$

$$u_{03}(X_1,X_2,t)=\sum_{n=1}^{\infty}\sum_{m=1}^{\infty}U_{3_{mn}}(t)sinkX_1\ sinlX_2\ e^{-i\beta t} \tag{18c}$$

$$\emptyset_{X_1}(X_1,X_2,t)=\sum_{n=1}^{\infty}\sum_{m=1}^{\infty}X_{X_{1_{mn}}}(t)coskX_1\ sinlX_2\ e^{-i\beta t} \tag{18d}$$

$$\emptyset_{X_2}(X_1,X_2,t)=\sum_{n=1}^{\infty}\sum_{m=1}^{\infty}Y_{X_{2_{mn}}}(t)sinkX_1\ coslX_2\ e^{-i\beta t} \tag{18e}$$

where $U_{1_{mn}}$, $U_{2_{mn}}$, $U_{3_{mn}}$, $X_{X_{1_{mn}}}$, $Y_{X_{2_{mn}}}$ are displacement coefficients, $k=m\pi/L_{X_1}$, $l=n\pi/L_{X_2}$, $\beta$ is the natural frequency and $i=\sqrt{-1}$. The temperature rising is defined as follows in the Navier solution;

$$\Delta T(X_1,X_2,X_3,t)=\sum_{n=1}^{\infty}\sum_{m=1}^{\infty}T_{mn}(X_3,t)sinkX_1\ sinlX_2 \tag{19a}$$

$$T_{mn}(X_3,t)=\frac{4}{L_XL_Y}\int_0^a\int_0^b\Delta S(X_1,X_2,X_3,t)sinkX_1sinlX_2\ dX_1dX_2 \tag{19b}$$

Substituting Eqs. (17-19) into Eqs. (15), and then using matrix procedure, the algebraic equations of free vibration problem can be expressed as follows;

$$\left(\begin{bmatrix}p_{11}&p_{12}&0&p_{14}&p_{15}\\p_{12}&p_{22}&0&p_{24}&p_{25}\\0&0&p_{33}&p_{34}&p_{35}\\p_{14}&p_{24}&p_{34}&p_{44}&p_{45}\\p_{15}&p_{25}&p_{35}&p_{45}&p_{55}\end{bmatrix}-\omega^2\begin{bmatrix}m_{11}&0&0&0&0\\0&m_{22}&0&0&0\\0&0&m_{33}&0&0\\0&0&0&m_{44}&0\\0&0&0&0&m_{55}\end{bmatrix}\right)\begin{Bmatrix}U_{1_{mn}}\\U_{2_{mn}}\\U_{3_{mn}}\\X_{X_{1_{mn}}}\\Y_{X_{2_{mn}}}\end{Bmatrix}=\begin{Bmatrix}0\\0\\0\\0\\0\end{Bmatrix} \tag{20}$$

where

$$\begin{aligned}&p_{11}=(A_{11}(T)k^2+A_{66}(T)l^2),\ \ p_{12}=(A_{12}(T)+A_{66}(T))kl\\&p_{14}=(B_{11}(T)k^2-B_{66}(T)l^2),\ p_{15}=(B_{12}(T)+B_{66}(T))kl,\\&p_{22}=(A_{66}(T)k^2+A_{22}(T)l^2),\ p_{24}=p_{15},\\&p_{25}=(B_{66}(T)k^2+B_{22}(T)l^2),p_{33}=K(A_{55}(T)k^2+A_{44}(T)l^2),\\&p_{34}=KA_{55}(T)k,\ \ p_{35}=KA_{44}(T)l,\\&p_{44}=(D_{11}(T)k^2+D_{22}(T)l^2+KA_{55}(T))\\&p_{45}=(D_{12}(T)+D_{66}(T))kl,\ p_{55}=(D_{66}(T)k^2+D_{22}(T)l^2+KA_{44}(T))k\\&m_{11}=I_0,\ m_{22}=I_0,\ m_{33}=I_0,\ m_{44}=I_2,\ m_{55}=I_2\end{aligned} \tag{21}$$

where $K$ is shear correction factor. Dimensionless fundamental frequency $\bar{\omega}$ is defined as follows;

$$\bar{\omega}_{mn}=\omega_{mn}({L_{X_2}}^2/\pi^2)\sqrt{\rho h/D_{22}} \tag{22}$$

## 3. Numerical Results

In numerical study, dimensionless frequencies of cross-ply laminated simply-supported plate are calculated obtained in figures for different temperature values, orientation angles and sequence of laminas in temperature-dependent physically property. The mechanical properties of manufactured using graphite epoxy and its material parameters are; $E_1$=150 GPa, $E_2$=9 GPa, $E_3$=9 GPa, $G_{12}$=7,1 GPa, $G_{23}$=2,5 GPa, $G_{13}$=7,1 GPa, $\rho$=1600 kg/m$^3$, $\nu_{12}$= $\nu_{21}$=0.3, $\alpha_1 = 1{,}1.10^{-6}$, $\alpha_1 = 25{,}2.10^{-6}$ at $30^{\circ}C$ (Li and Qiao [68], Oh vd. [69]). The dimensions of plate are considered as follows: $L_{X_1} = 4\text{m}$, $L_{X_2} = 4\text{m}$, $h$=0.2 m. In the obtaining the numerical results and figures, MATLAB program is used. It is noted that temperature rising of bottom surface $\Delta T_B$ is changed and the temperature of the top surface $\Delta T_T$ is constant $\Delta T_T = 20^{\circ}C$ in the numerical calculations.

In the numerical results, the relation between temperature rising and dimensionless natural frequencies is presented for different orientation angles and sequence of laminas. Also the difference between temperature dependent and independent physical properties on the dimensionless natural frequencies of laminated composite plate is discussed. For this purpose, figures 2,3,4 and 5 show the effect of the temperature rising on the first three lower dimensionless natural frequencies of the laminated plate for 0/0, 0/90, 90/0 and 90/90, respectively in two layer sequence in both temperature dependent and independent physical properties. Also, figures 6,7,8,9 and 10 show effect of temperature rising on first three lower dimensionless natural frequencies of the laminated plate for 0/0/0, 0/90/0, 90/0/90, 0/90/90 and 90/90/90, respectively in three layer sequence in both temperature dependent and independent physical properties.

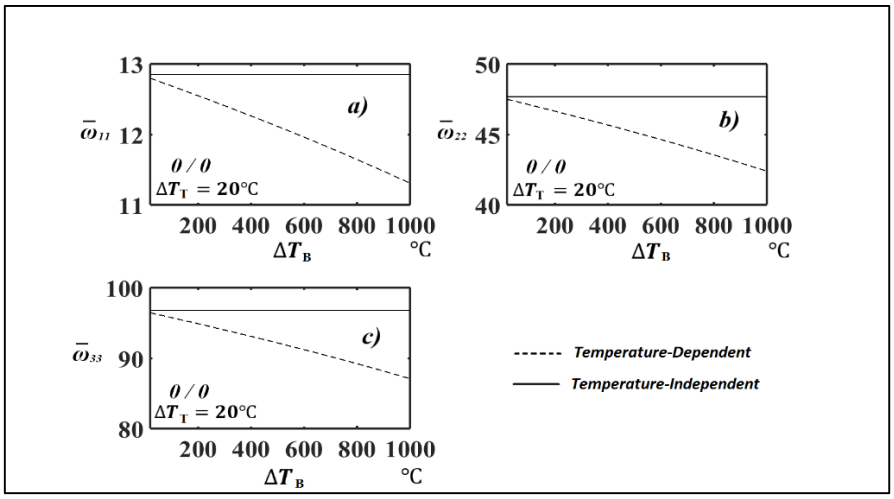


Fig. 2. The natural frequencies versus temperature rising for the two layers for stacking sequence 0/0 for a) $\bar{\omega}_{11}$ b) $\bar{\omega}_{22}$ and c) $\bar{\omega}_{33}$.

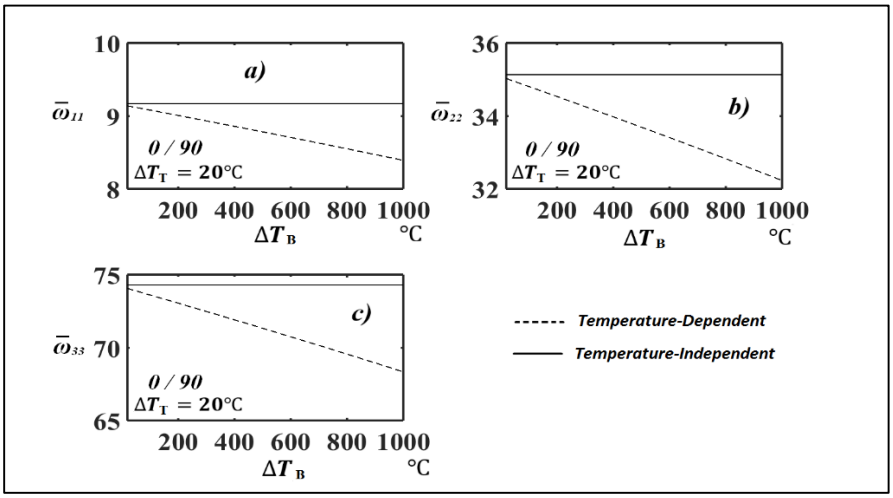


Fig. 3. The natural frequencies versus temperature rising for the two layers for stacking sequence 0/90 for a) $\bar{\omega}_{11}$ b) $\bar{\omega}_{22}$ and c) $\bar{\omega}_{33}$.

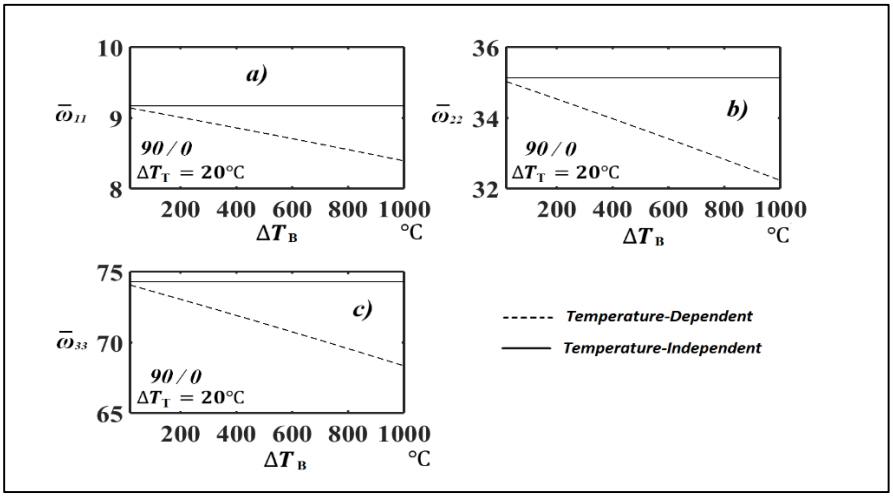


Fig. 4. The natural frequencies versus temperature rising for the two layers for stacking sequence 90/0 for a) $\bar{\omega}_{11}$ b) $\bar{\omega}_{22}$ and c) $\bar{\omega}_{33}$.

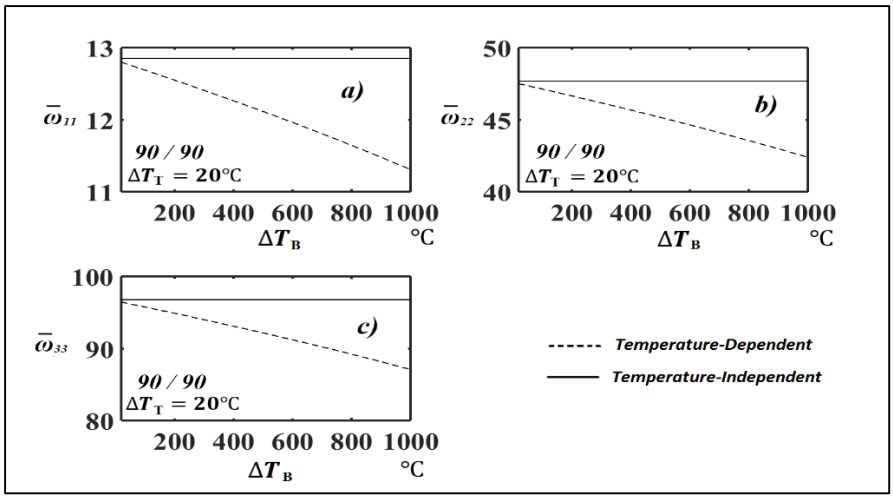


Fig. 5. The natural frequencies versus temperature rising for the two layers for stacking sequence 90/90 for a) $\bar{\omega}_{11}$ b) $\bar{\omega}_{22}$ and c) $\bar{\omega}_{33}$.

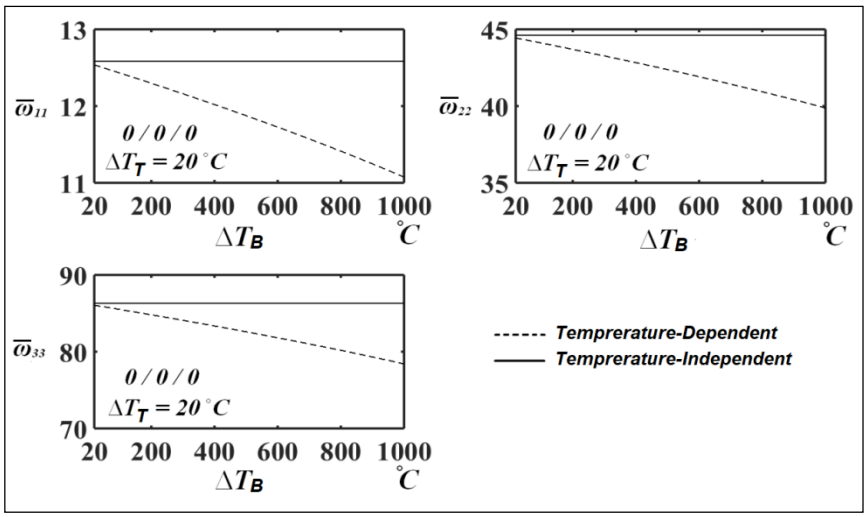


Fig. 6. The natural frequencies versus temperature rising for the three layers for stacking sequence 0/0/0 for a) $\bar{\omega}_{11}$ b) $\bar{\omega}_{22}$ and c) $\bar{\omega}_{33}$.

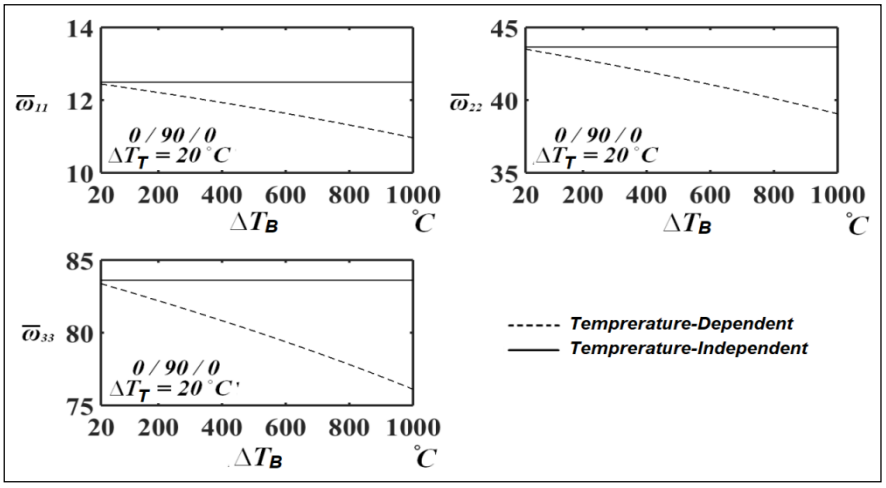


Fig. 7. The natural frequencies versus temperature rising for the three layers for stacking sequence 0/90/0 for a) $\bar{\omega}_{11}$ b) $\bar{\omega}_{22}$ and c) $\bar{\omega}_{33}$.

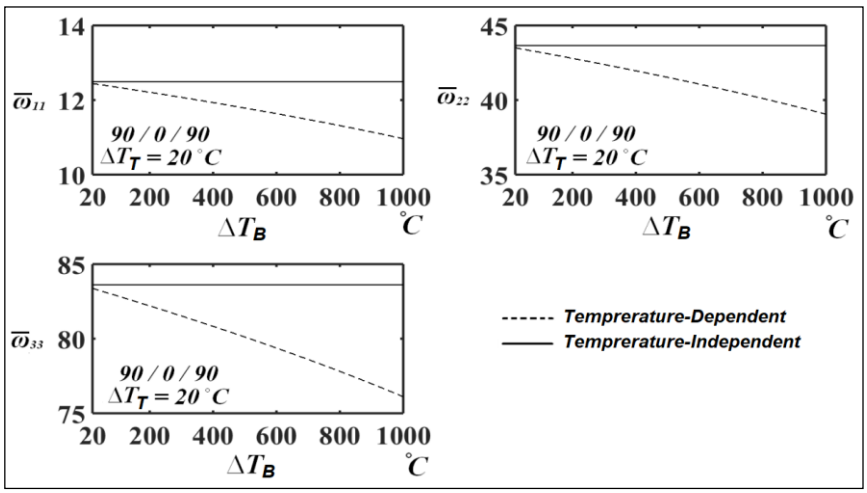


Fig. 8. The natural frequencies versus temperature rising for the three layers for stacking sequence 90/0/90 for a) $\bar{\omega}_{11}$ b) $\bar{\omega}_{22}$ and c) $\bar{\omega}_{33}$.

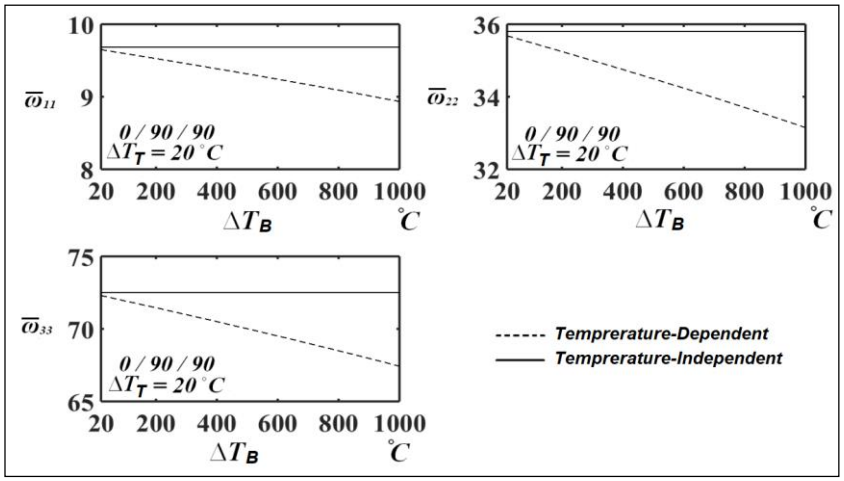


Fig. 9. The natural frequencies versus temperature rising for the three layers for stacking sequence 0/90/90 for a) $\bar{\omega}_{11}$ b) $\bar{\omega}_{22}$ and c) $\bar{\omega}_{33}$.

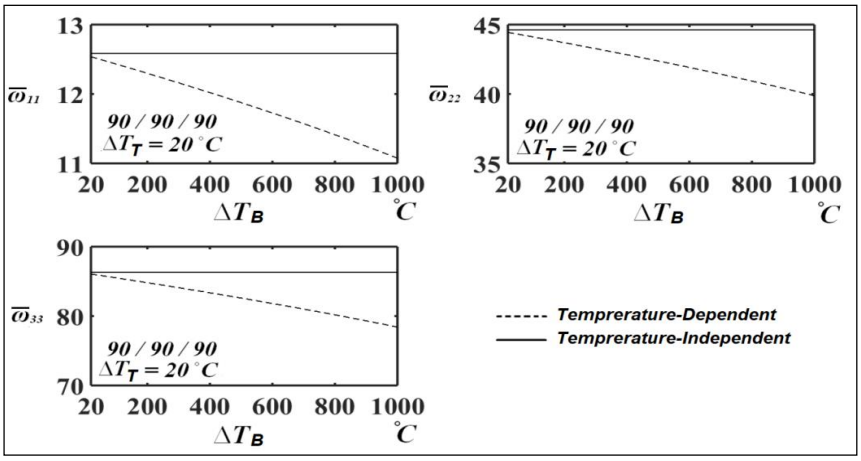


Fig. 10. The natural frequencies versus temperature rising for the three layers for stacking sequence 90/90/90 for a) $\bar{\omega}_{11}$ b) $\bar{\omega}_{22}$ and c) $\bar{\omega}_{33}$.

Figures 2-10 display that increasing in temperature, dimensionless frequency of laminated plate decreases significantly. With increasing temperature, the results of difference between temperature dependent and independent properties increase considerably.

Frequencies of temperature dependent are smaller than the frequencies of temperature independent. This is because; with the temperature increase, the strength of laminated plate decreases in the temperature dependent physical properties, so the frequencies decrease naturally. However, the strength of the laminated plate does not change with temperature increase in the temperature independent physical properties.

With changing the orientation angles, the dimensionless frequency change significantly. With increasing the orientation angles from 0 degree, the dimensionless frequency decrease considerably. Also, the stacking sequence play important role on vibration characterises of the laminated composite plate. In is observed from these figures that stacking sequence is very effective on thermal vibration responses.

## 4. Conclusions

In the presented paper, free vibration of a laminated plate is studied under thermal loading by using FSDPT in temperature-dependent physically properties. Cross-ply laminated sequence and simply-supported boundary conditions are considered. The Navier solution is implemented in the solution method. Effects of temperature, sequence of laminas and orientation angle of layers on the vibration characterises of laminated plate are investigated in temperature dependent physical properties. Also, difference between temperature dependent and independent are examined on the vibration results. As seen from the graphs that increasing temperature yields to increasing difference between the temperature dependent and independent results. Increasing fiber orientation angles and temperature yields to decreasing the frequency values. Frequencies of temperature dependent physical properties are smaller than those of temperature independent's. Stacking sequence and orientation angle of layers play important role on vibration behavior of composite laminated plates.

## Acknowledgments

This work has been supported by Research Fund of the Bursa Technical University. Project Number: 172L22.

## References

[1] Pal, M. C., Large amplitude free vibration of circular plates subjected to aerodynamic heating. *International Journal of Solids and Structures*, 6(3), 301-313, 1970.
[2] Chen, L.W., Chen, L.Y., Thermal buckling behavior of laminated composite plates with temperature-dependent properties. *Composite Structures*, 13(4), 275-287, 1989.
[3] Chen, L.W., Chen, L.Y., Thermal postbuckling behaviors of laminated composite plates with temperature-dependent properties. *Composite Structures*, 19(3), 267-283, 1991.
[4] Liu, C.F., Huang, C.H., Free vibration of composite laminated plates subjected to temperature changes. *Computers & Structures*, 60(1), 95-101, 1996.
[5] Lee, J.M., Chung, J.H., Chung, T.Y., Free vibration analysis of symmetrically laminated composite rectangular plates. *Journal of Sound and Vibration*, 199(1), 71-85 1997.
[6] Reddy, J.N., Chin, C.D., Thermomechanical analysis of functionally graded cylinders and plates. *Journal of Thermal Stresses*, 21(6), 593-626, 1998.
[7] Lee, H.J., Saravanos, D.A., The effect of temperature dependent material properties on the response of piezoelectric composite materials. *Journal of Intelligent Material Systems and Structures*, 9(7), 503-508, 1998.
[8] Reddy, J.N., Analysis of functionally graded plates. *International Journal for Numerical Methods in Engineering*, 47(1-3), 663-684, 2000.
[9] Jane, K.C., Hong, C.C., Thermal bending analysis of laminated orthotropic plates by the generalized differential quadrature method. *Mechanics Research Communications*, 27(2), 157-164, 2000.
[10] Shen, H.S., Thermal postbuckling behavior of imperfect shear deformable laminated plates with temperature-dependent properties. *Computer Methods in Applied Mechanics and Engineering*, 190(40-41), 5377-5390, 2001.
[11] Singha, M.K., Ramachandra, L.S., Bandyopadhyay, J.N., Thermal postbuckling analysis of laminated composite plates. *Composite Structures*, 54(4), 453-458, 2001.
[12] Sayman, O., Elastic-plastic and residual stresses in symmetric aluminum metal-matrix laminated plates under a linear thermal loading. *Journal of Thermal Stresses*, 26(4), 391-406, 2003.
[13] Patel, B.P., Lele, A.V., Ganapathi, M., Gupta, S.S., Sambandam, C.T., Thermo-flexural analysis of thick laminates of bimodulus composite materials. *Composite Structures*, 63(1), 11-20, 2004.

[14] Shukla, K.K., Huang, J.H., Nath, Y., Thermal postbuckling of laminated composite plates with temperature dependent properties. *Journal of Engineering Mechanics*, 130(7), 818-825, 2004.
[15] Liew, K.M., Yang, J., Kitipornchai, S., Thermal post-buckling of laminated plates comprising functionally graded materials with temperature-dependent properties. *Journal of Applied Mechanics*, 71(6), 839-850, 2004.
[16] Emery, T.R., Dulieu-Barton, J.M., Earl, J.S., Cunningham, P.R. A generalised approach to the calibration of orthotropic materials for thermoelastic stress analysis. *Composites Science and Technology*, 68(3-4), 743-752, 2008.
[17] Shen, H.S., Nonlinear bending of functionally graded carbon nanotube-reinforced composite plates in thermal environments. *Composite Structures*, 91(1), 9-19, 2009.
[18] Zenkour, A.M., Alghamdi, N.A., Bending analysis of functionally graded sandwich plates under the effect of mechanical and thermal loads. *Mechanics of Advanced Materials and Structures*, 17(6), 419-432, 2010.
[19] Vosoughi, A.R., Malekzadeh, P., Banan, M.R., Thermal postbuckling of laminated composite skew plates with temperature-dependent properties. *Thin-Walled Structures*, 49(7), 913-922, 2011.
[20] Kishore, M.H., Singh, B.N., Pandit, M.K., Nonlinear static analysis of smart laminated composite plate. *Aerospace Science and Technology*, 15(3), 224-235, 2011.
[21] Sahoo, R., Singh, B.N., A new inverse hyperbolic zigzag theory for the static analysis of laminated composite and sandwich plates. *Composite structures*, 105, 385-397, 2013.
[22] Carrera, E., Cinefra, M., Fazzolari, F.A., Some results on thermal stress of layered plates and shells by using unified formulation. *Journal of Thermal Stresses*, 36(6), 589-625, 2013.
[23] Sahoo, R., Singh, B.N., A new shear deformation theory for the static analysis of laminated composite and sandwich plates. *International Journal of Mechanical Sciences*, 75, 324-336, 2013.
[24] Chen, C.S., Chen, C.W., Chen, W.R., Chang, Y.C., Thermally induced vibration and stability of laminated composite plates with temperature-dependent properties. *Meccanica*, 48(9), 2311-2323, 2013.
[25] Torabizadeh, M.A., Fereidoon, A., Navier-type bending analysis of general composite laminates under different types of thermomechanical loading. *Mechanics*, 19(4), 380-389, 2013.
[26] Houmat, A., Nonlinear free vibration of laminated composite rectangular plates with curvilinear fibers. *Composite Structures*, 106, 211-224, 2013.
[27] Khorshid, K., Farhadi, S., Free vibration analysis of a laminated composite rectangular plate in contact with a bounded fluid. *Composite structures*, 104, 176-186, 2013.
[28] Akbaş, Ş.D., Free vibration characteristics of edge cracked functionally graded beams by using finite element method. *International Journal of Engineering Trends and Technology*, 4(10), 4590-4597, 2013.
[29] Akbaş, Ş.D., Free vibration and bending of functionally graded beams resting on elastic foundation. *Research on Engineering Structures and Materials*, 1(1), 2015.
[30] Akbaş, Ş.D., Free vibration of axially functionally graded beams in thermal environment. *International Journal Of Engineering & Applied Sciences*, *6*(3), 37-51, 2014.
[31] Akbaş, Ş.D., Free vibration of edge cracked functionally graded microscale beams based on the modified couple stress theory. *International Journal of Structural Stability and Dynamics*, 17(03), 1750033, 2017.
[32] Akbaş, Ş.D., Geometrically nonlinear static analysis of edge cracked Timoshenko beams composed of functionally graded material. *Mathematical Problems in Engineering*, 2013.
[33] Akbaş, Ş.D., On post-buckling behavior of edge cracked functionally graded beams under axial loads. *International Journal of Structural Stability and Dynamics*, *15*(04), 1450065, 2015.
[34] Akbaş, Ş.D. Free Vibration Analysis of Edge Cracked Functionally Graded Beams Resting on Winkler-Pasternak Foundation. *International Journal of Engineering & Applied Sciences*, *7*(3), 1-15, 2015.
[35] Akbaş, Ş.D., Thermal effects on the vibration of functionally graded deep beams with porosity. *International Journal of Applied Mechanics*, *9*(05), 1750076, 2017.
[36] Akbaş, Ş.D., Forced vibration analysis of functionally graded porous deep beams. *Composite Structures*, *186*, 293-302, 2018.
[37] Akbaş, Ş.D., Wave propagation of a functionally graded beam in thermal environments. *Steel and Composite Structures*, *19*(6), 1421-1447, 2015.

[38] Akbaş, Ş.D., Forced vibration analysis of cracked functionally graded microbeams. *Advances in Nano Research*, *6*(1), 39-55, 2018.
[39] Sayyad, A.S., Shinde, B.M., Ghugal, Y.M., Thermoelastic bending analysis of laminated composite plates according to various shear deformation theories. *Open Engineering (formerly Central European Journal of Engineering)*, 5(1), 18-30, 2015.
[40] Sayyad, A.S., Ghugal, Y.M., Mhaske, B. A. A four-variable plate theory for thermoelastic bending analysis of laminated composite plates. *Journal of Thermal Stresses*, 38(8), 904-925, 2015.
[41] Li, Z.M., Qiao, P., Thermal postbuckling analysis of anisotropic laminated beams with different boundary conditions resting on two-parameter elastic foundations. *European Journal of Mechanics-A/Solids*, 54, 30-43, 2015.
[42] Li, Z.M., Qiao, P., Buckling and postbuckling behavior of shear deformable anisotropic laminated beams with initial geometric imperfections subjected to axial compression. *Engineering Structures*, 85, 277-292, 2015.
[43] Akbaş, Ş.D. Static analysis of a nano plate by using generalized differential quadrature method. *International Journal Of Engineering & Applied Sciences*, *8*(2), 30-39, 2016.
[44] Ramos, I.A., Mantari, J. L., Zenkour, A.M., Laminated composite plates subject to thermal load using trigonometrical theory based on Carrera Unified Formulation. *Composite Structures*, 143, 324-335, 2016.
[45] Akbaş, Ş.D. Stability of a non-homogenous porous plate by using generalized differantial quadrature method. *International Journal of Engineering and Applied Sciences*, *9*, 147-155, 2017.
[46] Akbaş, Ş.D. Vibration and static analysis of functionally graded porous plates. *Journal of Applied and Computational Mechanics*, *3*(3), 199-207, 2017.
[47] Choudhury, A., Mondal, S.C., Sarkar, S. Effect of lamination angle and thickness on analysis of composite plate under thermo mechanical loading. *Strojnícky casopis–Journal of Mechanical Engineering*, 67(1), 5-22, 2017.
[48] Akbaş, Ş.D. Large deflection analysis of a fiber reinforced composite beam. *Steel and Composite Structures, An International Journal ,27*(5), 567-576, 2018.
[49] Akbaş, Ş.D. Post-buckling responses of a laminated composite beam. *Steel and Composite Structures*, *26*(6), 733-743, 2018.
[50] Akbaş, Ş.D. İki Malzemeli Kompozit Bir Kirişin Serbest ve Zorlanmış Titreşimlerinin İncelenmesi. *Politeknik Dergisi*, *21*(1), 65-73,2018.
[51] Akbaş, Ş.D. Geometrically nonlinear analysis of a laminated composite beam. *Structural Engineering and Mechanics, An International Journal , 66*(1), 27-36, 2018.
[52] Yüksel, Y.Z., Akbaş, Ş.D., Kara, İ.F., Sıcaklık Etkisi Altındaki Bir Plağın Serbest Titreşim Analizi. *20. Ulusal Mekanik Kongresi*, Bursa, Turkey, 2017.
[53] Yüksel, Y.Z., and Akbaş, Ş.D., Stress Analysis of a Laminated Composite Plate Under Temperature Rising. *7th International Conference on Advanced Technologies*, Antalya, Turkey, 2018.
[54] Baltacıoglu A.K., Akgoz, B., Civalek, O., Nonlinear static response of laminated composite plates by discrete singular convolution method. *Composite Structures* 93,153–161, 2010.
[55] Baltacıoglu, A.K., Civalek, O., Akgoz, B., Demir, F., Large deflection analysis of laminated composite plates resting on nonlinear elastic foundations by the method of discrete singular convolution. *International Journal of Pressure Vessels and Piping* 88, 290-300, 2011.
[56] Baltacıoglu, A.K., Akgoz, B., Civalek, O., Nonlinear static response of laminated composite plates by discrete singular convolution method. *Composite Structures* 93, 153–161, 2010.
[57] Civalek, O., Nonlinear dynamic response of laminated plates resting on nonlinear elastic foundations by the discrete singular convolution-differential quadrature coupled approaches. *Composites: Part B*, 50, 171–179, 2013.
[58] Shahba, A., Attarnejada, R., Hajilar, S., Free vibration and stability of axially functionally graded tapered Euler-Bernoulli beams. *Shock and Vibration*, 18,683–696, 2011.
[59] Civalek, O., Demir, C., Buckling and bending analyses of cantilever carbon nanotubes using the eulerbernoulli beam theory on non-local continuum model. *Asian Journal of Civil Engineering*, 12(5), 651-661, 2011.
[60] Akgöz, B, Civalek, O., Buckling analysis of cantilever carbon nanotubes using the strain gradient elasticity and modified couple stress theories. *Journal of Computational and Theoretical Nanoscience*, 8, 1821-1827, 2011.

[61] Wan Ji Chen, WJ., Li, XP., Size-dependent free vibration analysis of composite laminated Timoshenko beam based on new modified couple stress theory. *Arch Appl Mech*, 83, 431–444, 2013.
[62] Mercan, K., Civalek, O., DSC method for buckling analysis of boron nitride nanotube (BNNT) surrounded by an elastic matrix. *Composite Structures*, 143, 300–309, 2016.
[63] Demir, C., Mercan, K., Civalek, O. Determination of critical buckling loads of isotropic, FGM and laminated truncated conical panel. *Composites Part* B, 94,1-10, 2016.
[64] Mercan, K., Civalek, O., Buckling analysis of Silicon carbide nanotubes (SiCNTs) with surface effect and nonlocal elasticity using the method of HDQ. *Composites Part B*, 114, 34-45, 2017.
[65] Civalek, O., Free vibration of carbon nanotubes reinforced (CNTR) and functionally graded shells and plates based on FSDT via discrete singular convolution method. *Composites Part B*, 111,45-59, 2017.
[66] Mercan, K., Ersoy, H. and Civalek, O., (2016). Free vibration of annular plates by discrete singular convolution and differential quadrature methods. *Journal of Applied and Computational Mechanics*, 2(3), 128-133, 2017.
[67] Shen, H.S., Thermal postbuckling of imperfect shear-deformable laminated plates on two-parameter elastic foundations. *Mechanics of Composite Materials and Structures*, 6, 207-228, 1999.
[68] Li, Z.M. and Qiao, P., Thermal postbuckling analysis of anisotropic laminated beams with different boundary conditions resting on two-parameter elastic foundations. *European Journal of Mechanics-A/Solids*, 54, 30-43, 2015.
[69] Oh, I.K., Han, J.H., and Lee, I., Postbuckling and vibration characteristics of piezolaminated composite plate subject to thermo-piezoelectric loads. *Journal of Sound and Vibration*, 233(1), 19-40, 2000.

*International Journal of Engineering & Applied Sciences (IJEAS)*
*Vol.10, Issue 3 (2018) 190-206*
*http://dx.doi.org/10.24107/ijeas.456494*
Int J Eng Appl Sci 10(3) (2018) 190-206

# Thermo-resonance analysis of an excited graphene sheet using a new approach

*Mohammad Malikan [a*], Rossana Dimitri [b], Francesco Tornabene [c]*

*[a] Department of Mechanical Engineering, Islamic Azad University, Mashhad Branch, Mashhad, Iran,*
*[b,c] Department of Innovation Engineering, Università del Salento, Lecce, Italy,*
*E-mail address*: mohammad.malikan@yahoo.com [a], rossana.dimitri@unisalento.it [b],
francesco.tornabene@unisalento.it [c]

*Received date: 31.08.2018*
*Accepted date: 30.10.2018*

*ORCID numbers of authors*
0000-0001-7356-2168[a], 0000-0001-7153-4307[b], 0000-0002-5968-3382[c]

**Abstract**

*This paper analyzes the thermo-vibration response of a graphene sheet excited with a uniform harmonic The problem is here tackled with a novel approach combined with a nonlocal strain gradient theory (NSGT), in order to include the size-dependence and the nonlocality effect on impacts. Simply-supported plates are here studied analytically, according to the Navier's method. Thus, the thermo-forced vibration equations of the problem are here written and solved numerically for graphene sheets. The accuracy of the proposed theory is checked by means of several comparative evaluations with respect to the available results from literature. Another key aspect of the works is the sensitivity of the thermo-mechanical response of the plate structures to different thermal and mechanical input parameters. This could be of great interest for design purposes for many engineering applications, including nanoelectromechanical systems (NEMS), biosensors, piezoelectric devices, biomechanical tissues, among others.*

**Keywords:** Thermo-forced vibrations; A novel approach; Nonlocal theory of strain gradient

## 1. Introduction

Due to large variety of applications of graphene for many electronic components at the nanoscale, many studies in the literature on graphene materials have enhanced the development of lower-volume and high-speed electronic components. Graphene exhibits some physical properties usually not visible at a nanoscale level, namely, the high flexibility [1], the high thermal-mechanical resistance and elastic modulus [2]. More recently, an increased attention has been paid to graphene-based semiconductor photocatalysts [3], [4]. A graphene material is usually classified by means of a number of stacking layers, monolayer or multi-layer [5]. The use of a single-layer graphene nanoplate cannot only be a high-quality two-dimensional photocatalyst backup, but also can be a two-dimensional current circuit with a potentially significant potential for full redox and electrical properties [3]. To understand the main properties of single-layer graphene sheets, different works in literature have studied their mechanical and physical behavior. Among them, Ebrahimi and Barati [6] investigated the damped frequencies of nanoplates, according to a modified higher-order plate approach

combined with a general NSGT. The differential quadrature (DQ) technique has been applied to get numerical outcomes for simple edges. Radic and Jeremic [7] investigated the nonlocal stability of bi-layered nano sheets resting on a polymer foundation under in-plane thermal forces. Malikan et al. [8] employed the DQ technique to examine the stability of bi-layered nano sheets exposed to in-plane thermal and shear forces bridged on the polymer substrate. In the additional works by Malikan [9],[10], the author studied a laminated plate with graphene covering, subjected to in-plane mechanical forces, based on a refined couple stress theory [9], as well as the stability of nanoplates compressed nonuniformly [10]. The stability of nanoplates embedded on a polymer substrate was also analyzed by Shahsavari et al. [11] in a hygrothermal environment, while applying different NSGTs. Additional applications of nonlocal methods can be found in literature for stability problems of graphene sheets in thermal environment [12], or frequency problems of nano sheets under axial magnetic forces [13], nonlinear natural frequencies of beams made of graded materials reinforced with nanoplatelets [14]. Moreover, Gholami and Ansari [15] studied the nonlinear vibration of composite rectangular plates reinforced with graphene platelets, through the application of the third-order shear deformation model. Further relevant works on the topic can be found in [16-51], where different nanostructures have been considered for varying conditions.

Differently from the available literature on the topic, here we propose a refined plate approach with a reduced number of variables in comparison with the first-order shear deformation theory. The nanoplate is excited uniformly and harmonically under a transverse load. To model the thermo-vibration response, the nanoplate is considered in a thermal environment. The nonlocal reaction between atoms is here analyzed trough a nonlocal elasticity theory, whereby the mechanical behavior at a microscale and nanoscale accounts for the size-dependence of impacts and stiffness, in agreement with experimental evidences. Hence, the microstructural problem is here tackled with a modified couple stress method, whereas the nanostructural one is here studied accounting for the second order strain gradient term. A theoretical procedure is here proposed for the study of the thermomechanical behavior of simply supported nanoplates, while exploring the accuracy of the method and the sensitivity of the response to different input parameters.

## 2. Mathematical modeling

Fig. 1a shows an idealized and realistic model for graphene nanoplates. The plate is characterized by a length $L_x$, width $L_y$ and thickness $h$ in a Cartesian coordinate system, and it is pressured transversely by a uniform dynamic force in a thermal environment. More details about the dynamic force acting transversely on the body are depicted in Fig. 1b [52]. A novel plate model is here proposed, which assumes the following displacement field [53-59]

$$\begin{Bmatrix} U(x,y,z,t) \\ V(x,y,z,t) \\ W(x,y,z,t) \end{Bmatrix} = \begin{Bmatrix} u(x,y,t) - z\,\dfrac{\partial w_0(x,y,t)}{\partial x} \\ v(x,y,t) - z\,\dfrac{\partial w_0(x,y,t)}{\partial y} \\ w_0(x,y,t) + A\,\dfrac{\partial^2 w_0(x,y,t)}{\partial x^2} + B\,\dfrac{\partial^2 w_0(x,y,t)}{\partial y^2} \end{Bmatrix} \tag{1}$$

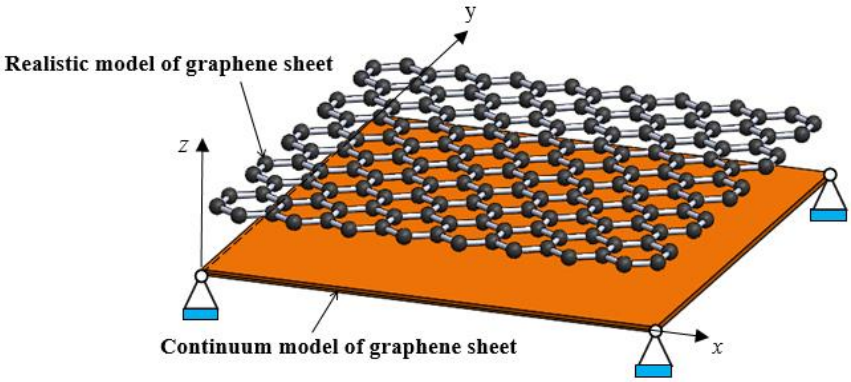


Fig.1a. Graphene nanoplate subjected to thermal environment in 3D Cartesian coordinate system

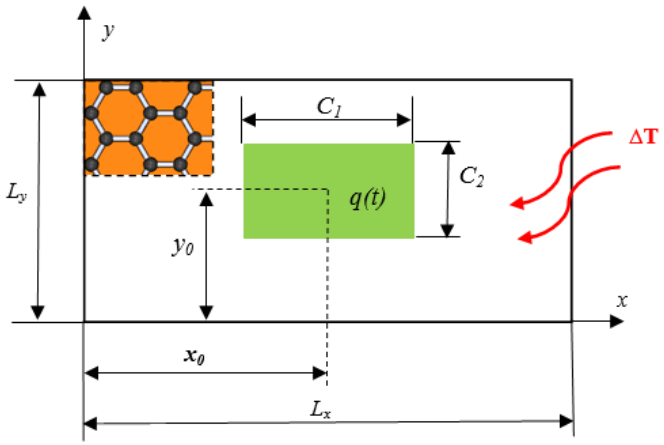


Fig.1b. The dynamic load acted harmonically and uniformly

As far as the Hamilton's approach is concerned, the potential energy of the model, *V*, is defined as [60]

$$\delta V = \delta \int_0^t (S + \Omega - T)dt = 0 \tag{2}$$

where $\delta\Omega$ is the variation of the external work, $\delta T$ refers to the variation of the kinetic energy and $\delta S$ is the variation of the strain energy. This last contribution is computed as

$$\delta S = \iiint_v \sigma_{ij} \delta\varepsilon_{ij} dV = 0 \tag{3}$$

Eq. (1) is substituted in the nonlinear Lagrangian strain filed, which leads to [58]

$$\begin{Bmatrix}\varepsilon_{xx}\\ \varepsilon_{yy}\\ \gamma_{xz}\\ \gamma_{yz}\\ \gamma_{xy}\end{Bmatrix}=$$

$$\begin{Bmatrix}\dfrac{\partial u}{\partial x}-z\,\dfrac{\partial^2 w_0}{\partial x^2}+\dfrac{1}{2}\left(A\,\dfrac{\partial^3 w_0}{\partial x^3}+B\,\dfrac{\partial^3 w_0}{\partial x\,\partial y^2}+\dfrac{\partial w_0}{\partial x}\right)^2\\ \dfrac{\partial v}{\partial y}-z\,\dfrac{\partial^2 w_0}{\partial y^2}+\dfrac{1}{2}\left(A\,\dfrac{\partial^3 w_0}{\partial x^2\partial y}+B\,\dfrac{\partial^3 w_0}{\partial y^3}+\dfrac{\partial w_0}{\partial y}\right)^2\\ A\,\dfrac{\partial^3 w_0}{\partial x^3}+B\,\dfrac{\partial^3 w_0}{\partial x\,\partial y^2}\\ A\,\dfrac{\partial^3 w_0}{\partial x^2\partial y}+B\,\dfrac{\partial^3 w_0}{\partial y^3}\\ \left(\dfrac{\partial u}{\partial y}+\dfrac{\partial v}{\partial x}\right)-2z\,\dfrac{\partial^2 w_0}{\partial x\,\partial y}+\left(A\,\dfrac{\partial^3 w_0}{\partial x^3}+B\,\dfrac{\partial^3 w_0}{\partial x\,\partial y^2}+\dfrac{\partial w_0}{\partial x}\right)\left(A\,\dfrac{\partial^3 w_0}{\partial x^2\partial y}+B\,\dfrac{\partial^3 w_0}{\partial y^3}+\dfrac{\partial w_0}{\partial y}\right)\end{Bmatrix} \quad (4)$$

Furthermore, the kinetic energy is defined as [52, 60]

$$T=\frac{1}{2}\int_A\int_{-h/2}^{h/2}\rho(z,T)\left(\left(\frac{\partial U}{\partial t}\right)^2+\left(\frac{\partial V}{\partial t}\right)^2+\left(\frac{\partial W}{\partial t}\right)^2\right)dz\,dA=0 \quad (5)$$

whereas its variational form reads as follows

$$\begin{aligned}\delta T=\int_A\int_{-h/2}^{h/2}\rho(z,T)\Bigg[\Bigg(&-z^2\frac{\partial^4 w_0}{\partial x^2\partial t^2}-z^2\frac{\partial^4 w_0}{\partial y^2\partial t^2}-\frac{\partial^2 w_0}{\partial t^2}-A^2\frac{\partial^6 w_0}{\partial x^4\partial t^2}\\ &-B^2\frac{\partial^6 w_0}{\partial y^4\partial t^2}-2A\frac{\partial^4 w_0}{\partial x^2\partial t^2}-2B\frac{\partial^4 w_0}{\partial y^2\partial t^2}-2AB\frac{\partial^6 w_0}{\partial x^2\partial y^2\partial t^2}\Bigg)\delta w_0\Bigg]dz\,dA=0\end{aligned} \quad (6)$$

The numerical terms in the Eq. (6) denote the mass moments of inertia, namely [52, 60]

$$(I_0,I_2)=\int_{-h/2}^{h/2}\rho(z,T)\left(1,z^2\right)dz \quad (7)$$

Thus, the governing equations of the problem read as follows

$$
\begin{aligned}
&-\frac{\partial^2 M_x}{\partial x^2}-\frac{\partial^2 M_y}{\partial y^2}-2\frac{\partial^2 M_{xy}}{\partial x\,\partial y}+A\frac{\partial^3 Q_x}{\partial x^3}+B\frac{\partial^3 Q_x}{\partial x\,\partial y^2}+A\frac{\partial^3 Q_y}{\partial x^2\partial y}+B\frac{\partial^3 Q_y}{\partial y^3}+\\
&N_x\left(A^2\frac{\partial^6 w_0}{\partial x^6}+B^2\frac{\partial^6 w_0}{\partial x^2\partial y^4}+\frac{\partial^2 w_0}{\partial x^2}+2AB\frac{\partial^6 w_0}{\partial x^4\partial y^2}+2A\frac{\partial^4 w_0}{\partial x^4}+2B\frac{\partial^4 w_0}{\partial x^2\partial y^2}\right)+\\
&N_y\left(A^2\frac{\partial^6 w_0}{\partial x^4\partial y^2}+B^2\frac{\partial^6 w_0}{\partial y^6}+\frac{\partial^2 w_0}{\partial y^2}+2AB\frac{\partial^6 w_0}{\partial x^2\partial y^4}+2A\frac{\partial^4 w_0}{\partial x^2\partial y^2}+2B\frac{\partial^4 w_0}{\partial y^4}\right)+\\
&N_{xy}\left(2A^2\frac{\partial^6 w_0}{\partial x^5\partial y}+4AB\frac{\partial^6 w_0}{\partial x^3\partial y^3}+4A\frac{\partial^4 w_0}{\partial x^3\partial y}+2B^2\frac{\partial^6 w_0}{\partial x\,\partial y^5}+4B\frac{\partial^4 w_0}{\partial x\,\partial y^3}+2\frac{\partial^2 w_0}{\partial x\,\partial y}\right)-\\
&I_2\left(\frac{\partial^4 w_0}{\partial x^2\partial t^2}+\frac{\partial^4 w_0}{\partial y^2\partial t^2}\right)-I_0\left(\frac{\partial^2 w_0}{\partial t^2}+A^2\frac{\partial^6 w_0}{\partial x^4\partial t^2}+B^2\frac{\partial^6 w_0}{\partial y^4\partial t^2}+2A\frac{\partial^4 w_0}{\partial x^2\partial t^2}+2B\frac{\partial^4 w_0}{\partial y^2\partial t^2}+\right.\\
&\left.2AB\frac{\partial^6 w_0}{\partial x^2\partial y^2\partial t^2}\right)=q\left(x,y,t\right)
\end{aligned}
\tag{8}
$$

where $N_i$, $Q_i$, and $M_i$ *(i= x, y, xy)* denote the stress resultants, in terms of axial forces, shear forces, and moments. Constants $D_{ij}$ (i, j = 1, 2, and 6) and $H_{44}$ are described by

$$
H_{44}=Gh,\ G=\frac{E}{2\left(1+\upsilon\right)},\ Q_{11}=\frac{E}{1-\upsilon^2}=Q_{22},\ Q_{12}=\frac{\upsilon E}{1-\upsilon^2},\ Q_{66}=G \tag{9}
$$

$$
D_{ij}=\int_{-\frac{h}{2}}^{\frac{h}{2}}\left(z^2\right)Q_{ij}dz\qquad\left(i=1,2,6\right) \tag{10}
$$

where $\nu$ is the Poisson′s ratio, $E$ is the Young's modulus, and $G$ is the shear modulus for isotropic graphene sheets. Some detail about the NSGT, here applied for the theoretical study, is presented in what follows [52, 58]

$$
\begin{aligned}
&\left(1-\mu_1\nabla^2\right)\left(1-\mu_0\nabla^2\right)\sigma_{ij}=C_{ijkl}\left(1-\mu_1\nabla^2\right)\varepsilon_{kl}-C_{ijkl}\,l^2\left(1-\mu_0\nabla^2\right)\nabla^2\varepsilon_{kl}\ ;\\
&\mu_0\left(nm^2\right)=\left(e_0a\right)^2,\ \mu_1\left(nm^2\right)=\left(e_1a\right)^2,\ \nabla^2=\frac{\partial^2}{\partial x^2}+\frac{\partial^2}{\partial y^2}
\end{aligned}
\tag{11}
$$

where, $\mu_0$ and $\mu_1$ refer to lower and higher-order nonlocal parameters, ($l$) is the length scale parameter. The local stress resultants read

$$
\left(N_x,N_y,N_{xy}\right)=\int_{-h/2}^{h/2}\left(\sigma_x,\sigma_y,\sigma_{xy}\right)dz \tag{12}
$$

$$
\left(M_x,M_y,M_{xy}\right)=\int_{-h/2}^{h/2}\left(\sigma_x,\sigma_y,\sigma_{xy}\right)zdz \tag{13}
$$

$$
\left(Q_x,Q_y\right)=\int_{-h/2}^{h/2}\left(\sigma_{xz},\sigma_{yz}\right)dz \tag{14}
$$

By combining Eqs. (4), (12)-(14), the stress resultants become

$$\begin{bmatrix} N_{xx} \\ N_{yy} \\ N_{xy} \\ M_{xx} \\ M_{yy} \\ M_{xy} \\ Q_y \\ Q_x \end{bmatrix} = \begin{bmatrix} A_{11} & A_{12} & 0 & 0 & 0 & 0 & 0 & 0 \\ A_{21} & A_{22} & 0 & 0 & 0 & 0 & 0 & 0 \\ 0 & 0 & A_{66} & 0 & 0 & 0 & 0 & 0 \\ 0 & 0 & 0 & D_{11} & D_{12} & 0 & 0 & 0 \\ 0 & 0 & 0 & D_{21} & D_{22} & 0 & 0 & 0 \\ 0 & 0 & 0 & 0 & 0 & D_{66} & 0 & 0 \\ 0 & 0 & 0 & 0 & 0 & 0 & H_{44} & 0 \\ 0 & 0 & 0 & 0 & 0 & 0 & 0 & H_{44} \end{bmatrix} \times$$

$$\begin{bmatrix} \dfrac{\partial u}{\partial x}+\dfrac{1}{2}\left(A\dfrac{\partial^3 w_0}{\partial x^3}+B\dfrac{\partial^3 w_0}{\partial x\,\partial y^2}+\dfrac{\partial w_0}{\partial x}\right)^2 \\ \dfrac{\partial v}{\partial y}+\dfrac{1}{2}\left(A\dfrac{\partial^3 w_0}{\partial x^2\partial y}+B\dfrac{\partial^3 w_0}{\partial y^3}+\dfrac{\partial w_0}{\partial y}\right)^2 \\ \left(\dfrac{\partial u}{\partial y}+\dfrac{\partial v}{\partial x}\right)+\left(A\dfrac{\partial^3 w_0}{\partial x^3}+B\dfrac{\partial^3 w_0}{\partial x\,\partial y^2}+\dfrac{\partial w_0}{\partial x}\right)\left(A\dfrac{\partial^3 w_0}{\partial x^2\partial y}+B\dfrac{\partial^3 w_0}{\partial y^3}+\dfrac{\partial w_0}{\partial y}\right) \\ -\dfrac{\partial^2 w_0}{\partial x^2} \\ -\dfrac{\partial^2 w_0}{\partial y^2} \\ -\dfrac{\partial^2 w_0}{\partial x\,\partial y} \\ A\dfrac{\partial^3 w_0}{\partial x^2\partial y}+B\dfrac{\partial^3 w_0}{\partial y^3} \\ A\dfrac{\partial^3 w_0}{\partial x^3}+B\dfrac{\partial^3 w_0}{\partial x\,\partial y^2} \end{bmatrix}$$

$$-\begin{Bmatrix} N^T \\ N^T \\ 0 \\ 0 \\ 0 \\ 0 \\ 0 \\ 0 \end{Bmatrix};\ N^0=-N^T=-Eh\alpha\Delta T\left(\frac{1+\upsilon}{1-\upsilon^2}\right) \tag{15}$$

where $N^T$ is the axial load associated to the thermal environment, $\alpha$ is the thermal expansion of the graphene sheet, and $\Delta T=T_2-T_1$ is the temperature variation in the thickness direction. Here we set a reference value for the temperature equal to $T_1=300K$. Then, we can use of Eq.

(11) to re-formulate the stress resultants, in order to obtain their nonlocal strain gradient form, namely

$$\left(1-\left(\mu_0+\mu_1\right)\nabla^2+\mu_0\mu_1\nabla^4\right)M_x=-\left[\left(1-\mu_1\nabla^2\right)-l^2\left(1-\mu_0\nabla^2\right)\nabla^2\right]\left(D_{11}\frac{\partial^2 w_0}{\partial x^2}+D_{12}\frac{\partial^2 w_0}{\partial y^2}\right) \quad (16)$$

$$\left(1-\left(\mu_0+\mu_1\right)\nabla^2+\mu_0\mu_1\nabla^4\right)M_y=-\left[\left(1-\mu_1\nabla^2\right)-l^2\left(1-\mu_0\nabla^2\right)\nabla^2\right]\left(D_{21}\frac{\partial^2 w_0}{\partial x^2}+D_{22}\frac{\partial^2 w_0}{\partial y^2}\right) \quad (17)$$

$$\left(1-\left(\mu_0+\mu_1\right)\nabla^2+\mu_0\mu_1\nabla^4\right)M_{xy}=-\left[\left(1-\mu_1\nabla^2\right)-l^2\left(1-\mu_0\nabla^2\right)\nabla^2\right]\left(D_{66}\frac{\partial^2 w_0}{\partial x\,\partial y}\right) \quad (18)$$

$$\left(1-\left(\mu_0+\mu_1\right)\nabla^2+\mu_0\mu_1\nabla^4\right)Q_x=\left[\left(1-\mu_1\nabla^2\right)-l^2\left(1-\mu_0\nabla^2\right)\nabla^2\right]H_{44}\left(A\frac{\partial^3 w_0}{\partial x^3}+B\frac{\partial^3 w_0}{\partial x\,\partial y^2}\right) \quad (19)$$

$$\left(1-\left(\mu_0+\mu_1\right)\nabla^2+\mu_0\mu_1\nabla^4\right)Q_y=\left[\left(1-\mu_1\nabla^2\right)-l^2\left(1-\mu_0\nabla^2\right)\nabla^2\right]H_{44}\left(A\frac{\partial^3 w_0}{\partial x^2\partial y}+B\frac{\partial^3 w_0}{\partial y^3}\right) \quad (20)$$

The thermo-excited vibration equations, can be obtained with combining Eq. (16)-(20) whilst inserting them into Eq. (8).

## 3. Analytical approach

This section employs the Navier's solution in order to study the behavior of simply-supported edges and solve the harvested equations, based on the following displacement equation [52, 56]

$$w_0\left(x,y,t\right)=\sum_{m=1}^{\infty}\sum_{n=1}^{\infty}W_{0mn}\exp\left(i\,\omega_n t\right)\sin\left(\frac{m\pi}{L_x}x\right)\sin\left(\frac{n\pi}{L_y}y\right) \quad (21)$$

In Eq. (21), $m$ and $n$ denote the half-wave numbers, $W_{0mn}$ is the displacement amplitude, and $\omega_n$ refer to the natural frequencies. The transverse dynamic loading applied uniformly and harmonically on the structure, reads [52, 56]

$$q\left(x,y,t\right)=\sum_{n=1}^{\infty}\sum_{m=1}^{\infty}q_m\exp\left(i\,\omega_{ex}t\right)\times\sin\left(\frac{m\pi}{L_x}x\right)\sin\left(\frac{n\pi}{L_y}y\right) \quad (22)$$

$$q_m=\frac{4q_0}{mn}\int_{y_0-c_2/2}^{y_0+c_2/2}\int_{x_0-c_1/2}^{x_0+c_1/2}\sin\left(\frac{m\pi}{L_x}x\right)\sin\left(\frac{n\pi}{L_y}y\right)dxdy=$$
$$\frac{16q_0}{mn\pi^2}\sin\left(\frac{m\pi}{L_x}x_0\right)\sin\left(\frac{m\pi}{L_x}\frac{c_1}{2}\right)\sin\left(\frac{n\pi}{L_y}y_0\right)\sin\left(\frac{n\pi}{L_y}\frac{c_2}{2}\right) \quad (23)$$

where, $q_m$ represents the Fourier coefficient, $q_0$ denotes the load amplitude, and $\omega_{ex}$ denotes the excitation frequency. The algebraic equations can be obtained by inserting Eq. (21) and (22) into thermo-excited vibration equations. Thus yields the following relation

$$\left(\left[k\right]-\Delta r^2\left[m\right]\right)\left\{W_{0mn}\right\}=\left\{\left(1-\left(\mu_0^2+\mu_1^2\right)\nabla^2+\mu_0^2\mu_1^2\nabla^4\right)q\left(x,y,t\right)\right\} \tag{24}$$

$$\Delta r=\frac{\omega_{ex}}{\omega_n} \tag{25}$$

where, $\Delta r$ stands for the excitation-to-natural frequency ratio, $k_{ij}$ ($i, j$=1, 2, 3) and $m_{ij}$ ($i, j$=1, 2, 3) refer to the stiffness and mass matrixes, respectively. After the enforcement of the null value to the determinant of the matrix coefficients, and after some mathematical manipulation, we can obtain the natural frequencies of the problem. Afterwards, by substituting the numerical frequencies into the thermo-excited vibration equations of the problem, the dynamic deflections can be found.

## 3. Numerical results

This section is devoted to the preliminary check for the accuracy of the proposed approach with respect to the available theories form the literature. Table 1 compares our results, based on a One Variable FSDT (OVFSDT), with respect to several well-known references [61-63] based on the molecular dynamics (MD), or a FSDT-DQM approach. As can be observed, growing the plate's length, makes the results nearer to the MD ones. Basically, the excellent agreement between our results and predictions from the literature verifies the high accuracy of the proposed theory. Further comparative evaluations of the results can be found in Table 2, with respect to a DQM and MD approach, in terms of mechanical stability of grapheme sheets compressed biaxially, while assuming $\mu=1.81nm^2$, $k_s=5/6$, $\upsilon=0.16$, $E=1TPa$.

Table 1. Validation for mechanical stability of graphene sheet compressed biaxially. $\mu=1.81nm^2$, $k_s=5/6$, $\upsilon=0.16$, $E=1TPa$.

| Stability load (*nN/nm*) | | | | |
|---|---|---|---|---|
| OVFSDT | FSDT-DQM [61] | FSDT-DQM [62] | MD results [63] | $L_x=L_y$ (*nm*) |
| 1.0274 | 1.0749 | 1.0809 | 1.0837 | 4.99 |
| 0.62151 | 0.6523 | 0.6519 | 0.6536 | 8.080 |
| 0.43832 | 0.4356 | 0.4350 | 0.4331 | 10.77 |
| 0.26122 | 0.2645 | 0.2639 | 0.2609 | 14.65 |
| 0.17075 | 0.1751 | 0.1748 | 0.1714 | 18.51 |
| 0.11963 | 0.1239 | 0.1237 | 0.1191 | 22.35 |
| 0.08856 | 0.0917 | 0.0914 | 0.0889 | 26.22 |
| 0.06918 | 0.0707 | 0.0705 | 0.0691 | 30.04 |
| 0.05568 | 0.0561 | 0.0560 | 0.0554 | 33.85 |
| 0.04488 | 0.0453 | 0.0451 | 0.0449 | 37.81 |

Table 2. Comparative evaluation of the mechanical stability of graphene sheet compressed biaxially compared to the FSDT-DQM [62] and MD [63]. $\mu=1.81nm^2$, $k_s=5/6$, $\upsilon=0.16$, $E=1TPa$.

| Stability load (*nN/nm*) | | | |
|---|---|---|---|
| OVFSDT | FSDT-DQM [62] | MD results [63] | $L_x / L_y$ |
| 0.52449 | 0.5115 | 0.5101 | 0.5 |
| 0.56223 | 0.5715 | 0.5693 | 0.75 |
| 0.64225 | 0.6622 | 0.6595 | 1.25 |
| 0.75576 | 0.7773 | 0.7741 | 1.5 |
| 1.0134 | 1.0222 | 1.0183 | 1.75 |
| 1.1703 | 1.1349 | 1.1297 | 2 |

Table 3. Mechanical properties of graphene sheets.

| | |
|---|---|
| Isotropic graphene sheet [8, 56] | $E=1\ TPa$, $v=0.3$<br>$h=0.34\ nm$, $Lx=Ly=10.2\ nm$,<br>$\rho=2250\ kg/m^3$, $\alpha=1.1e\text{-}6K$ |

To consider several cases of nonlocality against the transverse harmonic load, Figs. 2 and 3 are displayed. First of all, the higher-order nonlocal parameter has been investigated with the help of different dynamic loading conditions. As it is observed, the dynamic deflections decreased for increasing higher-order nonlocalities. Fig. 3 shows the conditions of lower-order NSGT by changing the lower-order nonlocal parameter. It is worth noticing that an increased value for the higher-order nonlocal parameter has an increased impact on the dynamic deflection, than the lower-order nonlocal parameter (please, compare the plots of Figs. 2 and 3)

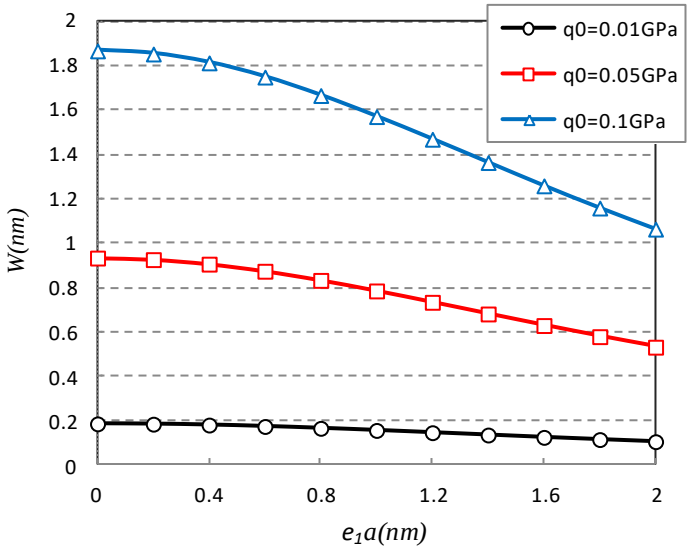


Fig.2. Transverse dynamic load vs. the higher-order nonlocal parameter. $e_0a=0.2\ nm$, $l=0.5h$, $m=n=1$, $\Delta r=0.1$, $\Delta T=200K$, $x_0=y_0=0.5L_x$, $c_1=c_2=L_x$.

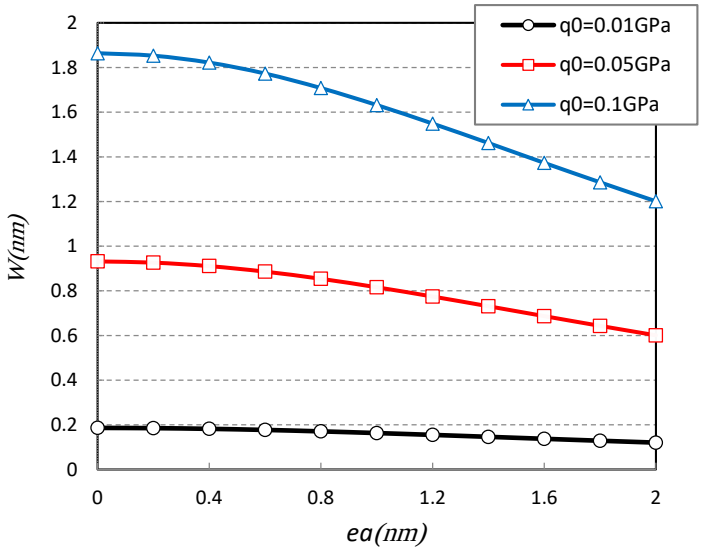


Fig.3. Transverse dynamic load vs. the nonlocal parameter. $e_0a= e_1a= ea$, $l=0.5h$, $\Delta r=0.1$, $m=n=1$, $\Delta T=200K$, $x_0=y_0=0.5L_x$, $c_1=c_2=L_x$.

Fig. 4 considers a higher-order NSGT for the graphene sheet under different excitation frequencies, and varying input geometrical parameters. As can be observed by these figures, the resonance situation occurs when $\Delta r=1$. Moreover, it is worth observing that after reaching the resonance condition, the dynamic deflections become smaller than those obtained before this resonance region. Naturally, if a large value of $\Delta r$ is assumed, the deflections cannot be significant, namely the system cannot have a vibrational response. It is interesting to note that a reduced distribution region for the transverse harmonic load, reduces the deformability of the structure. Furthermore, by comparing Fig. 4 and 5, we can observe that a farther distance of the centroid in the loaded region, yields meaningless deflections in the structure.

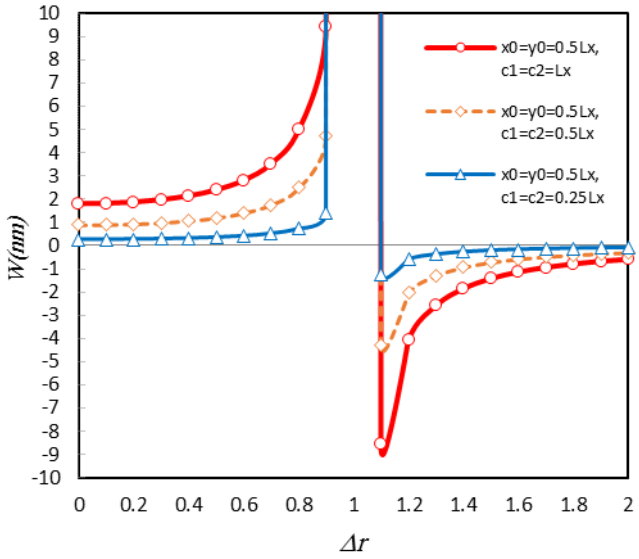


Fig.4. Distributed loads vs. the frequency ratio. $e_0a= 0.2$ nm, $e_1a= 0.4$ nm, $l=0.5h$, $q_0=0.1GPa$, $\Delta T=200K$.

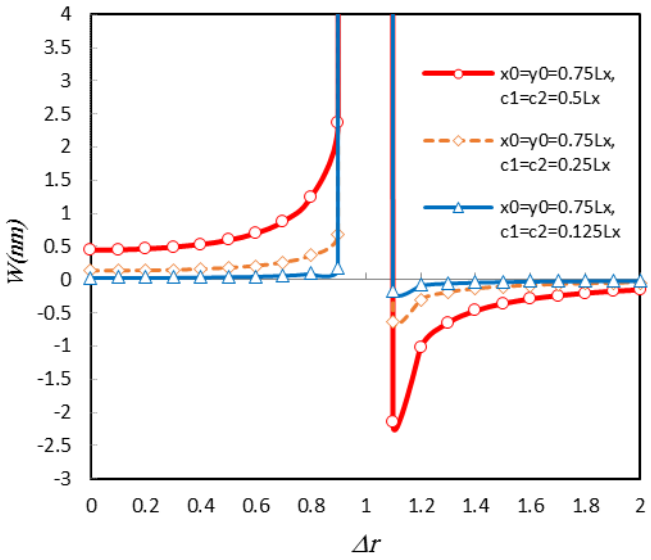


Fig.5. Distributed loads vs. the frequency ratio. $e_0a$= 0.2 nm, $e_1a$= 0.4 nm, $l$=0.5$h$, $q_0$=0.1GPa, $\Delta T$=200K.

Fig. 6 plots the displacement response of the nanoplate vs. the temperature, while keeping constant the following input parameters: $e_0a$=1$nm$, $e_1a$=0.5$nm$, and $e_0a$=0.5$nm$, $e_1a$=1$nm$. Based on a comparative evaluation of the results, the nonlocal input parameters affect significantly the structural response, especially for a high temperature conditions. These results confirm the great impact of higher-order NSGT on the mechanical behavior of graphene sheets.

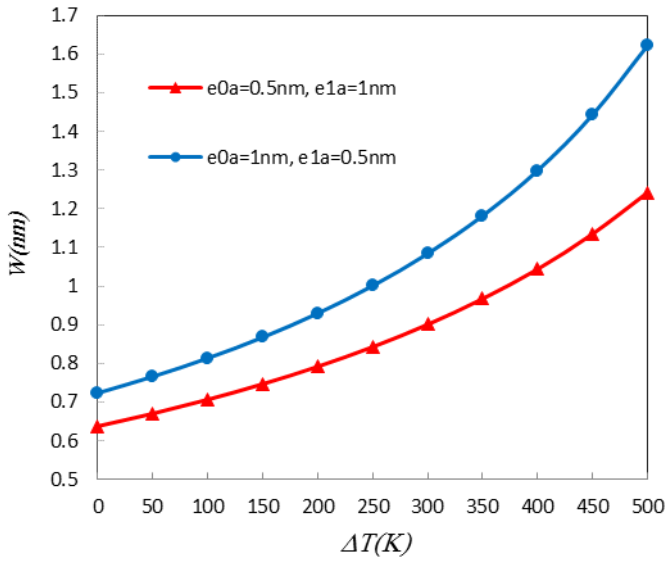


Fig.6. Higher and lower-order NSGT vs. the temperature variation. $l$=0.5$h$, $q_0$=0.05GPa, $\Delta r$=0.1, $m$=$n$=1, $x_0$=$y_0$=0.5$L_x$, $c_1$=$c_2$=$L_x$.

## 5. Conclusions

This article has investigated the thermo-forced vibration of graphene nanoplates, subjected to a transverse dynamic loading applied both uniformly and harmonically. A new plate approach is here proposed to determine the equations of motion, whereas the higher-order NSGT is

applied to evaluate the impacts at small scales. In addition, an analytic solution is here employed to check for the structural response. Based on a large parametric investigation, the following findings can be summarized as follows:

✓ The higher-order nonlocal parameter affects more significantly the structural response than other small scale parameters.
✓ A reduced sensitivity of the dynamic deflection when using higher-order nonlocality factors, within a higher-order NSGT context. This sensitivity of the response is less remarkable when a lower-order nonlocal parameter is applied.
✓ An increased value of the temperature emphasize the main differences in the structural results based on higher-order and lower-order nonlocal parameters. This means that, for high room temperatures, the higher-order nonlocal parameter play a key role.

## References

[1] Taghioskoui, M., Trends in graphene research. *Materials Today*, 12, 34–37, 2009.

[2] Park, S., Ruoff, R. S., Chemical methods for the production of graphenes. *Nature Nanotechnoly*, 4, 217-224, 2009.

[3] An, X., Yu, J. C., Graphene-based photocatalytic composites. *Royal Society of Chemistry Advances*, 1, 1426–1434, 2011.

[4] Xiang, Q., Yu, J., Jaroniec, M., Graphene-based semiconductor photocatalysts. *Chemical Society Reviews*, 41, 782–796, 2012.

[5] Esmaeili, A., Entezari, M. H., Facile and fast synthesis of graphene oxide nanosheets via bath ultrasonic Irradiation. *Journal of Colloid and Interface Science*, 432, 19-25, 2014.

[6] Ebrahimi, F., Barati, M. R., Damping vibration analysis of graphene sheets on viscoelastic medium incorporating hygro-thermal effects employing nonlocal strain gradient theory. *Composite Structures*, 185, 241-253, 2018.

[7] Radic, N., Jeremić, D., Thermal buckling of double-layered graphene sheets embedded in an elastic medium with various boundary conditions using a nonlocal new first-order shear deformation theory. *Composites Part B: Engineering*, 97, 201–215, 2016.

[8] Malikan, M., Jabbarzadeh, M., Sh. Dastjerdi, Non-linear Static stability of bi-layer carbon nanosheets resting on an elastic matrix under various types of in-plane shearing loads in thermo-elasticity using nonlocal continuum. *Microsystem Technologies*, 23, 2973-2991, 2017.

[9] Malikan, M., Buckling analysis of a micro composite plate with nano coating based on the modified couple stress theory. *Journal of Applied and Computational Mechanics*, 4, 1–15, 2018.

[10] Malikan, M., Analytical predictions for the buckling of a nanoplate subjected to nonuniform compression based on the four-variable plate theory. *Journal of Applied and Computational Mechanics*, 3, 218–228, 2017.

[11] Shahsavari, D., Karami, B., Mansouri, S., Shear buckling of single layer graphene sheets in hygrothermal environment resting on elastic foundation based on different nonlocal strain gradient theories. *European Journal of Mechanics / A Solids*, 67, 200-214, 2018.

[12] Farajpour, A., Haeri Yazdi, M. R., Rastgoo, A., Mohammadi, M., A higher-order nonlocal strain gradient plate model for buckling of orthotropic nanoplates in thermal environment. *Acta Mechanica*, 227, 1849–1867, 2016.

[13] Zhang, L. W., Zhang, Y., Liew, K. M., Vibration analysis of quadrilateral graphene sheets subjected to an inplane magnetic field based on nonlocal elasticity theory. *Composites Part B: Engineering*, 118, 96-103, 2017.

[14] Feng, C., Kitipornchai, S., Yang, J., Nonlinear free vibration of functionally graded polymer composite beams reinforced with graphene nanoplatelets (GPLs). *Engineering Structures*, 140, 110–119, 2017.

[15] Gholami, R., Ansari, R., Nonlinear harmonically excited vibration of third-order shear deformable functionally graded graphene platelet-reinforced composite rectangular plates. *Engineering Structures*, 156, 197–209, 2018.

[16] Civalek, O., The determination of frequencies of laminated conical shells via the discrete singular convolution method. *Journal of Mechanics of Materials and Structures*, 1, 163-182, 2006.

[17] Shen, J., Wang, H., Zheng, Sh., Size-dependent pull-in analysis of a composite laminated micro-beam actuated by electrostatic and piezoelectric forces: Generalized differential quadrature method. *International Journal of Mechanical Sciences*, 135, 353-361, 2018.

[18] Gürses, M., Civalek, O., Korkmaz, A., Ersoy H. Free vibration analysis of symmetric laminated skew plates by discrete singular convolution technique based on first-order shear deformation theory. *International journal for numerical methods in engineering*, 79, 290-313, 2009.

[19] Civalek, O., Nonlinear dynamic response of laminated plates resting on nonlinear elastic foundations by the discrete singular convolution-differential quadrature coupled approaches. *Composites Part B: Engineering*, 50, 171–179, 2013.

[20] Baltacıoglu, A. K., Akgoz, B., Civalek, O., Nonlinear static response of laminated composite plates by discrete singular convolution method. *Composite Structures*, 93, 153–161, 2010.

[21] Civalek, O., Analysis of thick rectangular plates with symmetric cross-ply laminates based on first-order shear deformation theory. *Journal of Composite Materials*, 42, 2853-2867, 2008.

[22] Baltacıoglu, A. K., Civalek, O., Akgoz, B., Demir, F., Large deflection analysis of laminated composite plates resting on nonlinear elastic foundations by the method of discrete singular convolution. *International Journal of Pressure Vessels and Piping*, 88, 290-300, 2011.

[23] Shahba, A., Attarnejada, R., Hajilar, S. Free vibration and stability of axially functionally graded tapered Euler-Bernoulli beams. *Shock and Vibration*, 18, 683–696, 2011.

[24] Civalek, O., Demir, C., Buckling and bending analyses of cantilever carbon nanotubes using the Euler Bernoulli beam theory based on non-local continuum model. *Asian Journal of Civil Engineering*, 12, 651-661, 2011.

[25] Akgöz, B., Civalek, O., Buckling analysis of cantilever carbon nanotubes using the strain gradient elasticity and modified couple stress theories. *Journal of Computational and Theoretical Nanoscience*, 8, 1821-1827, 2011.

[26] Civalek, O., Free vibration of carbon nanotubes reinforced (CNTR) and functionally graded shells and plates based on FSDT via discrete singular convolution method. *Composites Part B: Engineering*, 111, 45-59, 2017.

[27] Malikan, M., Electroelastic biaxial compression of nanoplates considering piezoelectric effects, *Journal of Polymer Science and Engineering*, (2018), http://dx.doi.org/10.24294/jpse.v0i0.558

[28] Malikan, M., Electro-mechanical shear buckling of piezoelectric nanoplate using modified couple stress theory based on simplified first order shear deformation theory. *Applied Mathematical Modelling*, 48, 196–207, 2017.

[29] Malikan, M., Tornabene, F., Dimitri, R., Nonlocal three-dimensional theory of elasticity for buckling behavior of functionally graded porous nanoplates using volume integrals. *Materials Research Express*, 5, 095006, 2018.

[30] Malikan, M., Electro-thermal buckling of elastically supported double-layered piezoelectric nanoplates affected by an external electric voltage. *Multidiscipline Modeling in Materials and Structures*, (2018), https://doi.org/10.1108/MMMS-01-2018-0010.

[31] Golmakani, M. E., Malikan, M., Sadraee Far, M. N., Majidi, H. R., Bending and buckling formulation of graphene sheets based on nonlocal simple first order shear deformation theory. *Materials Research Express*, 5, 065010, 2018.

[32] Malikan, M., Temperature influences on shear stability a nanosize plate with piezoelectricity effect. *Multidiscipline modeling in materials and structures*, 14, 125-142, 2018.

[33] Wan, J., Chen, W. J., Li, X. P., Size-dependent free vibration analysis of composite laminated Timoshenko beam based on new modified couple stress theory. *Archive of Applied Mechanics*, 83, 431–444, 2013.

[34] Mercan, K., Civalek, O., DSC method for buckling analysis of boron nitride nanotube (BNNT) surrounded by an elastic matrix. *Composite Structures*, 143, 300–309, 2016.

[35] Demir, C., Mercan K, Civalek, O. Determination of critical buckling loads of isotropic, FGM and laminated truncated conical panel. *Composites Part B: Engineering*, 94, 1-10, 2016.

[36] Mercan, K., Civalek, O., Buckling analysis of Silicon carbide nanotubes (SiCNTs) with surface effect and nonlocal elasticity using the method of HDQ. *Composites Part B: Engineering*, 114, 34-45, 2017.

[37] Jouneghani, F. Z., Dimitri, R., Bacciocchi, M., Tornabene, F., Free vibration analysis of functionally graded porous doubly-curved shells based on the first-order shear deformation theory. *Applied Sciences*, 7, 1-20, 2017.

[38] Nejati, M., Dimitri, R., Tornabene, F., Yas, M. H., Thermal buckling of nanocomposite stiffened cylindrical shells reinforced by Functionally Graded Wavy Carbon Nano-Tubes with temperature-dependent properties. *Applied Sciences*, 7, 1-24, 2017.

[39] Kiani, Y., Dimitri, R., Tornabene, F., Free vibration study of composite conical panels reinforced with FG-CNTs. *Engineering Structures*, 172, 472-482, 2018.

[40] Kiani, Y., Dimitri, R., Tornabene, F., Free Vibration of FG-CNT Reinforced Composite Skew Cylindrical Shells using Chebyshev-Ritz Formulation. *Composites Part B: Engineering*, 147, 169-177, 2018.

[41] Jouneghani, F. Z., Dimitri, R., Tornabene, F., Structural response of porous FG nanobeams under hygro-thermo-mechanical loadings. *Composites Part B: Engineering*, 152, 71-78, 2018.

[42] Fantuzzi, N., Tornabene, F., Bacciocchi, M., Dimitri, R., Free vibration analysis of arbitrarily shaped Functionally Graded Carbon Nanotube-reinforced plates. *Composites Part B: Engineering*, 115, 384–408, 2017.

[43] Nejati, M., Asanjarani, A., Dimitri, R., Tornabene, F., Static and free vibration analysis of functionally graded conical shells reinforced by carbon nanotubes. *International Journal of Mechanical Sciences*, 130, 383–398, 2017.

[44] Tornabene, F., Fantuzzi, N., Bacciocchi, M., Linear static response of nanocomposite plates and shells reinforced by agglomerated carbon nanotubes. *Composites Part B: Engineering*, 115, 449–476, 2017.

[45] Tornabene, F., Bacciocchi, M., Fantuzzi, N., Reddy, J. N., Multiscale approach for three-Phase CNT/Polymer/Fiber laminated nanocomposite structures. *Polymer Composite*, In Press, DOI: 10.1002/pc.24520.

[46] She, G. L., Yuan, F. G., Ren, Y. R., Thermal buckling and post-buckling analysis of functionally graded beams based on a general higher-order shear deformation theory. *Applied Mathematical Modelling*, 47, 340-357, 2017.

[47] She, G. L., Yuan, F. G., Ren, Y. R., Liu, H. B., Xiao, W. Sh., Nonlinear bending and vibration analysis of functionally graded porous tubes via a nonlocal strain gradient theory. *Composite Structures*, 203, 614-623, 2018.

[48] She, G. L., Yuan, F. G., Ren, Y. R., On wave propagation of porous nanotubes. *International Journal of Engineering Science*, 130, 62-74, 2018.

[49] She, G. L., Ren, Y. R., Yuan, F. G., Xiao, W. S., On vibrations of porous nanotubes. *International Journal of Engineering Science*, 125, 23-35, 2018.

[50] She, G. L., Ren, Y. R., Xiao, W. S., Liu, H. B., Study on thermal buckling and post-buckling behaviors of fgm tubes resting on elastic foundations. *Structural Engineering & Mechanics*, 66, 729-736, 2018.

[51] She, G. L., Yuan, F. G., Ren, Y. R., Xiao, W. S., On buckling and post-buckling behavior of nanotubes. *International Journal of Engineering Science*, 121, 130-142, 2017.

[52] Malikan, M., Nguyen, V. B., Tornabene, F., Electromagnetic forced vibrations of composite nanoplates using nonlocal strain gradient theory. *Materials Research Express*, 5, 075031, 2018.

[53] Malikan, M., Dimitri, R., Tornabene, F., Transient response of oscillated carbon nanotubes with an internal and external damping. *Composites Part B: Engineering*, 158, 198-205, 2019.

[54] Malikan, M., Nguyen, V. B., A novel one variable first-order shear deformation theory for biaxial buckling of a size-dependent plate based on the Eringen's nonlocal differential law. *World Journal of Engineering*, 2018. https://doi.org/10.1108/WJE-11-2017-0357

[55] Malikan, M., Nguyen, V. B., Tornabene, F., Damped forced vibration analysis of single-walled carbon nanotubes resting on viscoelastic foundation in thermal environment using nonlocal strain gradient theory. *Engineering Science and Technology, an International Journal*, 21, 778-786, 2018.

[56] Malikan, M., Dimitri, R., Tornabene, F., Effect of sinusoidal corrugated geometries on the vibrational response of viscoelastic nanoplates. *Applied Sciences*, 8, 1432, 2018.

[57] Malikan, M., On the buckling response of axially pressurized nanotubes based on a novel nonlocal beam theory. *Journal of Applied and Computational Mechanics*, (2018), DOI: 10.22055/JACM.2018.25507.1274

[58] Malikan, M., Nguyen, V. B., Buckling analysis of piezo-magnetoelectric nanoplates in hygrothermal environment based on a novel one variable plate theory combining with higher-order nonlocal strain gradient theory. *Physica E: Low-dimensional Systems and Nanostructures*, 102, 8-28, 2018.

[59] Malikan, M., Dastjerdi, Sh., Analytical buckling of FG nanobeams on the basis of a new one variable first-order shear deformation beam theory. *International Journal of Engineering & Applied Sciences*, 10, 21-34, 2018.

[60] Malikan, M., Sadraee Far, M. N., Differential quadrature method for dynamic buckling of graphene sheet coupled by a viscoelastic medium using neperian frequency based on nonlocal elasticity theory. *Journal of Applied and Computational Mechanics*. 4, 147-160, 2018.

[61] Golmakani, M. E., Rezatalab, J., Nonuniform biaxial buckling of orthotropic Nano plates embedded in an elastic medium based on nonlocal Mindlin plate theory. *Composite Structures*, 119, 238-250, 2015.

[62] Golmakani, M. E., Sadraee Far, M. N., Buckling analysis of biaxially compressed double-layered graphene sheets with various boundary conditions based on nonlocal elasticity theory. *Microsystem Technologies*, 23, 2145-2161, 2017.

[63] Ansari, R., Sahmani, S., Prediction of biaxial buckling behavior of single-layered graphene sheets based on nonlocal plate models and molecular dynamics simulations. *Applied Mathematical Modelling*, 37, 7338–51, 2013.

*International Journal of Engineering & Applied Sciences (IJEAS)*
*Vol.10, Issue 3 (2018) 207-236*
*http://dx.doi.org/10.24107/ijeas.458642*
Int J Eng Appl Sci 10(3) (2018) 207-236

# Stability Analysis of the FDE Mathematical Model Examining the Effects of the Specific Immune System Cells and the Multiple Antibiotic Concentration against Infection

*Bahatdin DAŞBAŞI [a*], İlhan ÖZTÜRK [b], Nurcan MENEKŞE [c]*

*[a*] Kayseri University, Department of Accounting and Finance Management, Faculty of Applied Sciences, TR-38039, Kayseri, Turkey,*
*[b] Erciyes University, Department of Mathematics, Faculty of Sciences, TR-38039, Kayseri, Turkey,*
*[c] Sınav College, 06170, Ankara, Turkey,*
*E-mail address: dasbasi_bahatdin@hotmail.com [a*],ozturki@erciyes.edu.tr [b] , n.menekse@outlook.com [c]*

*Received date: 10.09.2018*
*Accepted date: 31.10.2018*

*ORCID numbers of authors:*
*0000-0001-8201-7495[a*], 0000-0002-1268-6324[b], 0000-0003-2185-1798[c]*

**Abstract**

*In this study, the infection process in infectious individual is mathematically modeled by using a system of fractional order differential equations with multiple-orders. Qualitative analysis of the model was done. To mathematically examine the effects of Pseudomonas Aeruginosa and Mycobacterium tuberculosis and their treatment methods, the results of the proposed model are compared with numerical simulations with the help of datas obtained from the literature.*

**Keywords:** Fractional-Order Differential Equation, Infection model, Qualitative Analysis, Numerical Simulation.

**2010 Subject Classification:** 26A33, 34D20, 34K60, 92C50, 92D25

## 1. Introduction

In the process of forming and examining of mathematical models, the ordinary differential equations (ODE), the fractional-order differential equations (FDE) and the difference equations etc. are encountered in the literature. Especially, numerous literature on the application of fractional-order differential equations in nonlinear dynamics has recently been developed [1].

In the process of modeling real-life situations, the created models by using fractional-order differential and integration minimize the ignored errors that are caused by parameters, since the more general form of the concepts of integer-order differential and integration are

concepts of the fractional-order differential and integration. For this reason, the models formed by fractional-order differential equations are more realistic and feasible[2-11].

Fractional-order differential theory is based on the notes of Leibnitz in 1695. However, the earliest systematic studies on this subject were made by Liouville, Riemann and Holmgren in the 19th century [12]. At first this topic has been useful only in mathematics, but it has recently gained importance in other disciplines. FDE and its system are frequently used in the variety applications such as fluid mechanics, economics, viscoelasticity, biology, thermodynamics, physics and engineering [13-21]. Particularly, biology is a very rich resource for such models [22].

Considering the change of its size of a certain specy in population, the proposed models in the literature base on the mathematical growth models such as Malthus [23,24], Pearl-Verhulst Logistic [25,26], Gompertz [27-30] and Kemostat [31]. In addition that, there are interactive population models such as Lotka-Volterra prey-predator [32-34], Kolmogorov [35,35] and Epidemic [37] etc.

In this study, a mathematical model considering time-dependent changes of immune system cells, pathogen and drug concentrations in an infected individual receiving multiple drug treatment, is proposed. This model is in the form of fractional-order differential equations system. In this respect, the proposed model is mathematically different from the ones proposed in [38-41], since the different parameters under various scenarios have been added to the model in here.

## 2. Formation of Model

In this section, the infection model is introduced by giving the definitions of the used variables and parameters. In this sense, time-dependent changes of immune system cells and populations of susceptible bacteria to antibiotic and resistant bacteria to antibiotic in an individual receiving multiple antibiotic treatment in case of an infection have been investigated through mathematical modeling.

There are two types of immune system cells. These are *effector cells,* namely the first response or non-specific response of the immune system, and *memory cells,* namely the second response or specific response of immune system cells. When a sudden infection occurs in the host, first the effector cells and then the memory cells respond to the pathogen until the pathogen completely disappeared [42,43]. The effect of the memory cells of the immune system is investigated in the proposed model.

It has assumed that $B(t)$, $S(t)$, $R(t)$ and $A_i(t)$ for $i = 1,2,\dots,n$ symbolize the population size of specific immune system cells, the population size of susceptible bacteria to antibiotic, the population size of resistant bacteria to antibiotic and concentrations of antibiotics at time $t$, respectively. If the orders of the derivative in the system are accepted as $\alpha_j$ for $j = 1,2,\dots,n+3$, respectively, then $D^{\alpha_j}$ expresses fractional derivatives in the sense of Caputo from the $\alpha_j$-th order. By aforementioned assumptions, the nonlinear and autonomous FDEs system with multiple orders composed of $(n+3)$ equations is

$$\begin{aligned} D^{\alpha_1}B &= v(S+R)B - \omega_B B \\ D^{\alpha_2}S &= \beta_S S\left(1-\frac{S+R}{\Lambda}\right) - \omega_S S - S\sum_{i=1}^{n}\varepsilon_i A_i - S\sum_{i=1}^{n} d_i A_i - \gamma BS \\ D^{\alpha_3}R &= \beta_R R\left(1-\frac{S+R}{\Lambda}\right) - \omega_R R + S\sum_{i=1}^{n}\varepsilon_i A_i - \gamma BR \\ D^{\alpha_{i+3}}A_i &= \delta_i - \mu_i A_i, i = 1,2,\dots,n \end{aligned} \tag{1}$$

for $t \geq 0$. The $\alpha_j$ for $j = 1,2,\dots,n+3$ can be any real or complex vector. In this study, it is taken into account that these derivatives are nonnegative real numbers, and so, $\alpha_j \in (0,1|$. According to $B \equiv B(t)$, $S \equiv S(t)$, $R \equiv R(t)$, $A_1 \equiv A_1(t),\dots$, $A_n \equiv A_n(t)$, the initial conditions at the time $t = t_0$ are $B(t_0) = B_0$, $S(t_0) = S_0$, $R(t_0) = R_0$, $A_1(t_0) = A_{1_0},\dots,A_n(t_0) = A_{n_0}$. For the parameters used in the system (2.1), it is

$$\beta_S, \beta_R, \omega_S, \omega_R, \gamma, \Lambda, v, d_i, \varepsilon_i, \delta_i, \mu_i \in \mathbb{R}^+ \tag{2}$$

for $i = 1,2,\dots,n$.

The definitions of the parameters in (2) are given below. Because it is assumed that the bacteria have grown in accordance with the logistic rules, the parameters $\beta_S$ and $\beta_R$ are the growth rates of susceptible and resistant bacteria to multiple antibiotic, respectively, and the parameter $\Lambda$ indicates the carrying capacity of bacteria. Also, it is

$$\beta_S > \beta_R \tag{3}$$

due to fitness cost [41]. Immune system cells multiply at rate of $v$ by the current bacterial load [44,45]. Susceptible bacteria, resistant bacteria and immune system cells have the natural death rates $\omega_S$, $\omega_R$ and $\omega_B$, respectively. In addition that, the susceptible and resistant bacteria have death rates due to immune system cells and this rates is $\gamma$ [46]. During the administration of the $i$-th antibiotic, some resistant bacteria emerge due to mutations of susceptible bacteria exposed to this antibiotic. $\varepsilon_i$ for $i = 1,2,\dots,n$ is the mutation rate of susceptible bacteria exposured to the $i$-th antibiotic. Because susceptible bacteria are also killed by the action of antibiotics, $d_i$ for $i = 1,2,\dots,n$ is the death rate of susceptible bacteria exposured to the $i$-th antibiotic [38]. Lastly, the $i$-th antibiotic concentration is supplied at a constant rate $\delta_i$, and is taken up at a constant per capita rate $\mu_i$ [39].

Thus, the model (1) under the above scenarios is the mathematical form of a general bacterial infection and the relationships among the variables used in this model have showed schematically in Fig.1.

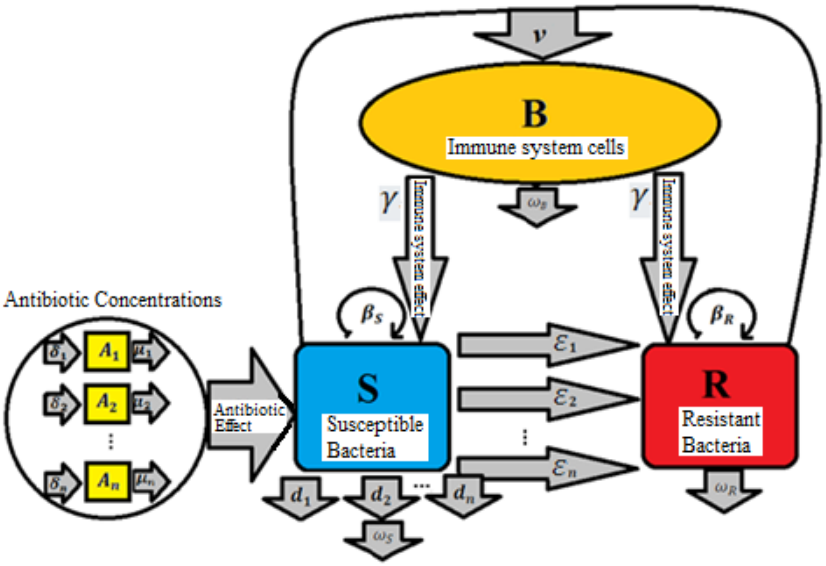


Fig.1. Schematic representation of the interaction among bacteria, immune system cells and antibiotic concentrations according to the parameters used in (1).

**Definition 2.1.** Let $i = 1,2,3,\dots,n+3$. Model in (1) can be rewritting in the matris form as following

$$\begin{aligned} D^{\alpha}X(t) &= f\big(X(t)\big) = UX(t) + x_2(t)N_2X(t) + x_3(t)N_3X(t) + P \\ X(0) &= X_0 \end{aligned} \tag{4}$$

where it is shown by $\alpha = [\alpha_1, \alpha_2, \alpha_3, \dots, \alpha_{n+3}]^T$ the derivatives, by $X(t) = [x_1(t), x_2(t), x_3(t), x_4(t) \dots, x_{n+3}(t)]^T = [B(t), S(t), R(t), A_1(t) \dots, A_n(t)]^T \in \mathbb{R}^{n+3}$ the variables, by $f = [f_1, f_2, f_3, \dots, f_{n+3}]^T \in \mathbb{R}^{n+3}$, $f_i: [0, +\infty)\mathrm{x}\mathbb{R}^{n+3} \to \mathbb{R}$ the functions. Also, when it is considered as $D^{\alpha} = [D^{\alpha_1}, D^{\alpha_2}, D^{\alpha_3}, \dots, D^{\alpha_{n+3}}]^T$, $D^{\alpha_i}$ expresses a fractional derivative in the sense of Caputo from the $\alpha_i$-th order. For $D^{\alpha}X(t) = [D^{\alpha_1}x_1(t), D^{\alpha_2}x_2(t), D^{\alpha_3}x_3(t), \dots, D^{\alpha_{n+3}}x_{n+3}(t)]^T$, (4) is defined as follows:

$$U=\begin{pmatrix}-\omega_B & 0 & 0 & 0 & \dots & 0\\ 0 & (\beta_s-\omega_S) & 0 & 0 & \dots & 0\\ 0 & 0 & (\beta_r-\omega_R) & 0 & \dots & 0\\ 0 & 0 & 0 & -\mu_1 & \dots & 0\\ \vdots & \vdots & \vdots & \vdots & \ddots & \vdots\\ 0 & 0 & 0 & 0 & \dots & -\mu_n\end{pmatrix},$$

$$P=\begin{pmatrix}0\\0\\0\\\delta_1\\\vdots\\\delta_n\end{pmatrix}, N_2=\begin{pmatrix}v & 0 & 0 & 0 & \dots & 0\\ -\gamma & -\frac{\beta_S}{\Lambda} & -\frac{\beta_S}{\Lambda} & -(\varepsilon_1+d_1) & \dots & -(\varepsilon_n+d_n)\\ 0 & 0 & -\frac{\beta_R}{\Lambda} & \varepsilon_1 & \dots & \varepsilon_n\\ 0 & 0 & 0 & 0 & \dots & 0\\ \vdots & \vdots & \vdots & \vdots & \ddots & \vdots\\ 0 & 0 & 0 & 0 & \dots & 0\end{pmatrix}, \tag{5}$$

$$N_3=\begin{pmatrix}v & 0 & 0 & 0 & \dots & 0\\ 0 & 0 & 0 & 0 & \dots & 0\\ -\gamma & -\frac{\beta_R}{\Lambda} & 0 & 0 & \dots & 0\\ 0 & 0 & 0 & 0 & \dots & 0\\ \vdots & \vdots & \vdots & \vdots & \ddots & \vdots\\ 0 & 0 & 0 & 0 & \dots & 0\end{pmatrix} \text{ and } X_0=\begin{pmatrix}B(0)\\S(0)\\R(0)\\A_1(0)\\\vdots\\A_n(0)\end{pmatrix}=\begin{pmatrix}x_1(0)\\x_2(0)\\x_3(0)\\x_4(0)\\\vdots\\x_{n+3}(0)\end{pmatrix}.$$

**Definition 2.2.** For $X(t)=\left(x_1(t)\ x_2(t)\ x_3(t)\ \ x_4(t)\ \dots\ x_{n+3}(t)\right)^T$, let $C^*[0,T]$ be a set of continuous column vectors in the interval $[0,T]$. Norm of the vector $X(t)\in C^*[0,T]$ definited in (4) is shown by $\|X(t)\|=\sum_{i=1}^{n+3} sup_t|x_i(t)|$.

**Proposition 2.1.** We have keep in mind Definition 2.1. In this sense, let us consider $X(t)=\left(x_1(t)\ x_2(t)\ x_3(t)\ \ x_4(t)\ \dots\ x_{n+3}(t)\right)^T$ in $\mathbb{R}_+^{n+3}=\{X\in R^{n+3}: X\geq 0\}$ and $D^\alpha f(x)\in C[a,b]$ for $f(X)\in C[a,b]$, $0<\alpha\leq 1$. According to generalized mean value theorem, it is $f(x)=f(a)+\frac{1}{\Gamma(\alpha)}D^\alpha f(\xi)(x-a)^\alpha$ for $\forall\ x\in[a,b]$ and $0\leq\xi\leq x$. Also,

- When $D^\alpha f(x)>0$ for $\forall\ x\in[a,b]$, the function $f(x)$ increases for each $x\in[a,b]$.
- When $D^\alpha f(x)<0$ for $\forall\ x\in[a,b]$, the function $f(x)$ decreases for each $x\in[a,b]$.

In addition to the above mentioned, the vector field is the points in $\mathbb{R}_+^{n+3}$, due to $D^\alpha x_1(t)|_{x_1=x_2=x_3=x_{i+3}=0}=0$, $D^\alpha x_2(t)|_{x_1=x_2=x_3=x_{i+3}=0}=0$, $D^\alpha x_3(t)|_{x_1=x_2=x_3=x_{i+3}=0}=0$ and $D^\alpha x_{i+3}(t)|_{x_1=x_2=x_3=x_{i+3}=0}=\gamma_i$ for $i=1,2,\dots,n$.

**Proposition 2.2.** If $X(t)\in C^*[0,T]$, then the system (4) has a single solution [47].

**Proof** Let $D^\alpha X(t)=UX(t)+x_2(t)N_2X(t)+x_3(t)N_3X(t)+P$. In this case, it is $F\big(X(t)\big)\in C^*[0,T]$ for the vector $X(t)\in C^*[0,T]$. For the vectors $X(t),Y(t)\in C^*[0,T]$ such that $X(t)\neq Y(t)$, we have the follows:

$$\left\|F\big(X(t)\big)-F\big(Y(t)\big)\right\|$$

$$=\|(UX(t)+x_2(t)N_2X(t)+x_3N_3X(t)+P)-(UY(t)+y_2(t)N_2Y(t)+y_3N_3X(t)+P)\|$$

$$=\|UX(t)+x_2(t)N_2X(t)+x_3N_3X(t)-UY(t)-y_2(t)N_2Y(t)-y_3N_3X(t)\|$$

$$= \left\| \begin{matrix} U\big(X(t)-Y(t)\big) + x_2(t)N_2X(t) + x_3N_3X(t) - y_2(t)N_2Y(t) - y_3N_3X(t) \\ -\Big(\underbrace{x_2(t)N_2Y(t) - x_2(t)N_2Y(t)}_{0}\Big) - \Big(\underbrace{x_3(t)N_3Y(t) - x_3(t)N_3Y(t)}_{0}\Big) \end{matrix} \right\|$$

$$= \left\| \begin{matrix} U\big(X(t)-Y(t)\big) + x_2(t)N_2\big(X(t)-Y(t)\big) + x_3(t)N_3\big(X(t)-Y(t)\big) \\ +\big(x_2(t)-y_2(t)\big)N_2Y(t) + \big(x_3(t)-y_3(t)\big)N_3Y(t) \end{matrix} \right\|$$

$$\leq \begin{pmatrix} \big\|U\big(X(t)-Y(t)\big)\big\| + \big\|x_2(t)N_2\big(X(t)-Y(t)\big)\big\| + \big\|x_3(t)N_3\big(X(t)-Y(t)\big)\big\| \\ +\big\|\big(x_2(t)-y_2(t)\big)N_2Y(t)\big\| + \big\|\big(x_3(t)-y_3(t)\big)N_3Y(t)\big\| \end{pmatrix}$$

$$\leq \begin{pmatrix} \|U\|\big\|\big(X(t)-Y(t)\big)\big\| + |x_2(t)|\|N_2\|\big\|\big(X(t)-Y(t)\big)\big\| + |x_3(t)|\|N_3\|\big\|\big(X(t)-Y(t)\big)\big\| \\ +\|N_2\|\big|\big(x_2(t)-y_2(t)\big)\big|\|Y(t)\| + \|N_3\|\big|\big(x_3(t)-y_3(t)\big)\big|\|Y(t)\| \end{pmatrix}$$

$$\leq \left( \begin{matrix} (\|U\| + |x_2(t)|\|N_2\| + |x_3(t)|\|N_3\|)\big\|\big(X(t)-Y(t)\big)\big\| + \\ \|N_2\| \underbrace{\big|\big(x_2(t)-y_2(t)\big)\big|}_{\leq\|(X(t)-Y(t))\|}\|Y(t)\| + \|N_3\| \underbrace{\big|\big(x_3(t)-y_3(t)\big)\big|}_{\leq\|(X(t)-Y(t))\|}\|Y(t)\| \end{matrix} \right)$$

$$\leq \begin{pmatrix} \|U\| + \|N_1\|\|Y(t)\| + \|N_2\||x_2(t)| + \\ \|N_2\|\|Y(t)\| + \|N_3\||x_3(t)| + \|N_3\|\|Y(t)\| \end{pmatrix} \big\|\big(X(t)-Y(t)\big)\big\|$$

$$\leq \left( \|U\| + \|N_2\| \left( \underbrace{|x_2(t)|}_{\leq\|X(t)\|} + \|Y(t)\| \right) + \|N_3\| \left( \underbrace{|x_3(t)|}_{\leq\|X(t)\|} + \|Y(t)\| \right) \right) \big\|\big(X(t)-Y(t)\big)\big\|$$

$$\leq \big(\|U\| + (\|N_2\| + \|N_3\|)(\|X(t)\| + \|Y(t)\|)\big)\big\|\big(X(t)-Y(t)\big)\big\|$$

and so,

$$\big\|F\big(X(t)\big) - F\big(Y(t)\big)\big\| \leq L\big\|\big(X(t)-Y(t)\big)\big\| \tag{6}$$

where $L = \|U\| + (\|N_2\| + \|N_3\|)(E_1 + E_2) > 0$ such that $E_1, E_2 \in \mathbb{R}^+$and $\|X(t)\| \leq E_1$, $\|Y(t)\| \leq E_2$ due to $X(t), Y(t) \in C^*[0,T]$. Hence, there is only one solution of (4).

## 3. Qualitative Analysis of Mathematical Model

In this section, the equilibrium points of the mathematical model expressed in (1) are found and stability analysis of these equilibrium points is made.

**Definition 3.1.** For the system (1), the threshold parameters $S_S$, $R_R$ and $S_R$ are defined as follows:

$$S_S = \frac{\left(\beta_S - \omega_S - \sum_{i=1}^{n}(\varepsilon_i + d_i)\frac{\delta_i}{\mu_i}\right)}{\frac{\beta_S}{\Lambda}}, R_R = \frac{(\beta_R - \omega_R)}{\frac{\beta_R}{\Lambda}}, S_R = \frac{\sum_{i=1}^{n}\varepsilon_i\frac{\delta_i}{\mu_i}}{\frac{\beta_R}{\Lambda}}. \tag{7}$$

where $S_R > 0$ and $S_S, R_R < \Lambda$ due to (2).

**Proposition 3.2.** We have presumed that the general expression of the equilibrium points of the system (1) is $E(\bar{B}, \bar{S}, \bar{R}, \overline{A_1}, \overline{A_2}, \ldots, \overline{A_n})$. If the threshold parameters in Definition 3.1 are taken into account, then the following expressions are provided:

- The infection-free equilibrium point is $E_0\left(0,0,0,\frac{\delta_1}{\mu_1},\frac{\delta_2}{\mu_2},\ldots,\frac{\delta_n}{\mu_n}\right)$, and this point always exists.
- If $R_R > 0$, then the equilibrium point $E_1\left(0,0,R_R,\frac{\delta_1}{\mu_1},\frac{\delta_2}{\mu_2},\ldots,\frac{\delta_n}{\mu_n}\right)$ exists.
- Let $S_S + S_R \neq R_R$. If $S_S > R_R$, then the equilibrium point $E_2\left(0,(S_S - R_R)\left(\frac{S_S}{S_S+S_R-R_R}\right),S_R\frac{S_S}{(S_S+S_R-R_R)},\frac{\delta_1}{\mu_1},\frac{\delta_2}{\mu_2},\ldots,\frac{\delta_n}{\mu_n}\right)$ exists.
- If $R_R - \frac{\omega_B}{v} > 0$, then the equilibrium point $E_3\left(\frac{R_R-\frac{\omega_B}{v}}{\frac{\gamma}{\frac{\beta_R}{\Lambda}}},0,\frac{\omega_B}{v},\frac{\delta_1}{\mu_1},\frac{\delta_2}{\mu_2},\ldots,\frac{\delta_n}{\mu_n}\right)$ exists.
- Let $S_S > max\left\{R_R,\frac{\omega_B}{v}\right\}$. In this case, the positive equilibrium point is $E_4\left(\frac{S_S-\frac{\omega_B}{v}}{\frac{\gamma}{\frac{\beta_S}{\Lambda}}},\frac{\omega_B}{v}\left(\frac{S_S-R_R}{S_S+S_R-R_R}\right),\frac{S_R\frac{\omega_B}{v}}{(S_S+S_R-R_R)},\frac{\delta_1}{\mu_1},\frac{\delta_2}{\mu_2},\ldots,\frac{\delta_n}{\mu_n}\right)$, and it exists.

**Proof** Let us remember that the equilibrium solution of (1) is denoted by $E(\bar{B}, \bar{S}, \bar{R}, \overline{A_1}, \overline{A_2}, \ldots, \overline{A_n})$. This solution is obtained from $D^{\alpha_1}B = D^{\alpha_2}S = D^{\alpha_3}R = D^{\alpha_{i+3}}A_i = 0$ for $i = 1,2,\ldots,n$. Therefore, we have

$$\begin{aligned}
&v(\bar{S}+\bar{R})\bar{B} - \omega_B\bar{B} = 0\\
&\beta_S\bar{S}\left(1-\frac{\bar{S}+\bar{R}}{\Lambda}\right) - \omega_S S - \bar{S}\sum_{i=1}^{n}\varepsilon_i\,\overline{A_\iota} - \bar{S}\sum_{i=1}^{n}d_i\,\overline{A_\iota} - \gamma\bar{B}\bar{S} = 0\\
&\beta_R\bar{R}\left(1-\frac{\bar{S}+\bar{R}}{\Lambda}\right) - \omega_R R + \bar{S}\sum_{i=1}^{n}\varepsilon_i\,\overline{A_\iota} - \gamma\bar{B}\bar{R} = 0\\
&\delta_i - \mu_i\overline{A_\iota} = 0,\ i = 1,2,\ldots,n.
\end{aligned} \tag{8}$$

Let us consider that the threshold parameters in Definition 3.1. The equilibrium value $\overline{A_\iota} = \frac{\delta_i}{\mu_i}$ is founded by the equation $\delta_i - \mu_i\overline{A_\iota} = 0$, which is the fourth equation of the system (8). If this value is rewritten in the second and third equations in (8), then it is founded that

$$\begin{aligned}
&v(\bar{S}+\bar{R})\bar{B} - \omega_B\bar{B} = 0\\
&\bar{S}\left(S_S - (\bar{S}+\bar{R}) - \frac{\gamma\Lambda\bar{B}}{\beta_S}\right) = 0\\
&\bar{R}R_R - \bar{R}(\bar{S}+\bar{R}) + \bar{S}S_R - \frac{\Lambda\gamma\bar{B}\bar{R}}{\beta_R} = 0
\end{aligned} \tag{9}$$

By the first equation of (9), it is either

$$\bar{B} = 0 \text{ or } (\bar{S}+\bar{R}) = \frac{\omega_B}{v} \tag{10}$$

**(i)** Let $\bar{B} = 0$. In this case, (9) tranforms to

$$\begin{aligned} &\bar{S}\left(S_S - (\bar{S} + \bar{R})\right) = 0 \\ &\bar{R}R_R - \bar{R}(\bar{S} + \bar{R}) + \bar{S}S_R = 0. \end{aligned} \tag{11}$$

From first equation in (11), it is founded either $\bar{S} = 0$ or $\bar{S} + \bar{R} = S_S$.

**a.** Let $\bar{S} = 0$. If this value is written in the second equation of (11), $\bar{R} = 0$ and $\bar{R} = R_R$ are obtained. Therefore, $E_0\left(0,0,0,\frac{\delta_1}{\mu_1},\frac{\delta_2}{\mu_2},\dots,\frac{\delta_n}{\mu_n}\right)$ and $E_1\left(0,0,R_R,\frac{\delta_1}{\mu_1},\frac{\delta_2}{\mu_2},\dots,\frac{\delta_n}{\mu_n}\right)$ are the equilibrium points. The equilibrium point $E_0$ is biological meaningful due to (2). On the other hand, the equilibrium point $E_1$ is biological meaningful when $R_R > 0$.

**b.** Let $\bar{S} + \bar{R} = S_S$. Taking into consideration the threshold parameters in (7), if this value is substituted in the second equation of the system (11), then

$$\begin{aligned} &\bar{S} + \bar{R} = S_S \\ &\bar{S}S_R + \bar{R}(R_R - S_S) = 0 \end{aligned} \tag{12}$$

is founded. From (12), we have $\bar{S} = \frac{S_S(S_S - R_R)}{S_S + S_R - R_R}$ and $\bar{R} = \frac{S_S S_R}{S_S + S_R - R_R}$ for $S_S + S_R - R_R \neq 0$. For $S_R > 0$ in (7), if $S_S > max\{R_R, 0\}$, then the equilibrium point $E_2\left(0,\frac{S_S(S_S - R_R)}{S_S + S_R - R_R},\frac{S_S S_R}{S_S + S_R - R_R},\frac{\delta_1}{\mu_1},\frac{\delta_2}{\mu_2},\dots,\frac{\delta_n}{\mu_n}\right)$ is biological meaning.

**(ii)** Let

$$(\bar{S} + \bar{R}) = \frac{\omega_B}{v}. \tag{13}$$

In this respect, the system (9) transforms to

$$\begin{aligned} &(\bar{S} + \bar{R}) = \frac{\omega_B}{v} \\ &\bar{S}\left(S_S - \frac{\omega_B}{v} - \frac{\gamma}{\frac{\beta_S}{\Lambda}}\bar{B}\right) = 0 \\ &\bar{R}\left(R_R - \frac{\omega_B}{v} - \frac{\gamma}{\frac{\beta_R}{\Lambda}}\bar{B}\right) + \bar{S}S_R = 0 \end{aligned} \tag{14}$$

From the second equation in the system (14), it is clear that either $\bar{S} = 0$ or $\bar{B} = \frac{S_S - \frac{\omega_B}{v}}{\frac{\gamma}{\frac{\beta_S}{\Lambda}}}$.

**a.** Let us assume $\bar{S} = 0$. In this sense, the values $\bar{R} = \frac{\omega_B}{v}$ and then $\bar{B} = \frac{R_R - \frac{\omega_B}{v}}{\frac{\gamma}{\frac{\beta_R}{\Lambda}}}$ are founded from (14), and so the equilibrium point is $E_3\left(\frac{R_R - \frac{\omega_B}{v}}{\frac{\gamma}{\frac{\beta_R}{\Lambda}}}, 0, \frac{\omega_B}{v}, \frac{\delta_1}{\mu_1}, \frac{\delta_2}{\mu_2}, \dots, \frac{\delta_n}{\mu_n}\right)$. If

$$R_R - \frac{\omega_B}{v} > 0, \tag{15}$$

then this point is biological meaningful due to (2).

**b.** Let $\bar{B} = \frac{S_S - \frac{\omega_B}{v}}{\frac{\gamma}{\frac{\beta_S}{\Lambda}}}$. If this value is substituted in the second equation of (14), then

$$\begin{aligned} &(\bar{S} + \bar{R}) = \frac{\omega_B}{v} \\ &\bar{S}S_R + \bar{R}(R_R - S_S) = 0 \end{aligned} \tag{16}$$

is obtained. By solving the equations in (16) for $S_S + S_R - R_R \neq 0$, the equilibrium values as $\bar{S} = \frac{\omega_B}{v}\left(\frac{S_S - R_R}{S_S + S_R - R_R}\right)$ and $\bar{R} = \frac{S_R\frac{\omega_B}{v}}{(S_S + S_R - R_R)}$ are obtained. Thereby, If $S_S > max\left\{R_R, \frac{\omega_B}{v}\right\}$ then, the equilibrium point $E_4\left(\frac{S_S - \frac{\omega_B}{v}}{\frac{\gamma}{\frac{\beta_S}{\Lambda}}}, \frac{\frac{\omega_B}{v}(S_S - R_R)}{S_S + S_R - R_R}, \frac{\frac{\omega_B}{v}S_R}{S_S + S_R - R_R}, \frac{\delta_1}{\mu_1}, \frac{\delta_2}{\mu_2}, \ldots, \frac{\delta_n}{\mu_n}\right)$ is biological meaningful due to (2) and (7).

The following table can be given with respect to the biological existence conditions depended on the parameters of the equilibrium points.

Table 1. The biological meaningful condition for equilibrium points of (1).

| **Equilibrium Point** | **Biological Existence Condition** |
|---|---|
| $E_0\left(0,0,0,\frac{\delta_1}{\mu_1},\frac{\delta_2}{\mu_2},\ldots,\frac{\delta_n}{\mu_n}\right)$ | Always |
| $E_1\left(0,0,R_R,\frac{\delta_1}{\mu_1},\frac{\delta_2}{\mu_2},\ldots,\frac{\delta_n}{\mu_n}\right)$ | $0 < R_R$ |
| $E_2\left(0,\frac{S_S(S_S - R_R)}{S_S + S_R - R_R},\frac{S_S S_R}{S_S + S_R - R_R},\frac{\delta_1}{\mu_1},\frac{\delta_2}{\mu_2},\ldots,\frac{\delta_n}{\mu_n}\right)$ | $max\{R_R, 0\} < S_S, S_S + S_R - R_R \neq 0$ |
| $E_3\left(\frac{R_R - \frac{\omega_B}{v}}{\frac{\gamma}{\frac{\beta_R}{\Lambda}}}, 0, \frac{\omega_B}{v}, \frac{\delta_1}{\mu_1}, \frac{\delta_2}{\mu_2}, \ldots, \frac{\delta_n}{\mu_n}\right)$ | $\frac{\omega_B}{v} < R_R$ |
| $E_4\left(\frac{S_S - \frac{\omega_B}{v}}{\frac{\gamma}{\frac{\beta_S}{\Lambda}}}, \frac{\frac{\omega_B}{v}(S_S - R_R)}{S_S + S_R - R_R}, \frac{\frac{\omega_B}{v}S_R}{S_S + S_R - R_R}, \frac{\delta_1}{\mu_1}, \frac{\delta_2}{\mu_2}, \ldots, \frac{\delta_n}{\mu_n}\right)$ | $max\left\{R_R, \frac{\omega_B}{v}\right\} < S_S, S_S + S_R - R_R \neq 0$ |

**Definition 3.2.** In the stability analysis of the equilibrium points of the system (1), we have assumed that

$$\alpha_1 = \alpha_2 = \cdots = \alpha_{n+3} = \alpha \tag{17}$$

for the orders of derivatives in this system.

**Proposition 3.3.** Let us assume that Definition 3.2. is provided. The following expressions for the equilibrium points of the system (1) are proved.

**(i)** If $S_S, R_R < 0$, then $E_0\left(0,0,0,\frac{\delta_1}{\mu_1},\frac{\delta_2}{\mu_2},\dots,\frac{\delta_n}{\mu_n}\right)$ is locally asymtotically stable.

**(ii)** Let $0 < R_R$. If $S_S < R_R < \frac{\omega_B}{v}$, then $E_1\left(0,0,R_R,\frac{\delta_1}{\mu_1},\frac{\delta_2}{\mu_2},\dots,\frac{\delta_n}{\mu_n}\right)$ is locally asymtotically stable.

**(iii)** Let $max\{R_R,0\} < S_S$ and $S_S + S_R - R_R \neq 0$. If $S_S < \frac{\omega_B}{v}$, then $E_2\left(0,\frac{S_S(S_S-R_R)}{S_S+S_R-R_R},\frac{S_S S_R}{S_S+S_R-R_R},\frac{\delta_1}{\mu_1},\frac{\delta_2}{\mu_2},\dots,\frac{\delta_n}{\mu_n}\right)$ is locally asymtotically stable.

**(iv)** Let $\frac{\omega_B}{v} < R_R$. If $\frac{\beta_S}{\beta_R}\left(S_S - \frac{\omega_B}{v}\right) < \left(R_R - \frac{\omega_B}{v}\right)$, then $E_3\left(\frac{R_R-\frac{\omega_B}{v}}{\frac{\gamma}{\frac{\beta_R}{\Lambda}}},0,\frac{\omega_B}{v},\frac{\delta_1}{\mu_1},\frac{\delta_2}{\mu_2},\dots,\frac{\delta_n}{\mu_n}\right)$ is locally asymtotically stable.

**(v)** Let $max\left\{R_R,\frac{\omega_B}{v}\right\} < S_S$ and $S_S + S_R - R_R \neq 0$. $E_4\left(\frac{S_S-\frac{\omega_B}{v}}{\frac{\gamma}{\frac{\beta_S}{\Lambda}}},\frac{\frac{\omega_B}{v}(S_S-R_R)}{S_S+S_R-R_R},\frac{\frac{\omega_B}{v}S_R}{S_S+S_R-R_R},\frac{\delta_1}{\mu_1},\frac{\delta_2}{\mu_2},\dots,\frac{\delta_n}{\mu_n}\right)$ is locally asymtotically stable, when $S_R < \frac{\omega_B}{v}$.

**Proof** The functions obtained from the system (1) for $i = 1,2,\dots,n$ are as the followings

$$\begin{aligned}
g_1(B,S,R,A_1,\dots,A_n) &= v(S+R)B - \omega_B B\\
g_2(B,S,R,A_1,\dots,A_n) &= \beta_S S\left(1-\tfrac{S+R}{\Lambda}\right) - \omega_S S - S\textstyle\sum_{i=1}^{n}\varepsilon_i A_i - S\sum_{i=1}^{n} d_i A_i - \gamma BS\\
g_3(B,S,R,A_1,\dots,A_n) &= \beta_R R\left(1-\tfrac{S+R}{\Lambda}\right) - \omega_R R + S\textstyle\sum_{i=1}^{n}\varepsilon_i A_i - \gamma BR\\
g_4(B,S,R,A_1,\dots,A_n) &= \delta_i - \mu_i A_i\\
&\vdots\\
g_{i+3}(B,S,R,A_1,\dots,A_n) &= \delta_i - \mu_i A_i
\end{aligned} \tag{18}$$

In this sense, the jacobian matrix of this system, which has the form $J = \begin{pmatrix} (g_1)_B & (g_1)_S & (g_1)_R & (g_1)_{A_1} & \dots & (g_1)_{A_n}\\ (g_2)_B & (g_2)_S & (g_2)_R & (g_2)_{A_1} & \dots & (g_2)_{A_n}\\ (g_3)_B & (g_3)_S & (g_3)_R & (g_3)_{A_1} & \dots & (g_3)_{A_n}\\ (g_4)_B & (g_4)_S & (g_4)_R & (g_4)_{A_1} & \dots & (g_4)_{A_n}\\ \vdots & \vdots & \vdots & \vdots & \ddots & \vdots\\ (g_{n+3})_B & (g_{n+3})_S & (g_{n+3})_R & (g_{n+3})_{A_1} & \dots & (g_{n+3})_{A_n} \end{pmatrix}$, is

$$J=\begin{pmatrix} v(S+R)-\omega_B & vB & vB & 0 & \dots & 0 \\ -\gamma S & \begin{pmatrix}\beta_s-\omega_S-2\frac{S\beta_s}{\Lambda}-\frac{R\beta_s}{\Lambda}\\ -\sum_{i=1}^{n}(\varepsilon_i+d_i)A_i-\gamma B\end{pmatrix} & -\frac{S\beta_s}{\Lambda} & -S(\varepsilon_1+d_1) & \dots & -S(\varepsilon_n+d_n) \\ -\gamma R & \left(-\frac{\beta_R R}{\Lambda}+\sum_{i=1}^{n}\varepsilon_i A_i\right) & \begin{pmatrix}\beta_R-\omega_R-\frac{\beta_R S}{\Lambda}\\ -2\frac{\beta_R R}{\Lambda}-\gamma B\end{pmatrix} & 0 & \dots & 0 \\ 0 & 0 & 0 & -\mu_1 & \dots & 0 \\ \vdots & \vdots & \vdots & \vdots & \ddots & \vdots \\ 0 & 0 & 0 & 0 & \dots & -\mu_n \end{pmatrix} \quad (19)$$

Let us remember that the values $\overline{A_\iota}=\frac{\delta_i}{\mu_i}$ for $i=1,2,\dots,n$ in all of the equilibrium points was founded in Proposition 3.2. By substituting these values in the Jacobian matrix in (19), this matrix transforms to

$$J^*=\begin{pmatrix} v(\bar{S}+\bar{R})-\omega_B & v\bar{B} & v\bar{B} & 0 & \dots & 0 \\ -\gamma\bar{S} & \frac{\beta_S}{\Lambda}\left(\begin{matrix}S_S-2\bar{S}-\\ \bar{R}-\frac{\gamma}{\frac{\beta_S}{\Lambda}}\bar{B}\end{matrix}\right) & -\frac{\bar{S}\beta_s}{\Lambda} & -\bar{S}(\varepsilon_1+d_1) & \dots & -\bar{S}(\varepsilon_n+d_n) \\ -\gamma\bar{R} & \frac{\beta_R}{\Lambda}(-\bar{R}+S_R) & \frac{\beta_R}{\Lambda}\left(\begin{matrix}R_R-\bar{S}-\\ 2\bar{R}-\frac{\gamma}{\frac{\beta_R}{\Lambda}}\bar{B}\end{matrix}\right) & 0 & \dots & 0 \\ 0 & 0 & 0 & -\mu_1 & \dots & 0 \\ \vdots & \vdots & \vdots & \vdots & \ddots & \vdots \\ 0 & 0 & 0 & 0 & \dots & -\mu_n \end{pmatrix} \quad (20)$$

where $\bar{B},\bar{S}$ and $\bar{R}$ are the components of the equilibrium points. From the matrix (20) evaluated at the equilibrium points showed in Table 3.1, it is assumed that the eigenvalues are denoted by $\lambda_i$ for $i=1,\dots,n+3$. Also, it is clear that $\lambda_{i+3}=-\mu_i<0$, which meant that the stability states of the equilibrium points with respect to Routh-Hurwitz criteria do not affect. Therefore, it should be examined the following block matrix

$$J^{*Block}=\begin{pmatrix} v(\bar{S}+\bar{R})-\omega_B & v\bar{B} & v\bar{B} \\ -\gamma\bar{S} & \frac{\beta_S}{\Lambda}\left(S_S-2\bar{S}-\bar{R}-\frac{\gamma}{\frac{\beta_S}{\Lambda}}\bar{B}\right) & -\frac{\beta_s}{\Lambda}\bar{S} \\ -\gamma\bar{R} & \frac{\beta_R}{\Lambda}(-\bar{R}+S_R) & \frac{\beta_R}{\Lambda}\left(R_R-\bar{S}-2\bar{R}-\frac{\gamma}{\frac{\beta_R}{\Lambda}}\bar{B}\right) \end{pmatrix} \quad (21)$$

**(i)** The matrix (21) evaluated at $E_0\left(0,0,0,\frac{\delta_1}{\mu_1},\frac{\delta_2}{\mu_2},\dots,\frac{\delta_n}{\mu_n}\right)$ is

$$J_{E_0}^{*Block}=\begin{pmatrix} -\omega_B & 0 & 0 \\ 0 & \frac{\beta_S}{\Lambda}S_S & 0 \\ 0 & \frac{\beta_R}{\Lambda}S_R & \frac{\beta_R}{\Lambda}R_R \end{pmatrix} \quad (22)$$

In this sense, the eigenvalues are $\lambda_1 = -\omega_B$, $\lambda_2 = \frac{\beta_S}{\Lambda} S_S$ and $\lambda_3 = \frac{\beta_R}{\Lambda} R_R$. These eigenvalues are real number and $\lambda_1 < 0$ due to (2). If

$$S_S, R_R < 0, \tag{23}$$

then $\lambda_1, \lambda_2 < 0$. In this case, $E_0$ is locally asymtotically stable.

**(ii)** Let $0 < R_R$. The matrix (21) evaluated at the point $E_1\left(0,0,R_R,\frac{\delta_1}{\mu_1},\frac{\delta_2}{\mu_2},\ldots,\frac{\delta_n}{\mu_n}\right)$ is

$$J_{E_1}^{*Block} = \begin{pmatrix} vR_R - \omega_B & 0 & 0 \\ 0 & \frac{\beta_S}{\Lambda}(S_S - R_R) & 0 \\ -\gamma R_R & \frac{\beta_R}{\Lambda}(-R_R + S_R) & -\frac{\beta_R}{\Lambda} R_R \end{pmatrix} \tag{24}$$

In this case, the eigenvalues obtained from (24) are $\lambda_1 = vR_R - \omega_B$, $\lambda_2 = \frac{\beta_S}{\Lambda}(S_S - R_R)$ and $\lambda_3 = -\frac{\beta_R}{\Lambda} R_R$. From (2) and (7), it is clear that these eigenvalues are real number. Moreover, if the biological existence condition of $E_1$ is taken into account, then it is seen $\lambda_3 < 0$. According to Routh-Hurwitz criteria, If

$$S_S < R_R < \frac{\omega_B}{v}, \tag{25}$$

then $\lambda_1$ and $\lambda_2$ are negatif real number, which meant that $E_1$ is locally asymtotically stable.

**(iii)** Let $S_S + S_R - R_R \neq 0$ and

$$max\{R_R, 0\} < S_S. \tag{26}$$

By the matrix (21) for $E_2\left(0,\frac{S_S(S_S-R_R)}{S_S+S_R-R_R},\frac{S_S S_R}{S_S+S_R-R_R},\frac{\delta_1}{\mu_1},\frac{\delta_2}{\mu_2},\ldots,\frac{\delta_n}{\mu_n}\right)$, it is

$$J_{E_2}^{*Block} = \begin{pmatrix} vS_S - \omega_B & 0 & 0 \\ \frac{-\gamma S_S(S_S-R_R)}{S_S+S_R-R_R} & -\frac{\beta_S}{\Lambda}\frac{S_S(S_S-R_R)}{S_S+S_R-R_R} & -\frac{\beta_s}{\Lambda}\frac{S_S(S_S-R_R)}{S_S+S_R-R_R} \\ -\gamma\bar{R} & \frac{\beta_R}{\Lambda}\frac{S_R(S_R-R_R)}{S_S+S_R-R_R} & \frac{\beta_R}{\Lambda}\left(R_R - S_S - \frac{S_S S_R}{(S_S+S_R-R_R)}\right) \end{pmatrix}. \tag{27}$$

One of the eigenvalues obtained from (27) is $\lambda_1 = vS_S - \omega_B$ and the others are founded by the following matrix

$$J_{E_2}^{**Block} = \begin{pmatrix} -\frac{\beta_S}{\Lambda}\left(\frac{S_S(S_S-R_R)}{S_S+S_R-R_R}\right) & -\frac{\beta_s}{\Lambda}\left(\frac{S_S(S_S-R_R)}{S_S+S_R-R_R}\right) \\ \frac{\beta_R}{\Lambda} S_R\left(\frac{S_R-R_R}{S_S+S_R-R_R}\right) & \frac{\beta_R}{\Lambda}\left(R_R - S_S - \frac{S_S S_R}{(S_S+S_R-R_R)}\right) \end{pmatrix}. \tag{28}$$

$\lambda_1$ is real number due to (2) and (7). Moreover, if

$$S_S < \frac{\omega_B}{v}, \tag{29}$$

then $\lambda_1 < 0$. To find the eigenvalues $\lambda_2$ and $\lambda_3$, the characteristic equation obtained from (28) is

$$\lambda^2 - \left[TrJ_{E_2}^{**Block}\right]\lambda + \left[DetJ_{E_2}^{**Block}\right] = 0 \tag{30}$$

where

$$\begin{aligned} TrJ_{E_2}^{**Block} &= -\left(\frac{\beta_R}{\Lambda}\left((S_S - R_R) + \frac{S_S S_R}{(S_S+S_R-R_R)}\right) + \frac{\beta_S}{\Lambda}\left(\frac{S_S(S_S-R_R)}{S_S+S_R-R_R}\right)\right) \\ DetJ_{E_2}^{**Block} &= \frac{\beta_S}{\Lambda}\frac{\beta_R}{\Lambda}S_S(S_S - R_R) \end{aligned} \tag{31}$$

Let us consider (26), namely the biological existence condition of $E_2$. In this case, $TrJ_{E_2}^{**Block} < 0$ and $DetJ_{E_2}^{**Block} > 0$. Therefore, it can be seen that all of the coefficients of (30) are positive real number. According to Routh-Hurwitz criteria, if the inequality in (29) is met, then all eigenvalues calculated at this equilibrium point are either complex numbers having negative real part or negative real numbers. In this case, $E_2$ is locally asymtotically stable.

**(iv)** Let

$$\frac{\omega_B}{v} < R_R. \tag{32}$$

In this respect, $E_3\left(\frac{R_R-\frac{\omega_B}{v}}{\frac{\gamma}{\frac{\beta_R}{\Lambda}}}, 0, \frac{\omega_B}{v}, \frac{\delta_1}{\mu_1}, \frac{\delta_2}{\mu_2}, \ldots, \frac{\delta_n}{\mu_n}\right)$ biologically exists. The Jacobian matrix (21) calculated at this point is

$$J_{E_3}^{*Block} = \begin{pmatrix} 0 & v\frac{R_R-\frac{\omega_B}{v}}{\frac{\gamma}{\frac{\beta_R}{\Lambda}}} & v\frac{R_R-\frac{\omega_B}{v}}{\frac{\gamma}{\frac{\beta_R}{\Lambda}}} \\ 0 & \frac{\beta_S}{\Lambda}\left(\left(S_S - \frac{\omega_B}{v}\right) - \frac{\beta_R}{\beta_S}\left(R_R - \frac{\omega_B}{v}\right)\right) & 0 \\ -\gamma\frac{\omega_B}{v} & \frac{\beta_R}{\Lambda}\left(S_R - \frac{\omega_B}{v}\right) & -\frac{\omega_B}{v}\frac{\beta_R}{\Lambda} \end{pmatrix} \tag{33}$$

From (33), it is $\lambda_1 = \frac{\beta_S}{\Lambda}\left(\left(S_S - \frac{\omega_B}{v}\right) - \frac{\beta_R}{\beta_S}\left(R_R - \frac{\omega_B}{v}\right)\right)$ and the eigenvalues $\lambda_2$ and $\lambda_3$ are obtained from the characteristic equation given as

$$\lambda^2 + \frac{\omega_B}{v}\frac{\beta_R}{\Lambda}\lambda + \omega_B\frac{\beta_R}{\Lambda}\left(R_R - \frac{\omega_B}{v}\right) = 0 \tag{34}$$

If

$$\frac{\beta_S}{\beta_R}\left(S_S - \frac{\omega_B}{v}\right) < \left(R_R - \frac{\omega_B}{v}\right), \tag{35}$$

then $\lambda_1$ is negative real number. That all coefficients in (34) are positive real number due to (2) and (32), which meant $TrJ_{E_3}^{Block} < 0$ and $DetJ_{E_3}^{Block} > 0$. In this respect, the eigenvalues $\lambda_2$ and $\lambda_3$ are either negative real numbers or complex numbers having negative real parts. In accord with Routh-Hurwitz criteria, if the inequality in (34) is provided, then $E_3$ is locally asymtotically stable.

**(v)** Let $S_S + S_R - R_R \neq 0$ and

$$max\left\{R_R, \frac{\omega_B}{v}\right\} < S_S. \tag{36}$$

By calculating the Jacobian matrix in (21) at the point $E_4\left(\frac{S_S - \frac{\omega_B}{v}}{\frac{\gamma}{\frac{\beta_S}{\Lambda}}}, \frac{\omega_B}{v}\frac{(S_S - R_R)}{(S_S + S_R - R_R)}, \frac{\omega_B}{v}\frac{S_R}{(S_S + S_R - R_R)}, \frac{\delta_1}{\mu_1}, \frac{\delta_2}{\mu_2}, \ldots, \frac{\delta_n}{\mu_n}\right)$, it is founded

$$J_{E_4}^{*Block} = \begin{pmatrix} 0 & v\bar{B} & v\bar{B} \\ -\gamma\bar{S} & -\bar{S}\frac{\beta_S}{\Lambda} & -\bar{S}\frac{\beta_s}{\Lambda} \\ -\gamma\bar{R} & \frac{\beta_R}{\Lambda}(S_R - \bar{R}) & \frac{\beta_R}{\Lambda}\left(-S_R\frac{\bar{S}}{\bar{R}} - \bar{B}\gamma\Lambda\left(\frac{\beta_S - \beta_R}{\beta_S\beta_R}\right) - \bar{R}\right) \end{pmatrix}, \tag{37}$$

where the values $\bar{B}$, $\bar{S}$ and $\bar{R}$ are in $E_4$. The characteristic equation for the eigenvalues $\lambda_1$, $\lambda_2$ and $\lambda_3$ obtained from the matrix (37) is

$$\lambda^3 + c_1\lambda^2 + c_2\,\lambda + \,c_3 = 0, \tag{38}$$

where

$$\begin{aligned} c_1 &= \frac{1}{\Lambda}\left(\beta_S\bar{S} + \beta_R\left(S_R\frac{\bar{S}}{\bar{R}} + \bar{B}\gamma\Lambda\left(\frac{\beta_S - \beta_R}{\beta_S\beta_R}\right) + \bar{R}\right)\right) \\ c_2 &= \left(\bar{B}v\,\gamma\frac{\omega_B}{v} + \frac{1}{\Lambda^2}\bar{S}\,\beta_R\,\beta_s\left(S_R + S_R\frac{\bar{S}}{\bar{R}} + \bar{B}\gamma\Lambda\left(\frac{\beta_S - \beta_R}{\beta_S\beta_R}\right)\right)\right) \\ c_3 &= \frac{\bar{S}\bar{B}v\,\gamma}{\Lambda}\beta_R\left(S_R + S_R\frac{\bar{S}}{\bar{R}} + \bar{B}\gamma\Lambda\left(\frac{\beta_S - \beta_R}{\beta_S\beta_R}\right)\right). \end{aligned} \tag{39}$$

Let us recall that if $c_1, c_3 > 0$ and $c_1 c_2 > c_3$ for the third-degreee characteristic polynomial in (38) according to Routh-Hurwitz criteria, then the equilibrium point is locally asymtotically stable. It is

$$c_1, c_2, c_3 > 0 \tag{40}$$

due to (2) and (3). Also, we have

$$c_1.c_2 - c_3 = \frac{1}{\Lambda}\left((L_2 + \beta_R L_1)\left(\bar{B} v\, \gamma \frac{\omega_B}{v} + \frac{1}{\Lambda^2}\bar{S}\, \beta_R\, \beta_S L_1\right) - \bar{S}\bar{B} v\, \gamma \beta_R L_1\right) \tag{41}$$

and so,

$$c_1.c_2 - c_3 = \frac{1}{\Lambda}\left(\frac{1}{\Lambda^2}\bar{S}\, \beta_R^2\, \beta_s {L_1}^2 + L_2 \bar{B} v\, \gamma \frac{\omega_B}{v} + \left[L_2 \frac{1}{\Lambda^2}\bar{S}\ \beta_s + \bar{B}\gamma v \underbrace{\left[\frac{\omega_B}{v} - \bar{S}\right]}_{*}\right]\beta_R L_1\right) \tag{42}$$

where

$$\begin{aligned} L_1 &= \left(S_R + S_R \frac{\bar{S}}{\bar{R}} + \bar{B}\gamma\Lambda\left(\frac{\beta_S - \beta_R}{\beta_S \beta_R}\right)\right) \\ L_2 &= (\beta_S \bar{S}\ - \beta_R S_R + \beta_R \bar{R}). \end{aligned} \tag{43}$$

In this sense, it is

$$0 < L_1 \tag{44}$$

due to (3). On the other hand, we have the follows

$L_2 = (\beta_S \bar{S} - \beta_R S_R + \beta_R \bar{R})$,

$L_2 = \left(\beta_S \frac{\omega_B}{v}\left(\frac{S_S - R_R}{S_S + S_R - R_R}\right) - \beta_R S_R + \beta_R \frac{\omega_B}{v}\frac{S_R}{(S_S + S_R - R_R)}\right)$,

$L_2 = \frac{1}{(S_S + S_R - R_R)}\left(\underbrace{\beta_S}_{>\beta_R \text{ due to (2.3)}} \frac{\omega_B}{v}(S_S - R_R) - \beta_R S_R\left(S_S - R_R + S_R - \frac{\omega_B}{v}\right)\right)$,

$L_2 > \frac{\beta_R}{(S_S + S_R - R_R)}\left(\frac{\omega_B}{v}(S_S - R_R) - S_R\left(S_S - R_R + S_R - \frac{\omega_B}{v}\right)\right)$,

$L_2 > \frac{\beta_R}{(S_S + S_R - R_R)}\left(\frac{\omega_B}{v}(S_S - R_R + S_R) - S_R(S_S - R_R + S_R)\right) = \beta_R\left(\frac{\omega_B}{v} - S_R\right)$,

$L_2 > \frac{\beta_R}{(S_S + S_R - R_R)}\left(\frac{\omega_B}{v}(S_S - R_R + S_R) - S_R(S_S - R_R + S_R)\right) = \beta_R\left(\frac{\omega_B}{v} - S_R\right)$,

and so,

$$L_2 > \beta_R\left(\frac{\omega_B}{v} - S_R\right). \tag{45}$$

If

$$S_R < \frac{\omega_B}{v}, \tag{46}$$

then

$$0 < L_2. \tag{47}$$

For the expression * in (42),

$$*= \left[\frac{\omega_B}{v} - \bar{S}\right] = \frac{\omega_B}{v} - \frac{\omega_B}{v}\left(\frac{S_S - R_R}{S_S + S_R - R_R}\right) = \frac{\omega_B}{v}\left[1 - \underbrace{\left(\frac{S_S - R_R}{S_S + S_R - R_R}\right)}_{<1 \text{ due to } (3.30)}\right] > 0 \tag{48}$$

is provided. To sum up, if (46) is provided, then it is

$$c_1.c_2 - c_3 > 0, \tag{49}$$

in (42), due to (44), (46) and (48). Let us consider (46). $E_4$ is locally asymtotically stable, when (40) and (49) are met.

As a result of this proposition, the following table can be given.

Table 2. Conditions of stability and biological meaningful for equilibrium points of (1).

| **Equilibrium Point** | **Biological Existence Condition** | **Stability Condition** |
|---|---|---|
| $E_0\left(0,0,0,\frac{\delta_1}{\mu_1},\frac{\delta_2}{\mu_2},\ldots,\frac{\delta_n}{\mu_n}\right)$ | Always | $S_S, R_R < 0$ |
| $E_1\left(0,0,R_R,\frac{\delta_1}{\mu_1},\frac{\delta_2}{\mu_2},\ldots,\frac{\delta_n}{\mu_n}\right)$ | $0 < R_R$ | $S_S < R_R < \frac{\omega_B}{v}$ |
| $E_2\left(0,\frac{S_S(S_S - R_R)}{S_S + S_R - R_R},\frac{S_S S_R}{S_S + S_R - R_R},\frac{\delta_1}{\mu_1},\frac{\delta_2}{\mu_2},\ldots,\frac{\delta_n}{\mu_n}\right)$ | $max\{R_R, 0\} < S_S$, $S_S + S_R - R_R \neq 0$ | $S_S < \frac{\omega_B}{v}$ |
| $E_3\left(\frac{R_R - \frac{\omega_B}{v}}{\frac{\gamma}{\frac{\beta_R}{\Lambda}}},0,\frac{\omega_B}{v},\frac{\delta_1}{\mu_1},\frac{\delta_2}{\mu_2},\ldots,\frac{\delta_n}{\mu_n}\right)$ | $\frac{\omega_B}{v} < R_R$ | $\frac{\beta_S}{\beta_R}\left(S_S - \frac{\omega_B}{v}\right) < \left(R_R - \frac{\omega_B}{v}\right)$ |
| $E_4\left(\frac{S_S - \frac{\omega_B}{v}}{\frac{\gamma}{\frac{\beta_S}{\Lambda}}},\frac{\frac{\omega_B}{v}(S_S - R_R)}{S_S + S_R - R_R},\frac{\frac{\omega_B}{v}S_R}{S_S + S_R - R_R},\frac{\delta_1}{\mu_1},\frac{\delta_2}{\mu_2},\ldots,\frac{\delta_n}{\mu_n}\right)$ | $max\left\{R_R,\frac{\omega_B}{v}\right\} < S_S$, $S_S + S_R - R_R \neq 0$ | $S_R < \frac{\omega_B}{v}$ |

## 4. Applications of the Proposed Model in (1)

In this section, the values obtained from the literature to the parameters used in the system (1) are given. The qualitative analysis of the proposed model was supported by numerical simulations. Two application have been done in this context.

### 4.1. Application for Pseudomonas Aeruginosa

The parameter values in the studies of Handel et al. [48] and Ternent et al. [40] are used. For an individual receiving Meropenem and Antivirulence drug in case of the infection caused by Pseudomonas Aeruginosa, they proposed a mathematical model in ODE form, based on the relationship among phagocyte (immune system cells), bacteria and drug concentrations.

Table 3. Parameter values used in system (1) for Pseudomonas Aeruginosa

| Parameter | Definition | Value | Reference |
|---|---|---|---|
| $\beta_S$ | The growth rate of susceptible Pseudomonas Aeruginosa | 24 $day^{-1}$ | [48] |
| $\beta_R$ | The growth rate of resistant Pseudomonas aeruginosa | 21.6 $day^{-1}$ | [40] |
| $\Lambda$ | The carrying capacity of Pseudomonas Aeruginosa | $10^9$ bakteri | [48] |
| $v$ | The growth rate of immune system cells in the presence of Pseudomonas Aeruginosa | 3 $day^{-1}$ | [40] |
| $\omega_S$ | The natural death rate of susceptible Pseudomonas Aeruginosa | 0.7 $day^{-1}$ | [40] |
| $\omega_R$ | The natural death rate of resistant Pseudomonas Aeruginosa | 0.7 $day^{-1}$ | [40] |
| $\omega_B$ | The natural death rate of immune system cells | 1.512 $day^{-1}$ | [49] |
| $\gamma$ | The death rate of Pseudomonas Aeruginosa due to immune system cells | $2.4 * 10^{-4} day^{-1}$ | [49] |
| $\varepsilon_1$ | The mutation rate of Pseudomonas Aeruginosa due to Meropenem | $10^{-6}$ mutxgen | [50,51] |
| $\varepsilon_2$ | The mutation rate of Pseudomonas Aeruginosa due to anti-virulence drug | 0 mutxgen | [40] |
| $d_1$ | The death rate of Pseudomonas Aeruginosa due to Meropenem | 8.47 $day^{-1}$ | [40] |
| $d_2$ | The death rate of Pseudomonas Aeruginosa due to anti-virulence drug | 2.93 $day^{-1}$ | [50,51] |
| $\delta_1$ | The daily dose of Meropenem | 4 mg/kg/day | [40,50,51] |
| $\delta_2$ | The daily dose of anti-virulence drug | 4 mg/kg/day | [40,50,51] |
| $\mu_1$ | The remove rate from the body of Meropenem | 0.15 $day^{-1}$ | [50,51] |
| $\mu_2$ | The remove rate from the body of anti-virulence drug | 0.15 $day^{-1}$ | [50,51] |
| $\alpha$ | The orders of the derivative in the system (1) | 0.9 | Hypothesis |
| $(B_0, S_0, R_0, A_{i_0})$ | Initial conditions for $i = 1,2$ | (1,6000,2,4,4) | [40,48] |

When parameter values in Table 3. are used, the threshold parameters in Definition 3.1. are $S_S = -11695802777$, $R_R = 967592592$ and $S_R = 1234567901$. From Proposition 3.2., the equilibrium points existed biologically are $E_0(0,0,0,26.66,26.66)$,

$E_1(0,0,967592592,26.66,26.66)$ and $E_3(87083.33,0,0.504,26.66,26.66)$, respectively. $E_3(87083.33,0,0.504,26.66,26.66)$ is locally asymtotically stable, because it is $\frac{\beta_S}{\beta_R}\left(S_S - \frac{\omega_B}{v}\right) = -\frac{2923950694376}{225} < \left(R_R - \frac{\omega_B}{v}\right) = 967592591.496$ in the Proposition 3.3. The drug dose and duration of treatment for this infection is determined by type and severity of the infection and the patient's condition. In the study of Handel et al.[48], they have investigated in a treatment duration of approximately 10 days. In this sense, we have considered the same treatment duration for this study. Thus, we have obtained the following figures.

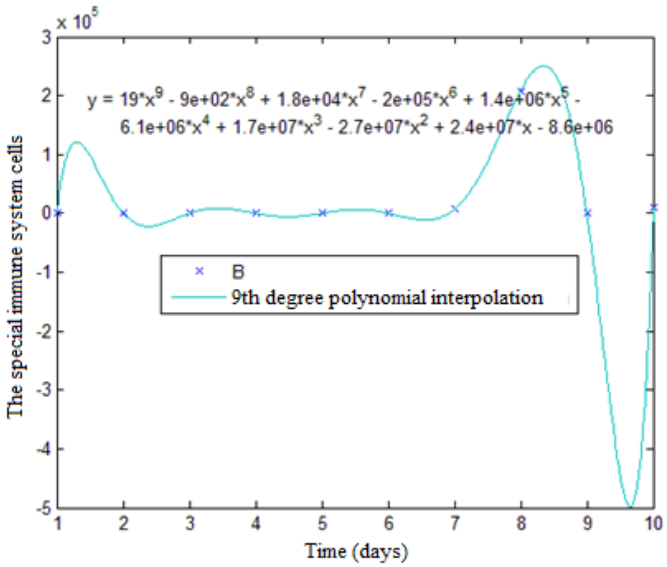


Fig.2. Time-dependent changes of the immune system cells during 10 days of the drug treatment according to Table 3.

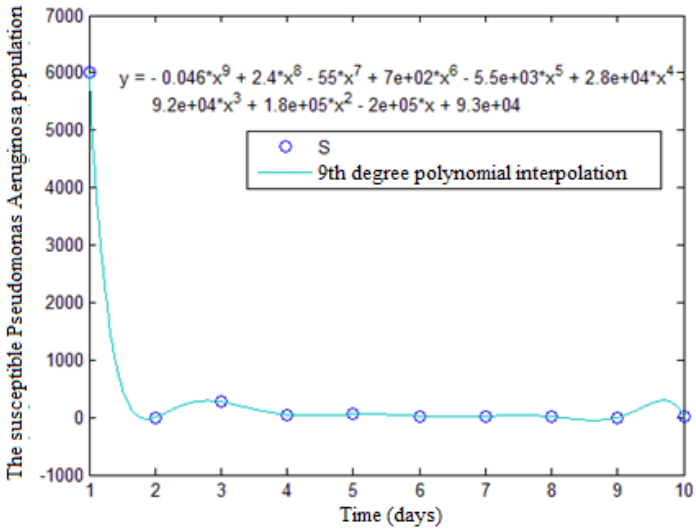


Fig.3. Time-dependent changes of the susceptible Pseudomonas Aeruginosa population during 10 days of drug treatment according to Table 3.

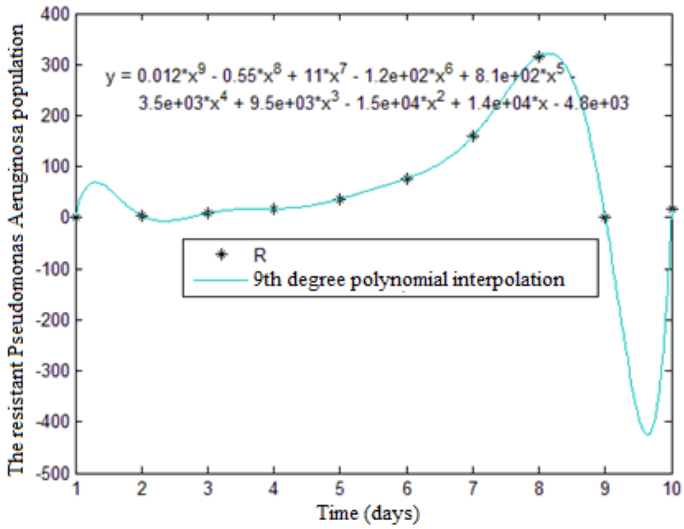


Fig.4. Time-dependent changes of the resistant Pseudomonas Aeruginosa population during 10 days of drug treatment according to Table 3.

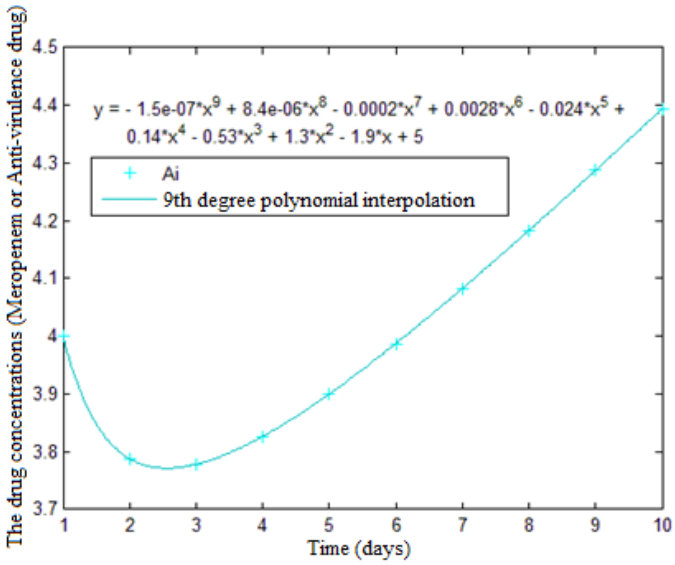


Fig.5. Time-dependent changes for the each drug concentrations (Meropenem or Anti-virulence drug) during 10 days of drug treatment according to Table 3.

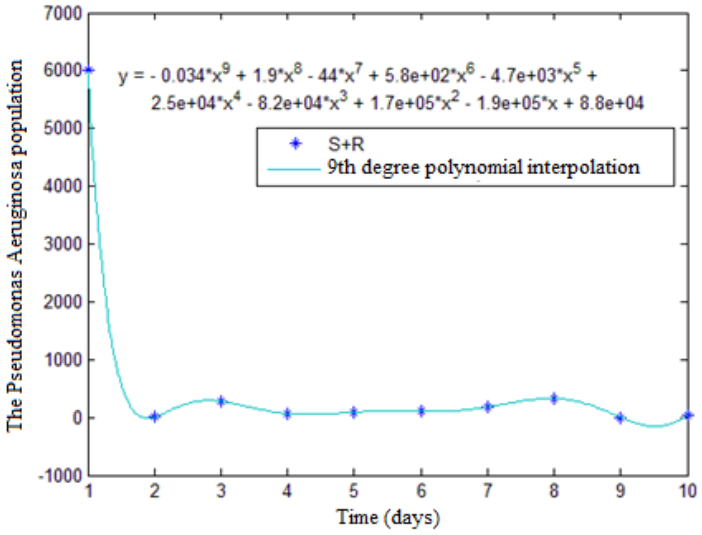


Fig.6. Time-dependent changes of the Pseudomonas Aeruginosa population during 10 days of drug treatment according to Table 3.

The daily ranges in quantities of the specific immune system cells, the susceptible Pseudomonas Aeruginosa population, the resistant Pseudomonas Aeruginosa population, the drug concentrations (Meropenem or Anti-virulence drug) and the Pseudomonas Aeruginosa population during the 10-day treatment period are shown respectively in Fig.2-6.

For ease of reviewing the daily values of the variables in these figures, the points on the graph were interpolated into polynomial at 9th degree (except for the initial conditions) to show the increase or decrease between consecutive days, due to it is a treatment method of 10 days.

Stability of the equilibrium points $E_3(87083.33,0,0.504,26.66,26.66)$ is seen in Fig. 7. Within 10 days of treatment, the antibiotic-resistant Pseudomonas aeruginosa population approaches 0.504 (quite small value) and the antibiotic-susceptible Pseudomonas aeruginosa population disappears. Also, it takes a long time that specific immune system cells approach to the value of 87083.33. As shown in Fig.7, this is due to the local stability and the parameters.

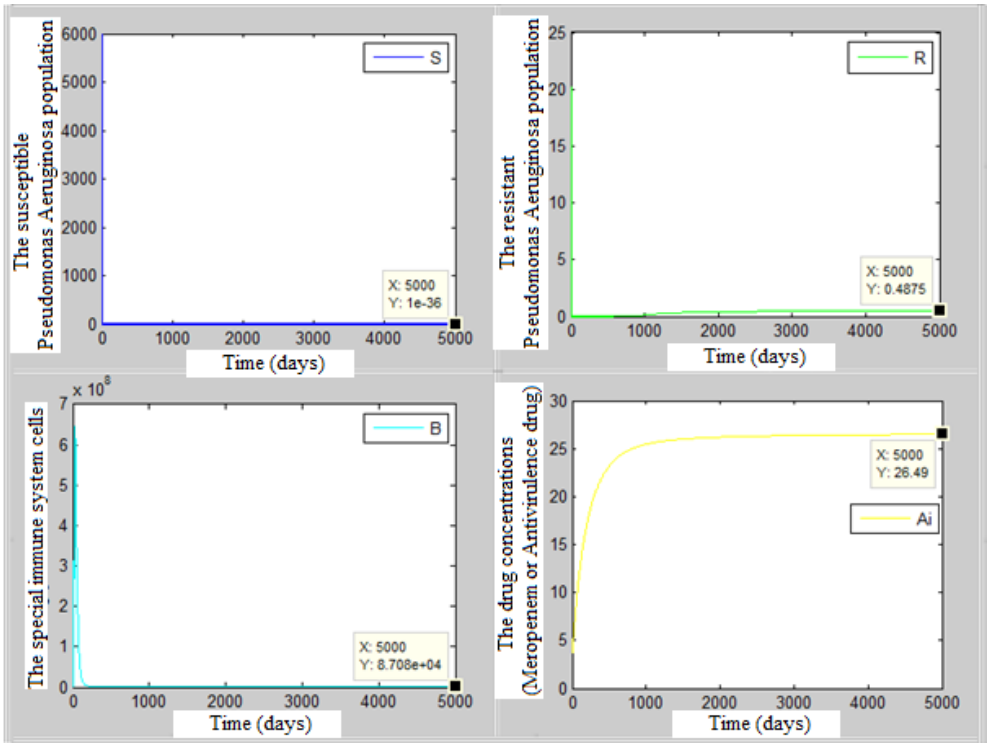


Fig.7. According to Table 3, Stability of the equilibrium point $E_3(87083.33,0,0.504,26.66,26.66)$.

### 4.2. Application for Mycobacterium Tuberculosis

The parameter values in the studies of Mondragón et al. [39] are used. For an individual receiving the antibiotics isoniazid (INH), rifampicin (RIF), streptomycin (SRT) and pyrazinamide (PZA) in case of the infection caused by Mycobacterium Tuberculosis, they proposed a mathematical model in ODE form, based on the relationship between bacteria and antibiotic concentrations. For this infection, the treatment time is about 6 months. In this sense, all of the antibiotics are used in the first two months and the antibiotics isoniazid and rifampicin are used in the remaining four months [52]. The parameter values used in the system (1) for numerical study are given in Table 4.

Table 4. Parameter values used in system (1) for Mycobacterium Tuberculosis

| Parameter | Definition | Value | Reference |
|---|---|---|---|
| $\beta_S$ | The growth rate of susceptible Mycobacterium Tuberculosis | 0.8 $day^{-1}$ | [39] |
| $\beta_R$ | The growth rate of resistant Mycobacterium Tuberculosis | 0.4 $day^{-1}$ | [39] |
| $\Lambda$ | The carrying capacity of Mycobacterium Tuberculosis | $10^9$ bakteri | [53] |
| $v$ | The growth rate of immune system cells in the presence of Mycobacterium Tuberculosis | 0.0002 $day^{-1}$ | Hypothesis |
| $\omega_S$ | The natural death rate of susceptible Mycobacterium Tuberculosis | 0.312 $day^{-1}$ | [39] |
| $\omega_R$ | The natural death rate of resistant Mycobacterium Tuberculosis | 0.312 $day^{-1}$ | [39] |
| $\omega_B$ | The natural death rate of immune system cells | 0.35 $day^{-1}$ | [54] |
| $\gamma$ | The death rate of Mycobacterium Tuberculosis due to immune system cells | $2.4 * 10^{-4}$ $day^{-1}$ | [49] |
| $\varepsilon_1$ | The mutation rate of Mycobacterium Tuberculosis due to isoniazid | $10^{-6}$ mutxgen | [55] |
| $\varepsilon_2$ | The mutation rate of Mycobacterium Tuberculosis due to rifampicin | $10^{-8}$ mutxgen | [55] |
| $\varepsilon_3$ | The mutation rate of Mycobacterium Tuberculosis due to streptomycin | 0 | [39] |
| $\varepsilon_4$ | The mutation rate of Mycobacterium Tuberculosis due to pyrazinamide | 0 | [39] |
| $d_1$ | The death rate of Mycobacterium Tuberculosis due to isoniazid | 0.0039 $day^{-1}$ | [56] |
| $d_2$ | The death rate of Mycobacterium Tuberculosis due to rifampicin | 0.00375 $day^{-1}$ | [39] |
| $d_3$ | The death rate of Mycobacterium Tuberculosis due to streptomycin | 0.0025 $day^{-1}$ | [53] |
| $d_4$ | The death rate of Mycobacterium Tuberculosis due to pyrazinamide | 0.00001625 $day^{-1}$ | [53] |
| $\delta_1$ | The daily dose of isoniazid | 5 mg/kg/day | [55] |
| $\delta_2$ | The daily dose of rifampicin | 10 mg/kg/day | [55] |
| $\delta_3$ | The daily dose of streptomycin | 15-25 mg/kg/ day | [55] |
| $\delta_4$ | The daily dose of pyrazinamide | 20-35 mg/kg/ day | [55] |
| $\mu_1$ | The remove rate from the body of isoniazid | 0.06 $day^{-1}$ | [57] |
| $\mu_2$ | The remove rate from the body of rifampicin | 0.05 $day^{-1}$ | [57] |
| $\mu_3$ | The remove rate from the body of streptomycin | 0.04 $day^{-1}$ | [57] |
| $\mu_4$ | The remove rate from the body of pyrazinamide | 0.03 $day^{-1}$ | [57] |
| $\alpha$ | The orders of the derivative in the system (1) | 0.9 | Hypothesis |
| $(B_0, S_0, R_0, A_{i_0})$ | Initial conditions for $i = 1,2,3,4$ | $(1000, 6000, 20,0,0,0,0)$ | Hypothesis |

Let us consider the parameter values in Table 4. and the treatment method mentioned above.

All antibiotics are used in the first two months of this treatment. In this sense, the threshold parameters are obtained as $S_S = -1919273333$, $R_R = 220000000$ and $S_R = 213333$. Considered in Table 1, the equilibrium points existing biologically are

$E_0(0,0,0,83{,}200{,}375{,}666)$, $E_1(0,0,220000000,83{,}200{,}375{,}666)$ and $E_3(0.5289575,0,1750,83{,}200{,}375{,}666)$. If the stability conditions of these equilibrium points with respect to Table 2. is considered, then it is obtained that $E_0$ is unstable due to $\underbrace{R_R}_{220000000} > 0$, $E_1$ is unstable due to $\underbrace{\frac{\omega_B}{v}}_{1750} < \underbrace{R_R}_{220000000}$ and $E_3$ is locally asymtotically stable due to $\underbrace{\frac{\beta_S}{\beta_R}\left(S_S - \frac{\omega_B}{v}\right)}_{-3838550166} < \underbrace{\left(R_R - \frac{\omega_B}{v}\right)}_{219998250}$. During the first two months of treatment, some of the resistant bacteria population survives and the sensitive bacterial population disappears.

Isoniazid and rifampicin as antibiotic are used in the last four months of this treatment. Therefore, the threshold parameters are recalculated as $S_S = -733856666$, $R_R = 220000000$ and $S_R = 213333$. The equilibrium points existing biologically are $E_0(0,0,0,83{,}200,0,0)$, $E_1(0,0,220000000,83{,}200,0,0)$ and $E_3(0.5289575,0,1750,83{,}200{,}375{,}666)$. Similar to the calculation results in the first two months of treatment, the equilibrium point $E_3(0.5289575,0,1750,83{,}200{,}375{,}666)$ is locally asymtotically stable, since $\underbrace{\frac{\beta_S}{\beta_R}\left(S_S - \frac{\omega_B}{v}\right)}_{-1467716832} < \underbrace{\left(R_R - \frac{\omega_B}{v}\right)}_{219998250}$.

For six months of treatment, the special immune system cells, the susceptible Mycobacterium Tuberculosis population and the resistant Mycobacterium Tuberculosis population approach to the values 0.5289575, 0 and 1750, respectively.

These situations are evident in the following figures.

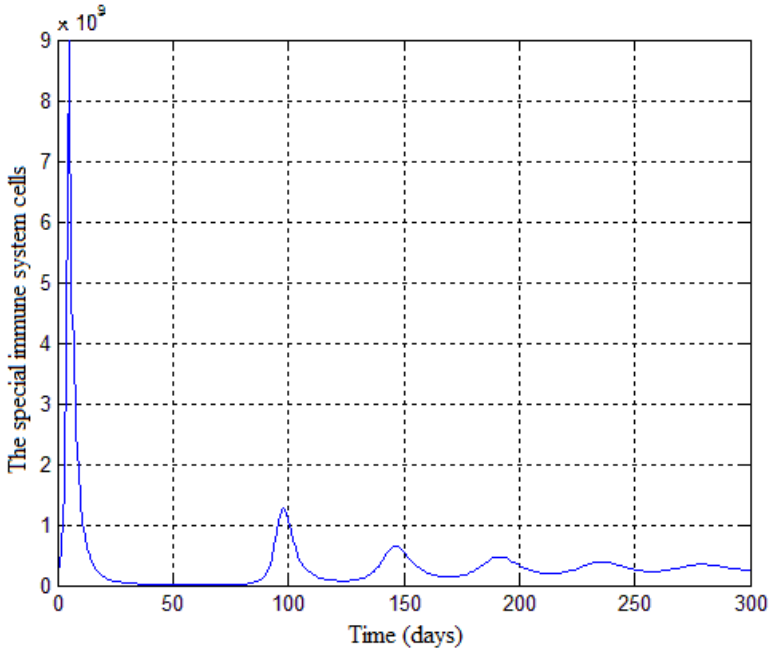


Fig.8. Time-dependent changes of the special immune system cells during 6 months of treatment according to Table 4.

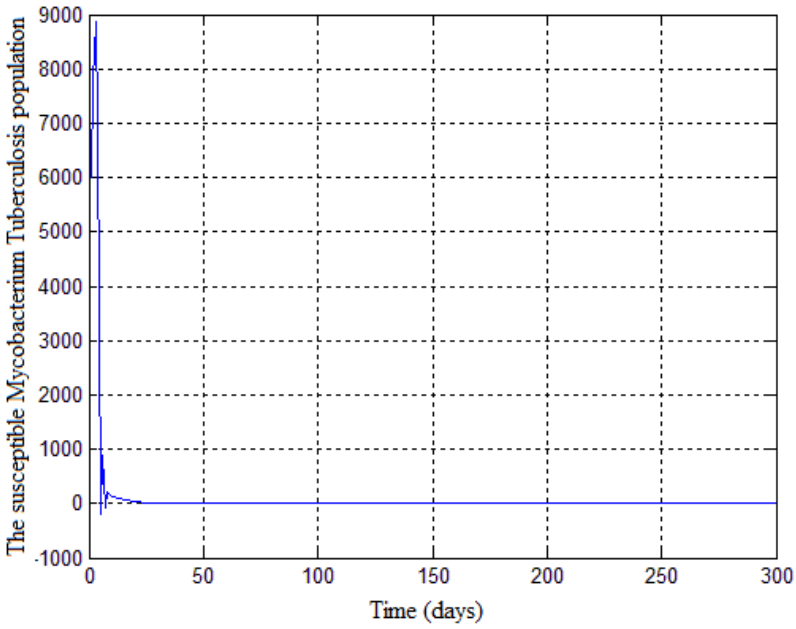


Fig.9 Time-dependent changes of the susceptible Mycobacterium Tuberculosis population during 6 months of treatment according to Table 4.

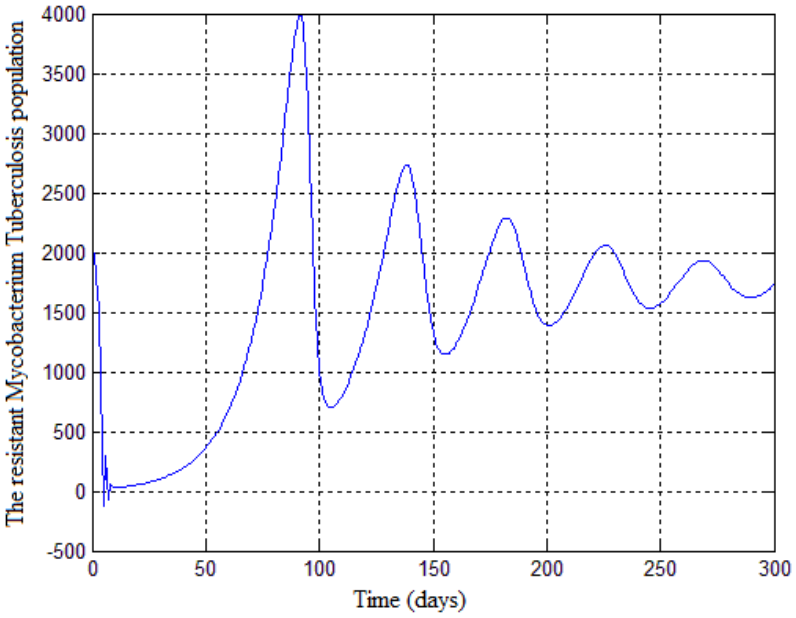


Fig.10. Time-dependent changes of the resistant Mycobacterium Tuberculosis population during 6 months of treatment according to Table 4.

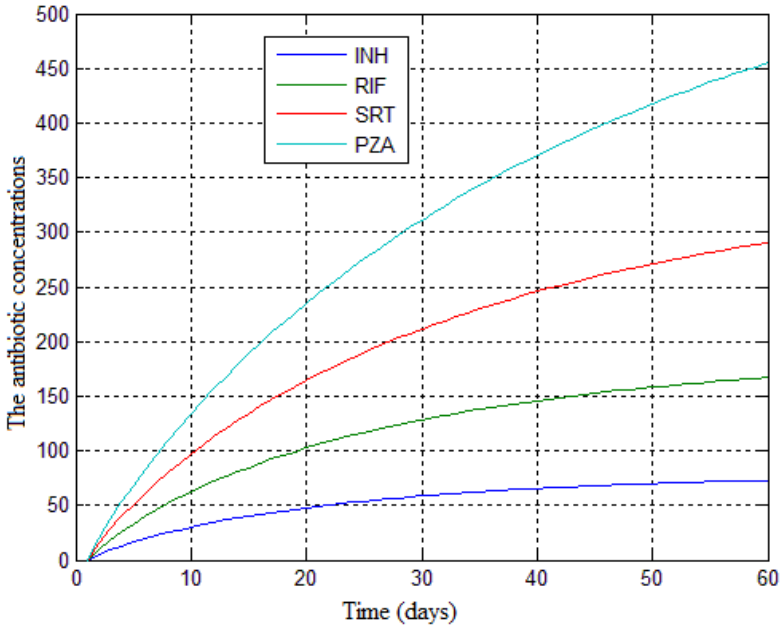


Fig.11. Time-dependent changes of the antibiotic concentrations during first 2 months of treatment according to Table 4.

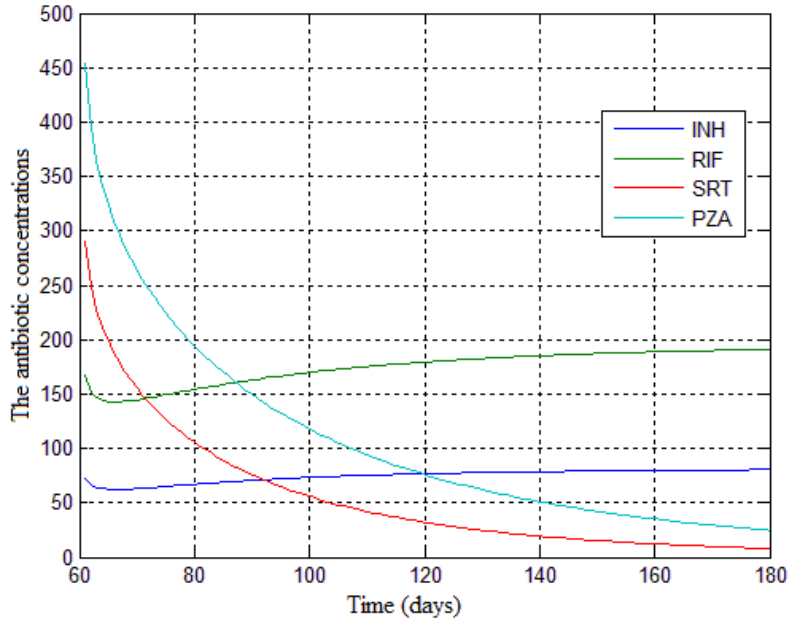


Fig.12. Time-dependent changes of the antibiotic concentrations during last 4 months of treatment according to Table 4.

## 5. Results and Discussions

As seen in the applications of the proposed model, while the susceptible bacteria population is disappeared and the resistant bacteria population is limited. Especially, the model is a useful model for explaining the recrudescence of a bacterial infection believed to have been destroyed when immune system of the individual is weakened. For example, the World

Health Organization explains that the rate of recurrence of Mycobacterium Tuberculosis is 5-10%. According to researchs conducted in recent years, about 9.2 million people suffer from this infection every year in the world and about 1.6 million of them die due to this infection. This rate is increasing due to the causes such as long-term or close contact with the infectious people, excessive stress and weakening of the immune system etc. Therefore, the model proposed in this study can be considered as a very useful tool to estimate the timing and the magnitude of both infection and possible re-infection.

## References

[1] Wang, J., Xu, T.-Z., Wei, Y.-Q. Wei, and Xie, J.-Q., Numerical solutions for systems of fractional order differential equations with Bernoulli wavelets. *International Journal Of Computer Mathematics*, DOI: 10.1080/00207160.2018.1438604, 1-20, 2018.

[2] Stankovic, T.M., Atanackovis, B., On a numerical scheme for solving differential equations of fractional order. *Mechanics Research Communications*, 35, 429 – 438, 2008.

[3] Daher Okiye, M.A., Aziz-Alaoui, M., Boundedness and global stability for a predator – prey model with modified Leslie – Gower and Holling-type II schemes. *Applied Math. Lett.*, 16, 1069-1075, 2003.

[4] Caputo, M., Linear models of dissipation whose Q is almost frequency independent. *Geophys. J. Int.*, 13, 5, 529–539, 1967.

[5] Clark, C.W., Mathematical models in the economics of renewable resources. *SIAM Rev.*, 21, 81 – 89, 1979.

[6] Mukherjee, T., Chaudhari, R.N., Das, K.S., Bioeconomic harvesting of a prey – predator fishery. *J. Biol. Dyn.*, 3, 447-462, 2009.

[7] Davis, H.D., *The Theory of Linear Operators*. Indiana: Principia Press, 1936.

[8] Peng, Y., Wang, R., Du, M., Effect of protection zone in the diffusive Leslie predator – prey model.. *J. Differ. Equ*, 3932 – 3956, 2009.

[9] El-Sayed, A.M.A., Multivalued fractional differential equations. *Aplied Math and Comput.*, 80, 1-11, 1994.

[10] El-Sayed, A.M.A., Fractional order evolution equations. *Journal Of Fractional Calculus*, 7, 89-100, 1995.

[11] Alidousti, K., Eshkaftaki, J., Ghaziani, B., Stability and dynamics of a fractional order Leslie-Gower prey-predator model. *Applied Math. Modelling*, 1-12, 2013.

[12] Podlubny, I., *Fractional Differential Equations*. New York: Academic Press, 1999.

[13] Jesus, I.S., Machado, J.A.T., Fractional control of heat diffusion systems. *Nonlinear Dynamics*, 54, 3, 2008.

[14] Vinagre, B.M., Petras, I., Merchan, P., Dorcak, L., Two Digital Realizations of Fractional Controllers: Application to Temperature Control of a Solid. in *Proceedings of the European Control Conference 2001* , Porto, Portugal, 2001, 1765-1767.

[15] Parada, F.J.V., Tapia, J.A.O., Ramirez, J.A., Effective medium equations for fractional Ficks law in porous media. *Physica A*, 373, 339-353, 2007.

[16] Torvik, P.J., Bagley, R.L., On the Appearance of the Fractional Derivative in the Behavior of Real Materials. *Transactions of the ASME*, 51, 294-298, 1984.

[17] Gaul, L., Klein, P., Kempfle, S., Damping description involving fractional operators. *Mech. Syst. Signal Process*, 5, 81-88, 1991.

[18] Miller, K.S., Ross, B., *An Introduction to the Fractional Calculus and Fractional Differential Equations*. New York: Wiley, 1993.

[19] Samko, G., Kilbas, A., Marichev, O., *Fractional Integrals and Derivatives: Theory and Applications*. Amsterdam: Gordon and Breach, 1993.

[20] Zaslavsky, G.M., *Hamiltonian Chaos and Fractional Dynamics*. Oxford: Oxford University Press, 2005.

[21] Matsuzaki, T., Nakagawa, M., A chaos neuron model with fractional differential equation. *J. Phys. Soc. Japan*, 72, 2678-2684, 2003.

[22] Ahmed, E., El-Sayed, A.M.A., El-Saka, H.A.A., Equilibrium points, stability and numerical solutions of fractional-order predator–prey and rabies models. *J. Math. Anal. Appl*, 325, 542-553, 2007.

[23] Turchin, P., Does population ecology have general laws?. *Oikos*, 94, 17-26, 2001.

[24] Malthus, T.R., *An Essay On The Principle Of Population as it Affects The Future Improvement of Society*. London: J. Johnson, 1798.

[25] Pearl, R., Reed, L.J., On the rate of growth of the population of the united states since 1790 and its mathematical representation. *Proceedings of the National Academy of Sciences*, 6, 6, 275 – 288, 1920.

[26] Verhuslt, P.F., Notice sur la loi que la population suit dans son accroissement. *Correpondance mathematique et Physique*, 10, 112–121, 1838.

[27] Winsor, C.P., The Gompertz curve as a growth curve. *Proceedings of the national academy of sciences*, 18, 1, 1-8, 1932.

[28] Gompertz, B., On the nature of the function expressive of the law of human mortality, and on a new mode of determining the value of life contingencies. *Philosophical Transactions of the Royal Society of London*, 115, 513-585, 1825.

[29] Durbin, P.W., Jeung, N., Williams, M.H., Arnold, J.S., Construction of a growth curve for mammary tumors of the rat. *Cancer Research*, 27, 1341-1347, 1967.

[30] Chow, G.C., Technological change and the demand for computers. *The American Economic Review*, 57, 5, 1117–1130, 1967.

[31] Stranndberg, P.E., The chemostat. Tech. rep.. *Univeristy of Linköping*, 2003.

[32] Gard, T.C., Hallam, T.G., Persistence in food webs: I Lotka-Volterra food chains. *Bull. Math. Biol.*, 41, 877-891, 1979.

[33] Lotka, A.J., *Elements of physical biology*. Baltimore: Williams and Wilkins, 1925.

[34] Volterra, V., Fluctuations in the abundance of a species considered mathematically. *Nature*, 118, 558–560, 1926.

[35] Kolmogorov, A.N., Sulla teoria di Volterra della lotta per l' esistenza. *Giornale Istituto Ital. Attuari*, 7, 74-80, 1936.

[36] May, R.M., Limit cycles in predator-prey communities. *Science*, 177, 900-902, 1972.

[37] Sterman, J.D., *Business dynamics: Systems Thinking and Modeling for a Complex World*., 2000.

[38] Daşbaşı, B., The Fractional-Order mathematical modeling of bacterial resistance against multiple antibiotics in case of local bacterial infection. *Sakarya University Journal of Science*, 251, 3, 1-13, 2017.

[39] Mondragón E.I., et al., Mathematical modeling on bacterial resistance to multiple antibiotics caused by spontaneous mutations. *BioSystems*, 117, 60–67, 2014.

[40] Ternent, L., Dyson, R.J., Krachler, A.M., Jabbari, S., Bacterial fitness shapes the population dynamics of antibiotic resistant and susceptible bacteria in a model. *J. Theor. Biol.*, 372, 1-11, 2014.

[41] Daşbaşı, B., Öztürk, İ., Mathematical modelling of bacterial resistance to multiple antibiotics and immune system response. *SpringerPlus*, 5, 408, 1-17, April 2016.

[42] Daşbaşı, B., Öztürk, İ., The dynamics between pathogen and host with Holling type 2

response of immune system. *Journal Of Graduate School of Natural and Applied Sciences*, 32, 1-10, 2016.

[43] Kostova, T., Persistence of viral infections on the population level explained by an immunoepidemiological model. *Math. Biosci.*, 206, 2, 309-319, 2007.

[44] Daşbaşı, B., Dynamics between Immune System-Bacterial Loads. *Imperial Journal of Interdisciplinary Research*, 2, 8, 526-536, 2016.

[45] Pugliese, A., Gandolfi, A., A simple model of pathogen–immune dynamics including specific and non-specific immunity. *Math. Biosci.*, 214, 73–80, 2008.

[46] Daşbaşı B., Öztürk, İ., On The Stability Analysis of The General Mathematical Modeling of Bacterial Infection. *International Journal Of Engineering & Applied Sciences*, 10, 2, 93-117, 2018.

[47] Ahmed, E., El-Sayed, A.M.A., El-Saka, H.A.A., Equilibrium points, stability and numerical solutions of fractional-order predator-prey and rabies models. *J. Math. Anal. Appl.*, 325, 542-553, 2007.

[48] Handel, A., Margolis, E., Levin, B., Exploring the role of the immune response in preventing antibiotic resistance. *J.Theor.Biol.*, 256, 655–662, 2009.

[49] Smith, A., McCullers, J., Adler, F., Mathematical model of a three-stage innate immune response to a pneumococcal lung infection. *J. Theor. Biol.*, 276, 106–116, 2011.

[50] Campion, J.J., McNamara, P.J., Evans, M.E., Pharmacodynamic modeling of ciprofloxacin resistance in Staphylococcus aureus. *Antimicrob. Agents Chemother*, 49, 1, 209-219, 2005.

[51] Chung, P., McNamara, P.J., Campion, J.J., Evans, M.E., Mechanism-based pharmacodynamic models of fluoroquinolone resistance in Staphylococcus aureus. *Antimicrob. Agents Chemother*, 50, 9, 2957–2965, 2006.

[52] Health Organization World, The Evolving Threat of Antimicrobial Resistance. in *Options for Action*, 2012, 1503-1518 ISBN: 978 924.

[53] Alavez, J., et al., Within-host population dynamics of antibiotic-resistant M. tuberculosis. *Math. Med. Biol.*, 24, 35-56, 2006.

[54] Mohtashemi, M., Levins, R., Transient dynamics and early diagnosis in infectious disease. *J. Math. Biol.*, 43, 446-470, 2001.

[55] Coll, P., Fármacos con actividad frente a Mycobacterium tuberculosis. *Enfer-medades Infecciosas y Microbiologa Clnica*, 27, 8, 474–480, 2009.

[56] Zhang, Y., Mechanisms of drug resistance in Mycobacterium tuberculosis. *Int. J. Tuberc. Lung Dis.*, 13, 11, 1320–1330, 2009.

[57] Romero, J., Ibargüen, E., Esteva, L., Un modelo matemático sobre bacteriassensibles y resistentes a antibióticos. *Matemáticas: Ensĕnanza Universitaria*, 20, 1, 55-73, 2011.

*International Journal of Engineering & Applied Sciences (IJEAS)*
*Vol.10, Issue 3 (2018) 237-251*
*http://dx.doi.org/10.24107/ijeas.458642*
Int J Eng Appl Sci 10(3) (2018) 237-251

# Critically Evaluate the Capabilities of Ultrasonic Techniques Used for Tracing Defects in Laminated Composite Materials

*Senan Thabet [a], Yaser A. Jasim [b] , Thabit H. Thabit [c*]*

*[a] Faculty of Computing, Engineering and Science, University of South Wales, Cardiff, UK*
*[b] Department of Accounting, Cihan University-Erbil, Erbil, Iraq*
*[c*] Collage of Electronic Engineering, Ninevah University, Mosul, Iraq*

*[*]E-mail address*: stc@englandmail.com [a], yaser.jasim@cihanuniversity.edu.iq [b] , thabit.acc@gmail.com [c*]*

*Received date: 30.09.2018*
*Accepted date: 31.10.2018*

*ORCID numbers of authors:*
*0000-0003-0251-7364[a], 0000-0003-3374-720X[b], 0000-0003-2033-6110[c]*

**Abstract**

*A Non-Destructive Test (NDT) technique is the fundamental strategy to look at a large portion of the materials, composite materials specifically. There are an excessive number of NDT techniques to assess the materials, for example, Visual Inspection, Liquid Penetrate Inspection, Eddy-Current Inspection, Phased Array Inspection, Magnetic Particle Inspection and Ultrasonic Inspection. The report delineates the Ultrasonic Test (UT) research centre examination that was directed with the group number 5 in the University lab, a few references and resources are utilised as a part of this investigation to completely exhibit the applications and deformity traceability of UT in covered composites. The paper finishes up the examination with the capacities and restrictions of the two systems and prescribes techniques to endeavour lessening the confinements.*

**Keywords:** Non-Destructive Testing, Ultrasonic Testing, and Composite Materials.

## 1. Introduction

Composite materials are a mix of two materials or more combined to get a specific basic properties, the blended materials don't break down totally in each other yet they act together as one strong material[1]. The reason for making composite materials is to get high pressure, low weight, fatigue resistance and corrosion resistance than the individual material. The request on composite materials has been expanded as the composite materials has expanded the execution and lessened the fuel utilisation particularly in aeronautics industry fields[2]. Since 60 years back Non-Destructive Test (NDT) has been in consistent advancement as it is the significant technique to decide and assess the composite materials[3]. In the most recent decades the vendors had an essential research for most composite materials to assess these sort of materials which are very surprising contrasted with ordinary materials[4]. The consolidated materials has supply the manufacturers with a one of a kind highlights that are inaccessible in typical materials. The designers advantage from the focal points offered by the composite materials that have light weight, hostile to consumption, high in opposition and incredible effectiveness proper for some applications in the mechanical area[5]. Because of

the complex tiny structure of these composite NDT techniques has been connected as often as possible to look at these entangled materials[6].

Presently nowadays ultrasonic tasting devices has a standout amongst the most utilised equipment and many well-known procedures worked to perform NDT appraisal on composite materials utilised as a part of aeronautical industry[7]. Despite of the unnecessarily various sorts of NDT materials examination, ultrasonic methodology is one of the broad strategies. In this investigation we will centre around ultrasonic technique which are extensively using ultrasonic area equipment and makes it possible to choose any disfigurements in numerous sorts of materials[8]. For evaluating composite materials ultrasonic procedures are for the most part used. With only a solitary access surface ultrasonic instrument are perfect to be used with either point column or straight line testing methodologies[9].

## 2. Discussion

### 2.1 Aims:

To discover any deformities in the composite materials by utilizing non-destructive test (NDT), with the ultrasonic equipment to trace any defects in the composite materials.

### 2.2 Objectives:

- Investigate ultrasonic technique as None-destructive testing method performed to asses laminated composites.
- Analyze their capabilities and limitations in tracking defects in composite structures.
- For effective NDT experiments, it is important to understand the nature of the material being tasted for better results.

In this paper we will review the carbon fibre as the ultrasonic investigation is appropriate for these sort of composites. In 1878 Sir Joseph Wilson Swan delivered glaring lights with carbon strings. Carbon fibre produced using around ten layers squeezed together under high weight, vacuumed and a sap topping off. Carbon fibre composite is a high temperature obstruction, weightless and fatigue, corrosion resistance[6].

A contact technique is been connected to examine composite materials by phase array method moved over the tasted piece[2]. A specific measure of frequency could be applied. The surface ought to be perfect and smooth, a medium called couplant is performed between the test and the inspect material to beat the power scattering which exists when the sound waves travel between the test and the surface of the composite and to fill the minute holes giving an exceptionally smooth surface to the test of the ultrasonic hardware to movement on[3].

In aeronautical industry NDT strategy considered as a much solid procedure to distinguish and recognize the deformities that can seriously influence the composite structure prompts terrible catastrophe particularly in formula1, ocean, aeronautical industry and more[5].

A specific frequency will be connected and it can shift between 5 MHz to 10 MHz through a test which is inside partitioned in to 64 sections to have the capacity to cover as much it

can[2]. This frequency will go through the composite make an interpretation of the outcome in to a diagram, frequency travelling would inverts if any deformity exists generally will bear on until the base surface of the composite, in the other word the information result of the ultrasonic device comes as a chart which would ready to clarified by the designers[1]**.**

## 2.3 Literature Review:

Because of past examinations have exhibited that the specialist and the planners dependably battle and striving to give best, powerful and solid devices at least conceivable cost with a superior execution to deliver the most precise gear that the designers could depend on to give a more secure condition.

In 1929 and 1935 ultrasonic waves contemplated by Sokolov to identify metal items. In 1931 Mulhauser obtained a patent in ultrasonic wave by utilizing two transducers to uncover abandons in solids. Firestone and Simons (1940) (1945) separately enhanced pulse ultrasonic testing by utilising a pulse-echo method. Josef Krautkrämer and Karl Deutsch 1949 in Germany both began in changes without the learning of each other. Josef Krautkrämer and his sibling the physicists Herbert working in oscilloscopes field. Karl Deutsch a mechanical specialist and Hans-Warner Branscheid a radar professional who had got some additional specialised understanding amid the second world two. The ultrasonic devices has been exhibited by the two organisations and as yet contending each other up to this point nowadays[10, 11]**.**

## 2.4 Ultrasonic Testing (UT) Implementations in Composites:

Notwithstanding the limitations of ultrasound testing system, this NDT strategy can give significant data to professionals while utilising them to assess composites[2]. At the point when UT is rehearsed on composites, it determines thickness estimations of composites and in addition mechanical deformities area and seriousness[1]. Broad inquires about and thinks about have been directed by a few organisations to comprehend the proliferation conduct of ultrasounds through laminated materials and its impact as shown in figure (1)[12].

In ultrasonic test devices, a sonic power is changed over from electrical power by methods for an equipment called a transducer (probe)[4]. The reason for a transducer is to transmit bunch of waves all through a test piece and get signals back to decide the state of a test composite[1]. As it were, pulse-echo ultrasound check uses high frequency to assess the separation by estimating it as far as time of flight[13]. To execute ultrasonic testing procedure on a test piece, there are three ultrasound testing basic techniques[14].


Fig. 1. The Ultrasonic Equipment

First Technique is called Through-Transmission Manner, in this technique we need to use two probes, we call the first one a sender and the second one is a receiver, to determine a composite the two probes need to be placed on both sides, the defect position is the scanning result.

Second Technique called Pitch-Catch technique, this technique in practice used for cylindrical materials, in this technique the ultrasonic waves travelling in shape of angle in the material and reflected back at the same transmitted angle.

Third Technique called Pulse-Echo technique, in this technique one probe only to be used, hence from one side only and to be placed perpendicular to the material and a bunch of ultrasonic waves send through and they are echoed back by the delamination or by reluctant material.

The reflected information of the ultrasonic waves is gathered and exhibited in different shapes yet, there are four general structures are presented in the NDT field as indicated by*:*

- A-scan: It is a graph, it presents the amount of reflected ultrasonic waves against the time as well as the depth of the defect in X and Y axis.

- B-scan: It displays the cross-sectional image of the composite shows the depth of the defect from the surface and it shows the exact position of the defect as well as the capability to detect for any other defects might be underneath previous defect found from C-scan as the ultrasonic waves won't be able to travel thorough defects.

- C-scan: It displays the top view image of the composite shows the number of the defects and the exact position of each defect in term of X and Y coordinates.

- S-scan: It displays the area only underneath the probe which is very limited but it is very effective as it is giving more details of every individual defect.

Phase Array system connected to examine laminated composites is a contact technique, where the test is physically moved over the examined piece[15]. A specific frequency is connected, which can change between 5 MHZ to 10 MHZ yet, any spectacular excess of the frequency can contrarily influence the ultrasonic wave reduction causing a wrong results outcomes[1]. A type of medium called Couplant is actualized between the probe and the surface of a material to beat power waste, which happens while ultrasonic waves venture out from the transducer to the material[3]. Ultrasonic testing NDT technique is a dependable method utilized as a part of composites to distinguish and recognize delamination that can severely impact the life cycle of the materials and lead to catastrophic disaster, particularly in aeronautical industry[12]. In different terms, phase array technique is a technique can be utilized to successfully in laminated composites and examine the depth of the sample.

## 2.5 Composite Materials

Composite materials define as two or more individual material combined together in one structure using pressure, heat and chemicals, as seen in figure (2). A high demand on materials with less weight and high rigidity particularly in aviation industry as the non-homogenous technology has raised the uniformity and solidity of the products as shown in figure (3)[16]. Composite materials can be classified in to three main types[6, 17]:

- Fiber Reinforced Composites (FRC) are mainly used to manufacturer bulletproof vests and in concrete as a hardening element by adding steel rods to increase the mechanical rigidity.

- Structural Materials are mainly used in aviation industry for its light weight, toughness, fatigue resistance and corrosion resistance made from two or more different types of materials bonded together to produce a rigid laminated materials.

- Practical-Reinforced Composite materials mainly used in civil engineering are consist of one or more materials such as sand and cement for example with some water place in a mold producing a tough material.

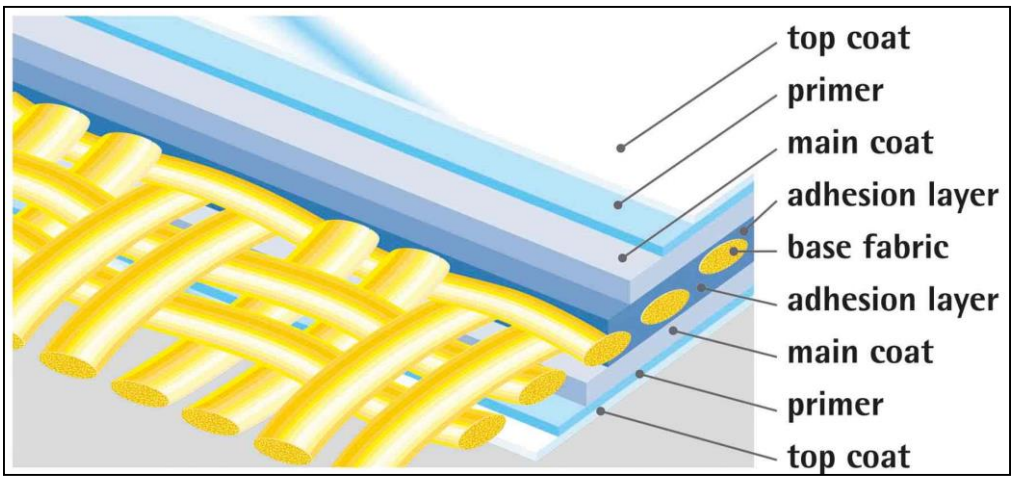


Fig. 2. Composite Materials

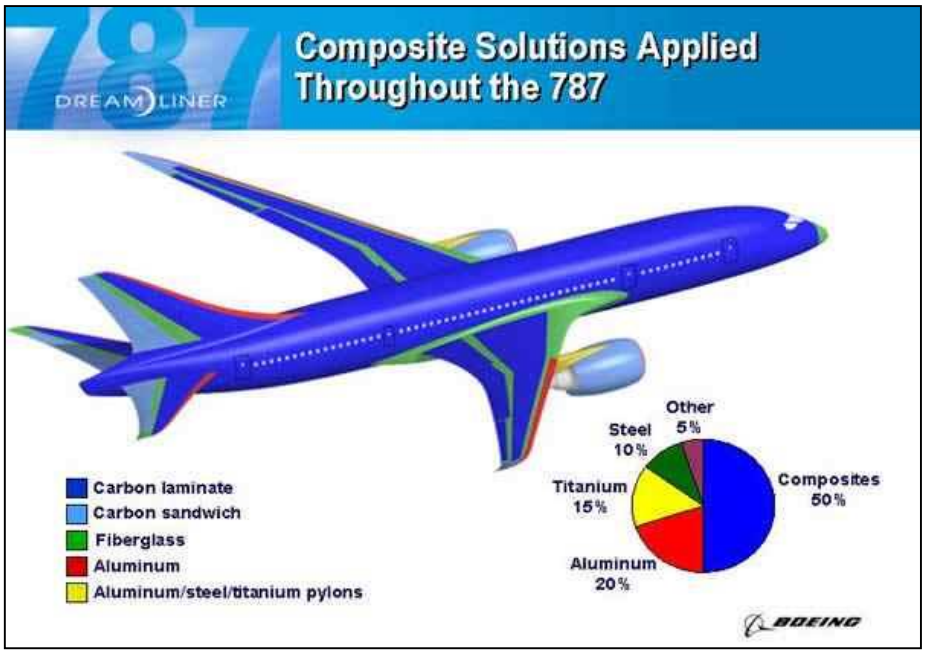


Fig. 3. Composite Materials in Aviation Industry

## 2.6 Capabilities:

The ultrasonic test is appropriate for testing the composite materials for very couple of reasons[18,19]:

- It can decide the size and the area of the defects.
- Resolution modification dislikes the other devices.
- Mobile and reduced, so it is so viable and could be conveyed to the area of the composite to be assessed which is extremely helpful particularly in aeronautical industry as the ultrasonic devices can be used in a work field without the prerequisite of research center condition .
- Ultrasonic test can guarantee composite materials thickness to assure life anticipation.
- The profundity of imperfections along the composite materials can be assessed.
- Ultrasonic test devices can be connected from one side if there is any confinement to get to the composite materials.
- The ultrasonic waves travel in both high density and low density but it will be slower in low density.

## 2.7 Limitations:

There are vary couple of impediments utilizing ultrasonic test on composite materials, such as[20,21]:

- To carry out an effective test, understanding and practicing are required.

- Thin materials are extremely hard to quantify.
- The composite surface must be spotless and smooth with couplant to be included.
- While the signal travelling from the probe to the surface a power loss may cause an inaccurate outcome.
- In some high level ends they are costly to purchase.
- Once the waves hit the defect it will reflect and we cannot see anything pass the defect.
- Ultrasonic waves won't be able to travel through a vacuum defect as it has a no density.

## 2.8 Ultrasonic Laboratory Experiment and Results:

### **2.8.1** Method:

At the university laboratory we were required to examine a piece of carbon-fibre material made from 10 layers (10*20) cm and 3mm thick with Olympus Omni equipment for any defects. The probe we used contains 64 elements and the more elements a higher resolution with 5 MHz frequency, we used a piece called wedge will hold the probe to keep the probe safe then we added a liquid called couplant to help the sound to transmit through different materials which is water based and the water is very conductive of sound plus this couplant would help to fill any gaps and make it smoother, after that we started to move the probe along the material bit by bit to cover the whole surface and get our results as explained in figures (4), (5), and (6).

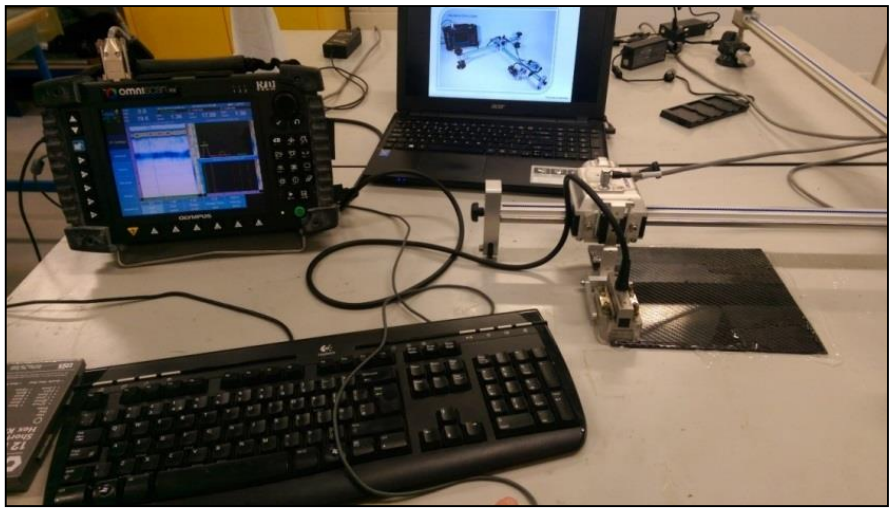

Fig. 4. Olympus Omni, Probe and Carbon-Fibre Spacemen

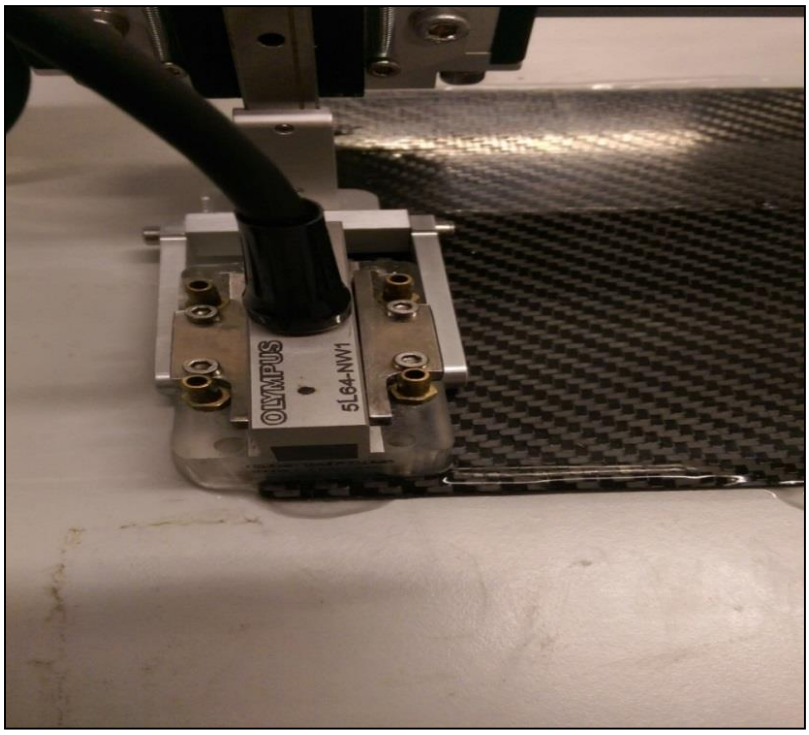


Fig. 5. The Probe

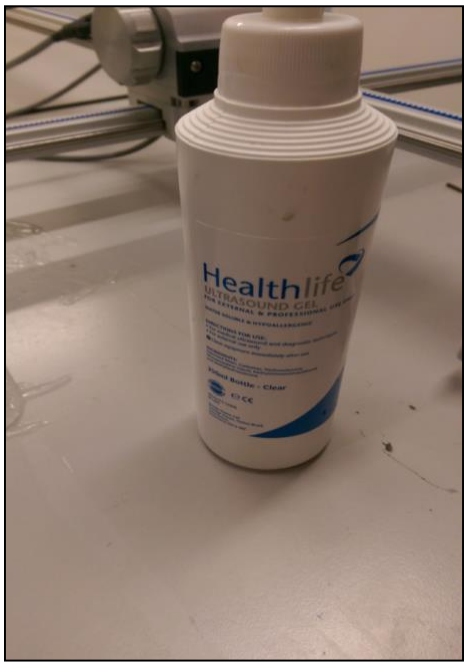


Fig. 6. Couplant

**2.8.2** Results:

In C-scan we found 5 defects, as seen in figure (7).

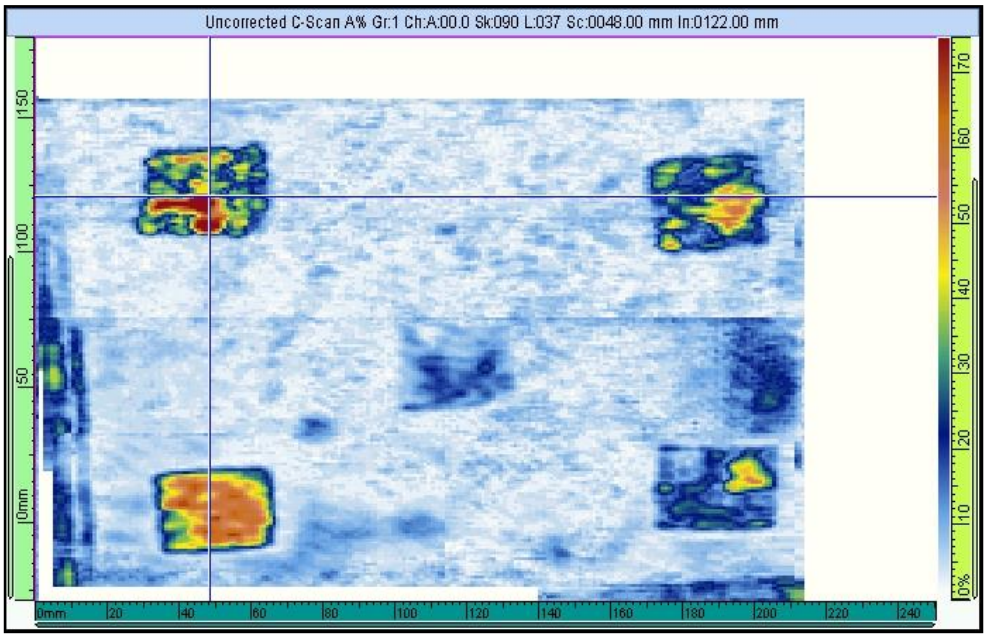


Fig. 7. 5 Defects in C-Scan

Figure (8) shows the 1st defect and the details as follows:

- A-Scan shows the defect is 0.25mm from the surface and the frequency bounced quicker.
- B-Scan shows the position of the defect which is around 0.25mm from the top surface and around 16mm from the right hand edge.
- C-Scan shows the number of the defects and their position.
- S-Scan shows the size of the defect and 0.25mm from the top surface.

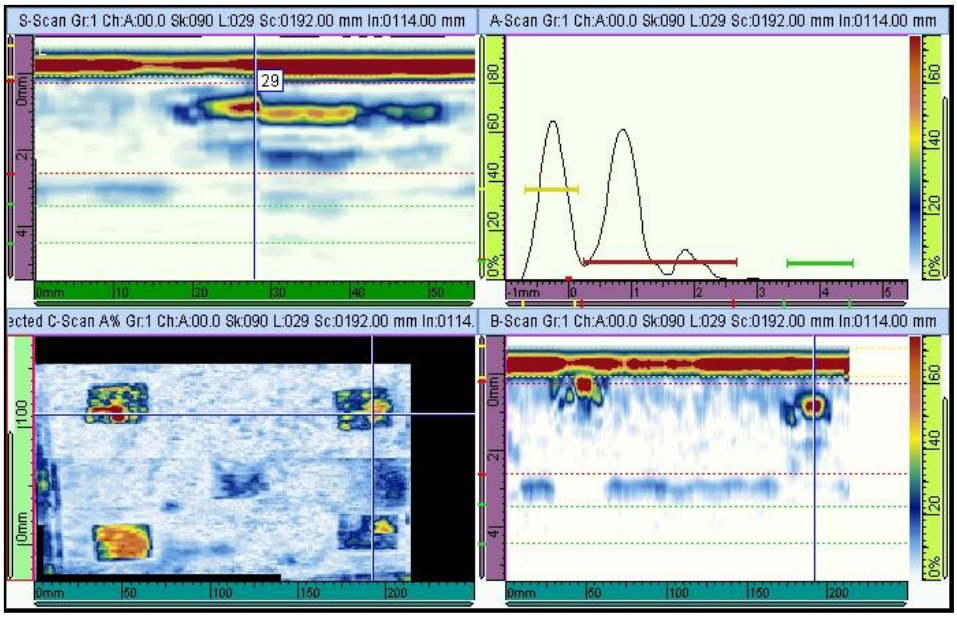


Fig. 8. Defect No.1

Figure (9) shows the 2nd defect, details as follow:

- A-Scan shows which is 2mm from the top surface and the frequency took much longer time.
- B-Scan shows which is around 2mm from the top surface and around 83mm from the right hand edge.
- C-Scan shows the number of the defects and their position.
- S-Scan shows the size of the defect and 2mm from the top surface.

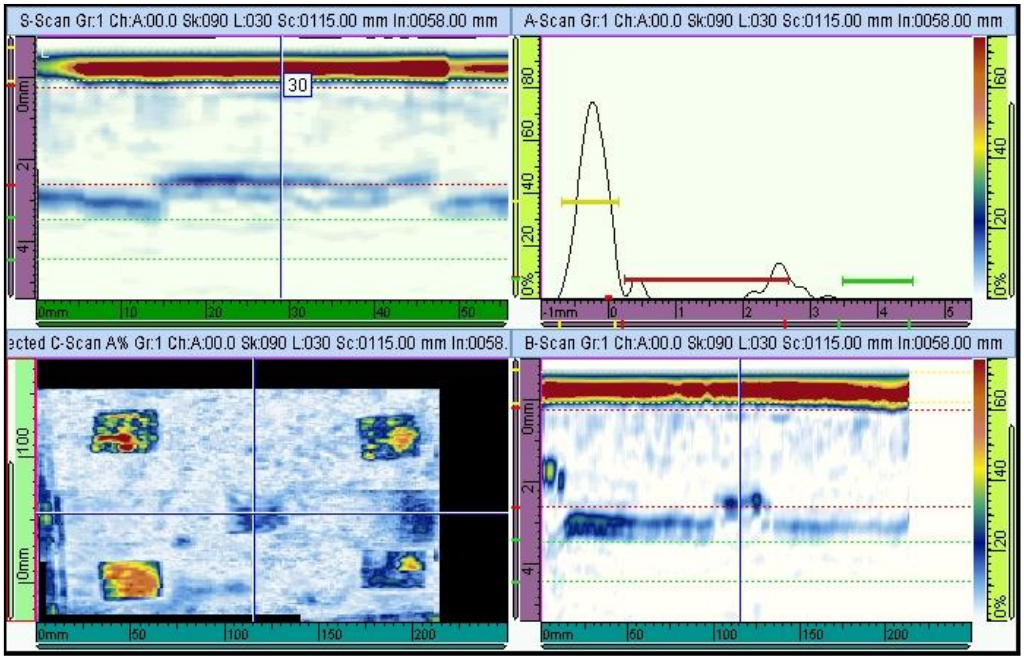


Fig. 9. Defect No.2

Figure (10) shows the 3rd defect, details as follow:

- A-Scan shows which is around 1.3mm from the top surface and the frequency took even much longer time.
- B-Scan shows which is around 1.3mm from the top surface and around 35mm from the left hand edge.
- C-Scan shows the number of the defects and their position.
- S-Scan shows the size of the defect and 1.3mm from the top surface.

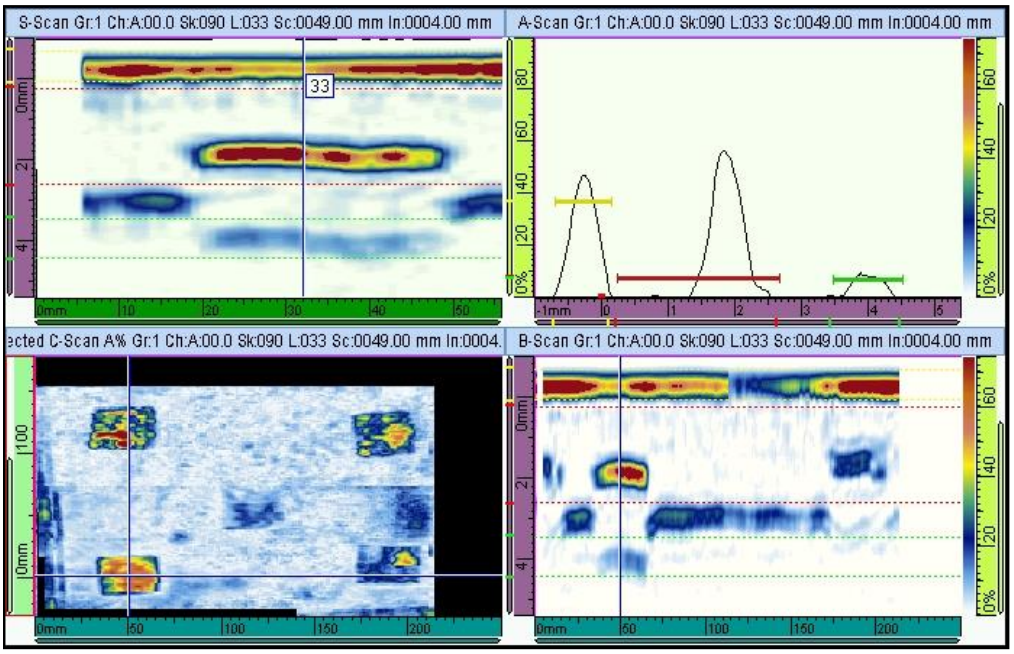


Fig. 10. Defect No.3

Figure (11) shows the 4th defect, details as follow:

- A-Scan shows is around 1.1mm from the top surface and the frequency took enough time to bounce.
- B-Scan shows which is around 1.1mm from the top surface and around 8mm from the right hand edge.
- C-Scan shows the number of the defects and their position.
- S-Scan shows the size of the defect and 1.1mm from the top surface.

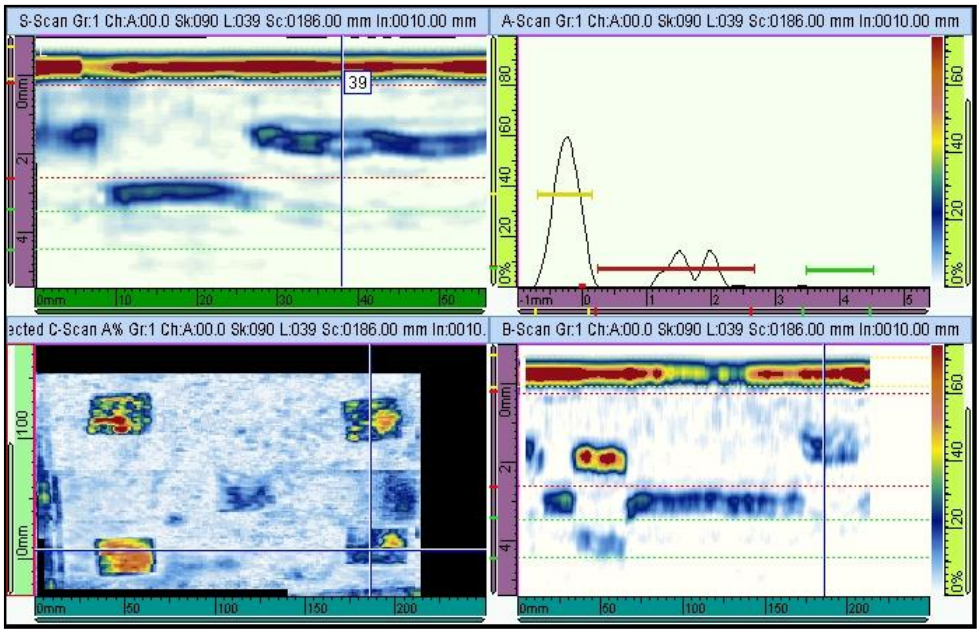


Fig. 11. Defect No.4

Figure (12) shows the 5th defect, details as follow:

- A-Scan shows is around 0.02mm from the top surface and the frequency took enough time to bounce.

- B-Scan shows which is around 0.02mm from the top surface and around 30mm from the left hand edge.

- C-Scan shows the number of the defects and their position.

- S-Scan shows the size of the defect and 0.02mm from the top surface.

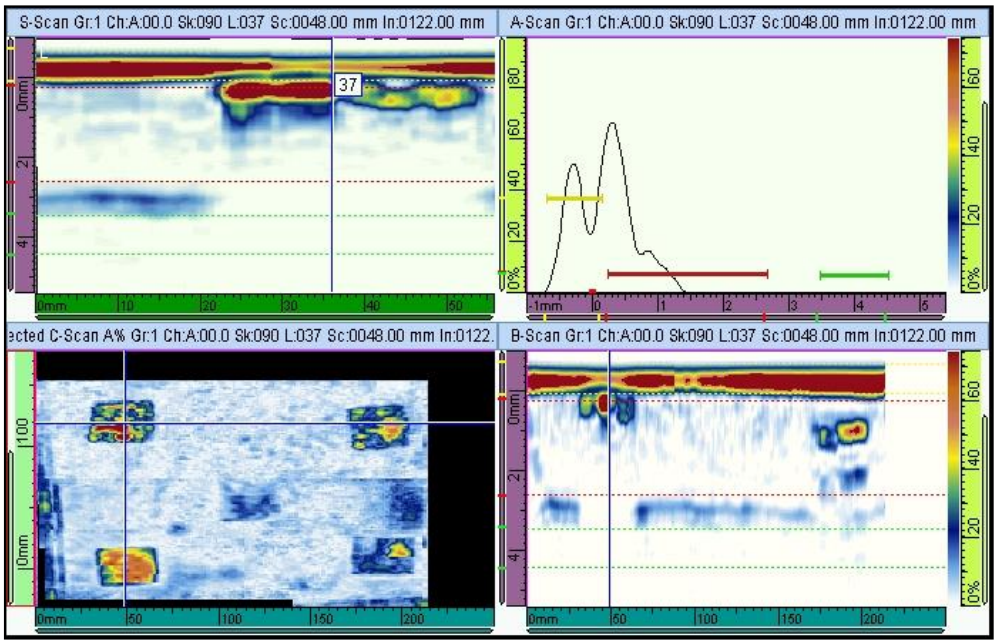


Fig. 12. Defect No.5

### **2.8.3** Omni Scan Report:

Table 1. Omni Scan Report

| Report Date | Report Version | Setup File Name | Inspection Date | Inspection Version | Save Mode |
|---|---|---|---|---|---|
| 2018 / 04 / 30 | MXU - 2.0R27 | 3MM_COMPOSITE_5L64NW1.ops | 2018 / 04 / 30 | MXU - 2.0R27 | Report |
| **OmniScan Type** | **OmniScan Serial #** | **Module Type** | **Module Serial #** | **Calibration Due** | **Data File Name** |
| OmniScan MX | OMNI-101144 | OMNI-M-PA16128 | OMNI-200577 | 2010 / 06 / 25 | team 5.opd |

**Group 1**

Setup

**A:00.0 Sk:090 L:001**

| Beam Delay | Start (Half Path) | Range (Half Path) | Max. PRF | Type | Averaging Factor |
|---|---|---|---|---|---|
| 17.76 us | -1.00 mm | 6.40 mm | 105 | PA | 1 |
| **Scale Type** | **Scale Factor** | **Video Filter** | **Pretrig.** | **Rectification** | **Band-Pass Filter** |
| Compression | 1 | On | 0.00 µs | FW | None (0.54 - 22 MHz) |
| **Voltage** | **Gain** | **Mode** | **Wave Type** | **Sound Velocity** | **Pulse Width** |
| 40 (Low) | 0.00 dB | PE (Pulse-Echo) | User-Defined | 4000.0 m/s | 100.00 ns |
| **Scan Offset** | **Index Offset** | **Skew** | | | |
| 0.00 mm | 0.00 mm | 90.0º | | | |

| Gate | Start | Width | Threshold | Synchro |
|---|---|---|---|---|
| I | -0.72 mm | 0.84 mm | 37.00 % | Pulse |
| A | 0.22 mm | 2.42 mm | 8.00 % | Pulse |
| B | 3.44 mm | 1.04 mm | 7.00 % | Pulse |

| TCG Point Number | Position (Half-Path) | Gain |
|---|---|---|
| 1 | 0.00 mm | 0.0 dB |

Calculator

| Used Element Qty. | First Element | Last Element | Resolution | Wave Type | Material Velocity |
|---|---|---|---|---|---|
| 8 | 1 | 64 | 1.0 | User-Defined | 4000.0 m/s |
| **Start Angle** | **Stop Angle** | **Angle Resolution** | **Focal Depth** | **Law Configuration** | |
| 0.0º | N/A | N/A | 20.00 mm | Linear at 0° | |

Part

| Material | Geometry | Thickness |
|---|---|---|
| PLEXIGLAS | Plate | 4.00 mm |

Scan Area

| Scan Start | Scan Length | Scan Resolution | Index Start | Index Length | Index Resolution |
|---|---|---|---|---|---|
| 0.00 mm | 250.00 mm | 1.00 mm | 0.00 mm | 285.00 mm | 57.00 mm |
| **Synchro** | **Max. Scan Speed** | | | | |
| Encoder | 105.00 mm/s | | | | |

| Axis | Encoder | Encoder Type | Encoder Resolution | Polarity |
|---|---|---|---|---|
| Scan | 2 | Quadrature | 13.00 step/mm | Inverse |
| Index | 1 | Quadrature | 13.00 step/mm | Inverse |

| A% | DA/ | PA/ | SA/ | A% | DA/ | ViA/ | VsA/ |
|---|---|---|---|---|---|---|---|
| 5.5 % | --- mm | --- mm | --- mm | 5.5 % | --- mm | --- mm | --- mm |

## 3. Conclusion and Recommendation:

As should be obvious from the examination has been done that the Non-Destructive Test technique is the most appropriate strategy for testing any materials and the composite materials as we utilized the ultrasonic review strategy, yet this technique was not ideal

strategy for this test as it has very couple of confinements restricting this technique to be an extraordinary technique in NDT. Our proposal is to pick the most appropriate NDT strategy as each material and composite materials have its own particular properties and in addition the assessment strategies had its own particular capabilities and limitations.

## References


[1] Salchak, Y., Zhvyrblya, V., Sednev, D., and Lider, A. (2016) Digitally focused array ultrasonic testing technique for carbon fiber composite structures, *IOP Conference Series: Materials Science and Engineering*, 135.

[2] Nesvijski, E. (1999) Phase Ultrasonic Testing of Joints in Multilayered Composite Materials. *Journal of Thermoplastic Composite Materials*, 12(2), pp.154-162.

[3] Gryzagoridis, J. (1989) Holographic non-destructive testing of composites, *Optics & Laser Technology*, 21(2), pp.113-116.

[4] Shen, Q., Omar, M., and Dongri, S. (2011) Ultrasonic NDE Techniques for Impact Damage Inspection on CFRP Laminates. *Journal of Materials Science Research*, 1(1), pp.3-14.

[5] Kamsu-Foguem, B. (2012) Knowledge-based support in Non-Destructive Testing for health monitoring of aircraft structures, *Advanced Engineering Informatics*, 26(4), pp.859-869.

[6] Reithmaier, L. and Sterkenburg, R. (2014) *Standard aircraft handbook for mechanics and technicians*, 7th edition, McGraw-Hill Education.

[7] Sharpe, R. (1976) Non-destructive testing, *Non-Destructive Testing*, 9(1), p.55.

[8] Thabit, Thabit H. (2013) *Adoption the Fuzzy Logic to Enhance the Quality of the Accounting Information to Operate Balanced Scorecard - Applied on Mosul Bank for Development & Investment in Nineveh Province*, M.Sc. thesis in accounting, University of Mosul, Mosul, Iraq.

[9] Thabit, Thabit H., and Jasim, Yaser A. (2015) A Manuscript of Knowledge Representation, *International Journal of Social Sciences & Economic Environment*, Vol.1, Issue 1, pp. 44-55.

[10] Thabet, S., and Thabit, Thabit H. (2018) Computational Fluid Dynamics: The Science of Future, *International Journal of Research and Engineering*, Vol.5, No. 6, pp. 430-433

[11] Thabet, Senan, and Thabit, Thabit H. (2018) CFD Simulation of the Air Flow around a Car Model (Ahmed Body), *International Journal of Scientific and Research Publications*, 8(8).

[12] Krautkrämer, J., and Krautkrämer, H. (1983) *Ultrasonic Testing of Materials*, Berlin, Heidelberg: Springer Berlin Heidelberg.

[13] Raj, B., Jayakumar, T., and Thavasimuthu, M. (2008) *Practical non-destructive testing*, Oxford, U.K.: Alpha Science International.

[14] Thabit, Thabit H., and Younus, Saif Q. (2018) Risk Assessment and Management in Construction Industries, *International Journal of Research and Engineering*, Vol. 5, No. 2, pp. 315-320.

[15] Bouden, T., Djerfi, F., and Nibouche, M. (2015) Adaptive split spectrum processing for ultrasonic signal in the pulse echo test, *Russian Journal of Nondestructive Testing*, 51(4), pp.245-257.

[16] Bates, C. (1969) Non-destructive testing techniques, *Non-Destructive Testing*, 2(1), pp.55.

[17] Thabet, Senan, Thabit, Thabit H., and Jasim, Yaser A. (2018), CFD Analysis of a Backward Facing Step Flows, *International Journal of Automotive Science and Technology*, Vol.2 , No.3 , pp.10-16.

[18] Berthelot, J. (2009) Damping Analysis of Sandwich Composite Materials, *Journal of Composite Materials*.

[19] Halmshaw, R. (1991) *Non destructive testing*, London.

[20] Hoagland (1979) Storage Technology: Capabilities and Limitations, *Computer*, 12(5), pp.12-18.

[21] Schall, W. (1968) *Non-destructive testing*, Brighton: Machinery Pub.

*International Journal of Engineering & Applied Sciences (IJEAS)*
*Vol.10, Issue 3 (2018) 252-263*
*http://dx.doi.org/10.24107/ijeas.468769*
Int J Eng Appl Sci 10(3) (2018) 252-263

# Vibration Analysis of an Axially Loaded Viscoelastic Nanobeam

*Mustafa ARDA* [a*]

[a]*Trakya University, Mechanical Engineering Department, Edirne, 22030 TURKEY*
[*]*E-mail address*: mustafaarda@trakya.edu.tr

*Received date: 09.10.2018*
*Accepted date: 02.11.2018*

*ORCID numbers of authors:*
*0000-0002-0314-3950*

**Abstract**

*Vibration of an axially loaded viscoelastic nanobeam has been studied in this paper. Viscoelasticity of the nanobeam has been modeled as a Kelvin-Voigt material. Equation of motion and boundary conditions for an axially compressed nanobeam has been obtained with help of Eringen's Nonlocal Elasticity Theory. Viscoelasticity effect on natural frequency and damping of nanobeam and critical buckling load have been investigated. Nonlocality effect on nanobeam structure in the view of viscoelasticity has been discussed.*

**Keywords:** viscoelastic nanobeam, nonlocal elasticity, vibration, axially loaded, buckling.

## 1. Introduction

Nano-sized structures are like carbon nanotubes (CNTs) taken interests of scientists over the years. The concept of design of a structure with superior properties getting attention of the industry. Possible applications of CNTs have increased day by day.

CNTs can be modeled by using continuum mechanics. Atomic interactions like small scale effect, surface stresses and long distance interaction can not be ignored in the nano-dimensional mechanics. Eringen [1,2] dealt with this problem and proposed the Nonlocal Elasticity Theory which includes the size effect and has been used in the most of the recent researches about modeling of CNTs.

Most of the papers about statics and dynamics of CNTs assumed that a CNT is an elastic structure. However, damping characteristics of CNT structures should be accounted in the continuum model for more realistic approach.

Lei et al. investigated the dynamic behavior of nonlocal viscoelastic Euler-Bernoulli [3] and Timoshenko nanobeams [4]. Dynamic stability and buckling of viscoelastic nanobeams studied by Chen et al. [5] and Pavlovic et al. [6]. Buckling of cantilever nanotubes [7,8], boron-nitride nanotubes [9] and silicon-carbide nanotubes [10] investigated by researchers. Karlicic et al. [11] carried out the free transverse vibration analysis of the multiple CNTs embedded in a viscoelastic polymer matrix which was affected by an axial magnetic field. Arani et al. [12] investigated the free and forced vibrations of double viscoelastic piezoelectric nanobeams with

the help of nonlocal viscoelasticity. Mohammadi [13] studied the vibration of rotating viscoelastic nanobeam with the thermal and humidity effect. Zhang et al. [14] investigated the transverse vibration of an axially loaded viscoelastic nanobeam embedded in elastic medium. Ebrahimi and Barati used the nonlocal strain gradient theory for the viscoelastic functionally graded (FG) nanobeams which resting on viscoelastic medium in the analysis of problems like: free vibration [15], hygro-thermal loading [16,17], surface and thermal effects [18] and size effect of nano-grains and nano-voids [19]. Attia and Mahmoud [20] modeled the viscoelastic nanobeam by using nonlocal couple-stress elasticity. Attia and Abdel Rahman [21] studied the free vibration of a FG viscoelastic nanobeams including the rotation and surface energy effects. Also, fractional nonlocal elasticity models have been proposed for dynamic analysis of viscoelastic nanobeams in recent studies [22–27] .

Present work assumes the CNT structure as a Kelvin-Voigt type viscoelastic material. Axial load effect through the buckling including nonlocal effect and viscoelasticity will be investigated. Variation of the non-dimensional frequency and damping of the nanobeam will be depicted in figures. Critical buckling load characteristics will be obtained.

## 2. Analysis

Viscoelastic nanobeams with simply supported and clamped-free boundary conditions are considered (Fig. (1)). The governing equation of motion for an axially loaded viscoelastic nanobeam can be interpreted as [28]:

$$E\left(1+\alpha\frac{\partial}{\partial t}\right)I\frac{\partial^4 w(x,t)}{\partial x^4}=-m\frac{\partial^2 w(x,t)}{\partial t^2}-P\frac{\partial^2 w(x,t)}{\partial x^2} \tag{1}$$

where $E$ is the Young's modulus, $m$ is the mass per unit length, $I$ is the moment of inertia, $w$ is the transverse displacement of the CNT, $\alpha$ is the viscous parameter of the viscoelastic material and $P$ is the axial load.

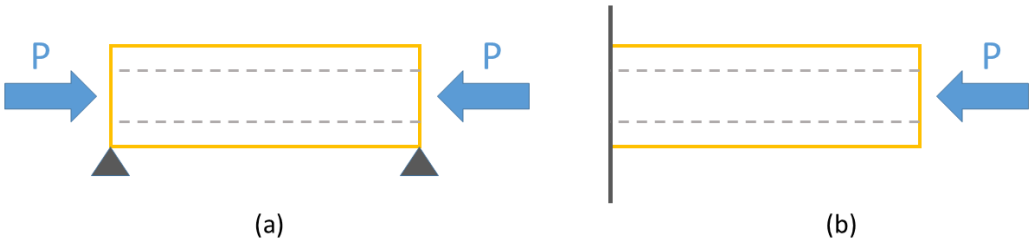


Fig. 1. Continuum Model of the Present Problem: a) Simply Supported Nanobeam b)Clamped-Free Nanobeam

### 2.1. Nonlocal Elasticity Approach

Nonlocal constitutive stress-strain relation can be expressed in differential form as [29]:

$$(1-\mu\nabla^2)\tau_{kl}=\lambda\varepsilon_{rr}\delta_{kl}+2G\varepsilon_{kl} \tag{2}$$

where $\tau_{kl}$ is the nonlocal stress tensor, $\delta_{kl}$ is the strain tensor, $\lambda$ and $G$ are the material constants and $\mu=(e_0 a)^2$ is called nonlocal parameter. Eringen obtained very close results to discrete theory results with a nonlocal continuum approach. With Eringen's assumption, the nonlocal model comprises both discrete and continuum approaches.

For isotropic viscoelastic carbon nanotube, nonlocal one dimensional relation in axial direction can be written as:

$$\left(1-\mu\frac{\partial^2}{\partial x^2}\right)\sigma = E\left(1+\alpha\frac{\partial}{\partial t}\right)\varepsilon \tag{3}$$

where $\varepsilon$ and $\sigma$ are the normal strain and the normal stress, respectively.

### 2.2. Nonlocal Equation of Motion and Boundary Conditions

If Eq. (3) is inserted into Eq. (1), one obtains [30,31]:

$$E\left(1+\alpha\frac{\partial}{\partial t}\right)I\frac{\partial^4 w(x,t)}{\partial x^4} = -\left(1-\mu\frac{\partial^2}{\partial x^2}\right)\left(m\frac{\partial^2 w(x,t)}{\partial t^2}+P\frac{\partial^2 w(x,t)}{\partial x^2}\right) \tag{4}$$

If Eq. (4) is reorganized according to D'Alambert Principle:

$$EI\alpha\frac{\partial^5 w(x,t)}{\partial x^4\partial t}+EI\frac{\partial^4 w(x,t)}{\partial x^4}+m\frac{\partial^2 w(x,t)}{\partial t^2}+P\frac{\partial^2 w(x,t)}{\partial x^2}-\mu m\frac{\partial^4 w(x,t)}{\partial x^2\partial t^2}-\mu P\frac{\partial^4 w(x,t)}{\partial x^4}=0 \tag{5}$$

Eq. (5) is the equation of motion of a viscoelastic nanobeam. If the nonlocal parameter and viscoelasticity parameter are assumed to be zero ($\mu$=0 , $\alpha$=0), the classical elasticity equation will be obtained. The boundary condition on both edges of nanobeam considered as simply supported (S-S) and clamped-free (C-F) which are defined below [32]:

$$\left.\begin{array}{l} x=0\ \begin{cases} w(0,t)=0 \\ -E\left(1+\alpha\frac{\partial}{\partial t}\right)I\frac{\partial^2 w(0,t)}{\partial x^2}+\mu P\frac{\partial^2 w(0,t)}{\partial x^2}+\mu m\frac{\partial^2 w(0,t)}{\partial t^2}=0 \end{cases} \\ x=L\ \begin{cases} w(L,t)=0 \\ -E\left(1+\alpha\frac{\partial}{\partial t}\right)I\frac{\partial^2 w(L,t)}{\partial x^2}+\mu P\frac{\partial^2 w(L,t)}{\partial x^2}+\mu m\frac{\partial^2 w(L,t)}{\partial t^2}=0 \end{cases} \end{array}\right\} S-S \tag{6}$$

$$\left.\begin{array}{l} x=0\ \begin{cases} w(0,t)=0 \\ \frac{\partial w(0,t)}{\partial x}=0 \end{cases} \\ x=L\ \begin{cases} -E\left(1+\alpha\frac{\partial}{\partial t}\right)I\frac{\partial^2 w(L,t)}{\partial x^2}+\mu P\frac{\partial^2 w(L,t)}{\partial x^2}+\mu m\frac{\partial^2 w(L,t)}{\partial t^2}=0 \\ -E\left(1+\alpha\frac{\partial}{\partial t}\right)I\frac{\partial^3 w(L,t)}{\partial x^3}-P\frac{\partial w(L,t)}{\partial x}+\mu P\frac{\partial^3 w(L,t)}{\partial x^3}+\mu m\frac{\partial^3 w(L,t)}{\partial x\partial t^2}=0 \end{cases} \end{array}\right\} C-F \tag{7}$$

The transverse displacement *w* can be expressed as:

$$w(x,t)=A(x)e^{\lambda t} \tag{8}$$

where *A(x)* and $\lambda$ is the amplitude function and characteristic value for viscoelastic nanobeam vibration, respectively. Inserting Eq. (8) into Eq. (5) gives following dimensionless equations of motion with the assumption of dimensionless nanotube length $\left(\bar{x}=\frac{x}{L}\right)$:

$$\frac{\partial^4 A(\bar{x})}{\partial\bar{x}^4}\left(1+\alpha\lambda-\frac{\mu}{L^2}\bar{P}\right)+\frac{\partial^2 A(\bar{x})}{\partial\bar{x}^2}\left(\bar{P}-\frac{\mu}{L^2}\Omega\lambda^2\right)+A(\bar{x})(\Omega\lambda^2)=0 \tag{9}$$

where $\bar{P}$ is the dimensionless axial load and $\Omega$ is the characteristic parameter coefficient which are defined as below:

$$\bar{P} = \frac{PL^2}{EI} \quad , \quad \Omega = \frac{mL^4}{EI} \tag{10}$$

Eq. (9) is a forth order differential equation and general solution can be written as:

$$A(\bar{x}) = C_1 e^{r_1 \bar{x}} + C_2 e^{r_2 \bar{x}} + C_3 e^{r_3 \bar{x}} + C_4 e^{r_4 \bar{x}} \tag{11}$$

where $C_i$ and $r_i$ ($i$=1,2,3,4) are the integration constants and the roots of the characteristic equation in Eq. (9), respectively. In Eqs. (6) and (7), boundary conditions should be written in matrix form using amplitude function in Eq. (8) for unknown coefficients as below:

$$\begin{bmatrix} P_{11} & P_{12} & P_{13} & P_{14} \\ P_{21} & P_{22} & P_{23} & P_{24} \\ P_{31} & P_{32} & P_{33} & P_{34} \\ P_{41} & P_{42} & P_{43} & P_{44} \end{bmatrix} \begin{bmatrix} C_1 \\ C_2 \\ C_3 \\ C_4 \end{bmatrix} = 0 \tag{12}$$

Eq. (12) is an eigen-value problem and the determinant of the coefficient matrix must be equal to zero for a nontrivial solution. Characteristic parameter (λ) for the viscoelastic nanobeam vibration can be obtained from determinant equation. λ is a complex number and its imaginary part defines the non-dimensional frequency (NDF) and real part defines the non-dimensional damping (NDD) of viscoelastic nanobeam.

Buckling is a structural stability loss and can be seen on axially loaded beams. It is a limit value problem that free vibration frequency of the structure drops to zero (See Eq. (13)).

$$\lim_{NDF \to 0} \bar{P} = P_{CR} \tag{13}$$

## 3. Numerical Results and Discussion

In this section, free transverse vibration analysis of the viscoelastic nanobeams has been carried out for various nonlocal parameter, viscous parameter and axial load.

Validation of the present nonlocal elastic CNT nanobeam model has been carried out in previous study [33]. Lattice dynamics results have been used in order to compare the nonlocal elastic stress gradient model. The nonlocal theory gives close results with the lattice dynamics results at the end of first Brillouin Zone.

In Fig. (2), the nonlocality and viscous effect on complex characteristic parameter of viscoelastic nanobeam in simply supported boundary condition can be seen. Softening effect of nonlocality has been addressed in previous works [34,35]. Nonlocal parameter reduces the NDF because of the softening. Viscous characteristics of the viscoelastic material also reduces with nonlocal parameter because nonlocality increases the elastic behavior of the material. Viscous parameter (α) decreases the NDF and increases the NDD. That is an expected result from the classical continuum mechanics approach. Clamped-free boundary condition results are shown in Fig. (3). Except one case, clamped-free boundary conditions gives same results with simply supported boundary case. In contrary to S-S case, clamped-free boundary condition increase the NDD and nanobeam buckles easily for higher nonlocal parameters. With applying compressive axial load, nanobeam can buckle easily in C-F boundary case and this situation can be seen clearly in Fig. (7).

In Figs. (4) and (5), axial compressive load effect on complex characteristic parameter of viscoelastic nanobeam can be seen. Axial load reduces the NDF and has no effect on NDD in simply supported boundary case. On the other hand, axial load change the vibration characteristics in clamped-free boundary case. Without the axial load, NDF and NDD increases with the help of nonlocality. With the axial load, NDF decreases and NDD increases reversely.

In the vibration of clamped-free nanobeams, nonlocal effect shows a strengthening effect on the material and fundamental frequency of nanobeam increases in contrary to other boundary conditions. This phenomena discussed by scientists in several studies [36–38] . Li et al. [39,40] pointed out that, both enhancing and weakening nonlocal effects are possible and correct. Nonlocal integral models have been used in recent studies to overcome this paradox [41–43].

Buckling of viscoelastic nanobeams can be seen in Figs. (6) and (7). NDF drops to zero with increasing effect of axial load. NDD doesn't change in S-S case but increases in C-F case with axial load. Viscoelasticity increases the NDF with nonlocal elasticity approach for a nanobeam without an axial load applied. This result is due to the nonlocal viscoelastic effects and contradicts with nonlocal elastic beam model.

Variation of critical buckling load is shown in Fig. (8) for the both boundary cases. Critical buckling load changes only with nonlocal parameter. Nonlocal parameters reduces CBL whereas viscous parameter couldn't change it.

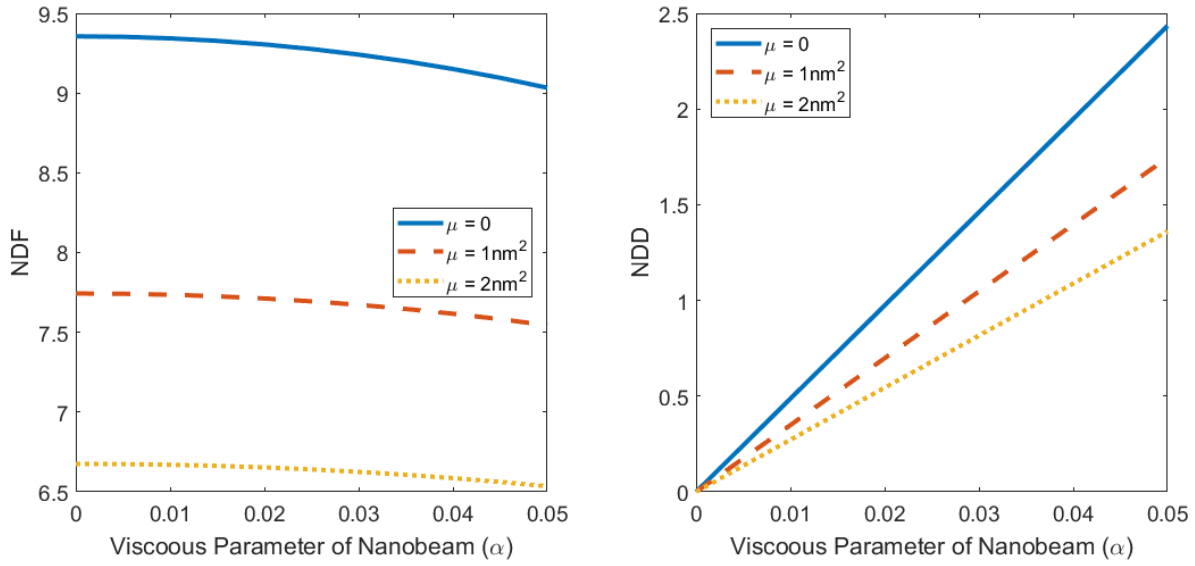


Fig. 2. Nonlocal and Viscous Parameter Effects on NDF and NDD in Simply Supported Boundary Condition ($\overline{P} = 1$)

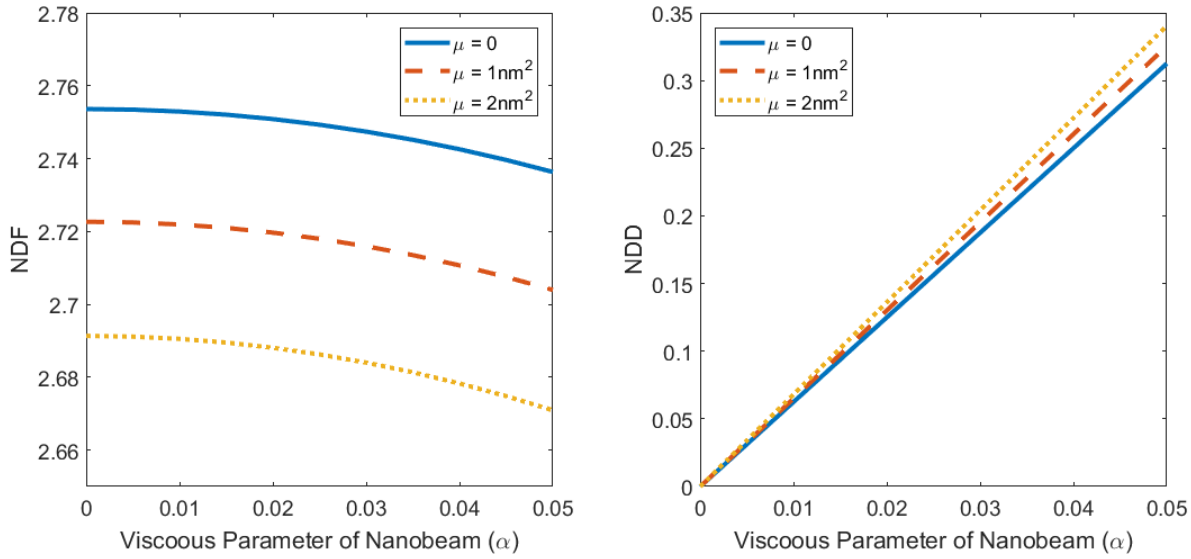


Fig. 3. Nonlocal and Viscous Parameter Effects on NDF and NDD in Clamped-Free Boundary Condition ($\overline{P} = 1$)

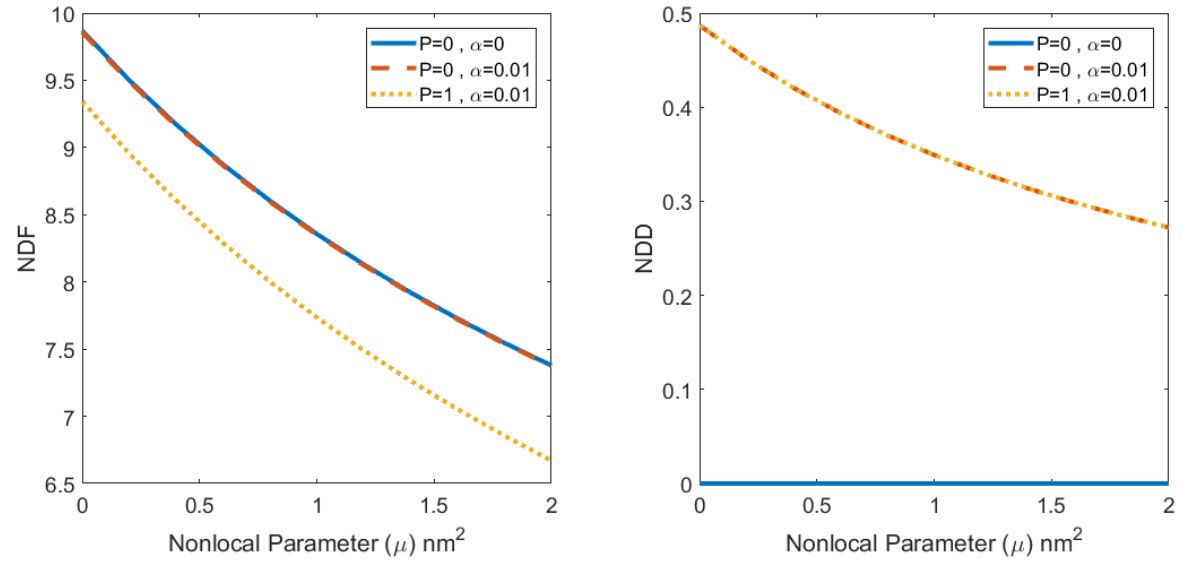


Fig. 4. Nonlocal, Viscous and Axial Load Effects on NDF and NDD in Simply Supported Boundary Condition

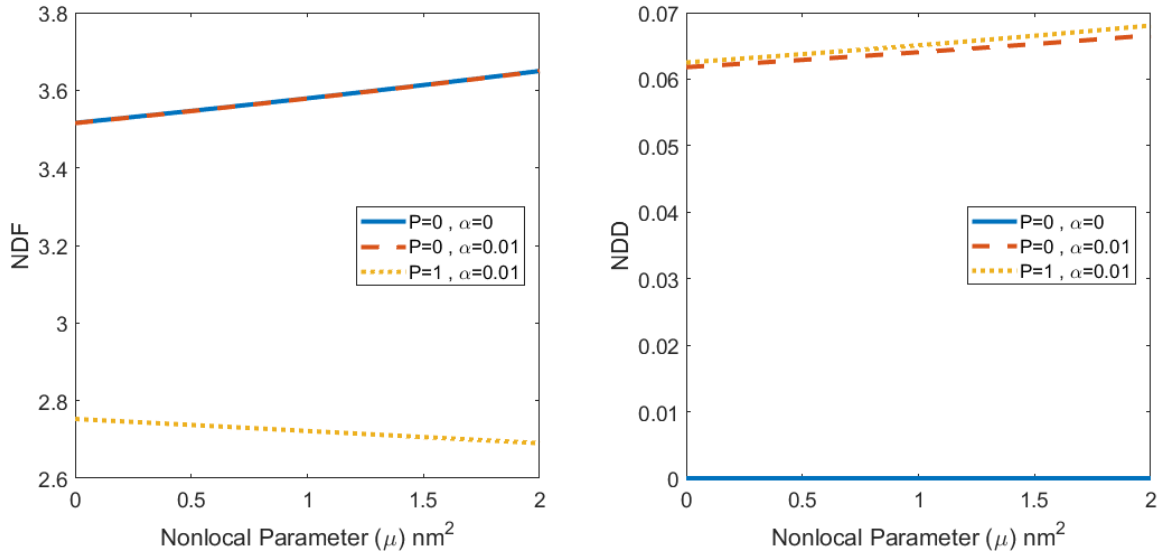


Fig. 5. Nonlocal, Viscous and Axial Load Effects on NDF and NDD in Clamped-Free Boundary Condition

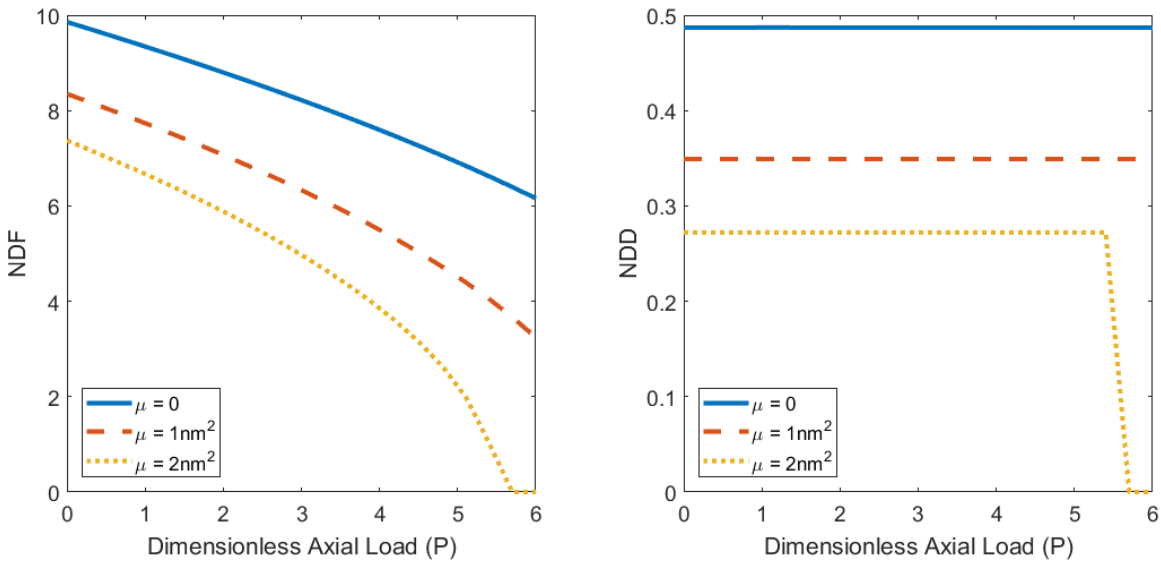


Fig. 6. Nonlocal Effect on Buckling of Viscoelastic Nanobeam in Simply Supported Boundary Condition (α=0.01)

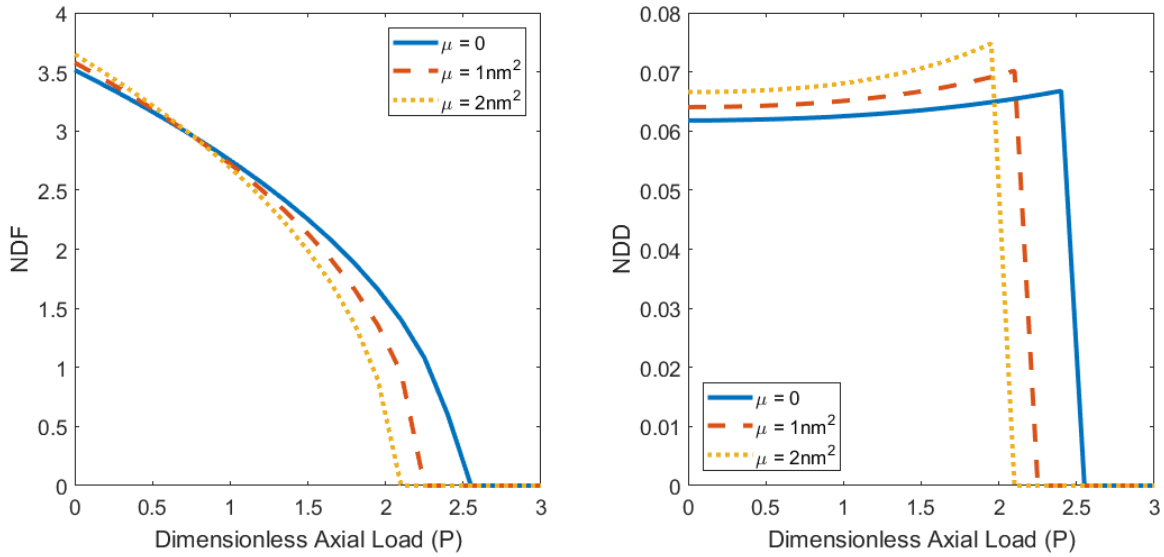


Fig. 7. Nonlocal Effect on Buckling of Viscoelastic Nanobeam in Clamped-Free Boundary Condition (α=0.01)

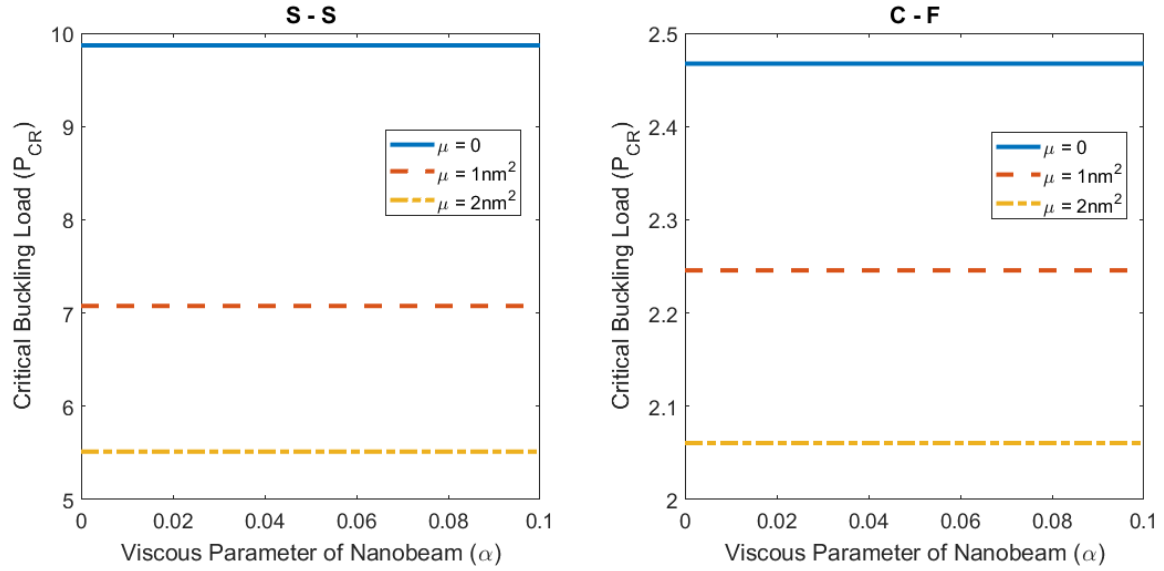


Fig. 8. Variation of Critical Buckling Load with Nonlocal and Viscous Parameters (NDF=NDD=0)

## 4. Conclusion

Present study deals with the vibration problem of an axially loaded viscoelastic nanobeam with simply supported and clamped-free boundary conditions. The nanobeam has been assumed as Kelvin-Voigt type viscoelastic material. Governing equations and boundary conditions have obtained with Eringen's Nonlocal Elasticity Theory. The viscous effect of viscoelastic medium decreases the complex characteristic parameter of nanobeam in simply supported boundary case. But in clamped-free boundary case, viscous effect increases the complex characteristic parameter because of the nonlocal boundary condition. Axial load and nonlocal effect shows

softening effect on nanobeam lattice structure. Results could be useful in designing a nano-mass sensor applications.

## References


[1] Eringen A.C., On differential equations of nonlocal elasticity and solutions of screw dislocation and surface waves, *Journal of Applied Physics*, 54, 4703–10, 1983. doi:10.1063/1.332803

[2] Eringen A.C., Nonlocal polar elastic continua, *International Journal of Engineering Science*, 10, 1–16, 1972. doi:10.1016/0020-7225(72)90070-5

[3] Lei Y., Murmu T., Adhikari S., Friswell M.I., Dynamic characteristics of damped viscoelastic nonlocal Euler-Bernoulli beams, *European Journal of Mechanics, A/Solids*, 42, 125–36, 2013. doi:10.1016/j.euromechsol.2013.04.006

[4] Lei Y., Adhikari S., Friswell M.I., Vibration of nonlocal Kelvin-Voigt viscoelastic damped Timoshenko beams, *International Journal of Engineering Science*, 66–67, 1–13, 2013. doi:10.1016/j.ijengsci.2013.02.004

[5] Chen C., Li S., Dai L., Qian C., Buckling and stability analysis of a piezoelectric viscoelastic nanobeam subjected to van der Waals forces, *Communications in Nonlinear Science and Numerical Simulation*, 19, 1626–37, 2014. doi:10.1016/j.cnsns.2013.09.017

[6] Pavlović I., Pavlović R., Ćirić I., Karličić D., Dynamic stability of nonlocal Voigt-Kelvin viscoelastic Rayleigh beams, *Applied Mathematical Modelling*, 39, 6941–50, 2015. doi:10.1016/j.apm.2015.02.044

[7] Civalek Ö., Demir C., Buckling and bending analyses of cantilever carbon nanotubes using the Euler-Bernoulli beam theory based on non-local continuum model, *Asian Journal of Civil Engineering*, 12, 651–62, 2011

[8] Akgöz B., Civalek Ö., Buckling Analysis of Cantilever Carbon Nanotubes Using the Strain Gradient Elasticity and Modified Couple Stress Theories, *Journal of Computational and Theoretical Nanoscience*, 8, 1821–7, 2011. doi:10.1166/jctn.2011.1888

[9] Mercan K., Civalek Ö., DSC method for buckling analysis of boron nitride nanotube (BNNT) surrounded by an elastic matrix, *Composite Structures*, 143, 300–9, 2016. doi:10.1016/j.compstruct.2016.02.040

[10] Mercan K., Civalek Ö., Buckling analysis of Silicon carbide nanotubes (SiCNTs) with surface effect and nonlocal elasticity using the method of HDQ, *Composites Part B: Engineering*, 114, 34–45, 2017. doi:10.1016/j.compositesb.2017.01.067

[11] Karličić D., Murmu T., Cajić M., Kozić P., Adhikari S., Dynamics of multiple viscoelastic carbon nanotube based nanocomposites with axial magnetic field, *Journal of Applied Physics*, 115, 234303, 2014. doi:10.1063/1.4883194

[12] Ghorbanpour-Arani A.H., Rastgoo A., Sharafi M.M., Kolahchi R., Ghorbanpour Arani A., Nonlocal viscoelasticity based vibration of double viscoelastic piezoelectric

nanobeam systems, *Meccanica*, 51, 25–40, 2016. doi:10.1007/s11012-014-9991-0

[13] Mohammadi M., Safarabadi M., Rastgoo A., Farajpour A., Hygro-mechanical vibration analysis of a rotating viscoelastic nanobeam embedded in a visco-Pasternak elastic medium and in a nonlinear thermal environment, *Acta Mechanica*, 227, 2207–32, 2016. doi:10.1007/s00707-016-1623-4

[14] Zhang Y., Pang M., Fan L., Analyses of transverse vibrations of axially pretensioned viscoelastic nanobeams with small size and surface effects, *Physics Letters, Section A: General, Atomic and Solid State Physics*, 380, 2294–9, 2016. doi:10.1016/j.physleta.2016.05.016

[15] Ebrahimi F., Barati M.R., Vibration analysis of viscoelastic inhomogeneous nanobeams incorporating surface and thermal effects, *Applied Physics A: Materials Science and Processing*, 123, 1–10, 2017. doi:10.1007/s00339-016-0511-z

[16] Ebrahimi F., Barati M.R., Hygrothermal effects on vibration characteristics of viscoelastic FG nanobeams based on nonlocal strain gradient theory, *Composite Structures*, 159, 433–44, 2017. doi:10.1016/j.compstruct.2016.09.092

[17] Ebrahimi F., Barati M.R., Effect of three-parameter viscoelastic medium on vibration behavior of temperature-dependent non-homogeneous viscoelastic nanobeams in a hygro-thermal environment, *Mechanics of Advanced Materials and Structures*, 25, 361–74, 2018. doi:10.1080/15376494.2016.1255831

[18] Ebrahimi F., Barati M.R., Vibration analysis of viscoelastic inhomogeneous nanobeams resting on a viscoelastic foundation based on nonlocal strain gradient theory incorporating surface and thermal effects, *Acta Mechanica*, 228, 1197–210, 2017. doi:10.1007/s00707-016-1755-6

[19] Ebrahimi F., Barati M.R., Damping Vibration Behavior of Viscoelastic Porous Nanocrystalline Nanobeams Incorporating Nonlocal–Couple Stress and Surface Energy Effects, *Iranian Journal of Science and Technology, Transactions of Mechanical Engineering*, 2017. doi:10.1007/s40997-017-0127-8

[20] Attia M.A., Mahmoud F.F., Analysis of viscoelastic Bernoulli–Euler nanobeams incorporating nonlocal and microstructure effects, *International Journal of Mechanics and Materials in Design*, 13, 385–406, 2017. doi:10.1007/s10999-016-9343-4

[21] Attia M.A., Abdel Rahman A.A., On vibrations of functionally graded viscoelastic nanobeams with surface effects, *International Journal of Engineering Science*, 127, 1–32, 2018. doi:10.1016/j.ijengsci.2018.02.005

[22] Oskouie M.F., Ansari R., Linear and nonlinear vibrations of fractional viscoelastic Timoshenko nanobeams considering surface energy effects, *Applied Mathematical Modelling*, 43, 337–50, 2017. doi:10.1016/j.apm.2016.11.036

[23] Oskouie M.F., Ansari R., Sadeghi F., Nonlinear vibration analysis of fractional viscoelastic Euler–Bernoulli nanobeams based on the surface stress theory, *Acta Mechanica Solida Sinica*, 30, 416–24, 2017. doi:10.1016/j.camss.2017.07.003

[24] Ansari R., Faraji Oskouie M., Rouhi H., Studying linear and nonlinear vibrations of

fractional viscoelastic Timoshenko micro-/nano-beams using the strain gradient theory, *Nonlinear Dynamics*, 87, 695–711, 2017. doi:10.1007/s11071-016-3069-6

[25] Ansari R., Faraji Oskouie M., Gholami R., Size-dependent geometrically nonlinear free vibration analysis of fractional viscoelastic nanobeams based on the nonlocal elasticity theory, *Physica E: Low-Dimensional Systems and Nanostructures*, 75, 266–71, 2016. doi:10.1016/j.physe.2015.09.022

[26] Ansari R., Faraji Oskouie M., Sadeghi F., Bazdid-Vahdati M., Free vibration of fractional viscoelastic Timoshenko nanobeams using the nonlocal elasticity theory, *Physica E: Low-Dimensional Systems and Nanostructures*, 74, 318–27, 2015. doi:10.1016/j.physe.2015.07.013

[27] Cajic M., Karlicic D., Lazarevic M., Nonlocal vibration of a fractional order viscoelastic nanobeam with attached nanoparticle, *Theoretical and Applied Mechanics*, 42, 167–90, 2015. doi:10.2298/TAM1503167C

[28] Marynowski K., Non-Linear Dynamic Analysis of an Axialy Moving Viscoelastic Beam, *Journal of Theoretical and Applied Mechanics*, 465–82, 2002

[29] Eringen A.C., Nonlocal Continuum Field Theories. Springer New York, 2007

[30] Civalek Ö., Demir Ç., Akgöz B., Static analysis of single walled carbon nanotubes (SWCNT) based on Eringen's nonlocal elasticity theory, *International Journal of Engineering and Applied Sciences*, 1, 47–56, 2009

[31] Akgöz B., Civalek Ö., Investigation of Size Effects on Static Response of Single-Walled Carbon Nanotubes Based on Strain Gradient Elasticity, *International Journal of Computational Methods*, 09, 1240032, 2012. doi:10.1142/S0219876212400324

[32] Reddy J.N., Pang S.D., Nonlocal continuum theories of beams for the analysis of carbon nanotubes, *Journal of Applied Physics*, 103, 2008. doi:10.1063/1.2833431

[33] Aydogdu M., A general nonlocal beam theory: Its application to nanobeam bending, buckling and vibration, *Physica E: Low-Dimensional Systems and Nanostructures*, 41, 1651–5, 2009. doi:10.1016/j.physe.2009.05.014

[34] Arda M., Aydogdu M., Buckling of Eccentrically Loaded Carbon Nanotubes, *Solid State Phenomena*, 267, 151–6, 2017. doi:10.4028/www.scientific.net/SSP.267.151

[35] Arda M., Aydogdu M., Nonlocal Gradient Approach on Torsional Vibration of CNTs, *NOISE Theory and Practice*, 3, 2–10, 2017

[36] Lu P., Lee H.P., Lu C., Zhang P.Q., Dynamic properties of flexural beams using a nonlocal elasticity model, *Journal of Applied Physics*, 99, 073510, 2006. doi:10.1063/1.2189213

[37] Eltaher M.A., Alshorbagy A.E., Mahmoud F.F., Vibration analysis of Euler-Bernoulli nanobeams by using finite element method, *Applied Mathematical Modelling*, 37, 4787–97, 2013. doi:10.1016/j.apm.2012.10.016

[38] Romano G., Barretta R., Diaco M., Marotti de Sciarra F., Constitutive boundary

conditions and paradoxes in nonlocal elastic nanobeams, *International Journal of Mechanical Sciences*, 121, 151–6, 2017. doi:10.1016/j.ijmecsci.2016.10.036

[39] Li C., A nonlocal analytical approach for torsion of cylindrical nanostructures and the existence of higher-order stress and geometric boundaries, *Composite Structures*, 118, 607–21, 2014. doi:10.1016/j.compstruct.2014.08.008

[40] Li C., Torsional vibration of carbon nanotubes: Comparison of two nonlocal models and a semi-continuum model, *International Journal of Mechanical Sciences*, 82, 25–31, 2014. doi:10.1016/j.ijmecsci.2014.02.023

[41] Challamel N., Reddy J.N., Wang C.M., Eringen's Stress Gradient Model for Bending of Nonlocal Beams, *Journal of Engineering Mechanics*, 142, 04016095, 2016. doi:10.1061/(ASCE)EM.1943-7889.0001161

[42] Eptaimeros K.G., Koutsoumaris C.C., Tsamasphyros G.J., Nonlocal integral approach to the dynamical response of nanobeams, *International Journal of Mechanical Sciences*, 115–116, 68–80, 2016. doi:10.1016/j.ijmecsci.2016.06.013

[43] Shaat M., Faroughi S., Abasiniyan L., Paradoxes of differential nonlocal cantilever beams: Reasons and a novel solution, 1–17, 2017

*International Journal of Engineering & Applied Sciences (IJEAS)*
*Vol.10, Issue 3 (2018) 264-275*
*http://dx.doi.org/10.24107/ijeas.471539*
Int J Eng Appl Sci 10(3) (2018) 264-275

# Defination of length-scale parameter in Eringen's Nonlocal Elasticity via Nolocal Lattice and Finite Element Formulation

*Büşra Uzun [a], Hayri Metin Numanoğlu [b], Ömer Civalek [c*]*

*[a] Uludağ University, Civil Engineering Department, Bursa, TURKIYE*
*[b,c] Akdeniz University, Civil Engineering Department, Antalya, TURKIYE*
*[*]E-mail address: uzunbusra34@gmail.com [a], metin_numanoglu@hotmail.com [b], civalek@yahoo.com [c*]*

*Received date: 10.10.2018*
*Accepted date: 03.11.2018*

*ORCID numbers of authors:*
*0000-0002-7636-7170[a], 0000-0003-0556-7850[b], 0000-0003-1907-9479[c]*

**Abstract**

*Nonlocal elasticity theory is one of the popular approaches for nano mechanic problems. In this study, nonlocal parameter is defined via different approach. Nonlocal finite element formulations for axial vibration of nanorods have been given and some parameters are compared with the lattice dynamics. Weak form and final finite element formulation for axial vibration case have been derived.*

**Keywords**: Nonlocal elasticity, finite element, axial vibration, rod, lattice dynamics.

## 1. Introduction

It is known that the general forms of the nonlocality are as follows [1]:

$$t_{kl,k} + \rho(f_1 - \ddot{u}_1) = 0 \tag{1}$$

$$t_{kl}(x) = \int_V \alpha(|x' - x|, \tau)\sigma_{kl}(x')dv(x'), \tag{2}$$

$$\sigma_{kl}(x') = \lambda e_{rr}(x')\delta_{kl} + 2\mu e_{kl}(x'), \tag{3}$$

$$e_{kl}(x') = \frac{1}{2}\left(\frac{\partial u_k(x')}{\partial x_l'} + \frac{\partial u_l(x')}{\partial x_k'}\right), \tag{4}$$

If the Eq. (2) is write in Eq. (1), we obtain

$$\frac{\partial \alpha}{\partial x_k}\sigma_{kl}(x') = -\frac{\partial \alpha}{\partial x'_k}\sigma_{kl}(x')$$

$$= -\frac{\partial}{\partial x'_k}\left[\alpha\sigma_{kl}(x')\right] + \alpha\frac{\partial \sigma_{kl}}{\partial x'_k} - \int_{\partial V}\alpha(|x'-x|)\sigma_{kl}(x')n'_k da(x') + \int_V \alpha(|x'-x|) \times \sigma_{kl,k}dv(x') + \rho(f_1 - \ddot{u}_1) = 0 \tag{5}$$

Here, the first integral through the surface represents the surface stresses. As a result, non-local elasticity theory includes surface physics, an important entity not included in classical theories. Again Eq. (3) and (4) introduce in Eq.(5), ones obtain

$$-\int_{\partial V}\alpha(|x'-x|)\left[\lambda u'_{r,r}\delta_{kl} + \mu(u'_{k,l} + u'k)\right]n'_k da' + \int_V \alpha(|x'-x|) \left[(\lambda+\mu)u'_{k,lk} + \mu u'_{l,kk}\right]dv' + \rho(f_1 - \ddot{u}_1) = 0 \tag{6}$$

In above equations the *(')* means depending on $x'$. Namely, $u' = u(x')$. If we solve the Eq.(6) under the suitable boundary and initial conditions, $u(x,t)$ displacement vector can be obtained. Initial conditions are depend $t_{kl}$ not $\sigma_{kl}$. So we can easily write $\tau_{\mathrm{kl}}n_k = t_{(n)l}$

## 2. Definition of nonlocal parameter in nonlocal elasticity

It is shown that the unit of nonlocal parameter located in Eq. (2) ($\alpha|x-x'|$) is (length)$^{-3}$. Thus, the non-local parameter will be dependent on a characteristic length ratio (*a/l*) in which an internal characteristic length a, (eg. lattice parameter, granular distance) and an external characteristic length *l* (eg, crack length, wavelength) is present. Thus it defined as

$$\alpha = \left(\alpha|x'-x|, \tau\right),\ \tau = \frac{e_0 a}{l} \tag{7}$$

Here $e_0$ will be different constant for each material. Some properties of nonlocal parameter are as follows:

- It reach the maximum value at $x' = x$ and decrease the value via $|x'-x|$ calculation.
- When $\tau \to 0$, the statement of $\alpha$ is become Dirac delta function. Hence, the boundary (limit) of the classical elasticity introduce the nearly zero value boundary of the internal length scale (a). Namely:

$$\lim_{\tau\to 0} = \left(\alpha|x'-x|, \tau\right) = \delta\left(\alpha|x'-x|\right) \tag{8}$$

So, it is easily said that “a” is a delta array.

- For small internal length scale value (such as $\tau \to 1$) nonlocal elasticity theory behave as atomic lattice dynamics.

By matching the wave distribution curves with the distribution curves of the atomic lattice dynamics (or experiments), we can determine "a"value for a certain material. Various forms have been obtained as a result of research [2-16]. Some of them are as follows:

One-dimensional parameter

$$\alpha(|x|,\tau)=\frac{1}{l\tau}\left(1-\frac{|x|}{l\tau}\right),|x|\le l\tau$$
$$\alpha(|x|,\tau)=0,\qquad |x|\ge l\tau \tag{9}$$

$$\alpha(|x|,\tau)=\frac{1}{2l\tau}e^{\sim\frac{|x|}{l\tau}} \tag{10}$$

$$\alpha(|x|,\tau)=\frac{1}{l\sqrt{\pi\tau}}e^{\frac{-x^2}{l^2\tau}} \tag{11}$$

Two-dimensional parameter

$$\alpha(|x|,\tau)=\frac{1}{2\pi l^2\tau^2}K_0\left(\frac{\sqrt{x\cdot x}}{l\tau}\right) \tag{12}$$

Here $K_0$ is a modified Bessel function.

Three-dimensional parameter

$$\alpha(|x|,t)=\frac{1}{8(\pi t)^{3/2}}e^{-\frac{x\cdot x}{4t}},t=\frac{l^2\tau}{4} \tag{13}$$

$$\alpha(|x|,\tau)=\frac{1}{4\pi l^2\tau^2\sqrt{x\cdot x}}e^{-\frac{\sqrt{x\cdot x}}{\pi l}} \tag{14}$$

When the equation 10 is examined, it is seen that the one-dimensional plane waves based on the Born-Kármán model, which is based on the theory of non-local elasticity and atomic lattice dynamics, fits perfectly with the distribution curve. When the two-dimensional parameter is analyzed, it is seen that the maximum error is 1.2% [1]. It is seen that all non-local parameters are normalized when the integrals are taken (over the length, area or volume). In addition, for

$\tau \to 0$ the Dirac delta function is obtained. With this feature, it is seen that when the term Dirac delta function is used in Equation 2, classical theory of elasticity is reverted and Hooke's law becomes valid. This observation was developed by Eringen [2] as follows:

If $\alpha$ is the linear differential operator Green function, we write

$$L\alpha\left(\left|x'-x\right|,\tau\right)=\delta\left(\left|x'-x\right|\right) \tag{15}$$

After used this Equation in Eq.(2), ones obtain

$$Lt_{kl}=\sigma_{kl} \tag{16}$$

Let be consider the L is a differential operator having constant coefficients

$$\left(Lt_{kl}\right)_{,k}=Lt_{kl,k} \tag{17}$$

So, we obtain the below equation

$$\sigma_{kl,k}+L\rho(f_1-\ddot{u}_1)=0 \tag{18}$$

Hence we obtain the differential equation instead of partial integral. For static case $L\rho(f_1-\ddot{u}_1)=0$

Finally, we can write below form

$$\sigma_{kl,k}=0 \tag{19}$$

If we sued the Eq. (19) in Eq.(3) we obtain the well-known Navier equation. So, differential operator as define via Eq.(3)

$$L=1-\tau^2 l^2\nabla^2 \tag{20}$$

After using this equation in Eq. (17) we obtained the following form

$$\left(1-\tau^2 l^2\nabla^2\right)t=\sigma \tag{21}$$

The accuracy of this result can be demonstrated by the atomic distribution relationship. For this purpose, the frequency expression obtained from the Born-Kármán model must be equal to the expression of non-local elasticity for plane waves.

## 3. Modeling by lattice dynamics

Lattice dynamics is known as harmonic approach provided that the displacements are small. In the chain, atoms can be connected with elastic springs (Figure 1).

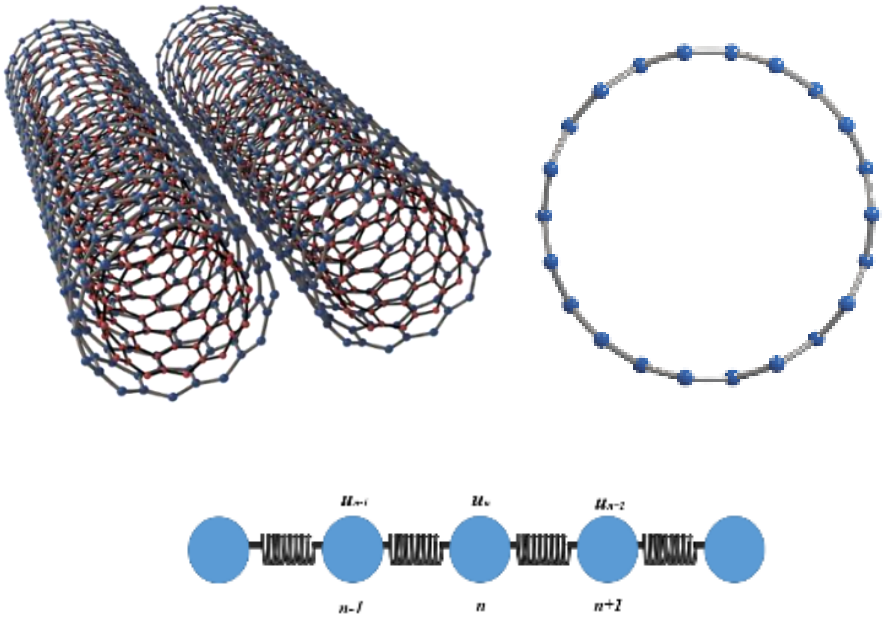

Fig. 1. One-dimensional lattice model

Therefore, force applied to the $n^{th}$ atom can be written as

$$F_n = K(u_{n+1} - u_n) + K(u_{n-1} - u_n) \tag{22}$$

Here K is the inter-atomic force (elastic) constant. Newton's second law applied to the $n^{th}$ atom

$$M\frac{d^2u_n}{dt^2} = F_n = K(u_{n+1} - u_n) + K(u_{n-1} - u_n) = -K(2u_n - u_{n+1} - u_{n-1}) \tag{23}$$

In the above expression M denotes the mass of the atom. Similarly, the equation for each atom in the cage should be written. N; In order to express the total number of atoms, the result is the N equation which must be solved simultaneously. In addition, the boundary conditions applied to the end of the cage must also be taken into account. The following conversion will be used for the solution

$$u_n = Ae^{i(kx_n - \omega t)} \tag{24}$$

Here, $x_n$ n. refers to the position of the atom and $x_n = na$. This equation represents a moving wave with q wavelength where all atoms oscillate at the same frequency ($q$) with the same $A$ amplitude. Equation (24) is written in Equation (23)

$$M(-\omega^2)e^{ikna} = -C(2e^{ikna} - e^{ik(n+1)a} - e^{ik(n-1)a}) \tag{25}$$

After some manipulation

$$M\omega^2 = C(2 - e^{ika} - e^{-ika}) = 2C(1 - \cos ka) \tag{26}$$

$$\frac{M}{C}\omega^2 = 2(1 - \cos ka) \tag{27}$$

Finally

$$\frac{M}{C}\omega^2 = 2(1 - \cos ka) = 4\sin^2\frac{ka}{2} \tag{28}$$

So, frequency and distribution relation is

$$\sqrt{\omega_j{}^2} = \sqrt{\frac{M}{C}\omega^2} = 2\left|\sin\frac{ka}{2}\right| \tag{29}$$

We expect the results obtained with the cage dynamics between the two atoms to be the same as the non-local elasticity results. In this case, the ratio of cage dynamics frequency distribution relation to bar frequency distribution relation

$$\alpha(k) = \frac{\omega_j{}^2(k)}{\omega_{oj}{}^2} = \left(\frac{2\kappa}{\pi k}\right)^2 \sin^2\left(\frac{\pi k}{2\kappa}\right) \tag{30}$$

Here angular frequency can be write as

$$\omega_{oj}{}^2 = c_0{}^2 k^2 \tag{31}$$

Also $c_0 = \sqrt{E/\rho}$. $\kappa$ is the Brillouin region is the value of the upper limit of k. This value is for one dimensional mesh dynamics. In the light of this information Equation (31) is reorganized

$$\alpha(k) = \frac{\omega_j{}^2(k)}{\omega_{oj}{}^2} = \left(\frac{2}{ka}\right)^2 \sin^2\left(\frac{ka}{2}\right) \tag{32}$$

If we write above equation as terms of cosine

$$\alpha(k) = \frac{\omega_j{}^2(k)}{\omega_{oj}{}^2} = \frac{2}{k^2a^2}(1 - \cos ka) \tag{33}$$

If the equation opens into the Maclaurin series

$$\cos ka = 1 - \frac{(ka)^2}{2!} + \frac{(ka)^4}{4!} - \frac{(ka)^6}{6!} + .... \tag{34}$$

$$1 - \cos ka = \frac{(ka)^2}{2!} - \frac{(ka)^4}{4!} + \frac{(ka)^6}{6!} - .... \tag{35}$$

After using these equations in Eq.(32), we obtain

$$\alpha(k) = \frac{2}{(ka)^2}(1 - \cos ka) = 1 - \frac{(ka)^2}{12} + \frac{(ka)^4}{360} - .... \tag{36}$$

Using the first-order approach and by using the first two-term of the Eq.36

$$\frac{1}{\alpha} = 1 + (e_0 a)^2 k^2 \tag{37}$$

After some arrangement

$$\alpha = \left(1 + e_0^2 a^2 k^2\right)^{-1},\ \left(1 + e_0^2 a^2 k^2\right)\bar{t}_{kl} = \bar{\sigma}_{kl},\ \left(1 - e_0^2 a^2 \nabla^2 - ...\right)t_{kl} = \sigma_{kl} \tag{38}$$

Hence, non-dimensional frequency via nonlocal elasticity is

$$\frac{\omega a}{c_0} = ka\left(1 + e_0^2 a^2 k^2\right)^{-1/2} \tag{39}$$

The relation of frequency distribution via lattice dynamics is as follows with the help of equation (29)

$$\frac{\omega a}{c_0} = 2\sin(ka/2) \tag{40}$$

If the Eq. (39) and Eq. (40) are equalized for $ka = \pi$

$$ka\left(1 + e_0^2 a^2 k^2\right)^{-1/2} = 2\sin(ka/2)$$

$$\pi\left(1 + e_0^2 \pi^2\right)^{-1/2} = 2\sin(\pi/2) \tag{41}$$

$$e_0 = 0.39$$

If second-order approach Eq. (36) extract the polynomial form in three-terms as

$$\frac{1}{\alpha} = 1 + (e_0 a)^2 k^2 + (\gamma_0 a)^4 k^4,\ \alpha = \left(1 + e_0^2 a^2 k^2 + {\gamma_0}^4 a^4 k^4\right)^{-1} \tag{42}$$

And nonlocal stress equation

$$\left(1 + e_0^2 a^2 k^2 + {\gamma_0}^4 a^4 k^4\right)\bar{t}_{kl} = \bar{\sigma}_{kl} \tag{43}$$

In this last equation $\bar{t}_{kl}$ and $\bar{\sigma}_{kl}$, means the Fourier transforms of $t_{kl}$ and $\sigma_{kl}$', respectively. If we take the inverse Fourier transform of Eq. (43)

$$\left(1 - e_0^2 a^2 \nabla^2 + {\gamma_0}^4 a^4 \nabla^4 - ...\right)t_{kl} = \sigma_{kl} \tag{44}$$

Also, the governing equation for stress in nonlocal case is

$$\sigma_{kl,k} + \left(1 - e_0^2 a^2 \nabla^2 + {\gamma_0}^4 a^4 \nabla^4\right)\left(\rho f_l - \rho \ddot{u}_l\right) = 0 \tag{45}$$

These equations replaced Navier's classical elasticity equations. New dimensionless frequency according to non-local elasticity theory is

$$\frac{\omega a}{c_0} = ka\left(1 + e_0^2 a^2 k^2 + {\gamma_0}^4 a^4 k^4\right)^{-1/2} \tag{46}$$

Lazar et al. [16]. Stated that $\varepsilon^4 = 4\gamma^4$. Frequency distribution relationship via lattice dynamics is as follows

$$\frac{\omega a}{c_0} = 2\sin(ka/2) \tag{47}$$

Eq. (46) and Eq. (47) are equalized for $ka = \pi$

$$\begin{gathered} ka\left(1 + e_0^2 a^2 k^2 + {\gamma_0}^4 a^4 k^4\right)^{-1/2} = 2\sin(ka/2) \\ \pi\left(1 + 2\gamma_0^2 \pi^2 + {\gamma_0}^4 \pi^4\right)^{-1/2} = 2\sin(\pi/2) \\ \gamma_0 = 0.24,\ \varepsilon_0 = 0.339 \end{gathered} \tag{48}$$

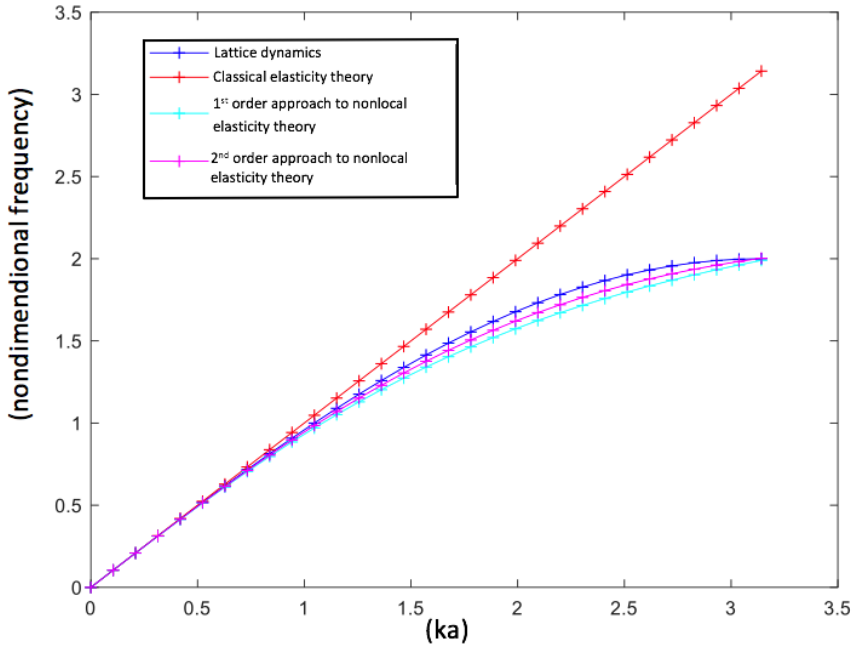


Fig. 2. Convergence of frequency value

The first and secon-order approaches of the theory of non-local elasticity, classical elasticity theory, and the frequency comparison of the lattice dynamics are presented in Figure 2. As can be seen from the figure, the frequency results for the second order approximation of non-local elasticity theory are closer to the lattice dynamic than the first-order approach. In more general case (under the axial foundation effect and thermal effect) free vibration form of axial vibration of elastic nanorod have been given as two different forms:

$$EA\frac{\partial^2 u}{\partial x^2} = \left(EA\alpha\Delta T\right)' - f(x) + k_w u(x) + \rho A\frac{\partial^2 u}{\partial t^2} + (e_0 a)^2 \frac{\partial^2}{\partial x^2}\left(f - k - \rho A\frac{\partial^2 u}{\partial t^2}\right) \tag{49}$$

$$\int_0^L \left[EA\frac{\partial u}{\partial x}\frac{\partial w}{\partial x} + EA\alpha_T\Delta_T\frac{\partial w}{\partial x} + wf(x) - wku(x) - \rho Aw\frac{\partial^2 u}{\partial t^2} - \mu f(x)\frac{\partial^2 w}{\partial x^2} - \mu k\frac{\partial w}{\partial x}\frac{\partial u}{\partial x} - \mu\rho A\frac{\partial^3 u}{\partial x\partial t^2}\frac{\partial w}{\partial x}\right]dx \tag{50}$$

Eq. (50) is the weak form for FEM approach of axial vibration. Some applications have also been listed in references related to macro, micro and nanomechanics [17-39].

## 4.Conclusion

Some comparison has been made for axial vibration. First and second order approach for nonlocal elasticity and lattice dynamics results have also been compared. Finally, weak form is given for axial vibration problem of nanorods.

## Acknowledgements

This study has been supported by The Scientific and Technological Research Council of Turkey (TÜBİTAK) with Project no: 117M495. This support is gratefully acknowledged.

## References

[1] Ari, N., Eringen A.C., Nonlocal Stress-Field at Griffith Crack, *Crystal Lattice Defects and Amorphous Materials*, 10(1), 33-38, 1983.

[2] Eringen, A. C., Linear theory of micropolar elasticity, *Journal of Mathematics and Mechanics*, 909-923, 1966.

[3] Eringen, A. C., A unified theory of thermomechanical materials, *International Journal of Engineering Science*, 4(2), 179-202, 1966.

[4] Eringen, A. C., Micropolar fluids with stretch, *International Journal of Engineering Science*, 7(1), 115-127, 1969.

[5] Eringen, A. C., Linear Theory of Nonlocal Elasticity and Dispersion of Plane-Waves, *International Journal of Engineering Science*, 10(5), 425-435, 1972.

[6] Thoft-Christensen, P., *Continuum Mechanics Aspects of Geodynamics and Rock Fracture Mechanics: Proceedings of the NATO Advanced Study Institute held in Reykjavik, Iceland, 11—20 August, 1974.* (Vol. 12), Springer Science & Business Media, 2012.

[7] Eringen, A. C., Nonlocal Polar Elastic Continua, *International Journal of Engineering Science*, 10(1), 1-16, 1972. doi: 10.1016/0020-7225(72)90070-5

[8] Eringen, A. C., On nonlocal fluid mechanics, *International Journal of Engineering Science*, 10(6), 561-575, 1972.

[9] Eringen, A. C., Nonlocal polar field theories, *Continuum physics*, 4(Part III), 205-264, 1976.

[10] Eringen, A. C., Screw Dislocation in Nonlocal Elasticity, *Journal of Physics D-Applied Physics*, 10(5), 671-678, 1976. doi: 10.1088/0022-3727/10/5/009.

[11] Eringen, A. C., On differential equations of nonlocal elasticity and solutions of screw dislocation and surface waves, *Journal of applied physics*, 54(9), 4703-4710, 1983.

[12] Eringen, A. C., *Nonlocal continuum field theories*, Springer Science & Business Media, 2002.

[13] Eringen, A. C., Edelen, D. G. B., On nonlocal elasticity, *International Journal of Engineering Science*, 10(3), 233-248, 1972.

[14] Eringen, A. C., Kim, B. S., Stress concentration at the tip of crack, *Mechanics Research Communications*, 1(4), 233-237, 1974.

[15] Eringen, A. C., Kim, B. S., Relation between Nonlocal Elasticity and Lattice-Dynamics, *Crystal Lattice Defects*, 7(2), 51-57, 1977.

[16] Lazar, M., Maugin, G. A., Aifantis, E. C., On a theory of nonlocal elasticity of bi-Helmholtz type and some applications, *International Journal of Solids and Structures*, 43(6), 1404-1421, 2006.

[17] Mercan, K., Civalek, O., DSC method for buckling analysis of boron nitride nanotube (BNNT) surrounded by an elastic matrix, *Composite Structures*, 143, 300-309, 2016.

[18] Baltacıoglu, A. K., Akgoz, B., Civalek, O., Nonlinear static response of laminated composite plates by discrete singular convolution method, *Composite Structures*, 93, 153–161, 2010.

[19] Civalek, O, Application of differential quadrature (DQ) and harmonic differential quadrature (HDQ) for buckling analysis of thin isotropic plates and elastic columns, *Engineering Structures*, 26, 171–186, 2004.

[20] Demir, C., Mercan, K., Civalek, O., Determination of critical buckling loads of isotropic, FGM and laminated truncated conical panel, *Composites Part B*, 94, 1-10, 2016.

[21] Civalek, O., *Finite Element analysis of plates and shells*, Elazığ, Fırat University, 1998.

[22] Phadikar, J. K., Pradhan, S. C., Variational formulation and finite element analysis for nonlocal elastic nanobeams and nanoplates, *Computational materials science*, 49(3), 492-499, 2010.

[23] Mercan, K., Ersoy, H., Civalek, Ö., Free vibration of annular plates by discrete singular convolution and differential quadrature methods, *Journal of Applied and Computational Mechanics*, 2(3), 128-133, 2016.

[24] Akgöz, B., Civalek, O., Buckling analysis of cantilever carbon nanotubes using the strain gradient elasticity and modified couple stress theories, *Journal of Computational and Theoretical Nanoscience*, 8(9), 1821-1827, 2011.

[25] Chen, Y., Lee, J. D., Eskandarian, A., Atomistic viewpoint of the applicability of microcontinuum theories, *International Journal of Solids and Structures*, 41(8), 2085-2097, 2004.

[26] Baltacıoglu, A.K., Civalek, O., Akgoz, B., Demir, F., Large deflection analysis of laminated composite plates resting on nonlinear elastic foundations by the method of discrete singular convolution, *International Journal of Pressure Vessels and Piping*, 88, 290-300, 2011.

[27] Omurtag, M. H., *Çubuk sonlu elemanlar*, Birsen Yayınevi, 2010.

[28] Civalek, O., Free vibration of carbon nanotubes reinforced (CNTR) and functionally graded shells and plates based on FSDT via discrete singular convolution method, *Composites Part B*, 111, 45-59, 2017.

[29] Peddieson, J., Buchanan, G. R., McNitt, R. P., Application of nonlocal continuum models to nanotechnology, *International Journal of Engineering Science*, 41(3), 305-312, 2003.

[30] Civalek, O., Nonlinear dynamic response of laminated plates resting on nonlinear elastic foundations by the discrete singular convolution-differential quadrature coupled approaches. *Composites: Part B*, 50, 171–179, 2013.

[31] Mercan, K., Civalek, O., Buckling analysis of Silicon carbide nanotubes (SiCNTs) with surface effect and nonlocal elasticity using the method of HDQ, *Composites Part B*, 114, 34-45, 2017.

[32] Chen, W. J., Li, X. P., Size-dependent free vibration analysis of composite laminated Timoshenko beam based on new modified couple stress theory, *Archive of Applied Mechanics*, 83, 431–444, 2013.

[33] Civalek, O., Demir, C., Buckling and bending analyses of cantilever carbon nanotubes using the euler-bernoulli beam theory based on non-local continuum model, *Asian Journal of Civil Engineering*, 12(5), 651-661, 2011.

[34] Narendar, S., Gopalakrishnan, S., Nonlocal scale effects on ultrasonic wave characteristics of nanorods, *Physica E: Low-dimensional Systems and Nanostructures*, 42(5), 1601-1604, 2010.

[35] Civalek, O., *Geometrically non-linear static and dynamic analysis of plates and shells resting on elastic foundation by the method of polynomial differential quadrature (PDQ)*, Elazığ, Fırat University, 2004.

[36] Houari, M. S. A., Bessaim, A., Bernard, F., Tounsi, A., Mahmoud, S. R., Buckling analysis of new quasi-3D FG nanobeams based on nonlocal strain gradient elasticity theory and variable length scale parameter, *Steel and Composite Structures*, 28, 13-24, 2018.

[37] Narendar, S., Nonlocal thermodynamic response of a rod, *Journal of Thermal Stresses*, 40(12), 1595-1605, 2017.

[38] Karlicic, D., Murmu, T., Adhikari, S., Mccarthy, M., *Non-local structural mechanics*, John Wiley & Sons, 2015.

[39] Zhang, Y. Q., Liu, X., Liu, G. R., Thermal effect on transverse vibrations of double-walled carbon nanotubes, *Nanotechnology*, 18(44), 445701, 2007.